Stomatal traits and the control of gas exchange

Robert Andrew Brench

A thesis submitted to the University of Sheffield for the degree of Doctor of Philosophy

The University of Sheffield

Faculty of Science

School of Biosciences

September 2023

Acknowledgements

Firstly, I would like to thank my supervisors, Julie Gray and Andrew Fleming, for their continual guidance and enthusiasm throughout my project. I have thoroughly enjoyed my PhD, in no small part due to the freedom and support you have both provided.

This project was funded by a BBSRC-DTP studentship. I am grateful to the BBSRC for the opportunity to pursue my PhD. I would also like to thank Tom Wilkinson and ADAS for hosting me during my PIPS placement.

This project would not have been possible without the support of colleagues who have supplied a seemingly endless source of knowledge and expertise. In particular, I would like to thank Sarah Carroll, whose guidance during my undergraduate degree gave me the confidence and enthusiasm to pursue this PhD. I would like to thank Sam Amsbury for the advice regarding antibody techniques and for never questioning my continued use of his stocks. Thank you to Natalia Hurtado-Castano for advice and cultivating of plant material. Thanks to Matt Wilson who taught me how to use a LICOR, sparking a long-term bitter-sweet relationship that was essential to much of the data I gathered. I am grateful to Shauni McGregor, who has provided advice and support throughout the project. I would also like to express my gratitude to the people who make up the C33 and D59 lab groups. I would like to thank Dr Silvere Vialet-Chabrand for advice and guidance modelling stomatal dynamics and Dr Lorna McAusland who's advice during the early stages of the project was invaluable. I would like to thank Thomas Hamer who has become a lifelong friend. His support throughout the last four years has enriched my PhD experience.

Finally, I would like to thank my parents for their constant support and encouragement throughout my life and PhD. I would also like to thank Samantha for her support and motivation throughout my PhD and making life outside of academia so fulfilling.

Abstract

Stomata are found on the aerial surfaces of land plants. These pores, which are composed typically of a pair of guard cells, are responsible for facilitating gaseous exchange between plants and their environment. Changes in guard cell turgor pressure causes pores to open and close to tightly regulate gas exchange. The stomata of a wide range of species are known to respond to light, but the speed and magnitude of stomatal responses has received less attention.

The magnitude and speed of stomatal responses was measured, using infra-red gas exchange analysis, across species from broad evolutionary lineages with a range of stomatal sizes, densities, geometries and distributions across both leaf surfaces. This revealed that guard cell geometry is a primary determinant of stomatal response speed and magnitude with dumbbell-shaped guard cells conveying an advantage. Interestingly, no relationship between stomatal size and speed was found, indicating that this may not be an important determinant of speed when looking across distantly related species.

It has been suggested that more rapid stomatal responses provide an advantage in a dynamic light environment by enabling plants to capture more carbon dioxide and minimise water loss. To investigate this further, plants were grown under constant daytime light or dynamic light conditions. Under well-watered conditions there was no difference in plant growth or water use between light conditions. Under drought conditions, plants grown under fluctuating light accumulated significantly less biomass and were less water-use efficient. Nonetheless, there was no significant advantage to having more rapid stomatal responses.

Stomatal opening and closure is fundamentally a mechanical process. Therefore, guard cell composition was investigated for species with kidney shaped guard cells. This revealed a large diversity in guard cell wall components across species from different evolutionary lineages and showed that arabinans contribute to the magnitude of stomatal response in soybean.

Table of contents

Table of Figures

List of Tables

Chapter 1. General introduction

One of the biggest challenges of the 21st century remains producing enough food for an increasing population. Already an estimated 800 million people currently live without access to sufficient and nutritious food (Wheeler and Von Braun, 2023). Climate change will likely compound this issue, adding strain to a system that is already failing to meet targets. Increased average global temperatures, severe weather events and droughts are likely challenges that current and future cropping systems will have to weather (Garnett *et al*., 2005). At the centre of efforts to mitigate these impacts are attempts to develop new elite crop cultivars. A deeper understanding of plant interactions with this changing environment will aid in the development of new crops better suited to provide consistently high yields.

Plants must exist in an environment that changes on scales of climate change over decades, to intermittent light flecks that can last seconds. One of the key adaptations that facilitates plant interactions with the environment is the stoma. Stomata are responsible for the exchange of gases between plants and their environment, of which, the uptake of CO_2 is vital for photosynthesis, a key determinant of crop yields. A trade-off to this is the loss of water through these pores. While the transpiration stream is essential for movement of water and nutrients, and evaporative cooling, excessive water loss can lead to drought stress. Taken together, carbon uptake and water loss make up plant water-use efficiency, a trait of central importance to global crop production (Kijne *et al*., 2003; Blum, 2009).

1.1. Stomatal patterning determines gas exchange potential

Stomata are found on the surfaces of plants and typically consist of a pair of guard cells that surround an adjustable pore (stomata of some mosses being a clear exception possessing only one guard cell) (Sack and Paolillo Jr., 1985). These guard cells function to control gas exchange through turgor driven inflation and deflation that acts to open and close the pore respectively. While stomata are found on the majority of land plants, their form and patterning on leaves have been shown to vary considerably (Hetherington and Woodward, 2003; Casson and Gray, 2008; Franks and Beerling, 2009; Dow and Bergmann, 2014a). Stomata can act to control gas exchange on short scales by opening and closing their pores, or on longer time scales by altering the development of stomatal density on the surface of the leaf (Hetherington and

Woodward, 2003; Franks and Beerling, 2009). Alteration of stomatal patterning influences leaf gas exchange, water-use efficiency and plant growth (Doheny-Adams *et al*., 2012; Franks *et al*., 2015 Bertolino *et al*., 2019; Caine *et al*., 2019).

As the facilitators of gaseous exchange in plants, stomatal size, density and patterning on the leaf epidermis can greatly impact on the assimilation of CO_2 (A) and water loss (Franks and Beerling, 2009; Lawson and Blatt, 2014). Theoretical maximum anatomical stomatal conductance ($g_{s\,max}$), calculated from size and density of stomata per leaf area, shows a strong positive correlation with empirical measurements of stomatal conductance (g_s; Franks and Farquhar, 2001; Franks and Beerling, 2009; Dow *et al*., 2014). Typically there is a trade-off between stomatal size and density, with maximum density being constrained by the one-cell spacing rule which describes how stomatal complexes are normally separated in the epidermal layer, by at least one pavement cell (Larkin *et al*., 1997; Hetherington and Woodward, 2003; Hara *et al*., 2007; Franks and Beerling, 2009). Throughout the evolution of land plants stomatal size and density have, in general, adjusted with prevailing environmental conditions, primarily atmospheric CO_2 concentration (Franks and Beerling, 2009) with suboptimal patterning of stomata incurring a cost to fitness (de Boer *et al.*, 2016). For a given total leaf pore area, models of smaller stomata result in a higher theoretical $g_{s\,max}$ than larger stomata due to their smaller diffusion depth through the pore (Franks and Beering, 2009). The evolution towards smaller stomata in the fossil record appears to coincide with periods of decreasing atmospheric CO_2 concentration, where highly efficient gas exchange was likely selected for in a carbon limiting environment (Raven, 2002; Hetherington and Woodward, 2003; Franks and Beerling, 2009). It has been shown experimentally in species sharing an ecological niche that maximum carbon assimilation (A_{max}) is negatively correlated with stomatal density, whereas $g_{s\,max}$ is positively correlated with stomatal density (Yin *et al*., 2020). This same study found no relationship between stomatal length and maximum operating g_s. When investigating one genus spanning wider ecological niches Drake *et al*. (2013) found a negative correlation between stomatal size and maximum operating g_s. When considering species from a wide range of taxa no relationship between stomatal patterning and g_s was found (Russo *et al*., 2010; McElwain *et al*., 2016). This indicates that if there is a relationship between stomatal patterning and gas exchange, this may be species and niche dependent. Indeed, Xiong and Flexas (2020) suggest that other traits may be important,

including the distribution of stomata on the abaxial and adaxial surfaces of leaves.Distribution of stomata across both the abaxial and adaxial leaf surface varies across plants, ranging from amphistomatous species (stomata on both leaf surfaces) to hypostomatous or hyperstomatous species (stomata only on the abaxial or adaxial surfaces respectively). In particular, the Gramineae family is notable for frequently displaying amphistomatous leaves, although the particular density and contribution to gas exchange of the abaxial and adaxial surface can vary (Pemadasa, 1979; Wall *et al*, 2022). Typically, amphistomatous species display a greater gas exchange capacity than hypostomatous species, likely due to reduced boundary resistance and shorter diffusive distances increasing mesophyll conductance (the diffusion pathway from sub-stomatal cavities to chloroplasts; Drake *et al*., 2019; Xiong and Flexas, 2020).

Stomatal distribution is far from the only innovation that can improve photosynthetic productivity. The evolution of C_4 photosynthesis has occurred over 62 times independently and is a key physiological adaptation that represents an improvement on the ancestral C_3 photosynthetic mechanism (Sage *et al*., 2011). C_4 photosynthesis increases efficiency by employing a carbon concentrating mechanism to increase the CO_2 concentration around Ribulose-1,5-bisphosphate carboxylase/oxygenase (Rubisco), minimising photorespiration (Hatch, 1987; von Caemmerer and Furbank, 2003; Lundgren *et al*., 2014). Interestly, species with C_4 anatomy have often been observed to have smaller stomata and more rapid stomatal responses (McAusland *et al*., 2016; Israel *et al*., 2022; Ozeki *et al*., 2022).

1.2. Stomatal development

One of the most striking examples of stomatal divergence and diversity are the commelinid monocots (including the grasses and cereals). While most plants, including the earliest known fossils, possess kidney-shaped guard cells, commelinid monocots possess dumbbell-shaped guard cells (**Figure 1.1; Figure 1.2A-D**). This is thought to be an adaptation to dry arid environments, with the suggestion that this altered morphology facilitates more rapid control of the stomatal pore (Raven, 2002; Franks and Farquhar, 2007; Chen *et al*., 2017). This alternative stomatal morphology is accompanied by alternative development. Grass stomata display a developmental gradient along the leaf (starting at the base), whereas stomata of all developmental stages can be found across the epidermis of growing dicots. Additionally,

dumbbell stomata are typically accompanied by subsidiary cells, which are thought to facilitate the stomatal response through enhancing the exchange of ions and acting as a source of increasing (or decreasing) mechanical advantage. While stomata with kidney-shaped guard cells can include adjacent subsidiary cells, this is not always the case and there is a wide diversity in subsidiary cell number, orientation and functional importance (Gray *et al*., 2020).

The molecular mechanisms that underpin stomatal development in dicots have been well characterised in the model organism *Arabidopsis thaliana* (Bergmann and Sack, 2017; Zoulias *et al*,. 2018; **Figure 1.3A**). Protodermal cells enter the stomatal lineage by transitioning to a meristemoid mother cell and an asymmetric division forms a meristemoid and a larger daughter cell (stomatal lineage ground cell; Larkin *et al*., 1997). The meristemoid may undergo multiple amplifying divisions, to create more daughter pavement cells, before transitioning to a guard mother cell (Larkin *et al*., 1997; Bergmann and Sack, 2007).

The development of stomata is coordinated by a network of genes and transcription factors, including three regulatory basic helix-loop-helix (bHLH) transcription factors; SPEECHLESS (SPCH), MUTE and FAMA (**Figure 1.3A**). SPCH is required for differentiation of protodermal cells into meristemoid mother cells, and the further asymmetric divisions to form meristemoids (MacAlister *et al*., 2007). MUTE controls the transition from meristemoids to guard mother cells (Pillitteri *et al*., 2007). The final symmetric division which forms a pair of guard cells is controlled by FAMA (Ohashi-Ito and Bergmann, 2006). These three core transcription factors heterodimerise with the transcription factors INDUCER OF CBP EXPRESSION 1/SCREAM (ICE1/SCRM) and SCREAM2 (SCRM2), which are essential to their function (Kanoaka *et al*., 2008).

In concert with the action of transcription factors, stomatal development is regulated by a peptide signalling pathway. Peptides are recognised by leucine-rich repeat receptor kinases (LRR-RKs) of the ERECTA (ER) family and the receptor-like protein TOO MANY MOUTHS (TMM) acting as a co-receptor. Together these activate a mitogen-activated protein kinase (MPK) cascade, which results in the phosphorylation of SPCH (Tori *et al*., 1996; Shpak *et al*., 2005; Lampard *et al*., 2008; Lampard *et al*., 2009).

The core signalling peptides that control stomatal development are EPIDERMAL PATTERNING FACTORS 1 and 2, (EPF1 and EPF2) and STOMAGEN (STOM; EPFL9), with EPFs 1/2 acting antagonistically with STOM by competing for ER and TMM binding sites (Hara *et al*., 2007; Hara *et al*., 2009; Hunt and Gray, 2008; Lee *et al*., 2015). The competitive binding of these peptides acts to regulate *SPCH*, with EPFs 1 and 2 suppressing progression through the stomatal lineage. Loss of *EPF1* and *EPF2* leads to an increase in stomatal density, whereas *epfl9* mutants show reduced stomatal density (Hara *et al*., 2007; Hunt and Gray, 2008; Hara *et al*., 2009; Hunt *et al*., 2010).

As discussed above, grass stomata show a distinct developmental gradient across the leaf with stomata arranged in parallel files across the leaf (Hepworth *et al*., 2018). The process begins with early division of precursor cells that are destined to make up a file. Then an asymmetric division leads to a smaller cell becoming a stomatal precursor. Further asymmetric divisions laterally produce subsidiary cells. Finally, the stomatal precursor (GMC) divides asymmetrically to differentiate into a guard cell pair (Raissig *et al*., 2016; **Figure 1.3B**). Despite the diversity in manner of development, the bHLH transcription factors (SPCH, MUTE, FAMA, ICE1 and SCREAM2) that are integral to *A. thaliana* stomatal development are also present in rice, maize and the model grass *Brachypodium distachyon* (Liu *et al*., 2016; Raissig *et al*., 2016; Raissig *et al*., 2017). While these orthologous bHLH transcription factors are shared between dicot and monocot lineages, their function shows divergence (Liu *et al*., 2016, Raissig *et al*., 2016). For example, while ICE1/SCRM and SCRM2 are functionally redundant in *A. thaliana*, mutation of *BdICE1* alone in *B. distachyon* results in a stomataless phenotype (Raissig *et al*., 2016). Conversely, while *Arabidopsis* has one copy of *AtSPCH*, *B. distachyon* has two partially redundant paralogs (*BdSPCH1* and *2*) which are involved early in stomatal development (Raissig *et al*., 2016). The transcription factor MUTE also acts differently in grasses as a mobile protein BdMUTE is able to initiate subsidiary cell development through the asymmetric division of the subsidiary mother cells (Raissig *et al*., 2017). Knockouts of *bdmute* (referred to hereafter as *B. distachyon* (SID)) display functioning (if less responsive) stomata that lack typical subsidiary cells (Raissig *et al*., 2017).

In addition to transcription factors, grasses also show similarity in signalling peptides. Orthologs of AtEPF1 and 2 have been characterised in barley (*HvEPF1;* Hughes *et al*., 2017). Overexpression of *HvEPF1* inhibits stomatal development, similar to overexpression of *AtEPF1*

and *2*. Additional evidence in rice supports a conserved role of EPFs in monocots, as *OsEPFL9a* knock-out mutants display a severe reduction in stomatal density (Yin *et al*., 2017).

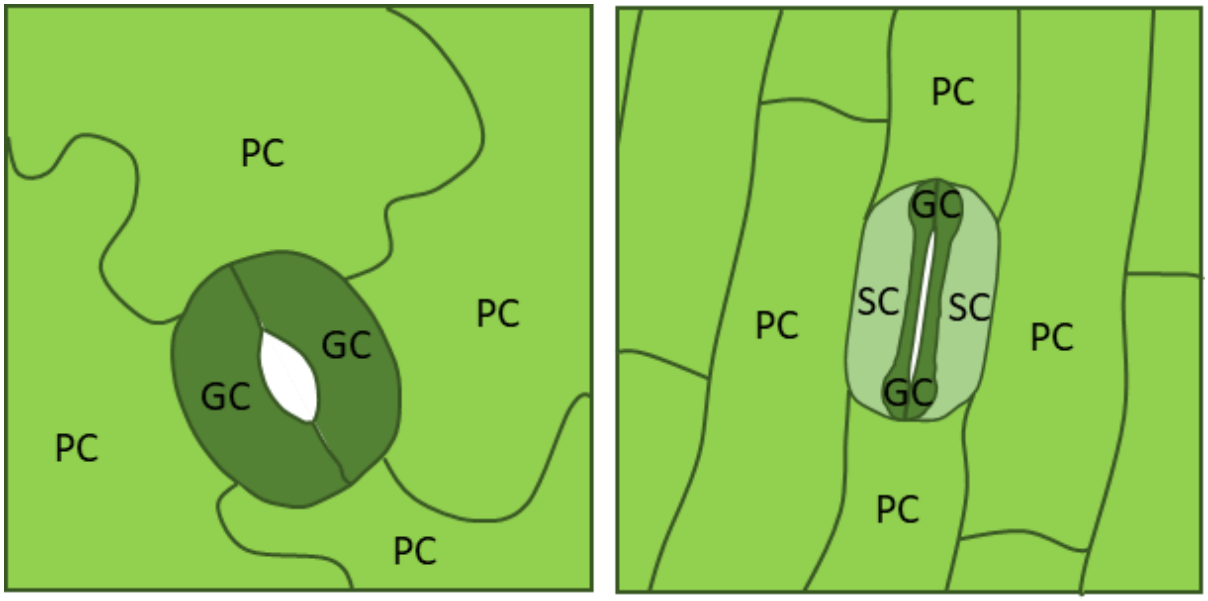

Figure 1.1. Dicot and non-commelinid monocot stomatal morphology
Examples of stomatal morphology in dicots (A) and non-commelinid monocots (B). Two guard cells (GC) are surrounded by epidermal pavement cells (PC). Additionally, guard cells can be flanked by subsidiary cells (SC).

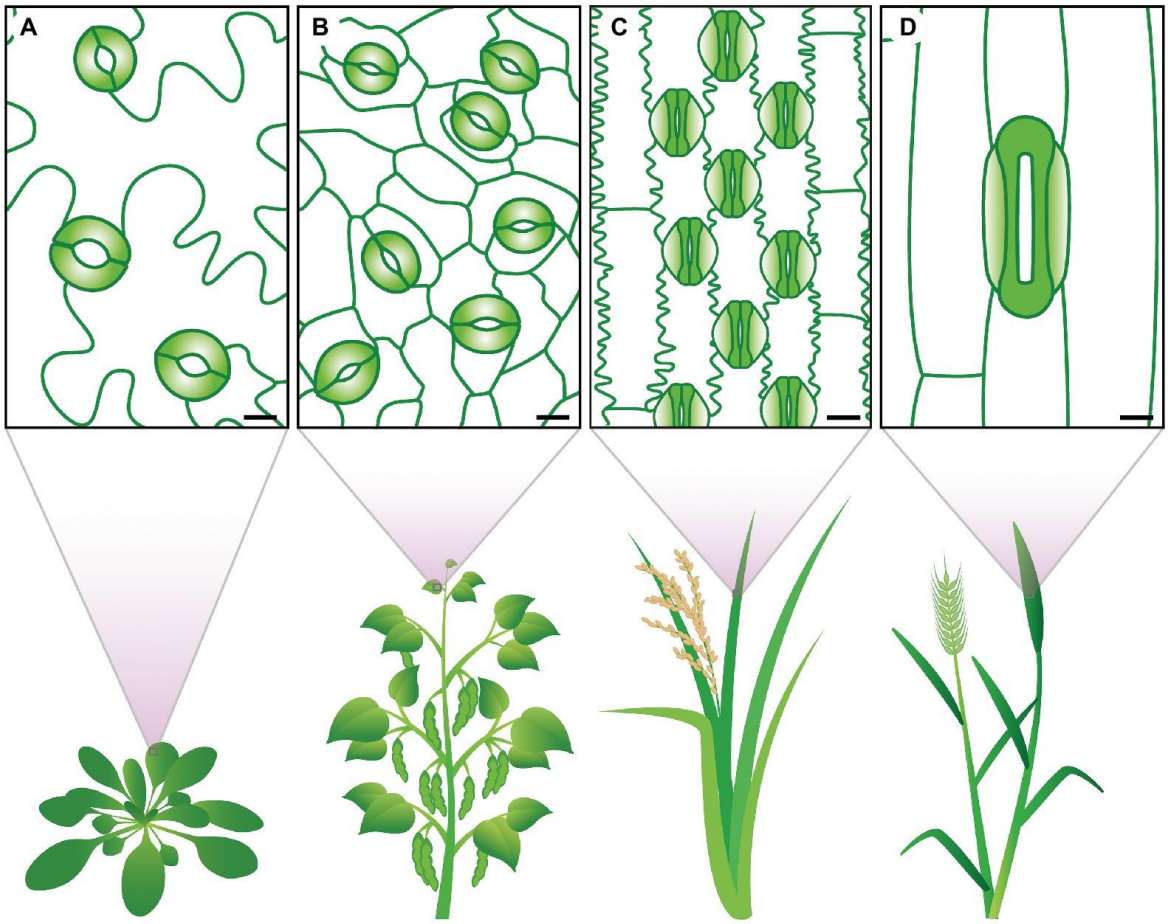

Figure 1.2. Stomatal morphology varies between species
Eudicot stomata of A) *Arabidopsis thaliana* and B) *Phaseolus vulgaris* have kidney-shaped guard cells. Whereas, C) *Oryza sativa* and D) *Triticum aestivum* have dumbbell-shaped guard cells. Scale bar = 10 µm. Figure from Bertolino *et al*., 2019.

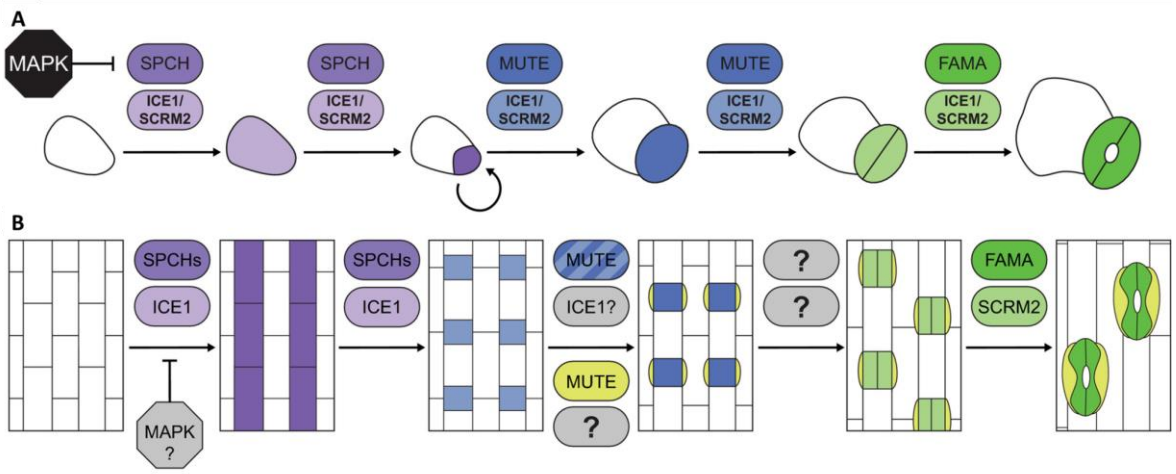

Figure 1.3. Kidney and dumbbell-shaped guard cell development pathways
Transcriptional controls of stomatal development from the model organisms **A)** *Arabidopsis thaliana* and **B)** *Brachypodium distachyon*. Comparison between the basic-helix-loop-helix (bHLH) transcription factors used in stomatal development. Question marks show transcription factors that are yet to be elucidated. Figure from McKown and Bergmann, 2020.

1.3. Molecular underpinnings of the stomatal response

While control of stomatal size and density are able to dictate absolute limits of gas exchange for the lifetime of the tissue, shorter scale alterations of the stomatal pore can control gas exchange to optimise carbon uptake and water loss (Franks and Beerling 2009). Plants must perceive a variety of often conflicting signals, resulting in a stomatal pore width that suits the plants needs (Lawson and Blatt., 2014). Changes in the stomatal aperture are achieved through movement of ions across the guard cell membrane, altering internal turgor (Heath, 1938; Blatt, 2000).

There are many signals that can elicit a stomatal response.g Light intensity, low internal CO_2 levels and the fungal toxin fusicoccin are all known to open stomata (Turner and Graniti, 1969; Brearly *et al*., 1997; Kinoshita and Hayashi, 2011). Low light intensity, high CO_2 and the plant hormone abscisic acid (ABA) are known to close stomata (Goh *et al*., 1996; Brearly *et al*., 1997). Ultimately, these signals drive changes in guard cell osmotic potential through

movement of ions into and out of the guard cell, which in turn drives changes in guard cell turgor. Generally, stomata open in response to both red and blue light with the notable exception of crassulacean acid metabolism (CAM) species which open their stomata in response to darkness (Cockburn, 1983). Stomatal responses to red and blue light differ both in the perception of light and the pathway that leads to a stomatal response (Zieger, 1984; Assmann *et al*., 1985; Matthews *et al*., 2020).

During light-induced opening, expulsion of H^+ from the guard cells by H^+-ATPase, leads to hyperpolarization of the guard cell membrane, the required driving force for the uptake of K^+ through KAT1/2 ion channels (Blatt, 2000; Assmann and Jegla, 2016). This is coupled with the uptake of Cl^- and malate as counter ions (Assmann and Jegla, 2016). The K^+/H^+ exchangers NHX1 and NHX2, chloride malate transporters (ALMT9) and chloride channel c (CLCc) facilitate transport of these ions into the vacuole (Jossier *et al*., 2010; De Angeli *et al*., 2013; Andrés *et al*., 2014).

The mechanisms underpinning the stomatal response to red light remain to be further elucidated, with conflicting data surrounding both the origin and nature of the signal (Matthews *et al*., 2020). The stomatal red light response has been linked to photosynthetic response of the leaf, with inhibitors of photosynthetic electron transport preventing stomatal movements (Kuiper, 1964; Sharkey and Raschke, 1981). It has been suggested that chlorophyll is likely the receptor involved in the red light stomatal response pathway, although the exact location remains unclear (Zieger *et al.*, 2002). Both mesophyll and guard cell chloroplasts have been suggested as candidates for the origin of this signal (Olsen *et al*., 2002; Lawson *et al*., 2014). The stomatal response to internal CO_2 concentration probably contributes to the red light response. Upon irradiance, light driven photosynthesis consumes intercellular CO_2 in the mesophyll, opening stomata (Mott, 1988). A beam of red light alone appears insufficient to drive guard cell specific ion transport, without additional alteration of surrounding CO_2 (Roelfsema *et al*., 2001; 2002). The protein kinase HIGH LEAF TEMPERATURE 1 (HT1), involved in the stomatal CO_2 response, is also involved in the stomatal red light response lending further support to intracellular CO_2 as a signal (Hashimoto *et al*., 2006; Matrosova *et al*., 2015). However, the mechanism of intercellular CO_2 as the primary signal driving the red light response has been called into question by observations that upon illumination with red light, g_s increases in systems when intercellular CO_2 remains constant (Messinger *et al*., 2006).

Furthermore, transgenic tobacco plants with reduced Ribulose-1,5-bisphosphate carboxylase/oxygenase (Rubisco) showed a decrease in carbon assimilation, but no change in stomatal response to red light compared to wild type regardless of higher intercellular CO_2 (von Caemmerer *et al*., 2004).

The blue light response has been demonstrated in epidermal peels, isolated from mesophyll derived signals (Zieger and Hepler, 1977) and hence is guard cell autonomous. Blue light is perceived by the phototropins PHOT1 and PHOT2 (Briggs and Christie, 2002). Upon perception of blue light, PHOT1 phosphorylates BLUE LIGHT SIGNALLING 1 (BLUS1) which activates guard cell plasma membrane H^+-ATPase and the associated exchanges of K^+ and Cl^- (Takemiya *et al*., 2013).

Stomatal closure is brought about by signalling pathways that act to increase ion channel flow out of guard cells and reduce turgor. Upon detection of high CO_2 or ABA, the S-type anion channel, SLOW ANION CHANNEL 1 (SLAC1) is activated facilitating the release of K^+ from guard cells (Vahisula *et al*., 2008; Kim *et al*., 2010; Yamomoto *et al*., 2016). ABA triggers OPEN STOMATA 1 (OST1), which in turn activates SLAC1 (Xue *et al*., 2011).

1.4. Stomatal evolution

Stomata are almost ubiquitous across extant land plants (Hetherington and Woodward, 2003). Phylogenomic analyses indicate that stomata were present in the common ancestor of all land plants (Harris *et al*., 2020). Notably, liverworts lack stomata, although this is thought to be a loss through evolution, as has been noted in other bryophytes, with over 60 independent losses in mosses (Harris *et al*., 2020; Renzaglia *et al*., 2020). The first confirmed stomata in the fossil record date back approximately 420 myo, although other putative stomata appear earlier in the fossil record (Edwards *et al*., 1998; Salamon *et al*., 2018; Clark *et al*., 2022).

The acquisition of stomata is thought to be a key innovation that allowed plants to colonise a terrestrial environment, along with a waxy cuticle (Raven, 2002). This waxy cuticle is almost completely impermeable to gaseous exchanges, necessitating pores that can facilitate uptake of CO_2 as well as evapotranspiration (Edwards *et al*., 1998). Stomata in mosses appear to have a function in spore release, through facilitating drying of the spore capsule (Duckett *et al*.,

2009; Chater *et al*., 2016). Interestingly, anthers of angiosperms have rows of stomata that are positioned to suggest that they may also be involved in facilitating pollen dehiscence (Bertolino et al, 2022). Unlike extant tracheophytes, stomata in moss appear only on the capsule, as opposed to the leafy photosynthetic gametophyte (Merced and Renzaglia, 2013; Merced and Renzaglia, 2016). The stomatal development pathway of the moss *Physcomitrium patens* has been studied as a model organism in order to understand the evolution of the stomatal development pathway (Ran *et al*., 2013; Chater *et al*., 2016; Harris *et al*., 2020).

The *P. patens* genome contains co-orthologs of bHLH transcription factor *AtFAMA* (*PpSMF1* and *PpSMF2*), which controls the final symmetric division in guard cell development (MacAlister and Bergmann, 2011; Ran *et al*., 2013; Chater *et al*., 2017). *P. patens* also contains orthologs of the *A. thaliana* bHLH transcription factor *AtSCRM1* (*PpSCRM1*; Chater *et al*., 2016). In *P. patens*, PpSMF1 and PpSCRM1 likely heterodimerize (as with SPCH, MUTE and FAMA with SCRM1 and 2 in *A. thaliana*), and knockouts of either of these genes result in mutants lacking stomata (Chater *et al*., 2016). Phylogenetic evidence suggests that a common ancestor of all embryophytes had SMF, FAMA and a gene similar to SPCH and MUTE, and these FAMA and SPCH/MUTE like genes were was subsequently lost in bryophytes (Harris *et al*., 2020).

As with the bHLH transcription factors, the signalling peptides and their transmembrane receptors that control stomatal development in *A. thaliana* have homologous genes in *P. patens* (*PpEPF1, PpTMM* and *PpERECTA1*; Caine *et al*., 2016). The EPF/TMM/ERECTA module appears to be an ancestral mechanism governing stomatal patterning. Loss of the *PpEPF1* signalling peptide results in an increase in stomatal density on the capsule (Caine *et al*., 2016). This is analogous to the action of *AtEPF1/2* in *A. thaliana* suggesting a conserved role of these genes (Hara *et al*., 2007; Hunt and Gray, 2009).

Some of the genes involved in the signalling network that controls stomatal aperture and has been well characterised in *A. thaliana*, also appear to have a conserved role across land plants (Harris *et al*., 2020). In *A. thaliana*, the protein kinase *OPEN STOMATA 1* (*OST1*) is essential for stomatal closure in response to ABA through activation of SLOW ANION CHANNEL 1 (SLAC1; Geiger *et al*., 2009; Lee *et al*., 2009). This pathway appears to be conserved in land plants, with *P. patens* containing homologs of *AtOST1* (Chater *et al*., 2011). *P. patens* knockout

mutants of *PpOST1* display a reduced ability to respond to ABA, similar to *AtOST1* knockout mutants in *A. thaliana* (Chater *et al*., 2011). Further evidence of the conserved role of *OST1* in land plants is demonstrated by the presence of orthologs of this gene in *Marchantia polymorpha* and *Selaginella uncinata* (Lind *et al*., 2015; Ruzsala *et al*., 2011). Complementation of *A. thaliana* knockouts of *AtOST1*, with a copy from *P. patens* or *S. moellendorffi*i orthologous *OST1* genes, rescues the stomatal ABA response (Chater *et al*., 2011; Ruzsala *et al*., 2011).

Environmental changes elicit guard cell responses (opening or closure), through detection by guard cell specific receptors or through plant hormones that are detected by the guard cell. These signals then typically activate ion channels that control guard cell turgor through the movement of ions between guard cells and surrounding cells. It has been suggested that plants from bryophyte, lycophyte and fern lineages operate their stomata in a hydropassive manner (Brodribb and McAdam, 2011). This theory suggests that the stomata of plants from these lineages close their stomata in response to leaf apoplastic water potential, rather than the direct movement of ions across the guard cell. Despite the contention that hydroactive stomatal responses (stomatal responses through movement of ions) evolved in the gymnosperms, there are multiple studies that show that extant members of the bryophyte, lycophyte and fern lineages respond to CO_2, ABA and light actively adjusting their stomatal pore, or that these stomata open in response to flagellin which activates H+-ATPases (Ruszala *et al*., 2011; Hõrak *et al*., 2017; Cai *et al*., 2021; Placket *et al*., 2021; **Figure 1.4**). Deletion of the *P. patens* OST1 homologue disrupts the stomatal response to ABA as mentioned above, indicating an active signalling response is present in bryophytes (Chater *et al*., 2011). For an in depth review of the evolution of stomatal responses see Harris *et al*. (2022).

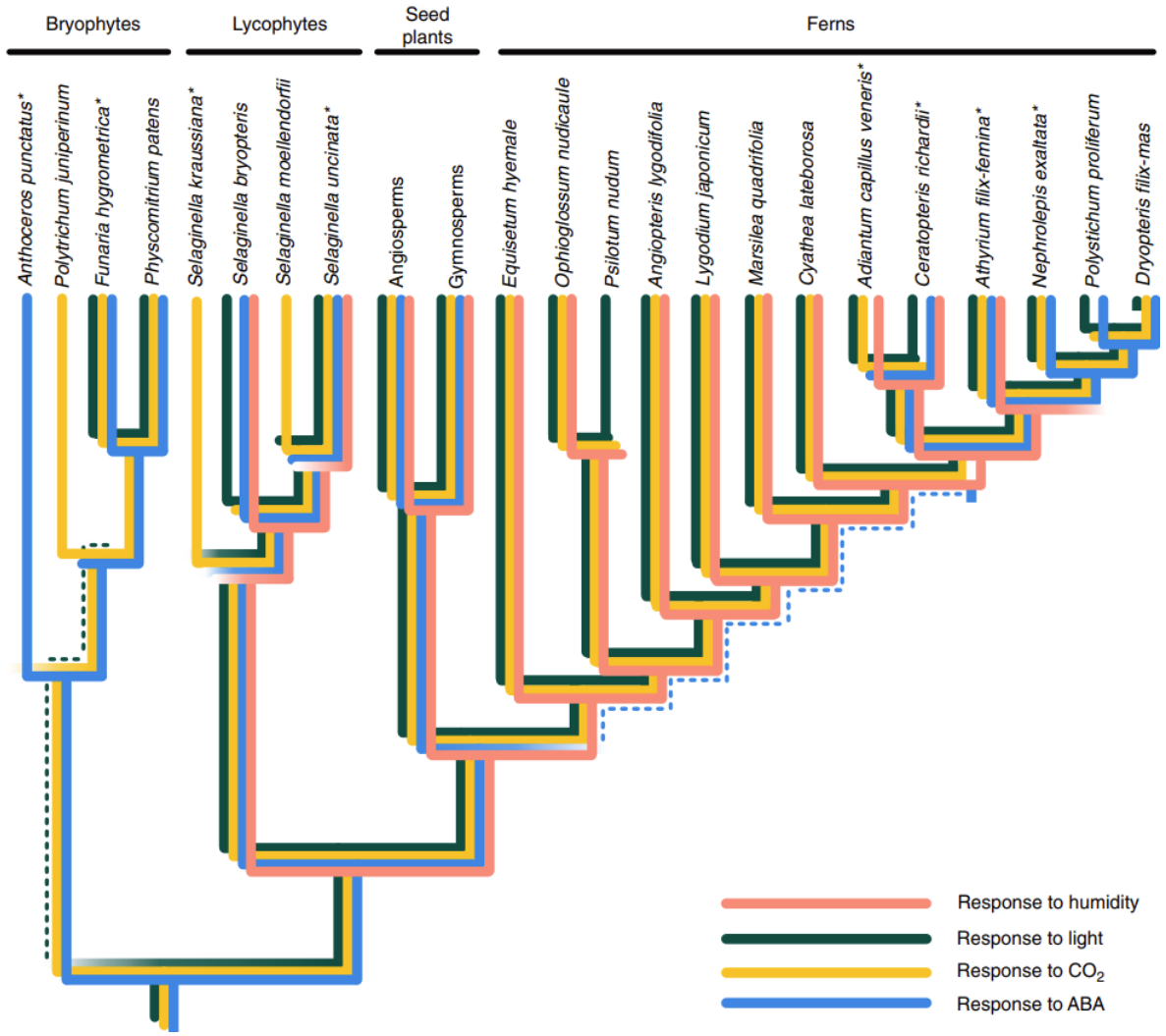

Figure 1.4. Stomatal responses across land plants
A phylogeny showing species which have been shown to have a stomatal response to humidity, light, CO_2 and ABA. Species with conflicting data are marked with an *. A lack of response displayed may mean a response is yet to be experimentally determined. Figure from Harris *et al*., 2022.

1.5. Speed of stomatal response

Under steady state conditions, there is a close relationship between the requirements of the mesophyll in terms of *A* and g_s (Wong *et al*., 1979). However, in dynamic conditions the stomata aperture response to stimuli is often much slower than photosynthetic regulation (Lawson and Blatt, 2014; McAusland *et al*., 2016; Vialet-Chabrand *et al*., 2017; Lawson and Vialet-Chabrand, 2019). This disconnect between *A* and g_s can have detrimental effects on water use efficiency, with slow stomatal opening limiting carbon acquisition and slow closing leading to excessive water loss (Farquhar and Sharkey, 1981; Knapp and Smith, 1987; Grantz and Assmann, 1991; McAusland *et al*., 2016; Matthews *et al*., 2017; Lawson and Vialet-Chabrand, 2019). While altering stomatal density on the surface of leaves remains an attractive solution to engineering favourable gas exchange in a variety of crops (Franks *et al*., 2015; Hepworth *et al*., 2015; Hughes *et al*., 2017; Caine *et al*., 2019; Dunn *et al*., 2019), increasing stomatal response speeds through manipulation of ion transport has yielded promising results (Qu *et al*., 2020; Horaruang *et al*., 2022). Improvements in WUE through enhancing the speed of stomatal response has provided empirical evidence for the modelled improvements in WUE estimated by reducing the limitation of slow stomata on *A* (Farquhar and Sharkey, 1982; Lawson and Blatt, 2014).

Understanding the physiological determinants of stomatal speed could aid in the engineering of crops with enhanced WUE. While the ability of stomata to respond hydroactively has been noted in species of all major extant land plants clades, the speed and magnitude of stomatal responses has been shown to vary considerably between species (Vico *et al*., 2011; Drake *et al*., 2013; Lawson and Blatt, 2014; McAusland *et al*., 2016; Elliot-Kingston *et al*., 2016; Deans *et al*., 2019; Cai *et al*., 2021; Harris *et al*., 2022; Zhang *et al*., 2022). Not only is there considerable variation in stomatal responses between species from different clades, but even between cultivars of the same crop species, albeit typically less than interspecies differences (Zhang *et al*., 2022). Stomatal size has often been thought to be important for determining the speed of stomatal opening and closure. Typically smaller stomata have been considered to open and close more quickly, due to their relatively larger surface area to volume ratio (Hetherington and Woodward, 2003; Franks and Beerling, 2009). This pattern has been reported in closely related species of the genus *Banksia* (Drake *et al*., 2003), in rainforest tree species that share an ecological niche (Kardiman and Ræbild, 2017) and some C_4 grass species

(Israel *et al*., 2022; Ozeki *et al*., 2022). However, stomatal opening and closure relies on both guard and pavement (or subsidiary) cell mechanics. This link between size and speed becomes more complicated when considering morphological variations in stomata such as the innovation of dumbbell shaped guard cells. Opening in these stomata relies on the pool of solutes stored in the subsidiary cells and the associated reduction in subsidiary cell mechanical advantage that occurs when these solutes are transported into the guard cells (Franks and Farquhar, 2007). Genetic ablation of these subsidiary cells results in impaired gas exchange and speed of stomatal response (Raissig *et al*., 2017). Additionally, the more rectangular shape of the dumbbell pore requires a much smaller increase in width to achieve a larger increase in pore area than an ellipsoid pore. This inherently provides grasses with an advantage in the speed of adjusting pore area, independent of size, compared to species with kidney shaped guard cells. Further, a negative relationship between stomatal size and speed relies on the assumption that the ion exchange capability is constant per unit surface area of the guard cell. This has been shown not to be the case (Lawson and Blatt, 2014). When looking at a more diverse group of species the relationship between stomatal size and speed appears more complicated and evidence contrary to a size-speed relationship exists. For example, experiments have shown that smaller stomata are faster in species with dumbbell but not kidney shaped guard cells (McAusland *et al*., 2016; Elliot-Kingston *et al*., 2016; Deans *et al*., 2019). However, a study looking at a panel of 5 horticultural crops with kidney-shaped stomata (totalling 19 varieties) did find a negative correlation between stomatal size and speed (Zhang *et al*., 2022).

It has been suggested that in some species stomatal speed is an adaptation to capturing light flecks, and that stomatal size is not always important. Indeed, data show that some ferns with large stomata are able to open more rapidly than gymnosperm and angiosperm species with smaller stomata (Deans *et al*., 2019). Leptosporangiate ferns have been shown to have faster stomatal responses to light when compared to *A. thaliana* and other fern clades, which is thought to be due to enhanced blue light signalling through an increased number of cryptochrome genes (Cai *et al*., 2020). These contrasting observations concerning the determinants of stomatal speed suggest that other factors, in addition to size, may contribute to stomatal speed. Indeed, experiments to engineer the activation of K+ channels have successfully increased the speed of stomatal responses (Papanatsiou et al, 2019).

1.6. Stomatal responses to a dynamic light environment

Light (in terms of both intensity and quality) in field conditions can be highly variable across spatial scale. Changes ranging from mean seasonal irradiance to sun flecks which can last less than a second make up a complex and dynamic environment in which plants must respond (Slattery *et al*., 2018). In the typical dense canopies commonly found in monoculture cropping, sunflecks have been shown to make up 20-93% of the photosynthetic photon flux density (PPFD) below the upper canopy hence, making use of these sunflecks can increase photosynthetic output (Pearcy *et al*., 1990; Slattery *et al*., 2018). Understanding the importance of fluctuating light intensity on plant growth and strategies to optimise photosynthesis in these conditions has been cited as a potential target for crop improvement (Yamori *et al*., 2016).

After an initial step increase in light, multiple biochemical limitations are imposed on photosynthesis, limiting output. The first steps (the activation of ribulose bisphosphate and activation of Rubsico) are typically limiting for up to 10 min (Pearcy, 1990). The final step, stomatal opening, can remain limiting for as long as an hour (Pearcy, 1990; Vico *et al*., 2011; McAusland *et al*., 2016). Reducing this final, longer limitation on photosynthesis is a strategy that has been approached through improvement of stomatal response speeds. The limitation of slow stomata on *A* has been estimated to be 10% and 15% in C_3 and C_4 crop species respectively (McAusland *et al*., 2016). Typical diurnal variation in light intensity results in incident light both above and below saturation. This lowers photosynthetic rate under lower PPFD and leads to periods of stress under higher light intensities that can cause damage to leaf photosynthetic machinery (Baker, 2008). Excess light energy results in build-up of excited chlorophylls and reduced electron carriers which can damage photosynthetic machinery through a build up of reactive oxygen species (ROS; Melis, 1999; Aro *et al*., 2005; Krieger-Liszkay, 2005). To prevent this, plants have developed a range of mechanisms to reduce damage termed photoprotection. These mechanisms include relocation of leaves and their chloroplasts, ROS scavenging, photorespiration and non-photochemical quenching (NPQ; Takahashi and Badger, 2011).

The limitation of g_s on *A* during stomatal opening seems to be context dependent, partially due to the conflicting needs of the plant to maximise *A* and limit water loss. The limitation of stomata on *A* during fluctuating PPFD is influenced by stomatal response speeds,

photosynthetic mechanism, time of day and environmental conditions such as drought (Mencuccini *et al*., 2000; McAusland *et al*., 2016; Matthew *et al*., 2017 Slattery *et al*., 2018; Sakoda *et al*., 2020). McAusland *et al*. (2016) observed rapid increases in *A* upon illumination of leaves, followed by much slower responses in g_s. This indicates that in order to facilitate a rapid increase in *A* upon a sudden increase in light intensity, g_s is maintained at a level higher than might be necessary, at least under well-watered conditions. Accordingly, under rapid illumination of the leaf, *A* is able to initially increase without limitation, but the level of stomatal gas exchange does eventually become limiting. However, under water limited conditions, leaves at low PPFD maintain a lower g_s likely to reduce water loss (McAusland *et al*., 2016; Slattery *et al*., 2018). Slow stomatal closure, such as during shading by cloud cover or by self-shading, further contributes to the asynchronicity between g_s and the needs of the plant (Lawson and Blatt, 2014; McAusland *et al*., 2016; Slattery *et al*., 2018; Wall *et al*., 2022). Excessive water loss (relative to carbon gained) during this slow closure decreases WUE.

Drought stress can play an important role in determining plant gas exchange, as it is one of the many complex signals that together determine stomatal aperture size. Hence, it can be a central factor underlying the trade-off between *A* and water loss. Drought stress is thought to impact *A* directly through a limitation of gaseous exchange and through inhibition of biochemical processes (Flexes *et al.,* 2004; Flexas *et al*., 2006; Sokado *et al*., 2022). Initially during drought, stomatal closure (to prevent water loss) reduces *A* by increasing the barrier to CO_2 diffusion into the leaf, followed by a decrease in mesophyll conductance (Flexas *et al*., 2004; Flexas *et al*., 2006; Mizokami *et al*., 2015; Sakoda *et al*., 2020).

Drought stress can contribute to damage to the leaf by excess light. A reduced availability of intracellular CO_2 reduces the rate of consumption by the Calvin cycle, potentially leading to a build up of ROS that can damage photosynthetic pigments and causes cellular damage (Long *et al*., 1994; Greico *et al*., 2020). Several biochemical pathways can be activated that reduce damage to the photosynthetic apparatus. This may include the production of anthocyanin pigments to reduce light absorption, and mechanisms to dissipate excess energy from photosystem II as heat or fluorescence, and a switch towards cyclic rather than linear electron transport.

1.7. Evidence for a rapid stomatal response being beneficial

Efforts to improve plant productivity in conditions more similar to field conditions than a constant daily PPFD growth chamber have yielded promising results. To introduce the variability of a field light regime, without the unpredictability of actual field trials, multiple experiments have been conducted that simulate real world light regimes in controlled growth chambers. By introducing plant with altered ion exchange capacity, the importance of a rapid stomatal response in maximising photosynthesis in a realistic dynamic PPFD environment can be directly assessed. In particular, the manipulation of the ion channels responsible for eliciting change in guard cell turgor has been a target for improving stomatal response speeds. Using these enhanced plants has provided a system to further investigate the importance of a rapid stomatal response in a dynamic environment.

The most commonly used species to date is *A. thaliana* with fewer studies translating the work into crop plants. *A. thaliana* plants overexpressing BLINK1 (blue light induced K^+ channel 1) displayed shorter opening and closing times through enhanced, blue light driven, ion transport (Papanatsiou *et al*., 2019). When grown under a fluctuating light environment, changing hourly between 10 and 150 µmol $m^{-2}s^{-1}$, BLINK1 plants achieved a 2.2 fold increase in biomass relative to the wild-type (Papanatsiou *et al*., 2019). Although this light regime does not replicate those found in field conditions, the data do suggest that improving stomatal response speeds may be a viable solution for improving plant performance under dynamic conditions.

Further evidence for manipulation of ion channels as an attractive solution to improve plant biomass under dynamic conditions comes from Kimurara *et al*., (2020). Utilising the *A. thaliana* plant with altered ion transport capacity: *ost1* (open stomata 1), *slac1* (slow anion channel-associated 1) and *PATROL1-ox* (proton ATPase translocation control 1) to cover a range of stomatal response phenotypes, the importance of stomatal response speed on biomass acquisition and WUE was investigated. Both *ost1* and *slac1* show impaired stomatal function, with consistently open stomata. On the other hand, *PATROL1-ox* displays enhanced stomatal response speeds. When grown together under a dynamic PPFD regime, *ost1* and *PATROL1-ox* achieved greater biomass than WT and *slac1.* Whereas, under constant light intensity there was no difference in biomass. The higher biomass achieved by *ost1* is likely attributed to the consistently open stomata, which led to a reduction in WUE. However,

PATROL1-ox displayed far more similar g_s to wild type, but with an increased dynamic range and faster responses, which appears to be the cause of the increased biomass under the dynamic light regime. Interestingly, during the fluctuating regime, the PPFD was increased or decreased every 5-10 minutes, far shorter than it takes to complete a stomatal opening response. It is noteworthy that both *BLINK1* and *PATROL1-ox* not only alter stomatal response time but also the magnitude of stomatal response, which may also play a role in the increased biomass achieved by these plants in dynamic conditions relative to wild-type.

Efforts have been made to translate advances in enhancing stomatal response speed to the field, in the economically important crop rice. Using GWAS and data on stomatal response speeds from 206 rice accessions, the ion transporter *OsNHX1* was identified to be associated with rapid stomatal closure (Qu *et al*., 2020). Rice lines overexpressing *OsNHX1* showed significantly shorter stomatal closing times and higher yield when grown in the field under drought.

Taken together, these experiments suggest that improving the speed of stomatal response is a valid avenue for improving crop yield and WUE in field conditions. However, these experiments focus heavily on plants, not only with altered stomatal response speeds, but often also altered steady state maximum and minimum g_s.

1.8. The plant cell wall is essential to guard cell function

One of the defining characteristics of the stomata of vascular plants is the ability to undergo reversible changes of the pore size. To facilitate this, guard cell walls must be capable of reversible deformation, suggesting a strong and flexible structure distinct from the surrounding pavement cells (Wu and Sharpe, 1979; Amsbury *et al*., 2016; Carter *et al*.,2017; Shtein *et al*., 2017; Woolfenden *et al*., 2017; Rui *et al.,* 2018; Chen *et al*., 2021; Carroll *et al*., 2022). This complex structure is primarily composed of polysaccharides that can be divided into cellulose, pectins and hemicelluloses.

Commonly, dicots and non-commelinid monocots have a type I cell wall, whereas monocots have a type II cell wall (Carpita, 1996). Both type I and II cell walls are typically rich in cellulose. Pectin content and composition varies between groups with type I cell walls containing more pectin (approximately 35% of the cell wall, mostly in the form of homoglacturonan: HGA) and

type II cell walls containing mostly rhamnogalacturonan (RG; approximately 2-10% of the cell wall; Mohnen, 2008; Vogel, 2008).

Cellulose, which consists of β-1,4-linked glucose, is synthesised at the plasma membrane by cellulose synthase enzymes and can subsequently form crystalised microfibrils from parallel chains (Hill *et al*., 2014; Li *et al*., 2014). Unlike cellulose, pectin and hemicellulose are synthesised in the golgi by glycosyltransferase enzymes and later transported to the cell wall (Oikawa *et al*., 2013). Although cellulose can aggregate to form microfibrils, its simple linear structure contrasts with the variably branched pectins and hemicelluloses (Atmojo *et al*., 2013; Voiniciuc *et al*., 2018).

Pectins are cell wall polysaccharides made up of four major groups. They are defined by a backbone that contains, α-1,4-linked D-galacturonic acid residues (O'Neill *et al*., 1990; **Figure 1.5A**). The simplest, and most common pectin in dicots is HGA (Mohnen, 2008). HGA is a polymer of linear α-1,4-linked D-galacturonic acid that can be methyl-esterified or acetylated. Xylogalacturonan has the same galacturonic acid backbone but is decorated with xylose residues (Zandleven *et al*., 2007). Rhamnogalacturonan II (RGII) is a less common pectin in dicots (Mohnen 2008). RGII is also a polymer of linear α-1,4-linked D-galacturonic acid that can be cross linked by borate diester bonds (Ishii and Matsunaga, 2006; O'Neill *et al*., 2004). Unlike HGA, RGII is often decorated with side chains composed of arabinose, rhamnose and fucose (O'Neill *et al*., 2004). Rhamnogalacturonan I (RGI) is composed of an alternating backbone of galacturonic acid and rhamnose. Rhamnose residues can be substituted with side chains of arabinose or galactose.

Hemicelluloses are all composed of β-1,4-linked backbones and include xyloglucans, xylans, mannans and glucomannans (Scheller and Ulvskov, 2010). Xyloglucan is found across all land plant lineages and is the most abundant hemicellulose found in type I cell walls (Scheller and Ulvskov, 2010). The xyloglucan backbone can be substituted with side chains, with letters indicating the composition of the xyloglucan units (G, X, L and F denote no substitution, xylose substitution, galactose substitution and fucose substitution respectively; **Figure 1.5B**). Xylans are formed from a backbone of xylose residues, which can be acetylated or have other decorations such as glucuronic acid and arabinose (Scheller and Ulvskov, 2010; Rennie and Scheller, 2014). Mannans are formed of a backbone of mannose.

1.9. Matrix polysaccharides in guard cell walls

Guard cell wall composition has been shown to vary across species in all three of the major cell wall polysaccharide components (Amsbury *et al*., 2016; Carter *et al*.,2017; Shtein *et al*., 2017; Brennan *et al*., 2019). Commelinid monocot guard cells appear to possess not only distinct morphology, but also a distinct cell wall composition compared to dicots and non-Commelinid monocots (Shtein *et al*., 2017; Brennan *et al*., 2019). In dicots the most common pectin is HGA. HGA is synthesised in a highly methyl-esterified form by pectin methyltransferases (PMTs; Mohnen, 2008; Wolf *et al*., 2009). These methyl groups can subsequently be removed by the action of pectin methyl esterase (PME) enzymes. HGA appears to be a highly conserved cell wall component (Mohnen, 2008). The action of PMEs has been cited as a mechanism by which cells can modulate wall stiffness. Removal of these methyl groups is thought to allow the formation of calcium cross links between adjacent HGA molecules, increasing stiffness (Mohnen, 2008; Wolf *et al*., 2009). This model is complicated by observations of un-esterified pectin being associated with cell wall loosening, likely due to the action of polygalacturonase enzymes (Voiniciuc *et al*., 2018). Current theory suggests that the manner of de-methyl-esterification of HGA determines the impact on cell wall flexibility with block-wise de-methyl-esterification allowing for the formation of calcium cross links, and random de-methyl-esterification marking HGA for degradation by polygalacturonases (Hocq *et al*., 2017).

The role of methyl-esterification of HGA in guard cells has been studied by Amsbury *et al*., (2016), who demonstrated that *A. thaliana* guard cells are enriched in un-esterified HGA. *A. thaliana* plants lacking PME6 (pectin methyl-esterase 6; a gene highly expressed in guard cells) showed guard cells with more methyl-esterified HGA, less un-esterified HGA and a reduced dynamic range of opening and closing. HGA methyl-esterification has also been shown to vary spatially across guard cells, with particular hotspots of un-esterified pectin located at the poles of stomata in *A. thaliana*, coinciding with areas of increased cell wall stiffness, detected using AFM (Carter *et al.,* 2017, Rui *et al*., 2017).

Another key pectic component of the cell wall that has been demonstrated to be important in guard cell function are short chains of arabinan, associated with RG1 (Jones *et al*., 2003; Jones *et al*., 2005; Carroll *et al*., 2022). Treatment of epidermal peels of *Commelina communis, Vicia faba* and *A. thaliana* with arabinase restricts proper function of guard cell opening and

closure (Jones *et al*., 2003; Jones *et al*., 2005; Carroll *et al*., 2022). Further, overexpression of the arabinan synthesis gene *ARABINASE DEFICIENT 1* (*ARAD1*) in *A. thaliana* led to an increase in both long and short chains of arabinan in guard cells and increased guard cell wall flexibility during opening (Carroll *et al*., 2022). The precise mechanism by which arabinan influences cell wall properties remains unknown. It has been suggested that arabinan can influence the formation of calcium cross bridges between HGA polymers (Jones *et al*., 2003). Alternatively, increasing evidence suggests that polymer entanglement may play an important role in cell wall mechanics, which arabinan side chains may impact (Carroll *et al*., 2022). HGA and arabinan have also been observed in the guard cells of the moss *Funaria hygrometrica*, with arabinan appearing to be exclusively in guard cells (Merced and Renzaglia, 2014). This may suggest a conserved role of guard cell arabinan in facilitating a stomatal response however, the function of moss stomata has been suggested to vary from that of tracheophytes (Chater *et al*., 2017). Nonetheless, arabinan may be functionally important in stomatal closure in mosses (Chater *et al*., 2011).

Xyloglucan is the primary hemicellulose in the cell walls of dicots (Carpita & Gibeaut, 1993; Cosgrove and Jarvis, 2012). Originally thought to have a role in the tethering of cellulose microfibrils together, the lack of a phenotype and any detectable xyloglucan in *A. thaliana* mutants lacking two *XYLOGLUCAN XYLOSYLTRANSFERASE* genes (*xxt1/xxt2*), indicates an alternative role for this hemicellulose (Carpita & Gibeaut, 1993; Cavalier *et al*., 2008; Cosgrove and Jarvis, 2012). *A. thaliana* lacking *xxt1/xxt2* achieve smaller stomatal pores during opening and closing, suggesting xyloglucan is important for correct guard cell function, likely due to altered cellulose fibril organisation during opening and closure (Rui and Anderson, 2016).

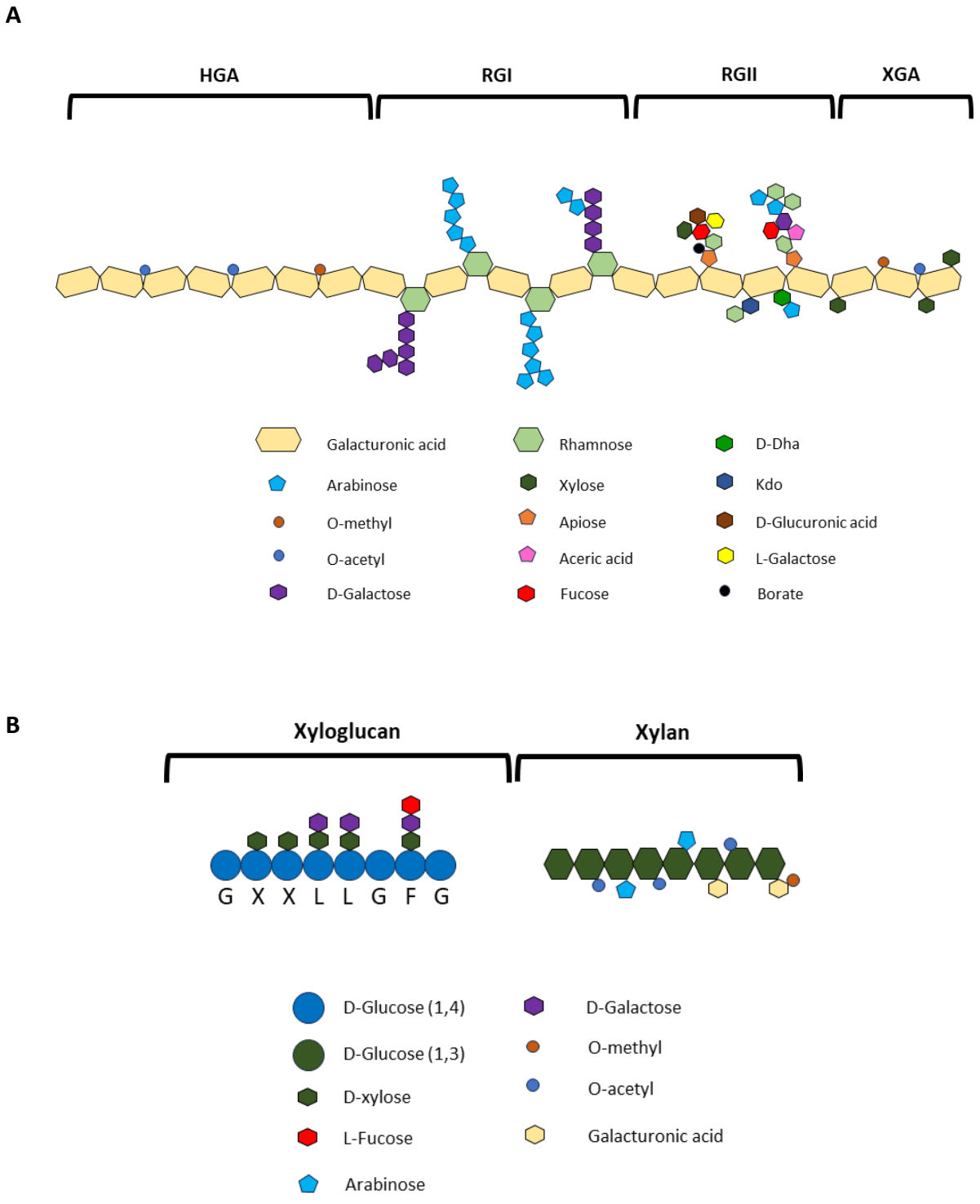

Figure 1.5. Pectin and hemicellulose cell wall components

A) The primary pectin forms in cell wall are homogalacturonan (HGA), rhamnogalacturonan I (RGI), rhamnogalacturonan II (RGII) and xylogalacturonan (XG). All have galacturonic acid backbones, but RGI has interspersed rhamnose units. HGA can be methyl or acetyl esterified. RGI can be decorated with side chains of arabinan, galactan or arabinogalactan. RGII has more complex side chains. XG is substituted with xylose. **B)** The most common hemicelluloses in dicots are xyloglucan and xylan. Xyloglucan has a backbone of β-1,4-linked D-glucose, which can be substituted with xylose, galactose and fucose shown by the single letter coding. Xylans have a backbone of β-1,4-linked xylose and can be substituted with galactose or methyl or acetyl esterified.

Table 1.1: Summary of plant cell wall components and their role in guard cell function.

Component	Backbone	Possible modifications	Distribution in plants	Role in guard cells
Homogalacturonan	α-1,4-linked D-galacturonic acid	Methyl and acetyl groups	Most abundant pectin in dicots	Can be de-methyl-esterified to alter cell wall flexibility (Amsbury *et al*., 2016)
Rhamnogalacturonan 1	Alternating galacturonic acid and rhamnose	Arabinose and galactose side chains	Most abundant pectin in monocots	Arabinose and galactose side chains have been suggested to modulate guard cell flexibility (Jones *et al*., 2003; Carroll *et al*., 2022)
Rhamnogalacturonan 2	α-1,4-linked D-galacturonic acid	Complex side chains	Most abundant pectin in monocots	Adjacent polymers can form borate diester bonds that may modulate stiffness (O'Neill *et al*., 2004)
Xylogalacturonan	α-1,4-linked D-galacturonic acid	Methyl and acetyl groups. Xylose residues	Often found in fruits and seeds	Little is known about the role of this component in guard cells
Xyloglucan	β-1,4-linked D-glucose	Xylose, galactose and fucose	Abundant across plants	Modulates correct cellulose orientation during stomatal opening and closure (Rui and Anderson, 2016)
Xylan	β-1,4-linked D-xylose	Arabinose, galacturonic acid and acetyl groups.	Commonly found in monocots and less so in dicots	A key component in grass guard cells that promotes guard cell flexibility (McGregor, 2021)

1.10. Aims and objectives

This thesis aims to increase the understanding of the diversity that exists across land plants in both stomatal response speeds and guard cell wall structure. By using representative species from major land plant clades, the diversity which exists in these traits can be captured.

Previous research has investigated the speed of stomatal response across species, but few studies have encompassed species from a broad range of clades, ecological niches, domesticated crop species and wild relatives. Investigating the diversity of stomatal response speeds and anatomical features of stomatal walls will improve the knowledge of what diversity exists across land plants and the contribution of anatomical characteristics to a rapid stomatal response. The primary questions raised were:

1. What diversity exists in the speed of stomatal responses across a broad range of species spanning ecological niche and stomatal morphology?
2. Can stomatal response speeds be attributed to morphological features such as size, density, shape or the presence of subsidiary cells?

Stomatal responses have often been cited as not only a key feature to the success of land plants, but also as a target to improve plant water use efficiency in crops. Using a panel of species with a range of stomatal speeds, the importance of a rapid stomatal response on plant efficiency and productivity in a dynamic light environment can be understood. Particularly:

1. Do species with a rapid stomatal response perform better in a dynamic environment?
2. Do plants grown under dynamic conditions show improved stomatal response speeds?

Further, the guard cell wall composition of these species will be examined. This will enable both the diversity in guard cell wall structure and the contribution of guard cell wall structure to a rapid stomatal response across different plant clades to be determined. While guard cell wall composition has been shown to be integral to stomatal function in a few model organisms, whether these observations are ubiquitous across land plants remains to be determined. This has led to the questions:

1. What diversity exists across land plants in stomatal, subsidiary and pavement cell wall composition?

2. Does guard cell wall composition change when looking at plants spanning evolutionary time?
3. Are certain cell wall components associated with a rapid or slow stomatal response?

Chapter 2. Materials and Methods

2.1. Plant material

2.1.1 Plant material and growth conditions

Where possible plants were grown from seed to control the conditions in which they developed prior to data collection. However, for some species this was not possible and measurements were taken on these species after new leaves had developed in stable growth conditions. For details of growth conditions see **Table 2.1**. *Selaginella plana* was kindly provided by the University of Bristol. *Athyrium filix-femina*, *Osmunda regalis, Illicium floridanum, Ginkgo biloba* and *Magnolia grandiflora* were purchased from Burncoose Nursery (Redruth, UK) and grown under a Valoya AP673L LED light source (Valoya, Helsinki, Finland). *Triticum aestivum* (Cougar)*, Triticum durum* (Voiler)*, Tradescantia rubra, Brachypodium distachyon* and *Hordeum vulgare* were taken from stocks at the University of Sheffield grown in a controlled growth chamber (Conviron PGR15; Conviron, Winnipeg, MB, Canada). *Solanum tuberosum* (King Edward)*, Solanum lycopersicum* (Moneymaker) and *Glycine max* were grown from stocks stored at the University of Sheffield and grown at the Arthur Willis controlled Environment Centre (AWEC, The University of Sheffield, UK). *Hordeum spontaneum, Triticum boeoticum* (Tr118344)*, Triticum araraticum* (Tr118358)*, Arabidopsis thaliana* (Col-0) and *Glycine soja* were taken from the stocks of Professor Colin Osborne (The University of Sheffield, Sheffield, UK). *B. distachyon* (SID) was provided by Professor Michael Raissig (The University of Heidelburg, Germany) and grown in a controlled growth chamber (Conviron PGR15; Conviron, Winnipeg, MB, Canada).

Species were chosen to span the plant phylogeny. Where possible species were chosen that have previously shown a stomatal response to light. Due to the time required to make measurements of response speed and availability of equipment, some clades are less well represented, such as the gymnosperms, with only *G. biloba* from this group. Crop species feature heavily in this study due to their economic importance and ease of material acquisition. Species were grown under conditions they were suited to rather than all under the same conditions to avoid taking measurements of stressed plants which would inevitably influence gas exchange (Table 2.1).

2.1.2 Phylogeny

To demonstrate the evolutionary relationship between species, a phylogeny was created using TimeTree (Kumar *et al*., 2022). Using this tool, estimates separating the most recent common ancestor between species used in this study were collated into a phylogeny (Wikström *et al*., 2001; Hedges and Kumar, 2009; Yuzawa *et al*., 2012; Clarke *et al*., 2011; Christin *et al*., 2014; Wu and Ge, 2012; Zhang *et al*., 2012; Givnish *et al*., 2000; Pafrey *et al*., 2011; Magallon *et al*., 2013).

2.2. Stomatal anatomical measurements

2.2.1. Stomatal density and size measurements

To calculate the size and density of stomata across the leaf epidermis impressions were made. Dental resin (Coltene Whaledent, Switzerland) spread across the leaf was used to make a negative impression. This was done on both the abaxial and adaxial surface from which (or as close to as possible) gas exchange measurements were taken. Nail varnish was then applied to the dental resin impressions to provide a positive impression. The dried nail varnish was then mounted on microscope slides under a cover slip and imaged using a light microscopy (Brunel). From this stomatal complex width and length could be measured. Using these two values, complex aspect ratio (width / length) was also calculated.

To measure stomatal density, four fields of view were analysed per leaf impression per side. Stomatal complexes within the field of view were counted and then scaled up to an equivalent density in $1mm^2$. Stomatal size was also calculated from these images. Two stomata per field of view were measured. The width and length of stomatal complexes was measured using ImageJ. Averages were calculated from at least 3 biological reps per species (see table 2.1 for exact replication numbers) in Chapter 3 and 5-6 biological reps per species in Chapter 4.

2.2.1. SEM imaging

To demonstrate physiological differences in stomatal morphology, SEM images were taken using a Hitachi benchtop SEM (Hitachi, Tokyo, Japan). At least 3 biological repeats were used per species and representative images are shown. Samples were mounted on adhesive stubs and placed in the SEM until a vacuum was achieved. Samples were then images using the TM30303Plus application.

2.3. Stomatal dynamics measurements

Section 2.3 outlines the methods used throughout chapter 3 and chapter 4.2.4

2.3.1. Infrared Gas Analysis

Carbon assimilation and stomatal conductance were calculated using a LI-COR 6800 portable photosynthesis system (LI-COR Biosciences, Lincoln, NE, USA) with a multiphase flash fluorometer (6800-01A) as a light source. The IRGA chamber was clipped onto a mature leaf which remained attached to the plant inside of the controlled environment growth chamber. See table 2.1 for details of where measurements were taken. The leaf was acclimated at low light intensity until a steady state was reached. At low PPFD data was logged every minute for 5 minutes, then for 90 minutes at high PPFD and then 90 minutes again at low light. For most of the species low PPFD was kept at 100 µmol $m^{-2}s^{-1}$ and high PPFD 1000 µmol $m^{-2}s^{-1}$. However, for four shade adapted species (*S. plana*, *A. filix-femina, O. reglais* and *A. thaliana*; denoted by '*' on **Table 2.1**) low and high PPFD were decreased to 20 µmol $m^{-2}s^{-1}$ and 500 µmol $m^{-2}s^{-1}$ as it was found that stomata were already open at 100 µmol $m^{-2}s^{-1}$. Similarly for *Z. mays* (which was grown at considerably higher light intensity than the other species used in this study; 1000 µmol $m^{-2}s^{-1}$) additional measurements were taken in which low and high PPFD were 100 µmol $m^{-2}s^{-1}$ and 2000 µmol $m^{-2}s^{-1}$ respectively (denoted by '^'). *A* and g_s under high and low PPFD were measured as a mean over 5 minutes, after 85 minutes under the relevant PPFD. Intrinsic water use efficiency (iWUE) was calculated as A/g_s after 85 minutes at high PPFD. See table 2.1 for replication numbers.

2.3.2. Stomatal dynamics calculations

To describe the stomatal response to a step change in light intensity, an asymmetric sigmoid response model outlined by Vialet-Chabrand *et al.* (2013) was utilised using an Excel macro (Vialet-Chabrand *et al*., 2016) and following the method outlined by McAusland *et al*. (2016):

$$g_s = (g_{smax} - r_0)\, e^{-e^{\left(\frac{\lambda - t}{k} + 1\right)}} + r_0 \qquad \text{Eqn 1}$$

This model comprised of an initial g_s value and final g_s value (r_0 and g_{smax} respectively), a time constant (k) denoting the time taken to achieve 63% of the change in g_s (equivalent to 1-e^{-1}; see Vialet-Chabrand *et al*., 2017 for more details) and a time lag (λ) to describe the time before g_s started to increase. Together these parameters can be used to get a total time to reach ~63% of opening or closing, including both λ and k (T_{63}). Using these parameters, the maximum slope of the sigmoidal response (Sl_{max}) was calculated:

$$Sl_{max} = \frac{k\,.(g_{smax} - r_0)}{e} \qquad \text{Eqn 2}$$

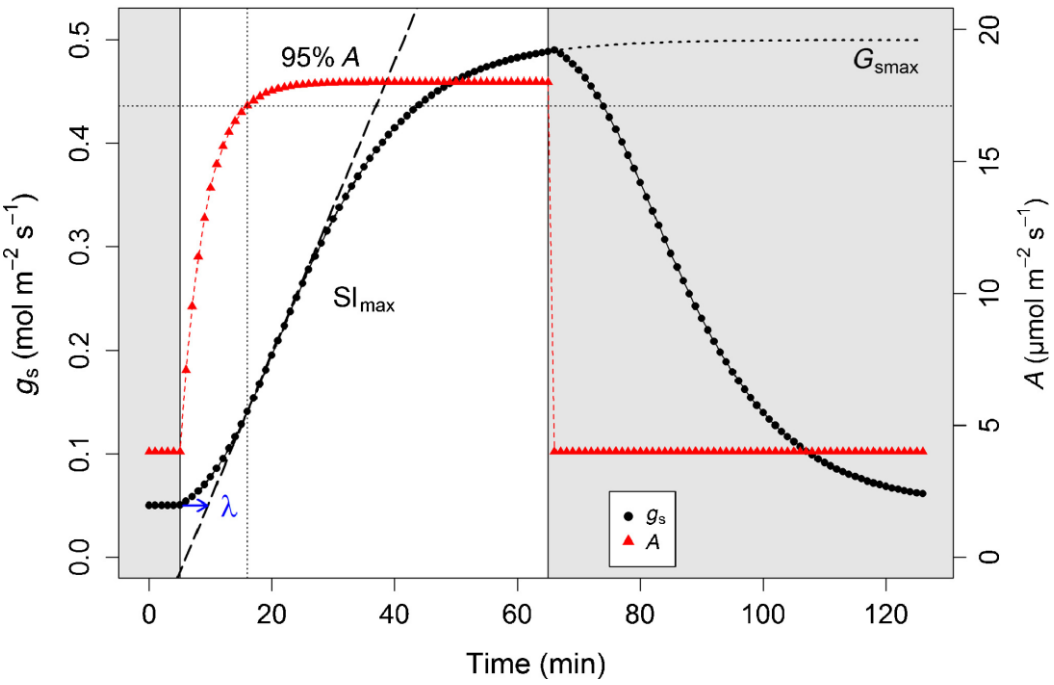

Figure 2.1. Sigmoidal modelling of a stomatal response.

Modelled response of g_s (black) and *A* (red) in response to a step change in PPFD. Grey shading represents low PPFD, white represents high PPFD. *Slmax* denotes the maximum rate of change of stomata during opening. λ denotes time lag. G_{smax} indicates steady state target of g_s during opening. McAusland *et al*. (2016).

Table 2.1: Plant growth conditions and gas exchange notes for chapters 3 and 5. * indicates species grown at low PPFD (shade adapted species). Brackets show biological replication per species for gas exchange measurements in Chapter 3. Where relative humidity (RH) was controlled, it is included below.

Species	Growth conditions	Growth Medium	IRGA notes
Selaginella plana (4)*	10h light/ 14h dark, 100 µmol $m^{-2}s^{-1}$ light intensity, 22°C temperature (constant).	Levongton F2S and sand compost	Measurements taken on the youngest growth.
Athyrium filix-femina (4)* *Osmunda regalis* (4)*	10h light/ 14h dark, 150 µmol $m^{-2}s^{-1}$ light intensity, 22°C temperature (constant).	Burncoose potting medium	Measurements taken on youngest fully expanded leaves of new growth after in stated conditions for at least 1 month.
Illicium floridanum (3)	10h light/ 14h dark, 200 µmol $m^{-2}s^{-1}$ light intensity, 22°C temperature (constant).	Burncoose potting medium	Measurements taken on youngest fully expanded leaves of new growth after in controlled conditions for at least 1 month.
Persea americana (6)	12h light/ 12h dark, 600 µmol $m^{-2}s^{-1}$ light intensity, 30°C/ 25°C temperature (day/night)	6:1 M3: perlite	Measurements taken on youngest fully expanded leaves.
Magnolia grandiflora (3) *Ginkgo biloba (3)*	14h light/ 10h dark, 600 µmol $m^{-2}s^{-1}$ light intensity, 22°C temperature (constant).	Burncoose potting medium	Measurements taken on youngest fully expanded leaves of new growth after in controlled conditions for at least 1 month.
Solanum tuberosum (5)	12h light/ 12h dark, 600 µmol $m^{-2}s^{-1}$ light intensity, 20°C/ 15°C temperature (day/night).	6:1 M3: perlite	Measurements were taken on the middle leaf of node 5 of 5 week old plants.
Solanum lycopersicum (7) *Glycine max*	16h light/ 8h dark, 600 µmol $m^{-2}s^{-1}$ light intensity, 25°C/ 21°C temperature (day/night).	6:1 M3: perlite	Measurements were taken on the middle leaf of node 5 of 5 week old plants.
Arabidopsis thaliana (7)*	12h light/ 12h dark, 125 µmol $m^{-2}s^{-1}$ light intensity, 22°C temperature (constant), 60% RH.	6:1 M3: perlite	Measurements taken on youngest fully expanded leaves.
Glycine soja (5)	16h light/ 8h dark, 400 µmol $m^{-2}s^{-1}$ light intensity, 21°C/ 16°C temperature (day/night), 60% RH.	6:1 M3: perlite	Measurements taken on youngest fully expanded leaves.
Tradescantia rubra (4)	16h light/ 8h dark, 150 µmol $m^{-2}s^{-1}$ light intensity, 22°C temperature (day/night), 60% RH.	6:1 M3: perlite	Measurements taken on youngest fully expanded leaves.
Zea mays ^ (4)	16h light/ 8h dark, 1000 µmol $m^{-2}s^{-1}$ light intensity, 28°C/ 20°C temperature (day/night), 70% RH.	5:1 John Innes No.3: Course horticultural sand	Measurements were taken on leaf 7, avoiding the midrib.
Brachypodium distachyon (6) *Brachypodium distachyon* (SID) (*5*) *Hordeum spontaneum (4)* *Hordeum vulgare (3)* *Triticum boeoticum (5), araraticum (4), durum (8) and aestivum (4)*	16h light/ 8h dark, 400 µmol $m^{-2}s^{-1}$ light intensity, 21°C/ 16°C temperature (day/night), 60% RH.	6:1 M3: perlite	Measurements were taken in the middle of leaf 5 of 4-5 week old plants.

2.4. Plant growth measurements under a fluctuating light environment

Section 2.4 outlines the methods used throughout chapter 4.

2.4.1. Plant material and growth conditions under fluctuating light intensity

Seeds of *Triticum aestivum, Tritucum durum, Triticum boeoticum, Triticum araraticum, Brachypodium distachyon, Glycine max, Solanum lycopersiucm* and *B. distachyon* (SID) were sown in module trays containing m3 compost (ICL, Suffolk, UK) and placed into a controlled environment growth chamber (Conviron PGR15; Conviron, Winnipeg, MB, Canada). These chambers were either set to constant PPFD (400 µmol $m^{-2}s^{-1}$) or fluctuating PPFD (daily light flux equal to a constant 400 µmol $m^{-2}s^{-1}$) replicating real world conditions taken from weather station data from the Arthur Willis controlled Environment Centre (AWEC, The University of Sheffield, S10 1AE, UK) in June 2020 (**Figure 4.1**). After approximately 10 days, seeds were transplanted into pots containing 6:1 M3 compost: perlite (Sinclair Pro, Cheshire, UK) each containing 5g Osmocote Exact 5-6 slow-release fertiliser (ICL, Suffolk, UK). For all measurements in 2.4, 5-6 biological replications were used.

2.4.2. Daily water loss, SPAD and dry mass measurements

In order to calculate the soil moisture capacity additional pots containing the same mass of soil mixture were prepared. These pots were either dried in an oven for 5 days or saturated with water for 24 hours. The masses of soil were calculated, and the soil moisture capacity was determined. 5-week-old plants were weighed and watered up to 70% (well-watered) or 30% (droughted) pot field capacity for 7 days to determine water loss. Every other day the plants and pots were weighed and the water mass lost was recorded before re-watering back to either 70% or 30%. Relative chlorophyll contents were calculated using a MultispecQ (PhotosynQ, Michigan, USA) on leaf 6 midway up the leaf. After 7 weeks of growth in either constant or fluctuating PPFD, above ground biomass was harvested and dried for 2 weeks at 60°C. The dry biomass was then weighed.

2.4.3. Carbon isotope discrimination

After 7 weeks of growth, leaves were harvested and dried for 2 weeks (leaf 7 for grasses; 5th node, middle leaf for *G. max* and *S. lycopersicum*). Samples were homogenised in a tissue lyser and between 1-2mg was sealed in a tin capsule and placed into an isotope ratio mass

spectrometer (IRMS, Sercon, UK) at the Sheffield Biomics Facility to determine the δ13C (carbon isotope composition) relative to the PeeDee belemnite carbonate standard (PDB) to correct for differences in the ambient air CO_2 environment between chambers. Equation 3.1 was used to calculate $\Delta^{13}C$. 5-6 plants were used per species.

$$\Delta^{13}C = \frac{\delta^{13}C_{air} - \delta^{13}C_{plant}}{1 + \delta^{13}C_{plant}} \qquad \text{Eqn 3}$$

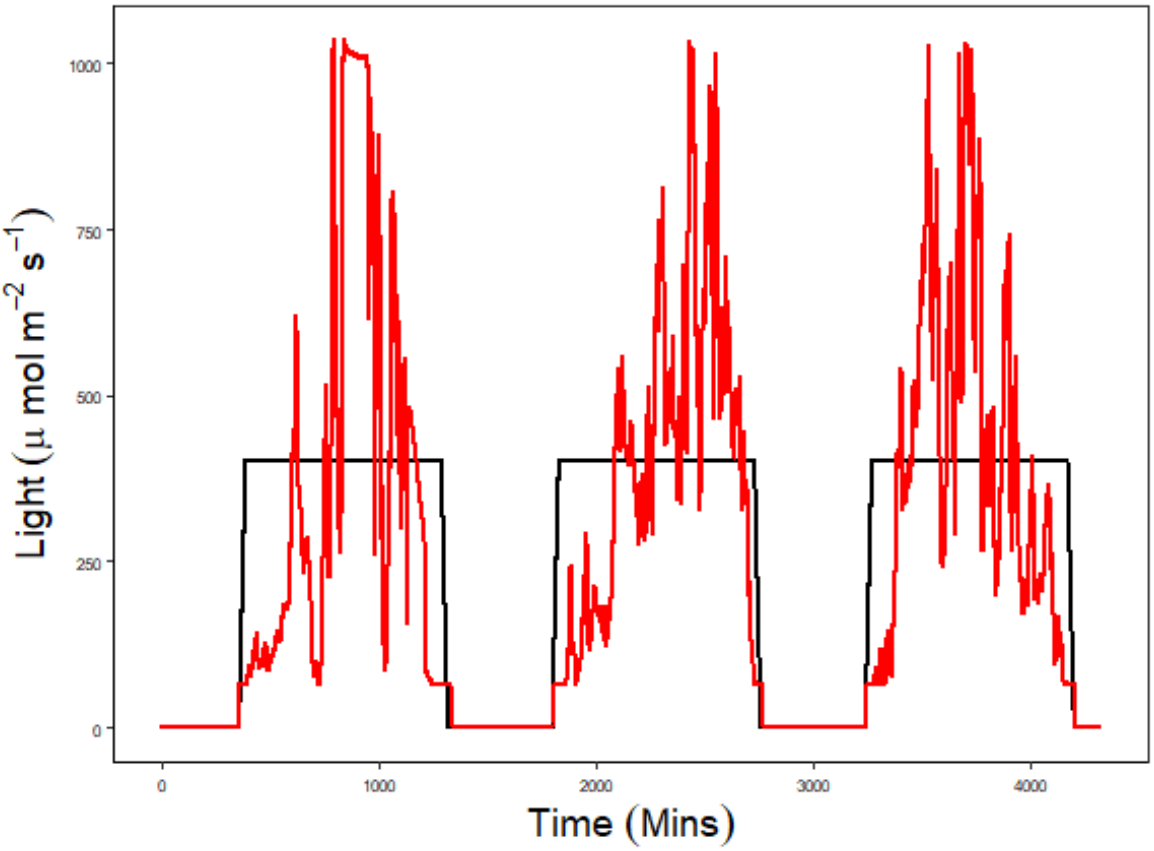

Figure 2.2. Chamber light regime
Chamber light regime showing a constant day chamber (black) and 3 days on repeat of fluctuating light (red) replicating field conditions taken from 3 days in July 2021 from the Arthur Willis Controlled Environment Centre, Sheffield, UK. Replicated field conditions were adjusted from the same net daily PPDF flux as the contant day chamber.

2.5. Immunolabelling

Section 2.5 outlines the methods used throughout chapter 5.

2.5.1. Tissue fixation

3mm by 3mm leaf strips were excised from the centre of the lamina and fixed in 4% (w/v) formaldehyde in PEM buffer (0.1 M PIPES, 10 mM EGTA, 1 mM $MgSO_4$, pH 7). Samples were vacuum infiltrated for 30 minutes and dehydrated in an ethanol dilution series (1 hour at 10%, 30%, 50%, 70%, 100% EtOH). Samples were infiltrated with LR white resin (London Resin Company) in EtOH (1 hour at 10%, 20%, 30%, 50%, 70% and 90%) followed by incubation at 100% LR White Resin for 3 x 8 hours. Samples were placed in gelatine capsules filled with resin and incubated at 37°C for 7 days until the resin had set. Leaf cross-sections were taken at 2 µm thickness using a Reichert-Jung Ultracut E microtome and a glass knife.

2.5.2. Immunolabelling

Sections were incubated with 3% (w/v) milk protein (Marvel, Premier Beverages, UK) in phosphate-buffered saline solution (PBS, pH 7.2) (referred to as MP). Sections were subsequently incubated with a ten-fold dilution of primary antibody for 1 hour at room temperature. Samples were then washed with PBS 3 times for 5 minutes and incubated with secondary antibody (anti-rat-IgG coupled to alexafluor 488) with a hundred-fold dilution for 1 hour. Samples were kept in the dark. Samples were counterstained with a ten-fold dilution of 0.25% (w/v) Calcofluor White for 5 minutes, before mounting on slides with Citifluor AF1 anti-fade solution (Agar Scientific, UK). Samples were visualised on an Olympus BX51 microscope with epifluorescence optics fitted and images were captured using a DP51 camera. Alexafluor 488 was visualised with a 460-490 nm excitation filter, a 510-550 nm emission filter and a 505 nm dichroic mirror. Calcofluor White was visualised using a 400-410 nm excitation filter, a 455 nm emission filter and a 455 nm dichroic mirror. Image processing was carried out in FIJI (ImageJ).

Table 2.2. Antibody specificities.

Antibody	Specificity	Reference
JIM7	Partially methyl-esterified HGA	Verhertbruggen *et al*., 2009
LM19	Partially methyl-esterified HGA/ un-esterified HGA	Verhertbruggen *et al*., 2009
LM20	Partially methyl-esterified HGA/ highly methyl-esterified HGA	Verhertbruggen *et al*., 2009
LM6M	(1-5)-L-arabinan	Cornuault *et al*., 2017
LM13	Linearised (1-5)-L-arabinan	Moller *et al*., 2008
LM5	Non-reducing end of (1-4)-β-D-galactan	Jones *et al*., 1997
LM26	Branched (1-4)-β-D-galactan	Torode *et al*., 2018
LM10	Non-reducing end of (1-4)-β-D-xylan	McCartney *et al*., 2005
LM11	Non-reducing end of (1-4)-β-D-xylan/arabinoxylan	McCartney *et al*., 2005
LM25	XXXG/galactosylated xylan	Pedersen *et al*., 2012
LM15	XXXG xylan	Pedersen *et al*., 2012
LM24	Galactosylated xylan	Pedersen *et al*., 2012
LM21	Heteromannan	Marcus *et al*., 2010

2.6. Stomatal function bioassays

2.6.1. Arabinase stomatal bioassay

Whole leaf sections approximately 3 mm by 3 mm were excised from 5 week old plants and floated into a resting buffer (10mM MES, 10mM KCl , 0.1mM $CaCl_2$, pH 6.2) containing either 10 units/mL arabinase (Arabinase from *Cellvibrio japonicus*, Megazyme) or no enzyme for 1 hour. Samples were then floated onto an opening buffer (50 mM KCl, 10 mM MES, pH 6.2) abaxial side down supplemented with either ABA to a final concentration of 10 µM, 2 µM or a control solvent solution, and ambient air was bubbled through. Samples were mounted on slides and imaged after 2 hours at room temperature with exposure to 150 µmol m^{-2} s^{-1} PPFD. Sections from 6 plants per species were imaged under a light microscope and pore dimensions of 14 stomata per leaf section were measured using ImageJ. Pore area was assumed to be elliptical and calculated using the following equation:

$$Pore\ area\ =\ \pi\ *\ (\frac{Pore\ width}{2})\ *\ (\frac{Pore\ length}{2}) \qquad \text{Eqn 3}$$

2.7. Data analysis

Statistical analysis was carried out using R software (www.r-project.org; version 3.5.3). Datasets were assessed for normality. One-way analysis of variance (ANOVA) was used to identify significant differences in stomatal responses between species. Statistical significance was determined if $P < 0.05$. When significance was detected, Tukey's HSD test was used as a multiple comparison test to determine differences between species. While ANOVAs are robust to modest differences in sample size, it is worth noting that the different replication number for each species measured throughout chapter 3 may reduce that statistical power of such a test.

Covariance between gas exchange and stomatal morphological traits was analysed using general linear regression. The significance value was determined by a Bonferroni correction for these regressions (with a corresponding value of significance of $P < 0.00625$). Due to the

large number of variables, principal component analysis combining stomatal morphological and speed traits was performed.

Significant differences between plants grown under constant or fluctuating PPFD were identified using an unpaired, two-tailed t test ($P = <0.05$). Covariance between plant growth metrics and stomatal speed was analysed using general linear regression.

Chapter 3. Stomatal response speed and implications for carbon capture and WUE across evolution.

3.1.1. Introduction

As sessile organisms, plants have evolved mechanisms to detect and respond to fluctuations in the external environment. Not only must plants be able to take up carbon dioxide for photosynthesis, but also limit excessive water loss. The establishment of an impermeable cuticle and stomata has enabled plants to tightly regulate the exchange of gases between the leaf interior and the environment (Raven, 2002; Hetherington and Woodward, 2003). Through changes in intracellular turgor, stomata are able to open and close to tightly control gaseous exchange to the needs of the plant. As a driver of photosynthetic output, light is one of the most dynamic signals that governs stomatal responses (Woods and Turner, 1971). The speed at which stomata respond to changes in light intensity has implications for both carbon acquisition and water loss. These traits determine the water use efficiency (WUE) of plants. Given the importance of carbon capture for global crop yields and the current reliance of agriculture on a diminishing water supply, stomatal kinetics and their impact on WUE are of great importance to global food production and primary productivity.

Conditions in the field are rarely static and so plants must be able to actively sense and respond to a variety of signals that drive stomatal pore changes. In particular, changing light environments are particularly important for driving changes in stomatal pore apertures, with stomatal responses often an order or magnitude slower than changes in photosynthetic induction (Lawson and Blatt, 2014; McAusland *et al*., 2016; Vialet-Chabrand *et al*., 2017; Lawson and Vialet-Chabrand, 2019). This disconnect between A and g_s has been modelled to limit photosynthesis by up to 10-15% in C_3 and C_4 crops (McAusland *et al*., 2016). Across species there has shown to be large variation in stomatal response speeds however, the determinants that dictate stomata response speed remain a matter of some debate (Vico *et al*., 2011; Drake *et al*., 2013; Lawson and Blatt, 2014; McAusland *et al*., 2016; Elliot-Kingston *et al*., 2016; Haworth *et al*., 2018; Deans *et al*., 2019; Cai *et al*., 2021; Harris *et al*., 2022; Zhang *et al*., 2022).

In particular, morphological traits, such as size and geometry, have been implicated as determinants of stomatal speed. The increased surface area to volume ratio of smaller

stomata has been hypothesised to aid in more rapid stomatal responses, although this assumes uniform distribution of ion transporters across stomata of different sizes (Hetherington and Woodward, 2003; Franks and Beerling, 2009; Lawsona and Blatt, 2014). While smaller stomata have been observed to respond faster in closely related species and species that share an ecological niche this observation is far from ubiquitous when considering the breadth of land plants (Drake *et al*., 2013, McAusland *et al*., 2016, Kardiman and Ræbild, 2017; Zhang *et al*., 2019; Ozeki *et al*., 2022). Other studies looking across clades and more distantly related species suggest that size is less important (Elliot-Kingston *et al*., 2016; Deans *et al*., 2019). The innovation of the dumbbell guard cells does seem key to enhanced stomata response speed, potentially superseding any size-speed relationship. These dumbbell guard cells are typically coupled with a pair of subsidiary cells that act as a pool of ions and a source of reducing mechanical advantage that aids in the stomatal response, with their removal hampering opening and closure (Raissig *et al*., 2016; Durney *et al*., 2023).

Few studies have attempted to quantify the stomatal opening and closing response speeds across species spanning the major clades of land plants, including representatives from a broad range of ecological niches. Where this has been attempted, key innovations such as the dumbbell shaped stomata have been often excluded or under-represented.

3.1.2. Aims

The experiments described in this chapter aimed to quantify the speed of stomatal responses to a step change in PPFD across a diverse panel of species. A wide range of species with a variety of stomatal sizes, densities and morphologies were sampled to investigate the relative importance of these physiological parameters in an efficient stomatal response. Further, by studying species from multiple evolutionary clades and growth habits the stomatal speeds of distinct groups were compared.

3.2. Results

3.2.2. Species relatedness and stomatal morphology

Species were sampled from across a broad range of clades to provide representatives from the breadth of land plants that produce stomata on their leaves (**Figure 3.1**). Bryophytes, an early diverging clade of land plants, were not included in this study as extant species produce stomata only on their sporangia and these are believed to function primarily in sporangium drying, and the release of spores. In particular, commelinid monocots were heavily sampled. These included several cereal grass species of the grasses due to their specialised dumbbell shaped guard cell and subsidiary cell geometry and importance as global food crop staples, and also one species of the Commelinales order with subsidiary cells and kidney shaped guard cells. SEM images of the species used in this study were taken, demonstrating the diversity in stomatal morphologies (**Figure 3.2**). As expected, the earlier diverging lineages of lycophytes, ferns, gymnosperms, ANA grade and magnoliids, and the asterids and rosids all had stomata formed from pairs of kidney shaped guard cells. One of the later diverging monocot species (Commelinales species *T. rubra*) also had kidney shaped guard cells, and all of the cereal grass species of grasses had dumbbell shaped guard cells. All of the monocot species, with either kidney or dumbbell shaped guard cells, had well-defined subsidiary cells.

To aid in the visualisation of associations between stomatal parameters and evolutionary clade, the results figures in this chapter have, where possible, been arranged by phylogeny, from early to later diverging lineages, left to right. To allow comparisons between stomatal morphologies, species with kidney shaped guard cells are represented by red symbols, and those with dumbbell shaped guard cells by blue symbols. The role of subsidiary cells was investigated using a *B. distachyon* subsidiary cell deficient mutant, SID, and this is represented by violet coloured symbols on all figures. Additionally, preliminary experiments (not shown) demonstrated that plants grown at low PPFD (100-150 µmol $m^{-2}s^{-1}$; *Selaginella plana*, *Athyrium filix-femina*, *Osmunda regalis* and *Arabidopsis thaliana*) already had open stomata when analysed under the lower PPFD level of 100 µmol $m^{-2}s^{-1}$. Therefore, the PPFD levels were shifted down to 20 and 500 µmol $m^{-2}s^{-1}$ for low and high PPFD respectively. These four species will henceforth be referred to as shade-adapted species and indicated with an *.

3.2.3. There is significant variation in stomatal size and density across species

Stomatal size and density were measured across all of the 21 species shown in **Table 2.1**, plus the *B. distachyon* (SID) mutant. The mean densities and sizes (where possible) of stomata were calculated from both abaxial and adaxial sides of mature leaves (Materials and methods 2.2). The combined stomatal density from both sides of the leaf varied significantly across these species (ANOVA, $F_{(21,228)} = 8.81$, $P < 0.0001$; **Figure 3.3A**). There was a nearly 24-fold difference between the species, with the highest and lowest stomatal density coming from the kidney shaped magnoliid species *P. americana* (141 mm^{-2}) and the kidney shaped monocot species *T. rubra* (6.19 m^{-2}) respectively. Species also showed significant variance in stomatal complex area (ANOVA, $F_{(21,190)} = 296.5$, $P < 0.0001$; **Figure 3.3B**). Similar to stomatal density, there was a 25-fold difference in stomatal complex area between the largest and smallest complex areas, *T. rubra* (2522 μm^2) and the dumbbell shaped grass species *B. distachyon* (101.3 μm^2). There was no obvious correlation between stomatal morphology (i.e., kidney or dumbbell shaped guard cells) and either stomatal density or size, although kidney shaped species exhibited a larger range of both sizes and densities than dumbbell shaped species. Across this range of species, the data collected here, support the hypothesis that stomatal size and density are inversely correlated. As shown in **Figure 3.3C** a general trend of decreasing stomatal density with increasing stomatal size was observed across phylogenies and stomatal morphologies, in line with previous studies (Franks & Beerling, 2009).

To investigate whether there were differences in the pattern of stomatal distribution across the two surfaces of the leaf, the ratios of stomata on the adaxial to abaxial surfaces were calculated (**Figure 3.3D**). Species from the earlier diverging lineages of lycophytes, ferns, gymnosperms, ANA grade and magnoliids were all hypostomatous with stomata only on the abaxial side. All of the asterids, rosids, the monocot with kidney shaped guard cells (*T. rubra*) and the monocot grass species with dumbbell shaped guard cells were all amphistomatous. Thus, it appears that the earliest diverging clades were hypostomatous with only abaxial stomata, and across evolutionary time amphistomatous species arose and there was a gradual increase in the proportion of adaxially localised stomata. Interestingly, this did not lead to an increase in the total stomatal density on the leaves of later diverging lineages.

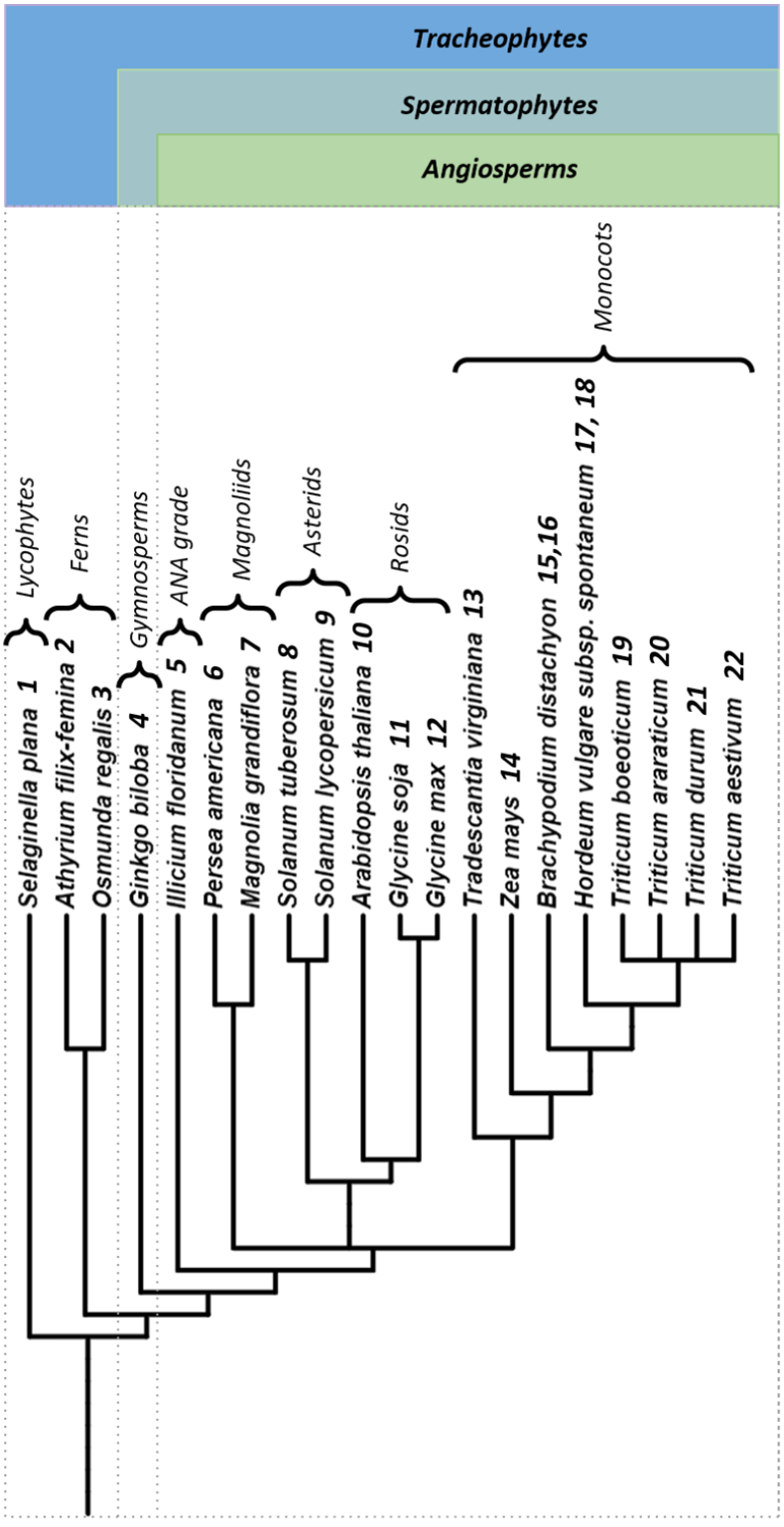

Figure 3.1. Phylogenetic tree of species.

Phylogenetic tree of species used in this study (Generated using phyloT). Numbers are used for reference to later figures *Tradescantia virginiana* is used instead of *rubra* as it is one of the *Tradescantia* species crossed to make this variety. Brackets indicate clade. Species 14-22 are grasses with dumbbell shaped guard cells.

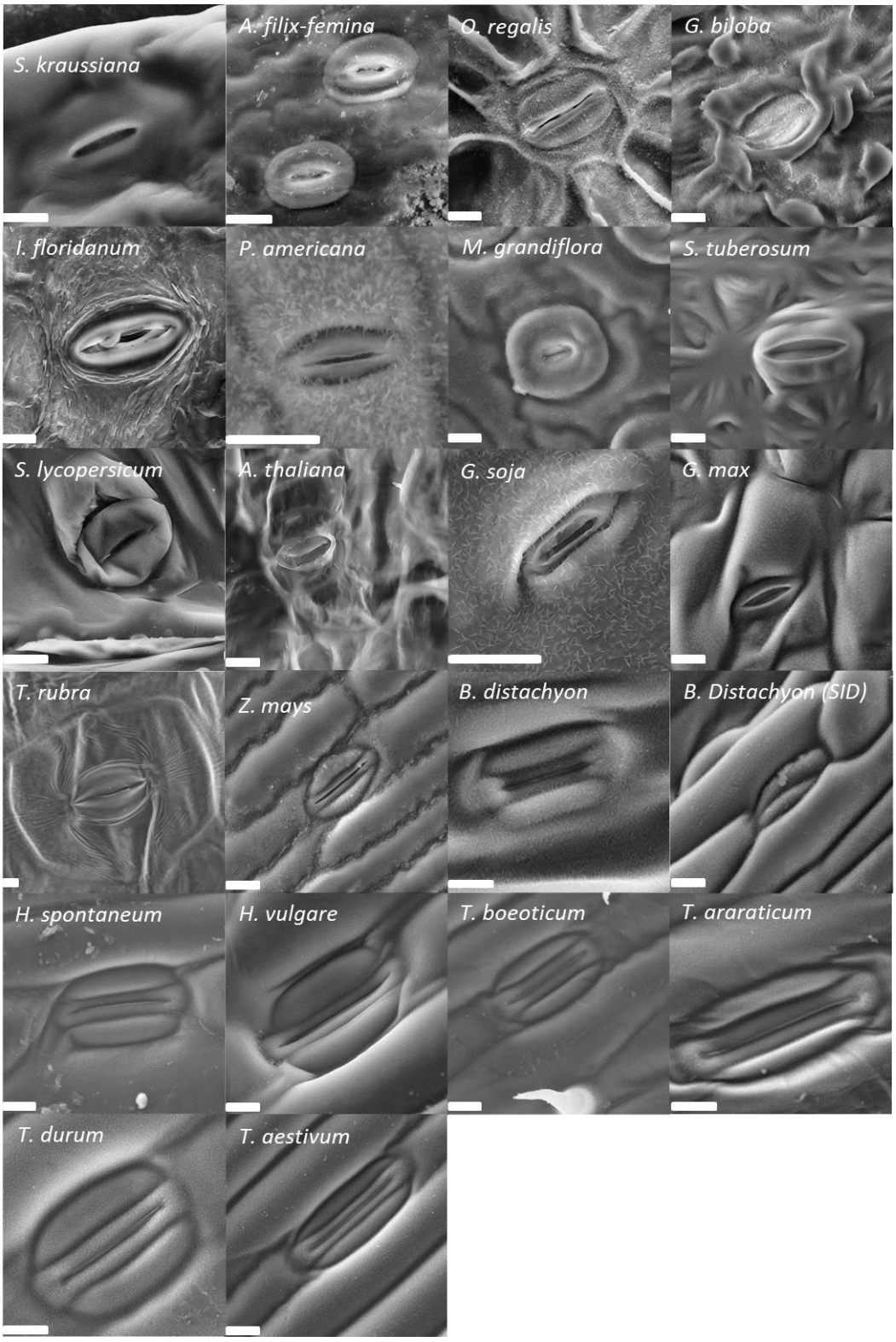

Figure 3.2. Variation in stomatal morphology

Representative SEM images of stomata for species used. *Selaginella krausianna* is presented in place of *Selaginella plana*. Scale bar = 10 µm.

A

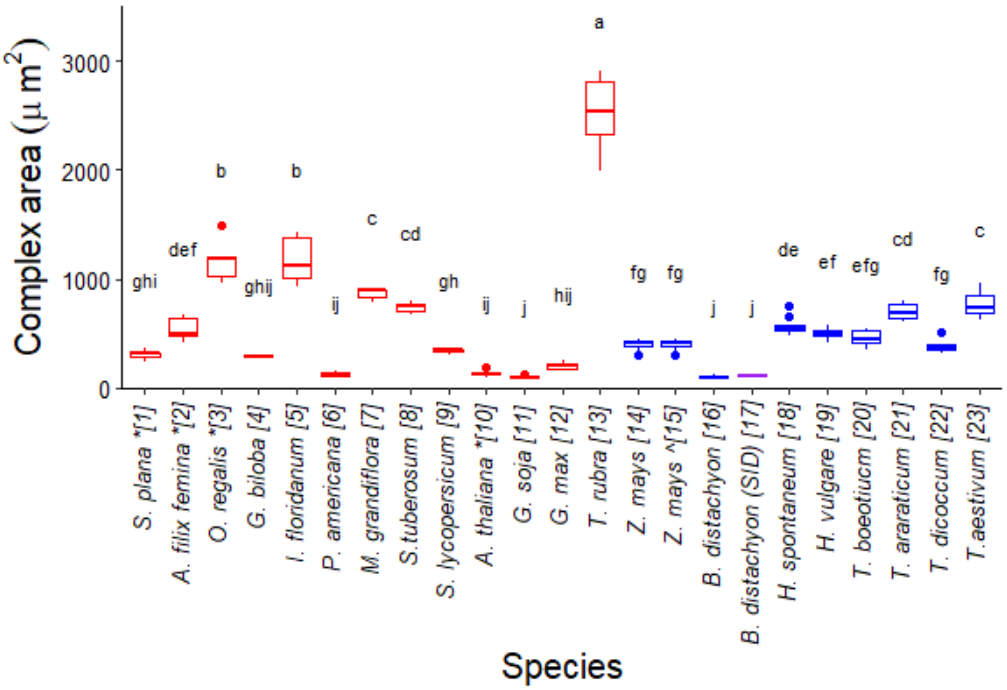
Complex area (μ m²)
3000
2000
1000
0
ghi
def
b
ghij
b
iii
c
cd
gh
iii
j
hij
a
fg
fg
j
j
de
ef
efg
cd
fg
c
S. plana *[1]
A. filix femina *[2]
O. regalis *[3]
G. biloba [4]
I. floridanum [5]
P. americana [6]
M. grandiflora [7]
S.tuberosum [8]
S. lycopersicum [9]
A. thaliana *[10]
G. soja [11]
G. max [12]
T. rubra [13]
Z. mays [14]
Z. mays ^[15]
B. distachyon [16]
B. distachyon (SID) [17]
H. spontaneum [18]
H. vulgare [19]
T. boeotiucm [20]
T. araraticum [21]
T. dicoccum [22]
T.aestivum [23]
Species

B

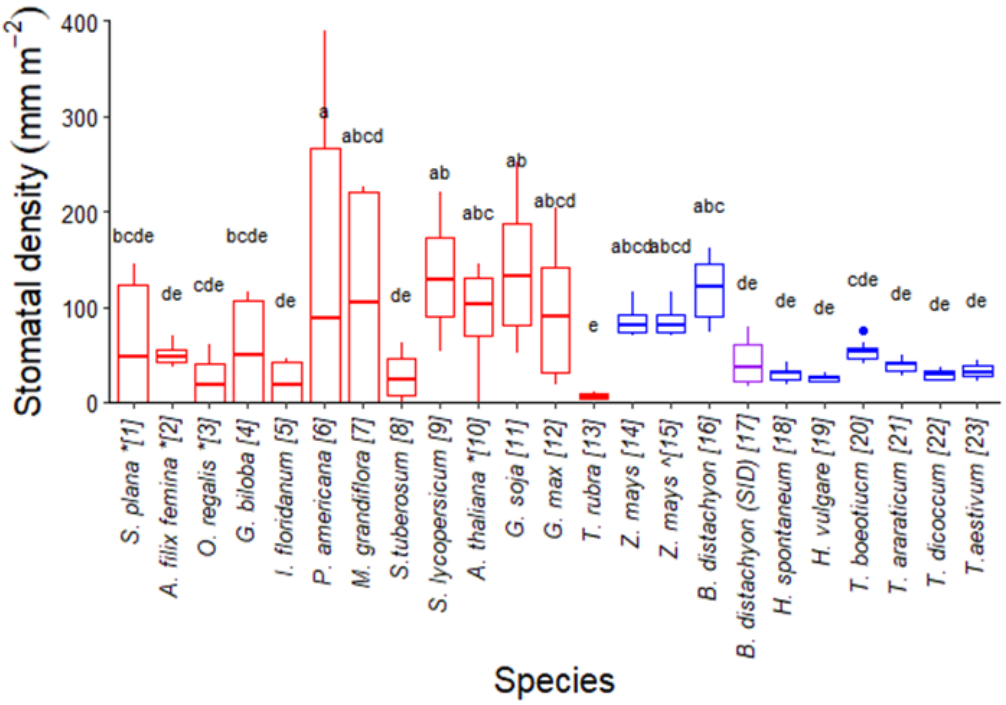
Stomatal density (mm m⁻²)
400
300
200
100
0
bcde
de
cde
bcde
de
a
abcd
de
ab
abc
ab
abcd
e
abcdabcd
abc
de
de
de
cde
de
de
de
S. plana *[1]
A. filix femina *[2]
O. regalis *[3]
G. biloba [4]
I. floridanum [5]
P. americana [6]
M. grandiflora [7]
S.tuberosum [8]
S. lycopersicum [9]
A. thaliana *[10]
G. soja [11]
G. max [12]
T. rubra [13]
Z. mays [14]
Z. mays ^[15]
B. distachyon [16]
B. distachyon (SID) [17]
H. spontaneum [18]
H. vulgare [19]
T. boeotiucm [20]
T. araraticum [21]
T. dicoccum [22]
T.aestivum [23]
Species

C

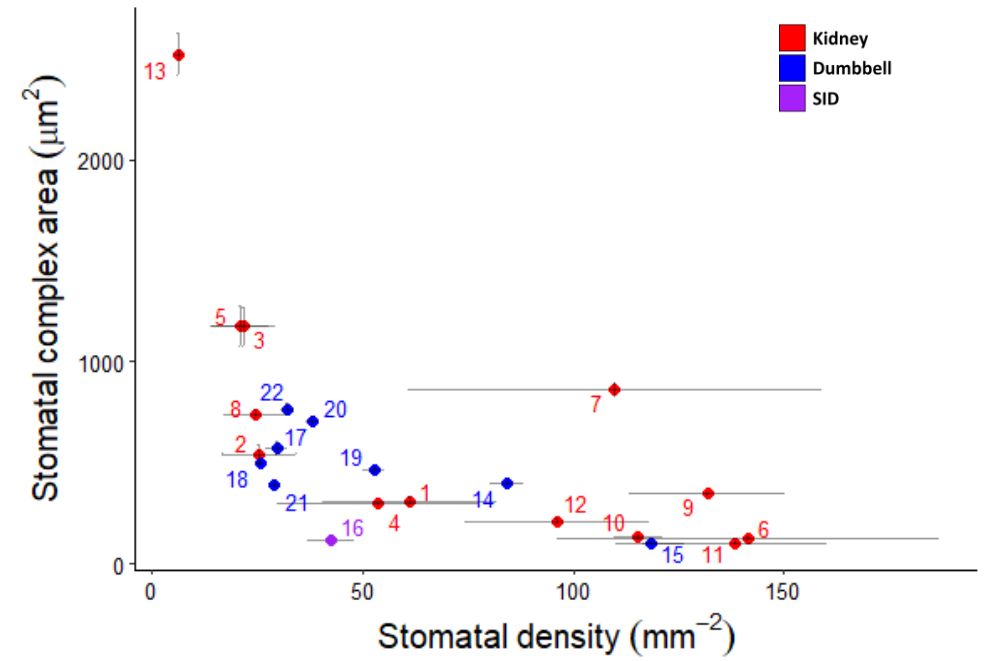

D

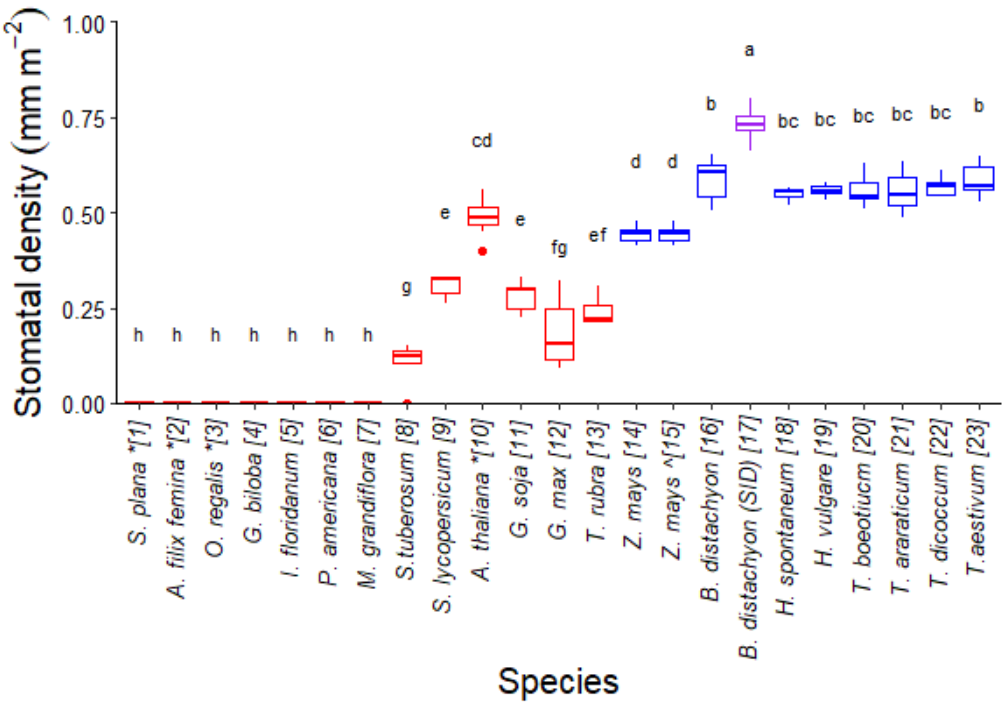

Figure 3.3. There is variation in stomatal patterning between species.

A) Mean stomatal complex area and **B), C)** density across species. Mean density is shown across abaxial and adaxial surfaces. Mean size is calculated from both abaxial and adaxial surfaces where possible. Numbers correspond to phylogeny. **D)** Stomatal ratio (adaxial/abaxial number) between species aligned by phylogeny. Symbols: kidney = red; dumbbell = blue; SID = purple. Species that cannot be distinguished from each other at 0.05 confidence limit are indicated by different letters as determined by ANOVA with a Tukey HSD. Data shown are the mean ± SE. n = minimum of 3 per species.

3.2.4. Species respond to a step change in light intensity through altering gas exchange

In order to measure and compare the speed of stomatal responses, the same set of plants were subjected to step changes in light intensity inside of an IRGA leaf chamber, from low to high to low PPFD (see methods section 2.3) whilst gas exchange rates were measured. All species studied responded to the step increase and decrease in light intensity by increasing and decreasing g_s and A, respectively (**Figure 3.4A**). However, while all species responded to altered light intensity, not all species were able to adjust A and g_s to the same extent, with the magnitude of changes in A and g_s differing greatly between species. To better compare the response rates of species to light, traces were normalised to values between 0 and 1 (**Figure 3.4B**). The shapes of the resulting curves differed between species. In the following section these differences in the magnitude and speed of stomatal responses are discussed.

3.2.5. There is significant variation in gas exchange in high and low PPFD

In order to understand the variation in gas exchange potential across species, steady state gas exchange measurements were made and levels of A, g_s and iWUE were calculated. 'Steady state' values of A, g_s and iWUE were taken for 5 minutes after 85 minutes at either low or high PPFD. Preliminary experiments indicated that 85 minutes was sufficient time for plants to acclimate to a constant or near constant rate of gaseous exchange.

The diverse species analysed in this study come from a broad range of ecological niches and therefore their requirements from photosynthetic output and gas exchange differed, meaning that some species had to be analysed under different light environments. However, in general the results indicated that there has been an increase in gas exchange capacity (gs and A) across plant evolution with the early diverging lycophyte and fern species having the lowest rates of photosynthesis and the later diverging grasses having the highest rates.

Across species there was a significant variance in steady state assimilation at low PPFD (A_{low}; ANOVA, $F_{(20,85)} = 9.648$, $P < 0.0001$; **Figure 3.5A**). The highest A_{low} recorded was from grass species *T. aestivum* (7.40 µmol m^{-2} s^{-1}). The lowest A_{low} recorded was from the fern *O. regalis* a shade adapted species (0.48 µmol m^{-2} s^{-1} measured at 20 µmol $m^{-2}s^{-1}$ PPFD) and the early angiosperm *I. floridanum* (3.28 µmol m^{-2} s^{-1}) for those measured at PPFD of 100 µmol m^{-2} s^{-1} . When removing the four shade adapted species and *Z. mays* measured at higher PPFD (*Z.*

mays ^), across the 18 species studied at the same light intensity, the species with dumbbell shaped guard cells displayed a higher mean A_{low} than kidney-shaped species (6.02 and 4.42 µmol m^{-2} s^{-1} respectively; ANOVA, $F_{(1,15)} = 10.24$, $P < 0.01$). When gas exchange measurements were taken at high PPFD (A_{high}) there was a significant variance across species in A_{high} (ANOVA, $F_{(20,88)} = 47.71$, $P < 0.0001$; **Figure 3.5B**). The species with the highest A_{high} was the only C4 species tested, *Z. mays* ^ (49.6 µmol m^{-2} s^{-1}). However, this measurement was taken at a higher PPFD. When only considering measurements taken at 1000 µmol m^{-2} s^{-1}, *Z. mays* still achieved the highest A_{high} (39.8 µmol m^{-2} s^{-1}). The shade adapted species that displayed the lowest A_{high} was the lycophyte *S. plana* (1.72 µmol m^{-2} s^{-1}), and *I. floridanum* (5.76 µmol m^{-2} s^{-1}) was the lowest of those measured at 1000 µmol m^{-2} s^{-1} of PPFD. When removing shade adapted species and *Z. mays* measured at higher PPFD, dumbbell shaped species achieved greater A_{high} than kidney species (28.8 and 11.7 µmol m^{-2} s^{-1} respectively; ANOVA, $F_{(1,15)} = 41.13$, $P < 0.001$). Thus, grass species with dumbbell shaped guard cells appeared better able to maximise photosynthesis at both low and high PPFD.

As with *A*, there was significant variation in steady state g_s at low PPFD ($g_{s\,low}$) between species (ANOVA, $F_{(20,88)} = 14.94$, $P < 0.0001$; **Figure 3.6A**). Interestingly, the species with the highest $g_{s\,low}$ (*T. boeoticum*; 0.286 µmol m^{-2} s^{-1}) was not the same as the species with the highest A_{low}. When removing shade adapted species and *Z. mays* measured at higher PPFD, there was no significant difference in $g_{s\,low}$ between dumbbell and kidney species (ANOVA, $F_{(1,15)} = 2.562$, $P > 0.05$). There was significant variation in steady state $g_{s\,high}$ between species (ANOVA, $F_{(20,88)} = 22.69.$, $P < 0.0001$; 3.6B), again the species with the highest $g_{s\,high}$ (*T. boeoticum;* 0.55µmol m^{-2} s^{-1}) was the same as the species with the highest A_{high}, when *Z. mays* ^ was excluded due to the higher PPFD used. When removing shade adapted species and *Z. mays* ^ measured at higher PPFD, there was a significant difference in $g_{s\,high}$ between dumbbell and kidney species (ANOVA, $F_{(1,15)} = 20.77$, $P < 0.001$). All dumbbell shaped guard cell species supported higher rates of stomatal gas exchange than kidney shaped species, with the exception of *S. tuberosum* and *G. max,* both domesticated crop species.

These parameters (*A* and g_s) were used to calculate iWUE (with the assumption that stomatal opening was no longer limiting A_{high} after 85 minutes at high PPFD). It was found that there was a significant variation in iWUE across species (ANOVA, $F_{(22,85)} = 4.078$, $P < 0.001$; **Figure 3.7**). However, when removing the four shade adapted species which were measured at lower

PPFD, and *Z. mays* measured at higher PPFD, there was no significant difference in $iWUE_{high}$ between dumbbell and kidney shaped species (ANOVA, $F_{(1,15)} = 0.021$, $P > 0.05$). Thus, despite a trend towards increasing levels of stomatal gas exchange and photosynthesis across evolutionary timescales, this has not resulted in generally higher water use efficiencies.

A

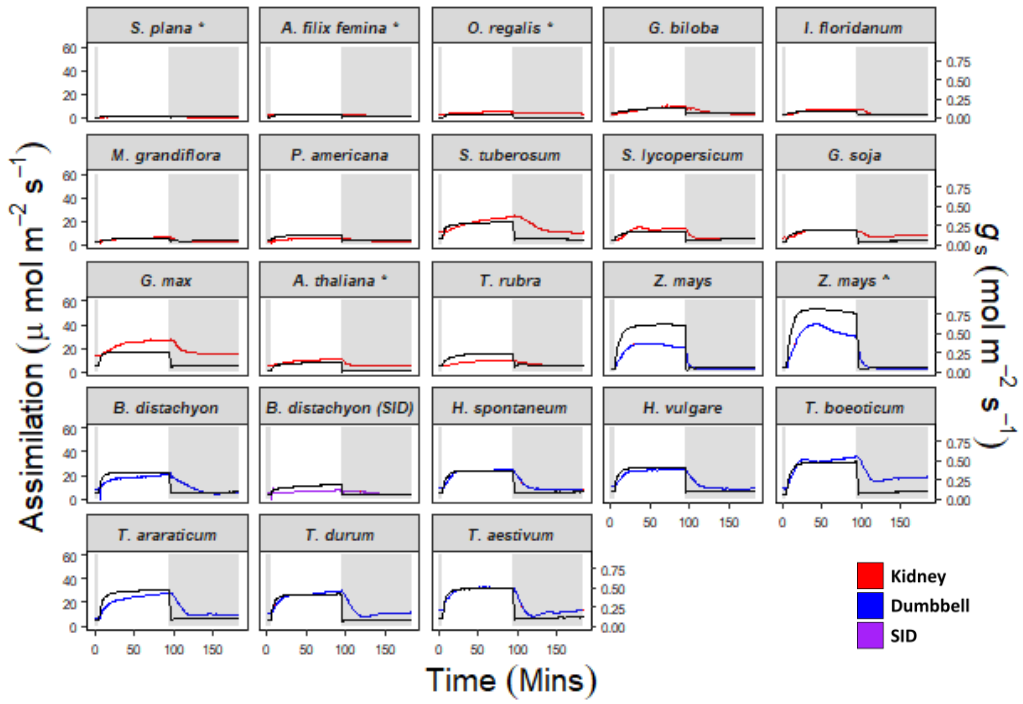

B

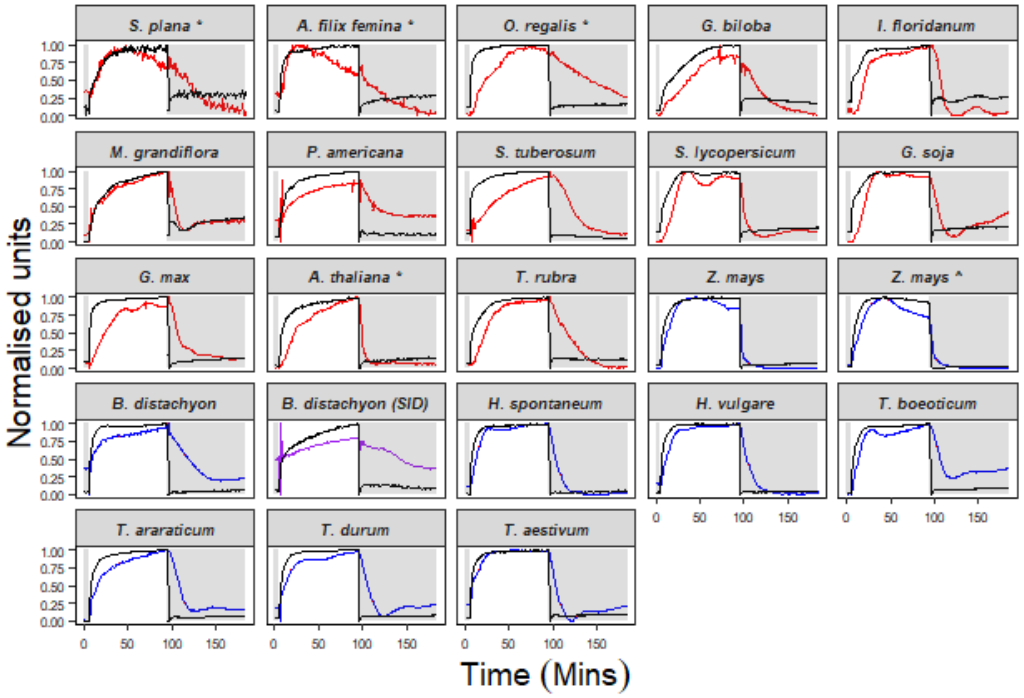

Figure 3.4. All species show a response of g_s and *A* in response to a step change in PPFD.
A) Response of stomatal conductance (gs) and assimilation (A; grey) in species with kidney shaped (red) and dumbbell shaped (blue) stomata to a change in PPFD at 5 minutes from 100 µmol $m^{-2}s^{-1}$ (shaded area) to 1000 µmol m^{-2} s^{-1} for 90 minutes, followed by a decrease to 100 µmol $m^{-2}s^{-1}$ for 90 minutes (20 µmol $m^{-2}s^{-1}$ to 500 µmol $m^{-2}s^{-1}$ to 20 µmol $m^{-2}s^{-1}$ for shade adapted species '*') Violet indicates the *B. distachyon* SID mutant **B)** The same data with values normalised between 0 and 1. Data shown are the mean ± SE (n = 3).

A

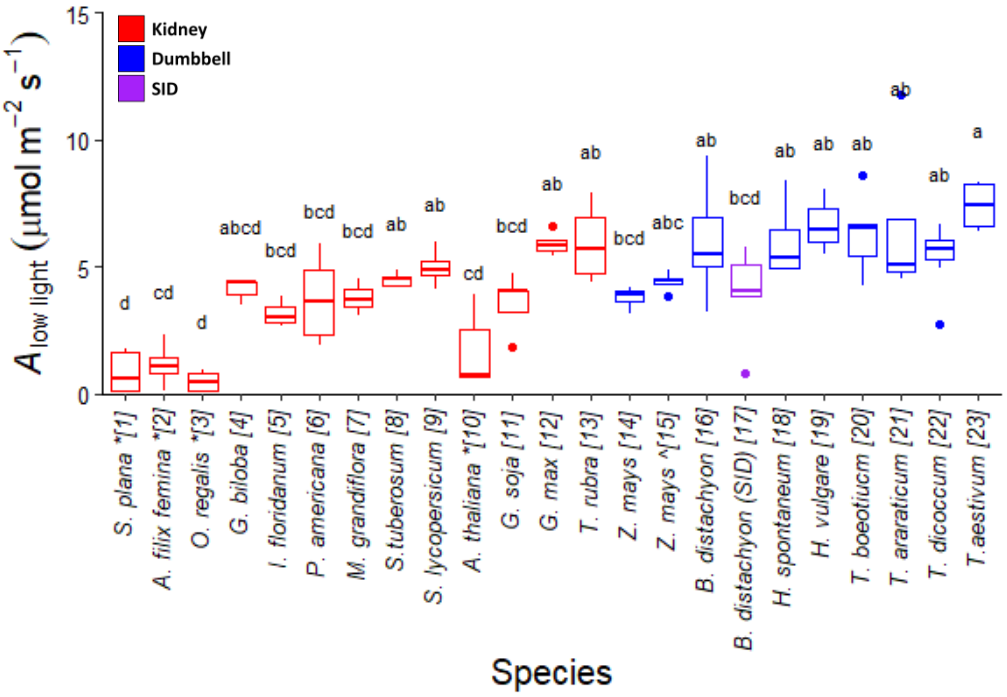

B

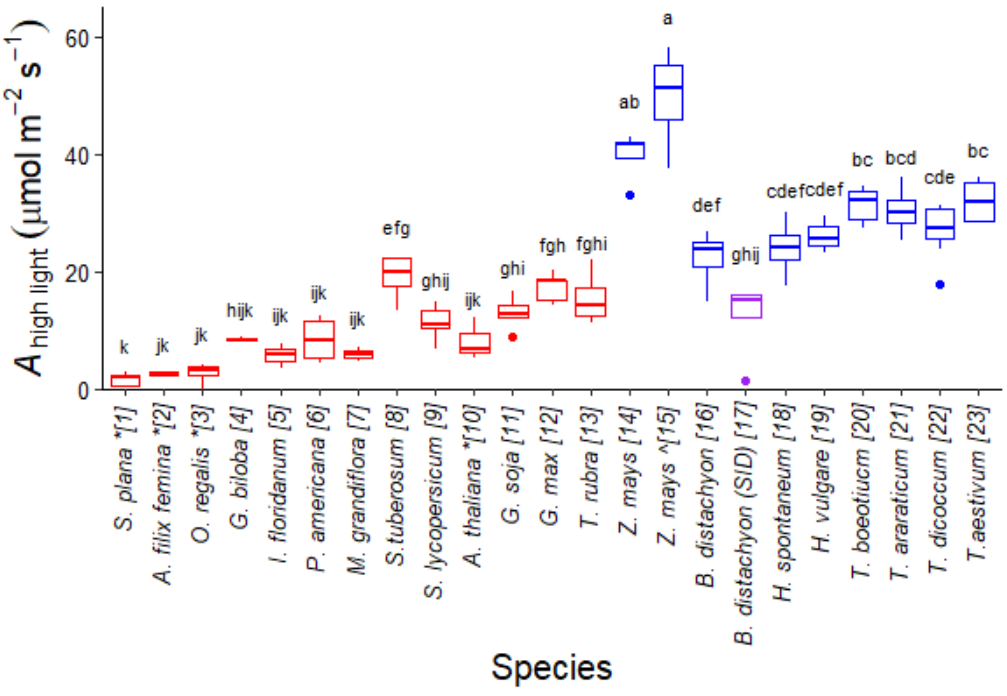

Figure 3.5. Carbon assimilation in the low and high PPFD varies by species.

A) Mean *A* under low PPFD conditions (100 µmol m^{-2} s^{-1}, 20 µmol m^{-2} s^{-1} for species indicated by *). **B)** Mean *A* under high PPFD conditions (1000 µmol m^{-2} s^{-1}, 500 µmol m^{-2} s^{-1} for species indicated by *, 2000 µmol m^{-2} s^{-1} for species indicated by ^. Symbols: kidney = red; dumbbell = blue; SID = purple. Species that cannot be distinguished from each other at 0.05 confidence limit are indicated by different letters as determined by ANOVA with a Tukey HSD. Data shown are the mean ± SE (n = 3-7).

A

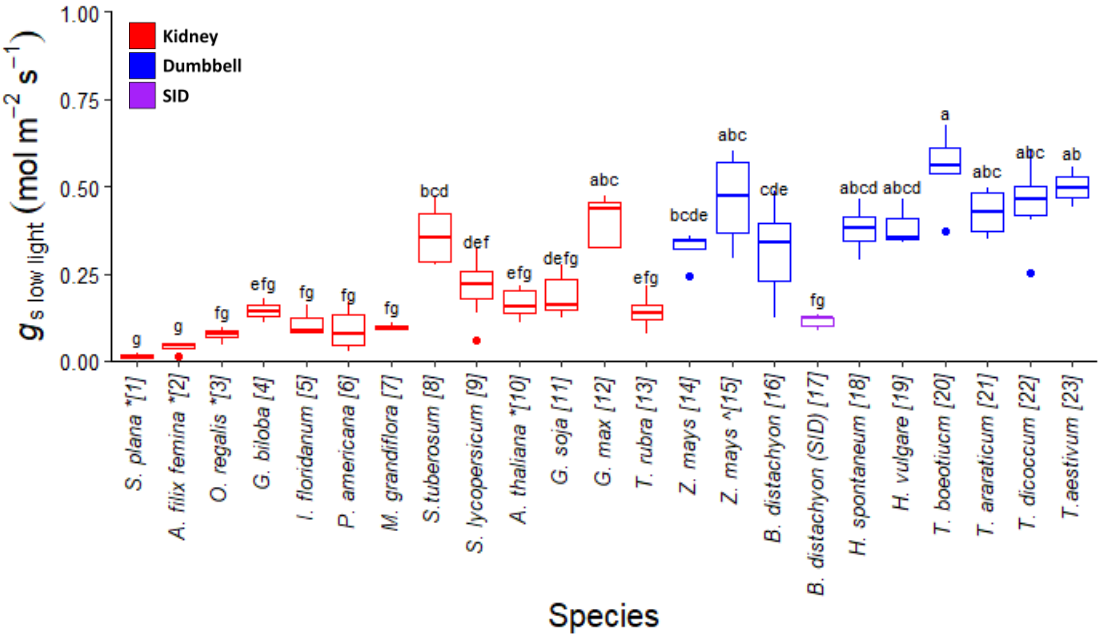

B

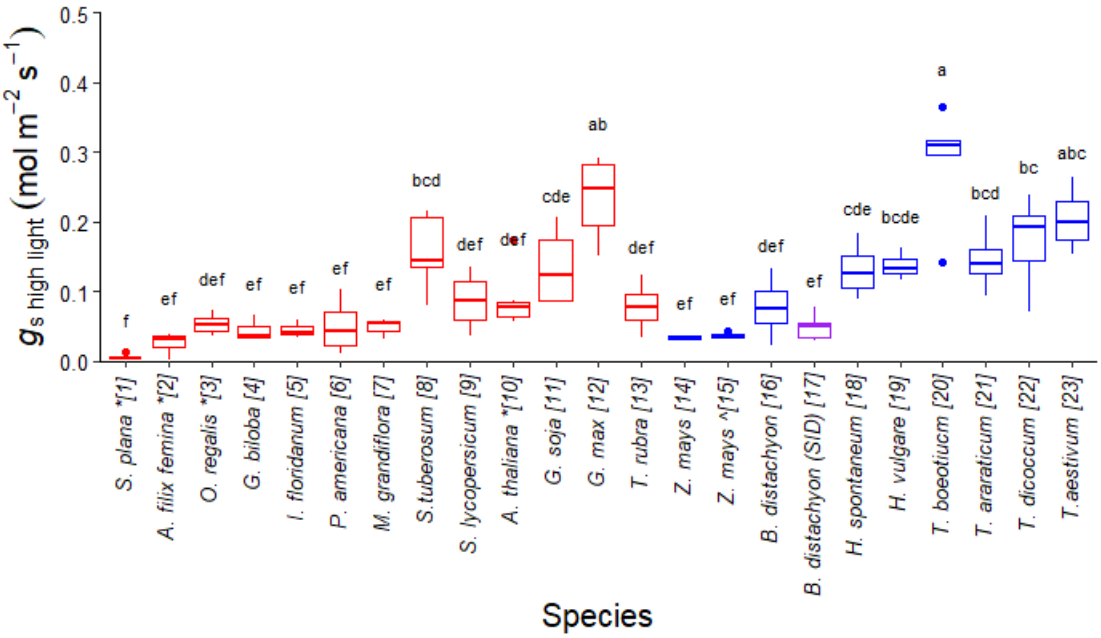

Figure 3.6. Stomatal conductance at low and high PPFD varies by species.

A) Mean *A* under low PPFD conditions (100 µmol m^{-2} s^{-1}, 20 µmol m^{-2} s^{-1} for species indicated by *). **B)** Mean *A* under high PPFD conditions (1000 µmol m^{-2} s^{-1}, 500 µmol m^{-2} s^{-1} for species indicated by *, 2000 µmol m^{-2} s^{-1} for species indicated by ^. Symbols: kidney = red; dumbbell = blue; SID = purple. Species that cannot be distinguished from each other at 0.05 confidence limit are indicated by different letters as determined by ANOVA with a Tukey HSD. Data shown are the mean ± SE (n = 3-7).

A

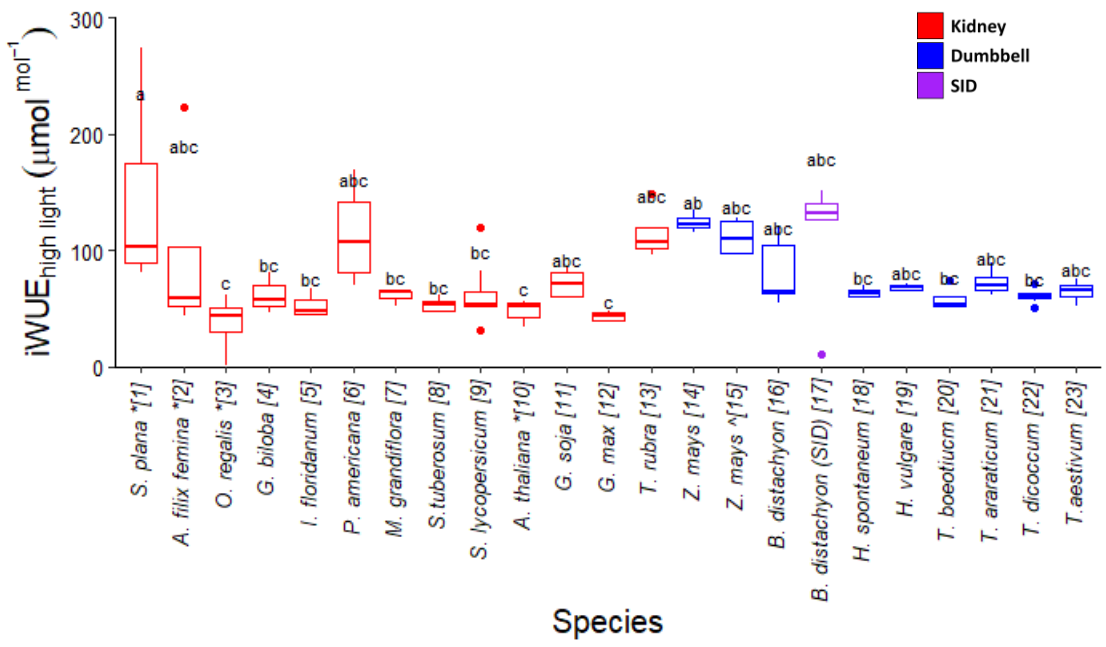

Figure 3.7. Intrinsic WUE varies by species.

Mean iWUE under high PPFD conditions (1000 µmol m^{-2} s^{-1}, 500 µmol m^{-2} s^{-1} for species indicated by *, 2000 µmol m^{-2} s^{-1} for species indicated by ^). Symbols: kidney = red; dumbbell = blue; SID = purple. Species that cannot be distinguished from each other at 0.05 confidence limit are indicated by different letters as determined by ANOVA with a Tukey HSD. Data shown are the mean ± SE (n = 3-7).

3.2.6. There is a significant positive correlation between *A* and g_s

As g_s represents the rate of gas exchange in plants the relationship between g_s and *A* was examined between species. A co-variance analysis was performed for steady state values of species at low and high PPFD (**Figure 3.8A-B**). It was found that A_{low} and $g_{s\ low}$ were significantly positively correlated (Pearson correlation, $r^2 = 0.41$, $P < 0.001$). When considering high PPFD, A_{high} and $g_{s\ high}$ were also positively correlated (Pearson correlation, $r^2 = 0.73$, $P < 0.0001$). The relationship between *A* and g_s was stronger at high PPFD than low PPFD.

3.2.7. Stomatal geometry dictates stomatal opening and closing metrics

Three metrics were used to quantify and compare the speed of stomatal opening and closing from IRGA measurements (Materials and methods 2.3). After a step change in PPFD the stomatal response was characterised by the lag (λ), if any, before g_s changed. The subsequent stomatal response was characterised by the time taken to achieve 63% of the total variation in g_s (k) and the maximum slope was fitted to the response (Sl_{max}; McAusland *et al*., 2016). There was significant variance across species in time lag during opening (λ_{op}; **Figure 3.9A**; ANOVA, $F_{(22,86)} = 8.72$, $P < 0.0001$). Half of the dumbbell shaped grass species had no measurable λ_{op}, while the rest were characterised by short lag times. The early angiosperm *I. floridanum* had the highest λ_{op} taking almost 9 minutes to respond. When grouped by geometry, the kidney shaped species showed a significantly longer λ_{op} and a larger degree of variation than the dumbbell shaped species (ANOVA, $F_{(1,19)} = 7.75$, $P < 0.05$, **Figure 3.12A**). There was also a significant variance across species in time lag during closing (λ_{cls}; **Figure 3.10A**; ANOVA, $F_{(22,83)} = 4.67$, $P < 0.0001$). However, there was no significant variance in λ_{cls} when species were grouped by guard cell morphology (ANOVA, $F_{(1,19)} = 0.353$, $P > 0.05$; **Figure 3.12B**). The angiosperm *S. tuberosum* with kidney shaped guard cells, took about 13 minutes to respond to a reduction in PPFD whereas the shade adapted lycophyte and ferns and some dumbbell shaped grass species, had no discernable lag period. Most species showed differences between their λ_{op} and their λ_{cls}. When comparing the means of opening and closing lag times by morphology, the dumbbell shaped grasses tended towards shorter lag times during opening compared to closing. Kidney species showed no such bias however, most species displayed a bias towards either shorter λ_{op} or λ_{cls} (**Figure 3.11A**).

The maximum rate of opening ($SI_{max\ op}$) varied significantly across species (ANOVA, $F_{(22,86)}$ = 22.5, P < 0.0001) with a clear trend for the dumbbell shaped grass species to operate with a higher $SI_{max\ op}$ (ANOVA, $F_{(1,19)}$ = 50.7, P < 0.0001; **Figure 3.9C**; **Figure 3.12E**). When grouped by guard cell morphology, dumbbell shaped species had a mean $SI_{max\ op}$ of 0.327 mmol m^{-2} s^{-2} whereas kidney species had a much lower mean $SI_{max\ op}$ of 0.0588 mmol m^{-2} s^{-2} (**Figure 3.12E**). Despite this clear divide based on morphology, there still was a large degree of variation within these groups. The species with the highest $SI_{max\ op}$ was the grass *T. boeoticum* (0.565 mmol m^{-2} s^{-2}), which was also the species with the highest steady state values for g_s. The kidney species with the fastest $SI_{max\ op}$ was *S. lycopersicum* (0.156 mmol m^{-2} s^{-2}). There was significant variation in the maximum rate of closing ($SI_{max\ cl}$) across species (ANOVA, $F_{(22,86)}$ = 13.88, P < 0.0001; **Figure 3.10C**). The C_4 grass *Z. mays* displayed the highest $SI_{max\ cl}$ (1.12 mmol m^{-2} s^{-2}), more than a 2-fold higher than the comparative $SI_{max\ op}$ (**Figure 3.11C**). Mean $SI_{max\ cl}$ was higher than $SI_{max\ op}$ when species were grouped by morphology (dumbbell and kidney achieving mean $SI_{max\ cl}$ rates of 0.463 and 0.106 mmol m^{-2} s^{-2} respectively; **Figure 3.12E-F**). Notably, the shade adapted species displayed the opposite response exhibiting faster opening than closing (**Figure 3.11C**).

While SI_{max} is useful for quantifying the maximum rate of change of response, this metric can be further broken down into components that define the stomatal response. The time constant k can be used to define a stomatal response in terms of time alone. Interestingly, while k during opening (k_{op}) showed significant variance across species (ANOVA, $F_{(22,86)}$ = 6.85, P < 0.0001) there was no significant difference between dumbbell and kidney species (means of 5.92 and 10.7 minutes respectively; ANOVA, $F_{(1,19)}$ = 3.2, P > 0.05; **Figure 3.9B**; **3.12C**). This indicates that some of the difference in $SI_{max\ op}$ between dumbbell and kidney species can be attributed to magnitude of opening and closing, rather than the time taken for the response alone. The range of k_{op} for dumbbell shaped species remained small with only 4.96 minutes separating the fastest and slowest species, whereas for kidney species the fastest and slowest were separated by 24.5 minutes. There was a significant variance in k during closing (k_{cls}) between species (ANOVA, $F_{(21,83)}$ = 15.1, P < 0.0001). As with opening, during closure there was no significant difference in k_{cls} when species were grouped by morphology (mean k_{cls} of 4.67 and 9.63 minutes for dumbbell and kidney species respectively; ANOVA, $F_{(1,19)}$ = 2.36, P > 0.05 ; **Figure 3.12C-D**).

3.2.7. Stomatal patterning plays a limited role in governing dynamic responses to light

Stomatal size is proposed to be an important factor in stomatal response speeds. Smaller stomata (often occurring at high stomatal density) are hypothesised to have faster rates of opening and closing due to their greater relative surface area to volume ratio and the implications this has for effecting a change in internal turgor. To test this hypothesis a co-variance analysis between stomatal patterning characteristics and speed metrics was conducted. For this analysis the mutant *B. distachyon* (SID) was excluded and data was separated by guard cell morphology. It was found that there was no significant correlation between stomatal response speeds (either k or SI_{max}) and either stomatal size or density during opening or closing, except in dumbbell shaped species which showed a negative correlation (Pearson correlation, $r^2 = 0.66$, $P < 0.01$) between stomatal density and k_{cls}. Thus, the analysis reported here does not support the hypothesis that smaller stomata can adjust their apertures faster.

Measures of stomatal traits including size, density, length and aspect ratio (width/length) along with measures of stomatal response speed were included in a PCA to further understand how multiple stomatal traits together impact opening and closure speeds (**Figure 3.14**). During opening, the fist axis accounted for 38.1% of the variation and the second axis accounted for 29.4% of the variation. During closure, the fist axis accounted for 35.2% of the variation and the second axis accounted for 33.5% of the variation. When considering stomatal opening, stomatal size and density separated along the second principle axis and SI_{max} and k separated along the first principle axis, as might be expected from the relationship between these parameters. Interestingly, leaf aspect ratio was positively associated with k and negatively associated with SI_{max} during both opening and closure, suggesting that more round stomata were slower to respond. This could be due to some of the notably faster species with kidney-shaped guard cells possessing long and thin stomata (such as soybean). However, the tendency for species with dumbbell-shaped guard cells to have long and thin stomata, and respond rapidly, has likely driven this separation. For both opening and closure, maximum slope and complex area separated from each other however, this was only in the second principle axis for each response.

3.2.8. Subsidiary cells support stomatal responses

To understand the importance of subsidiary cells in facilitating a stomatal response, the mutant line *B. distachyon* (lacking subsidiary cells) was used and compared to the wild type *B. distachyon*. In each of the three stomatal response parameters across both opening and closing, *B. distachyon* (SID) had a substantially different response than *B. distachyon* (**Figure 3.9-3.10 A-C**). Across both opening a closure, λ and k was longer, and SI_{max} was smaller. In general, the mutant line *B. distachyon* (SID) had speed values more similar to kidney species than *B. distachyon* or other dumbbell shaped species. In particular, *B. distachyon* (SID) was more similar to the slower species with kidney shaped-guard cells, than those species that responded more quickly. This suggests that the innovation of dumbbell guard cells relies heavily on the surrounding subsidiary cells and that it is the complementary nature of this 4-celled system that is key to the success of the grass stomata.

Interestingly, *B. distachyon* (SID) achieved a higher WUE than the wild type. This agrees with carbon isotope discrimination data that suggests that *B. distachyon* (SID) has reduced g_s compared to the wild type (Raissig *et al*., 2017).

A

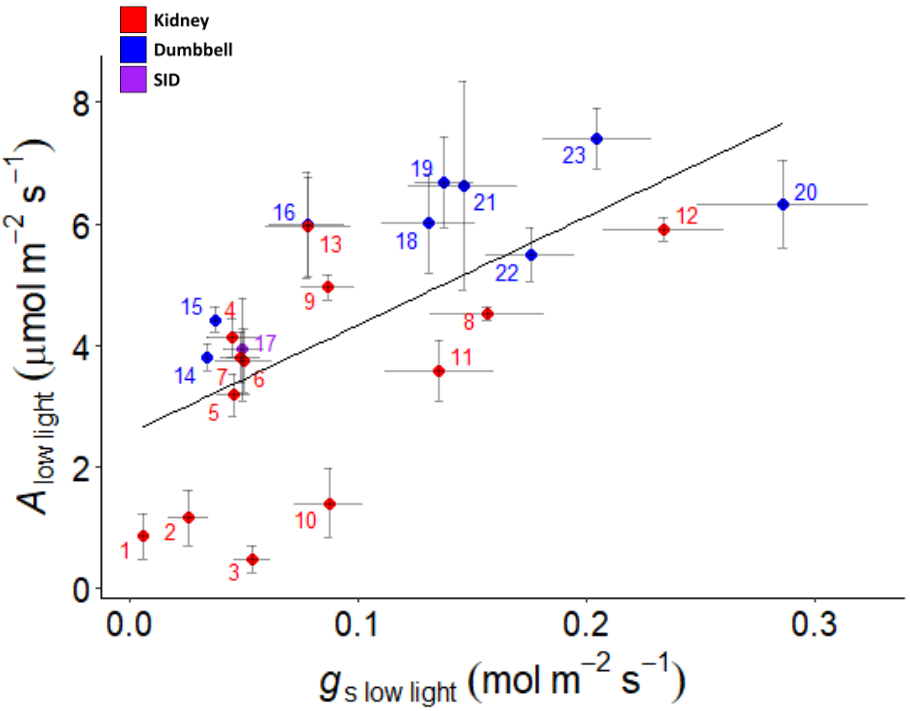

B

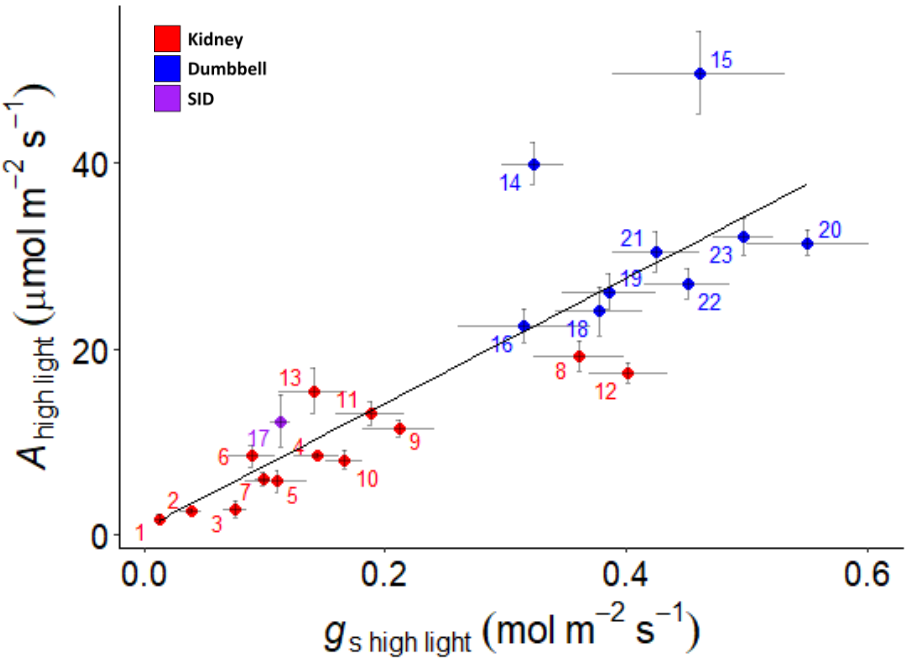

Figure 3.8. *A* and g_s are positively correlated.

Mean g_s against *A* at low **A)** and high **B)** PPFD. Symbols: kidney = red; dumbbell = blue; SID = purple. Data shown are the mean ± SE. n = minimum of 3 per species.

A

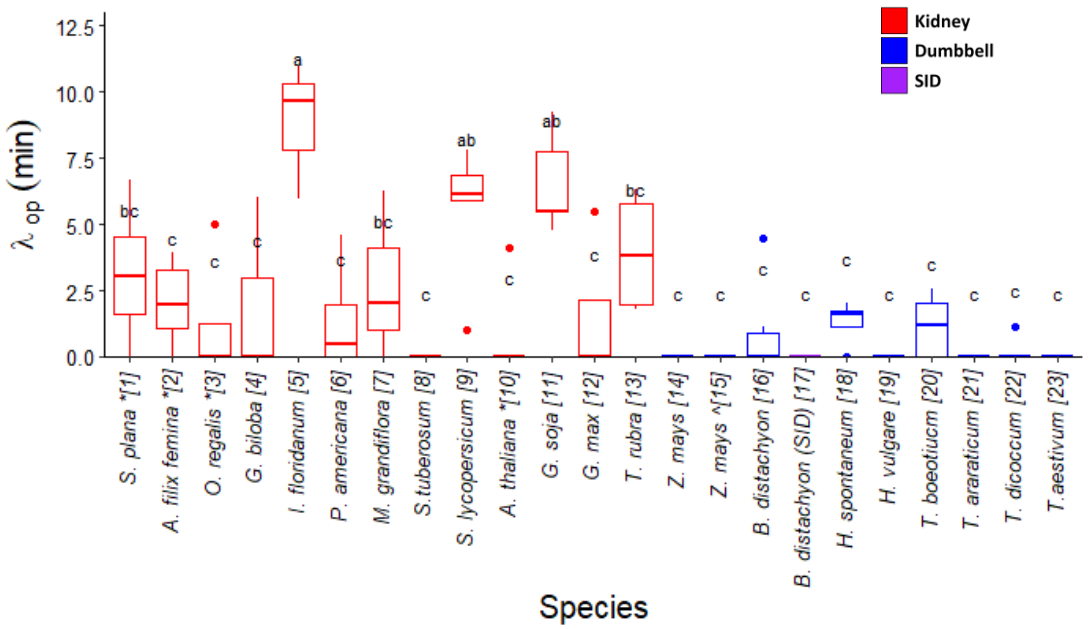
Kidney
Dumbbell
SID
λ op (min)
12.5
10.0
7.5
5.0
2.5
0.0
S. plana *[1]
A. filix femina *[2]
O. regalis *[3]
G. biloba [4]
I. floridanum [5]
P. americana [6]
M. grandiflora [7]
S.tuberosum [8]
S. lycopersicum [9]
A. thaliana *[10]
G. soja [11]
G. max [12]
T. rubra [13]
Z. mays [14]
Z. mays ^[15]
B. distachyon [16]
B. distachyon (SID) [17]
H. spontaneum [18]
H. vulgare [19]
T. boeotiucm [20]
T. araraticum [21]
T. dicoccum [22]
T.aestivum [23]
Species

B

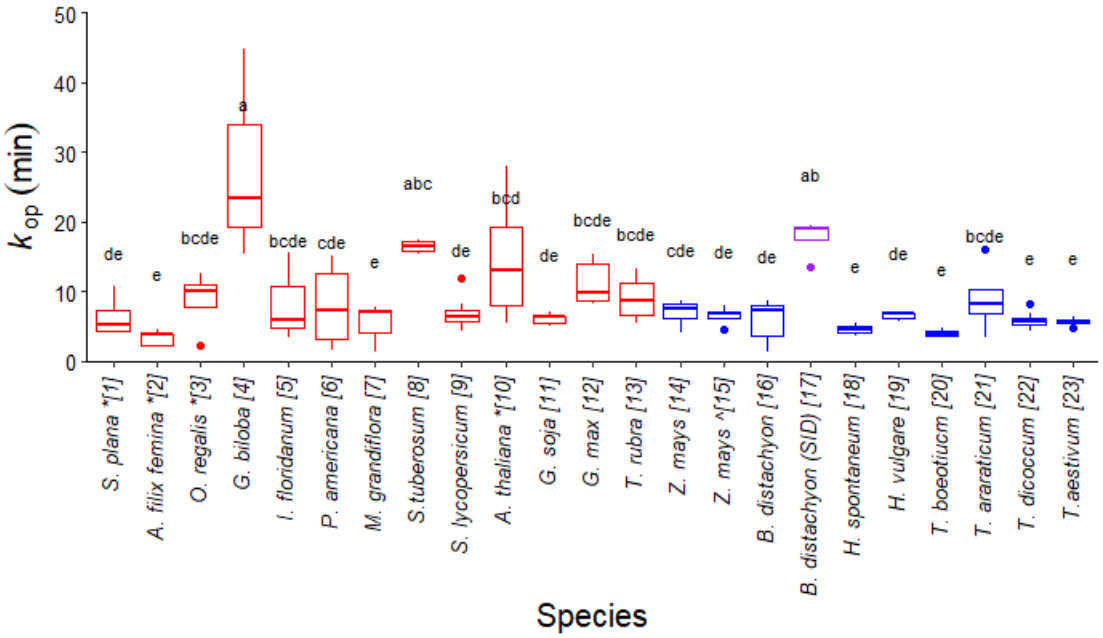
kop (min)
50
40
30
20
10
0
S. plana *[1]
A. filix femina *[2]
O. regalis *[3]
G. biloba [4]
I. floridanum [5]
P. americana [6]
M. grandiflora [7]
S.tuberosum [8]
S. lycopersicum [9]
A. thaliana *[10]
G. soja [11]
G. max [12]
T. rubra [13]
Z. mays [14]
Z. mays ^[15]
B. distachyon [16]
B. distachyon (SID) [17]
H. spontaneum [18]
H. vulgare [19]
T. boeotiucm [20]
T. araraticum [21]
T. dicoccum [22]
T.aestivum [23]
Species

C

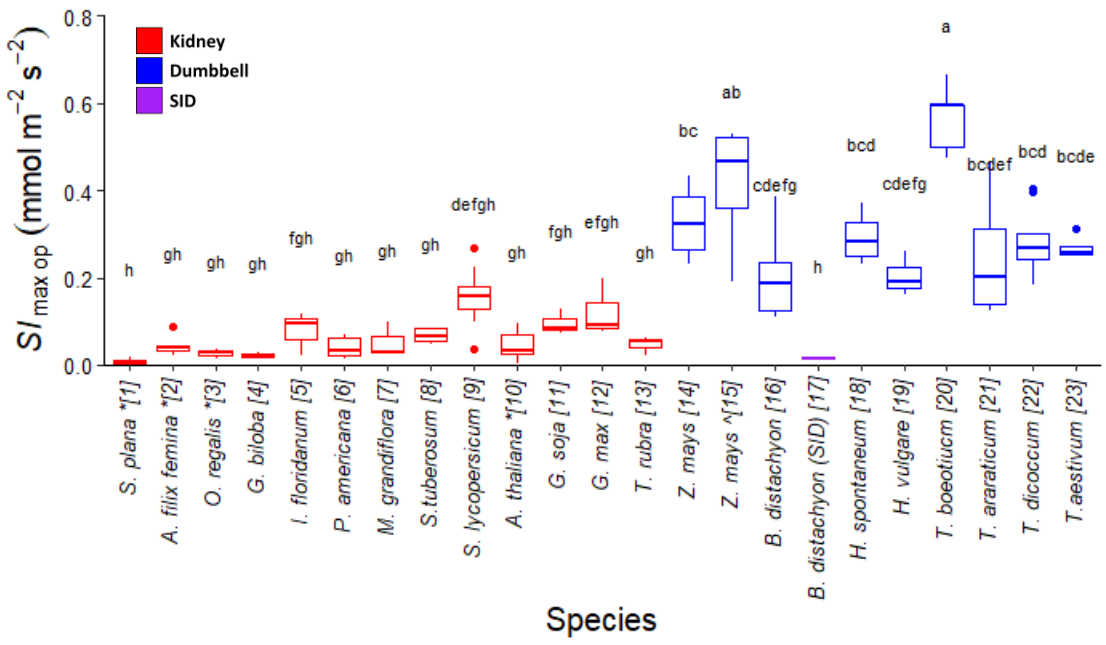

Figure 3.9. Geometry dictates the speed and magnitude of the stomatal response during opening.

A) Mean time lag by species during stomatal opening. **C)** Mean *k* by species during stomatal opening. **C)** Mean maximum rate SI_{max} by species during stomatal opening. Symbols: kidney = red; dumbbell = blue; SID = purple. Species that cannot be distinguished from each other at 0.05 confidence limit are indicated by different letters as determined by ANOVA with a Tukey HSD. Data shown are the mean ± SE. n = minimum of 3 per species.

A

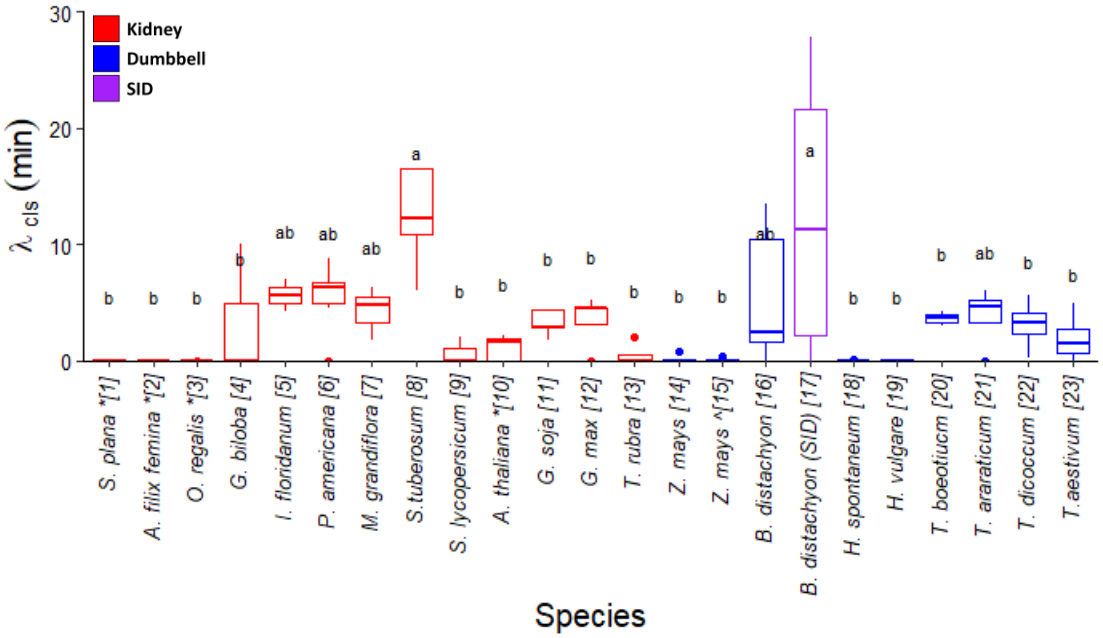
Kidney
Dumbbell
SID
λ cls (min)
30
20
10
0
b b b b ab ab ab a b b b b b b b b b ab a b b b ab b b
S. plana *[1]
A. filix femina *[2]
O. regalis *[3]
G. biloba [4]
I. floridanum [5]
P. americana [6]
M. grandiflora [7]
S.tuberosum [8]
S. lycopersicum [9]
A. thaliana *[10]
G. soja [11]
G. max [12]
T. rubra [13]
Z. mays [14]
Z. mays ^[15]
B. distachyon [16]
B. distachyon (SID) [17]
H. spontaneum [18]
H. vulgare [19]
T. boeotiucm [20]
T. araraticum [21]
T. dicoccum [22]
T.aestivum [23]
Species

B

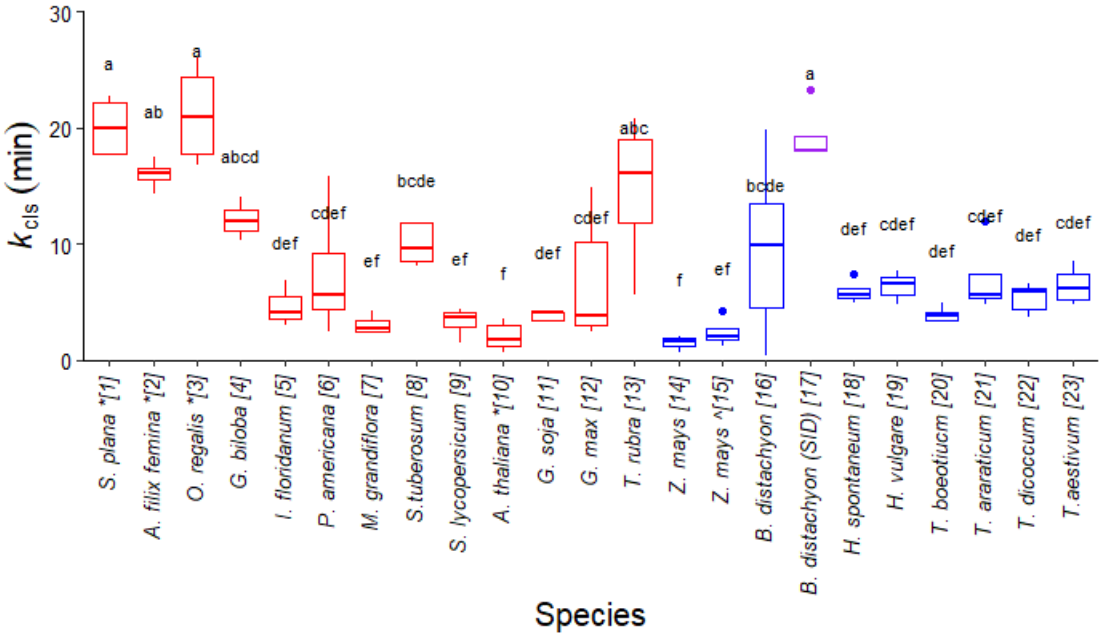
k cls (min)
30
20
10
0
a ab a abcd def cdef ef bcde ef f def cdef abc f ef bcde a def cdef def cdef def cdef
S. plana *[1]
A. filix femina *[2]
O. regalis *[3]
G. biloba [4]
I. floridanum [5]
P. americana [6]
M. grandiflora [7]
S.tuberosum [8]
S. lycopersicum [9]
A. thaliana *[10]
G. soja [11]
G. max [12]
T. rubra [13]
Z. mays [14]
Z. mays ^[15]
B. distachyon [16]
B. distachyon (SID) [17]
H. spontaneum [18]
H. vulgare [19]
T. boeotiucm [20]
T. araraticum [21]
T. dicoccum [22]
T.aestivum [23]
Species

C

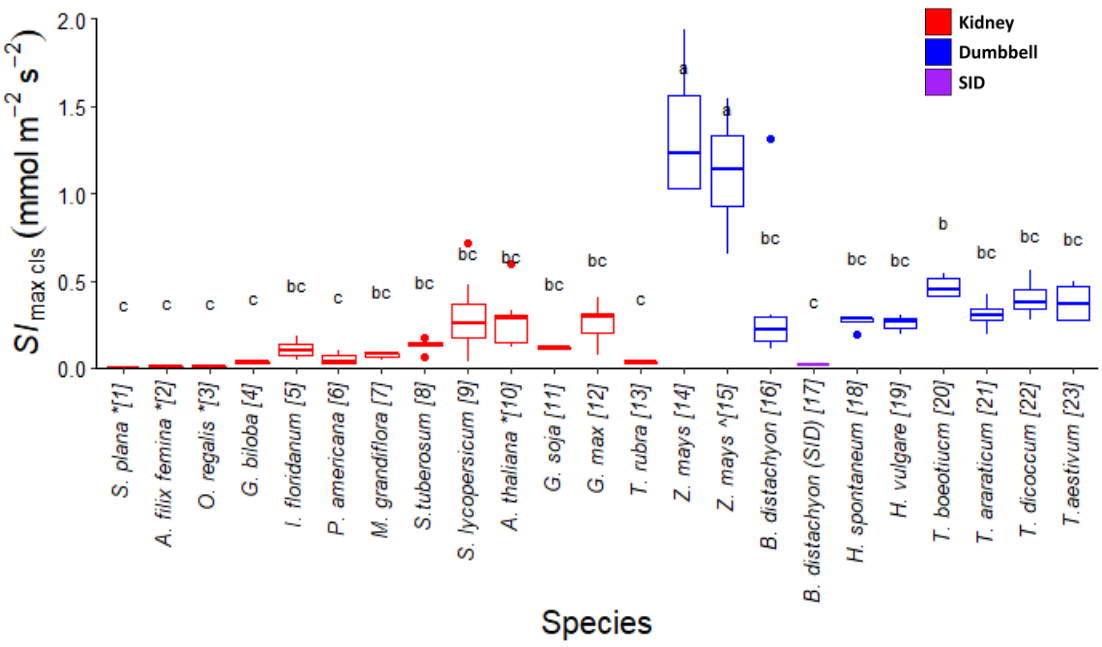

Figure 3.10. Geometry dictates the speed and magnitude of the stomatal response during closing.

A) Mean time lag by species during stomatal closing. **C)** Mean *k* by species during stomatal closing. **C)** Mean SI_{max} by species during stomatal closing. Symbols: kidney = red; dumbbell = blue; SID = purple. Species that cannot be distinguished from each other at 0.05 confidence limit are indicated by different letters as determined by ANOVA with a Tukey HSD. Data shown are the mean ± SE. n = minimum of 3 per species.

A

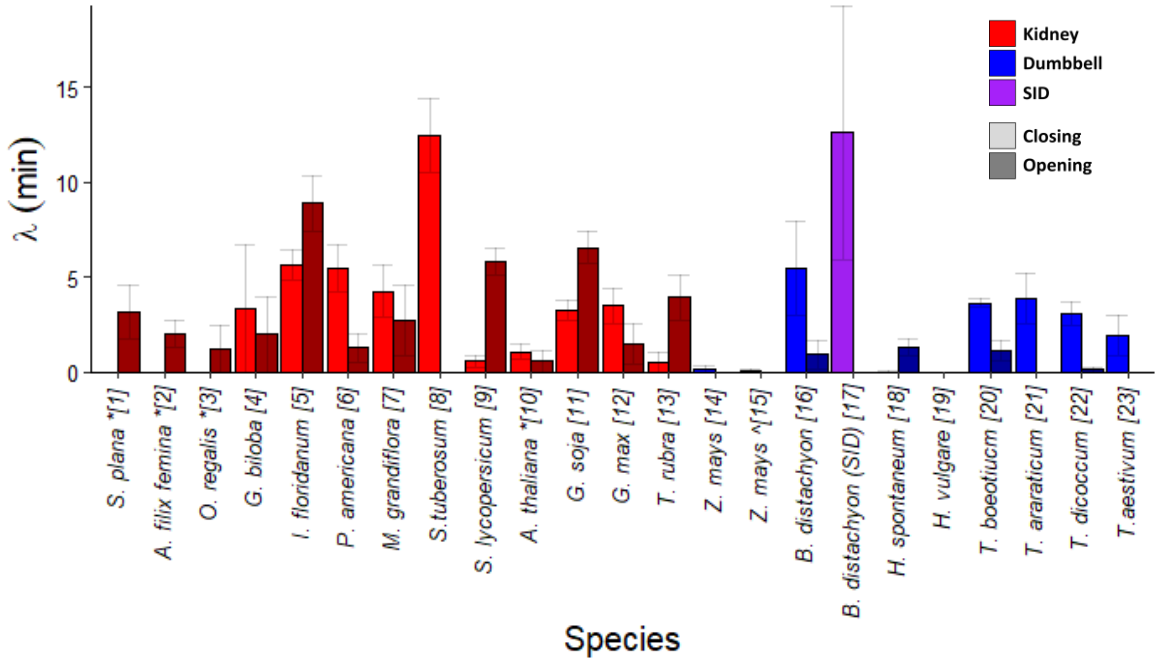
Kidney
Dumbbell
SID
Closing
Opening
λ (min)
0
5
10
15
S. plana *[1]
A. filix femina *[2]
O. regalis *[3]
G. biloba [4]
I. floridanum [5]
P. americana [6]
M. grandiflora [7]
S.tuberosum [8]
S. lycopersicum [9]
A. thaliana *[10]
G. soja [11]
G. max [12]
T. rubra [13]
Z. mays [14]
Z. mays ^[15]
B. distachyon [16]
B. distachyon (SID) [17]
H. spontaneum [18]
H. vulgare [19]
T. boeotiucm [20]
T. araraticum [21]
T. dicoccum [22]
T.aestivum [23]
Species

B

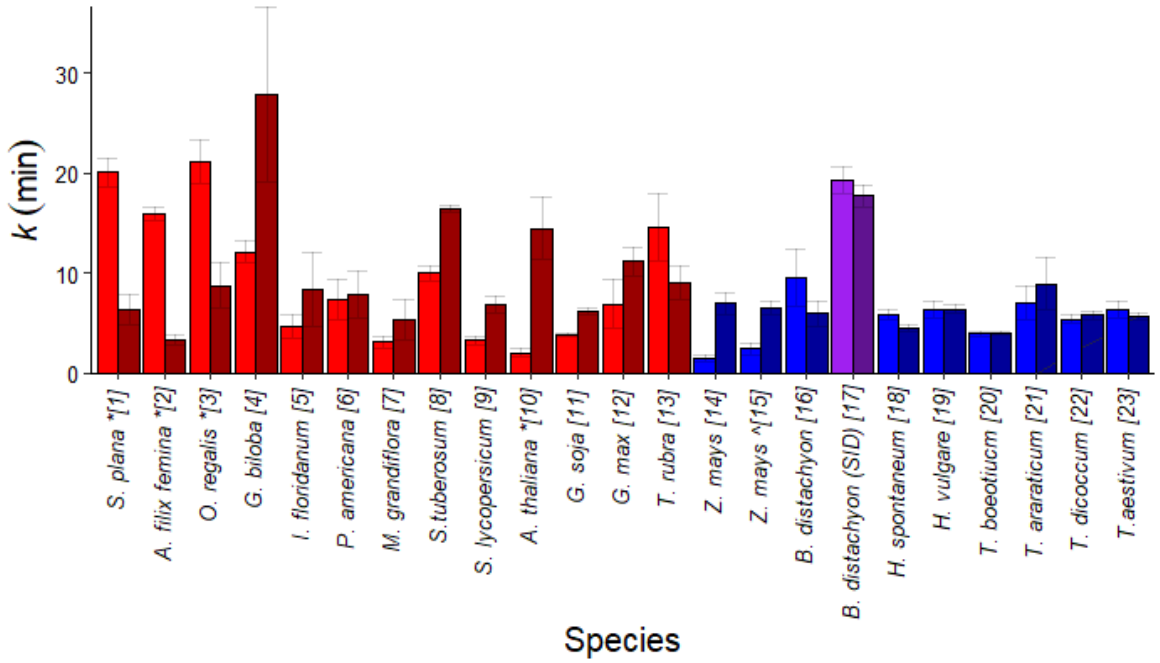
k (min)
0
10
20
30
S. plana *[1]
A. filix femina *[2]
O. regalis *[3]
G. biloba [4]
I. floridanum [5]
P. americana [6]
M. grandiflora [7]
S.tuberosum [8]
S. lycopersicum [9]
A. thaliana *[10]
G. soja [11]
G. max [12]
T. rubra [13]
Z. mays [14]
Z. mays ^[15]
B. distachyon [16]
B. distachyon (SID) [17]
H. spontaneum [18]
H. vulgare [19]
T. boeotiucm [20]
T. araraticum [21]
T. dicoccum [22]
T.aestivum [23]
Species

C

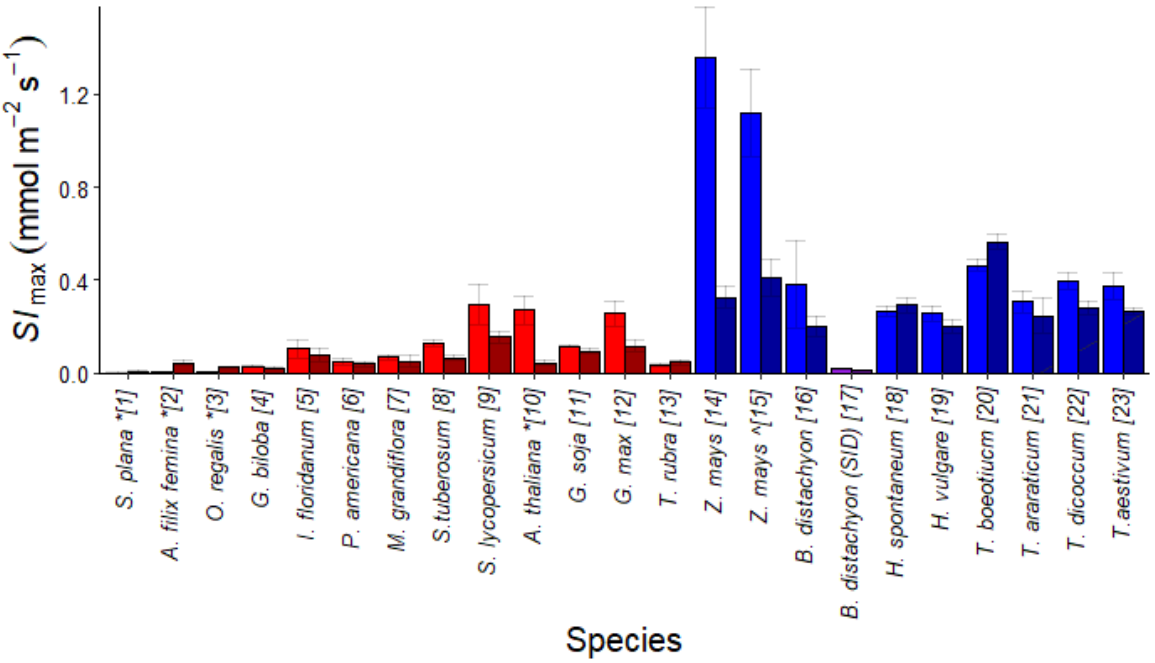

Figure 3.11. Stomatal opening and closing is not the same across species.

A) Mean time lag by species during stomatal opening and closure. **C)** Mean *k* by species during stomatal opening and closure. **C)** Mean SI_{max} by species during stomatal opening and closure. Shading indicates opening. Symbols: kidney = red; dumbbell = blue; SID = purple. Data shown are the mean ± SE. n = minimum of 3 per species.

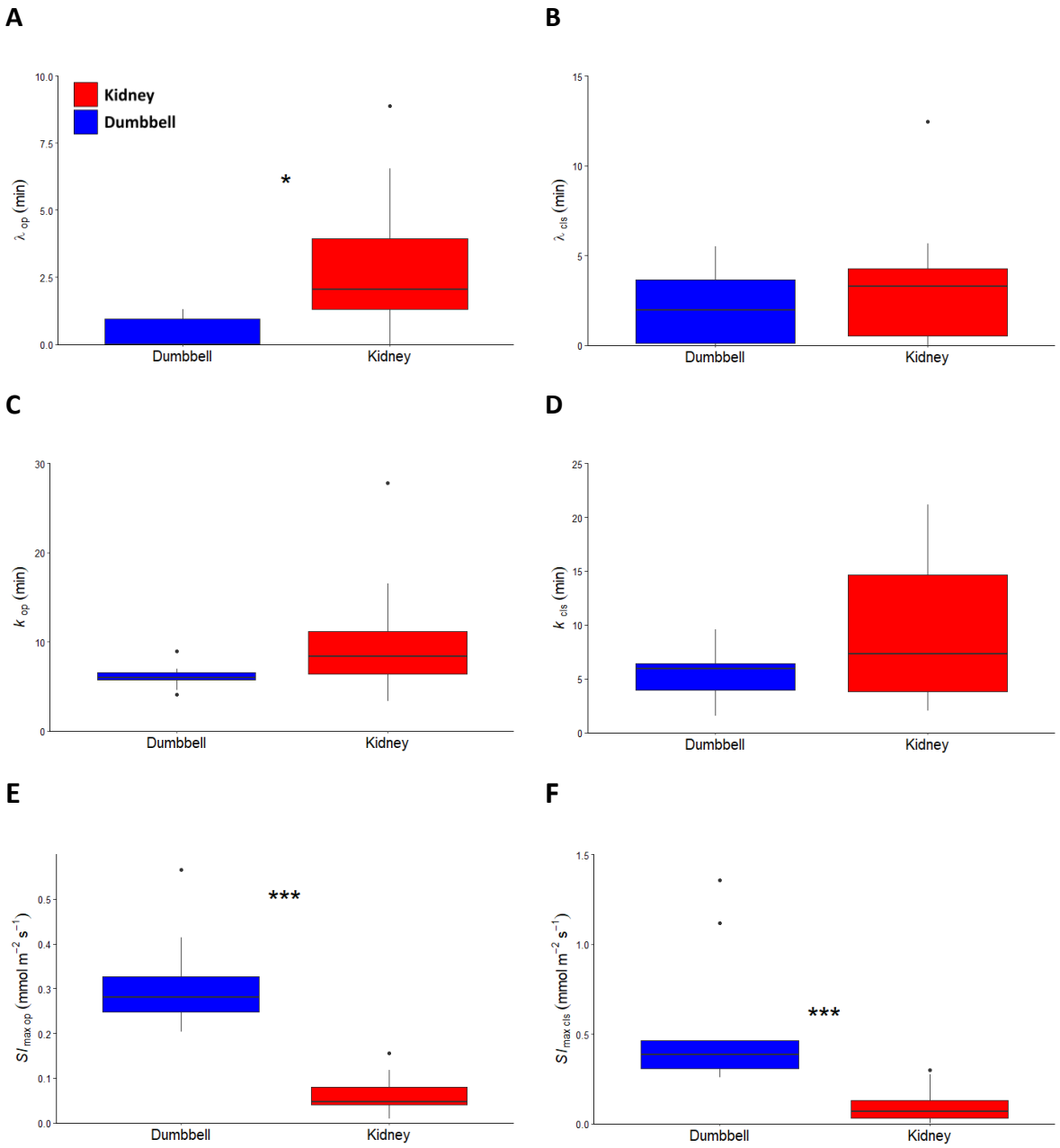

Figure 3.12. Dumbbell shaped species are able to achieve a higher maximum change in g_s during opening and closure.

A) Mean time lag during (λ_{cls}) opening grouped by morphology. **B)** Mean time lag during (λ_{cls}) closing grouped by morphology. **C)** Mean time constant (k_C)during opening grouped by morphology. **D)** Mean time constant (k_C)during closing grouped by morphology. **E)** Mean Sl_{max} during opening grouped by morphology. **F)** Mean Sl_{max} during closing grouped by morphology. Colours: kidney = red; dumbbell = blue. *B. distachyon* (SID) was excluded. Asterisks indicate significant differences (* indicates p=<0.05, *** indicates p=<0.001). Data shown are the mean ± SE. n = minimum of 3 per species.

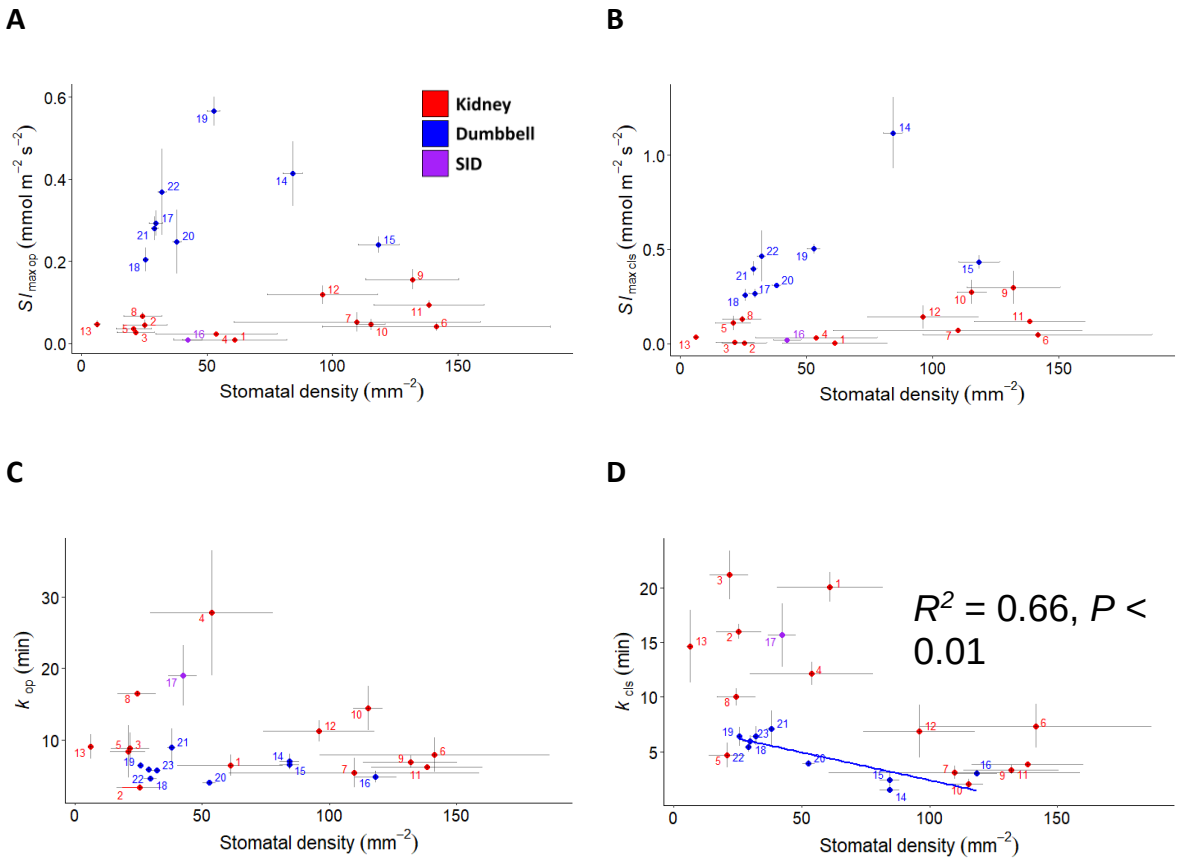

Figure: 3.13. Stomatal opening and closing metrics show no correlation with stomatal density, except for k_{cks} for dumbbell guard cells when data is grouped my geometry

A) The relationship between $SI_{max\ op}$ and stomatal density. **B)** The relationship between $SI_{max\ cls}$ and stomatal density. **C)** The relationship between $k_{c\ op}$ and stomatal density. **D)** The relationship between $k_{c\ cls}$ and stomatal density. Symbols: kidney = red; dumbbell = blue. *B. distachyon* (SID) was excluded. Data shown are the mean ± SE. n = minimum of 3 per species.

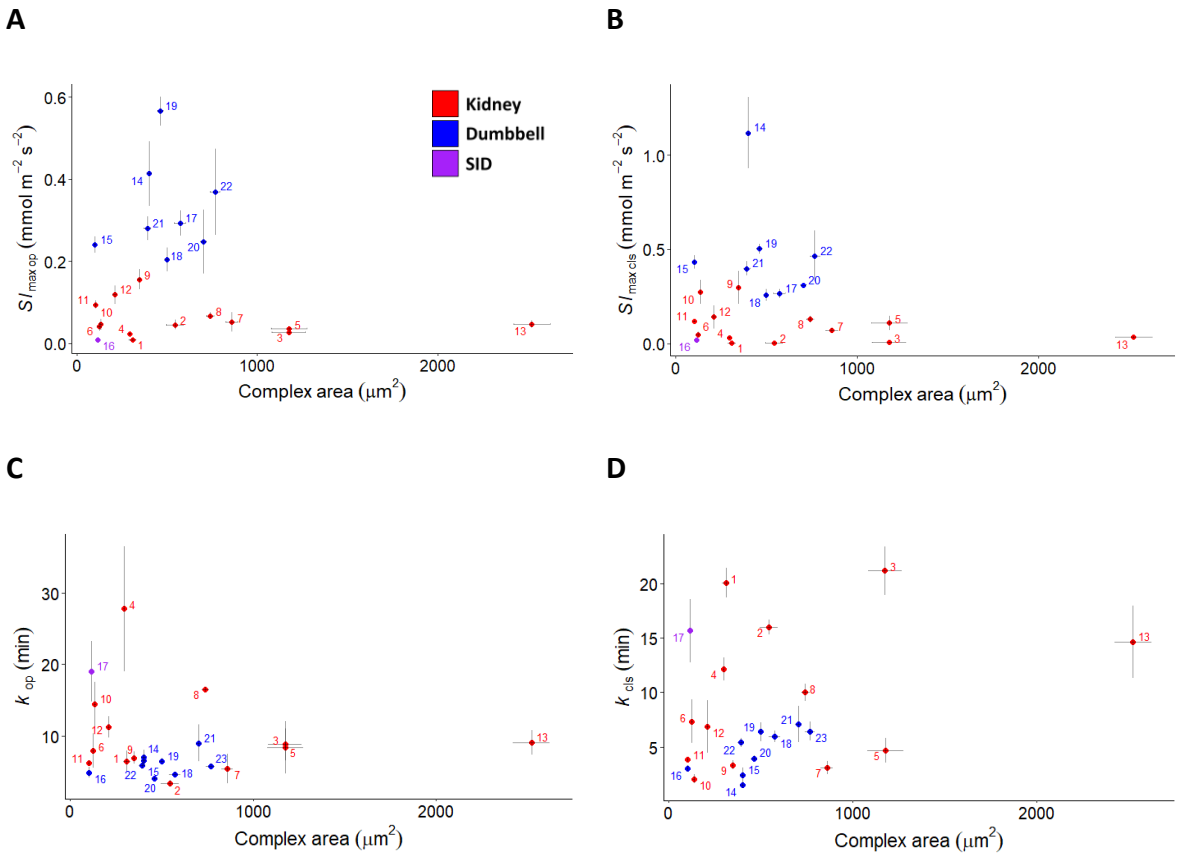

Figure 3.15. Stomatal opening and closing metrics show no correlation with stomatal size when data is group by stomatal geometry

A) The relationship between $SI_{max\ op}$ and stomatal complex area. **B)** The relationship between $SI_{max\ cls}$ and stomatal complex area. **C)** The relationship between $k_{c\ op}$ and stomatal complex area. **C)** The relationship between k_{cls} and stomatal complex area. Symbols: kidney = red; dumbbell = blue. *B. distachyon* (SID) was excluded. Data shown are the mean ± SE. n = minimum of 3 per species.

A

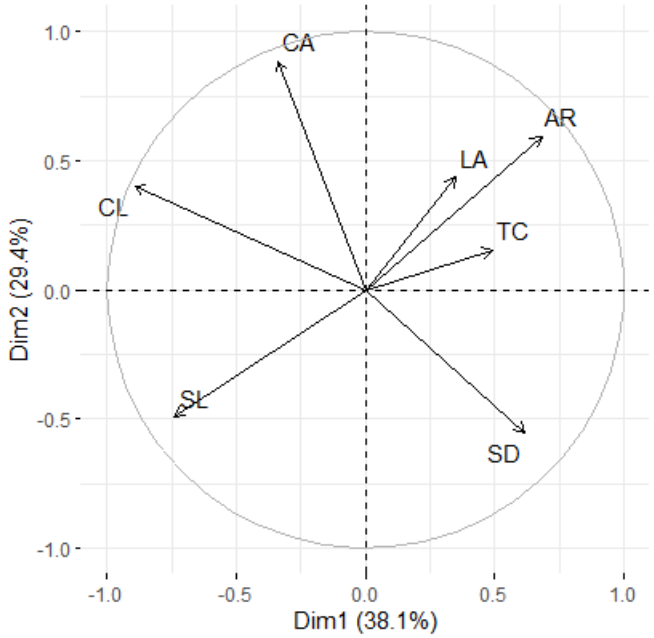

B

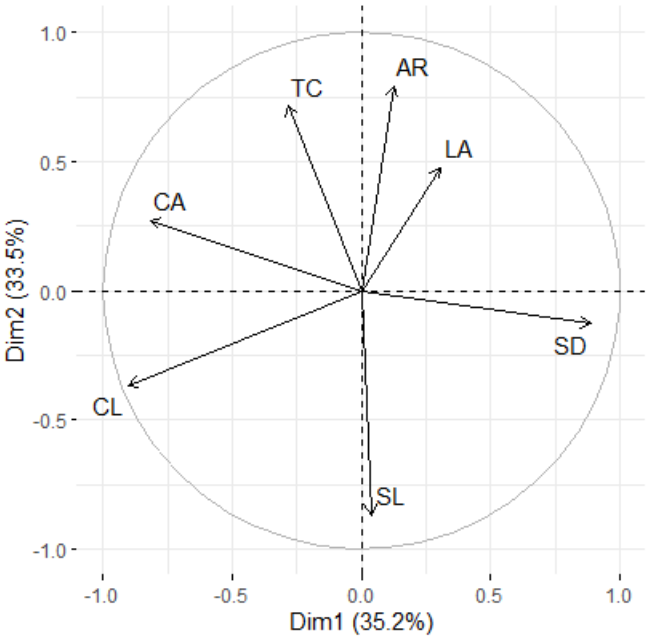

Figure: 3.14. Principle component analysis (PCA) of stomatal morphological and response traits

A principle component analysis among complex length (CL), complex area (CA), stomatal density (SD), Stomatal length (SL), time lag (LA), time constant (TC) and Sl_{max} (SL) during stomatal **A)** opening **B)** and closure.

3.3. Discussion

Light is one of the main drivers of photosynthesis and can fluctuate significantly at the canopy level. Plant responses to this dynamic stimulus manifest as modulation of A and g_s (Pearcy, 1990). The rapidity and magnitude of the response of gas exchange across a wide range of plants was measured, adding to the growing understanding of the importance of a dynamic stomatal response in carbon acquisition and WUE (Drake *et al*., 2013; McAusland *et al*., 2016, Elliot-Kingston *et al*., 2016; Haworth *et al*., 2018). This chapter aimed to not only quantify the response of stomata to a step change in PPFD, but also understand the impact of stomatal morphological and geometric traits on the efficiency of this response. Using species from a wide range of evolutionary backgrounds that occupy broad ecological niches, sample plants were samples that spanned a large spectrum of traits, including differing sizes, patterning and stomatal morphologies.

3.3.1. Species show diverse stomatal distribution and gas exchange potential

Plants adjust gas exchange capacity through alterations of stomatal size and density (Hetherington and Woodward, 2003) and ultimately it is the combination of these two characteristics that determines maximum rates of gaseous exchange with the external environment. One of the most stark differences in stomatal density across species was in how plants partition stomatal distribution across the abaxial and adaxial surfaces of the leaves. Species studied here that diverged prior to the Asterids had stomata only on the abaxial surface, whereas members of the monocot clade were characterised by amphistomatous leaves. However, it should be noted that hypostomaty is still found in later evolving angiosperms (Yang *et al*., 2014). The distribution presented here is the result of selection bias. Amphistomaty has been suggested as a beneficial adaptation to fast growing annual crops, with a potential trade off being additional sites of pathogen entry (McKown *et al*., 2014; Drake *et al*., 2018). Indeed, all grasses had an almost equal distribution of stomata across both sides of the leaf as previously reported (Pemadasa, 1979; Wall *et al*, 2022). The only non-grass monocot sampled, *Tradescantia rubra*, also had amphistomatous leaves but tended towards more stomata on the abaxial surface, as did members of the Asterid and Rosid clades (*Solanum*, *Glycine* and *Arabidopsis* species). These findings are consistent with previous observations (Muir *et al*., 2014; Muir 2015). Interestingly, it appears that the amphistomatous

model plant *A. thaliana*, may not represent the majority of land plant species when considering stomatal distribution across leaves.

The relationship between gas exchange capacity and distribution of stomata across the leaf surfaces has previously been observed in studies comparing species from diverse evolutionary lineages (Haworth *et al*., 2018). This suggests that the distribution of stomata across both surfaces of the leaf may play an important role in achieving these higher rates of gas exchange. This may be an effect of the reduced diffusive distance in amphistomatous leaves, coupled with the isobilateral (palisade mesophyll on both leaf surfaces) nature of grass leaves (Drake *et al*., 2018). Interestingly, *S. tuberosum* had amphistomatous leaves but with very few adaxial stomata and only an adaxial palisade layer, yet still maintained high g_s suggesting this is not a necessity for increasing gas exchange.

Despite the equal distribution of stomata across both leaf surfaces, the grasses tended towards having a lower stomatal density when considering both leaf surfaces. Thus, high gas exchange achieved by grasses is likely facilitated by the more rectangular pore created by their dumbbell shaped guard cells. Under the higher PPFD, and to a lesser extent low PPFD, amphistomatous species, particularly the grasses were able to achieve much higher *A* and g_s despite their relatively lower stomatal density and comparable stomatal size to other species.

As expected, the C_4 crop maize achieved greater *A* for a given g_s, than the C_3 grasses however, conclusions about the role of C_4 in this are difficult to draw as it was the only C_4 species included. Previous studies comparing C_4 and C_3 grasses have also observed the increased *A* compared to C_3 species (McAusland *et al*., 2016; Israel *et al*., 2022; Ozeki *et al*., 2022). These increased rates of *A* compared to given g_s naturally increase WUE in C_4 plants as seen for *Z. mays* here and in the aforementioned studies (Osborne and Sack, 2012; McAusland *et al*., 2016; Israel *et al*., 2022; Ozeki *et al*., 2022). Interestingly, as was observed here, these previous studies have reported more rapid stomatal responses for C_4 species, which has often been attributed to their smaller stomata size compared to C_3 species (McAusland *et al*., 2016; Israel *et al*., 2022; Ozeki *et al*., 2022).

3.3.2. All species responded to a step change in PPFD

As light is a driver of photosynthetic output it would be expected for all plants to respond to a step increase in light, which mimics a short, intense sun fleck in the field (Chazdon and Pearcy, 1991; Grantz and Assmann, 1991). All species tested here responded to an increase in light intensity, achieving higher values of *A* and g_s than at low PPFD. Interestingly, all species were able to increase *A* within minutes at a much quicker rate than g_s, demonstrating the established non-synchronous relationship between these parameters (Farquhar and Sharkey, 1982). This rapid increase in *A* before the associated increase in g_s indicates that at low PPFD g_s was higher than the requirement of *A* (Lawson and Blatt, 2014, McAusland *et al*., 2016). This is likely an adaptation that 'primes' plants to maximise *A* upon a sudden increase in PPFD. Following a step increase in light intensity, after an initial rapid increase, *A* eventually showed limitation by a slower stomatal g_s response in all species. While all species opened their stomata in response to an increase in PPFD, there were clear species-specific differences in the capacity of both *A* and g_s. As expected, *A* and g_s were both positively correlated at steady state however, there was a much stronger relationship at high PPFD. A strong positive correlation between *A* and g_s has previously been reported across species with a wide range of physical stomatal traits (McElwain *et al*., 2016; Xiong and Flexas, 2020).

After initial experiments with four 'shade adapted species' demonstrated a limited response of g_s to step change in PPFD from 100 to 1000 µmol m^{-2} s^{-1}, these measurements were repeated under a lower PPFD shift from 20 to 500 µmol m^{-2} s^{-1}. This lower PPFD shift induced the typical stomatal opening response to PPFD and was therefore included when analysing stomatal responses to a step change in PPFD intensity. It is likely that at 100 µmol m^{-2} s^{-1} these shade adapted species had already opened their stomata. Consequently, any further increase in PPFD intensity yielded a limited stomatal response. As the primary aim of the chapter is concerned with quantifying stomatal response speed, the data taken at the lower light level for these species was presented. Likewise for *Z. mays*, which was grown at a much higher light intensity than other species, data was collected at an additional 100 to 2000 µmol m^{-2} s^{-1} light shift. This data is presented alongside that taken at the typical 100 to 1000 µmol m^{-2} s^{-1} as stomata responded under both light regimes.

Typically, the grass species with dumbbell shaped guard cells were able to achieve much higher steady state *A* and g_s in high PPFD conditions. This held true when shade adapted

species were excluded due to the clear bias a low light intensity would have on these parameters. The tendency for species with dumbbell shaped guard cells to achieve higher *A* and g_s has previously been reported (Xiong and Flexas, 2020). These higher gas exchange values could be due to stomatal patterning. Alternatively, higher gas exchange could be due to the shape of the dumbbell guard cells. This cellular morphology could lead to reduced boundary resistance and shorter diffusive distances increasing mesophyll conductance (Drake *et al*., 2019; Xiong and Flexas, 2020).

Interestingly, despite their apparent adaptation to dry and arid conditions the grasses did not display improved iWUE under steady state high PPFD conditions. While grasses achieved higher rates of *A* this was also coupled with high g_s, lowering iWUE. While high g_s and *A* may have been selected for in crop species it does not explain the equally high rates reached in the wild relatives of these species. In field conditions a steady state is rarely experienced by plants. Thus, it may be the ability of grasses, equipped with dumbbell guard cells, to modulate their stomatal pore area quickly that provides a competitive advantage in dry and arid conditions.

3.3.3. Guard cell geometry dictates stomatal response speed

As species diversify and adapt to different environmental niches it might be expected that new stomatal traits may arise. In order to investigate the adaptations that may appear in different groups, species were arranged in order of evolutionary divergence and the metrics describing the rapidity of the stomatal response were examined. The grasses clearly occupied a separate group demonstrating higher SI_{max} and lower (although not significantly) *k* for both opening and closing than kidney species, as has been noted in other studies focussing on crop species (McAusland *et al*., 2016; Haworth *et al*., 2018). It has been hypothesised that the morphology of the dumbbell guard cells enables more efficient adjustments in stomatal pore area (Raven, 2002). A meta-analysis conducted on time of opening and closing suggested that grasses responded more quickly (Vico *et al*., 2011). A combination of the thin shape of the guard cells requiring less flux of solutes to elicit opening and a more rectangular pore shape are hypotheses that explain a more rapid adjustment of the stomatal pore (Franks and Farquhar, 2007; Vico *et al*., 2011; Raven, 2014). A smaller change in pore width can cause a large change in aperture size compared to the more elliptical kidney pore (Hetherington and

Woodward, 2003). Interestingly, despite a large SI_{max} of dumbbell guard cells compared to kidney, there was less of a difference in *k* during opening and closing. While dumbbell shaped species did on average demonstrate a shorter *k*, this difference was insignificant. As *k* is independent of the magnitude of response this implies that the superior ability of grasses to rapidly respond to changing light comes from their large dynamic range of g_s, rather than the time taken to effect a change alone.

Broadly speaking, species responded similarly during both stomatal opening and closure. However, there was a trend for species to close slightly more quickly than they opened when grouped by morphology. When looking at individual species there is far more variability between stomatal opening and closing. In particular, the ferns and lycophytes showed a bias towards opening far more rapidly than they closed. This is consistent with the theorised need of ferns and lycophytes, which are typically adapted to life in understory environments, to maximise rare sun flecks which penetrate a dense canopy above (Woods and Turner 1971; Chazon and Pearcy, 1987). During the incidence of a rapid sun fleck, a fast stomatal opening response would allow plants to maximise photosynthesis in an otherwise light impoverished environment. The subsequent closure of stomata appears slow, consistent with an environment with high water availability and reduced need to rapidly close stomata when the sun fleck has ceased (Knapp and Smith, 1987; Chazdon and Pearcy, 1991; Deans *et al*., 2019; Cai *et al*., 2021). This slow response may also be an adaptation to utilise subsequent sun flecks that may occur (Ooba and Takahashi, 2003; Vico *et al*., 2011; Deans *et al*., 2019; Cai *et al*., 2020). The relative speed of fern stomata during opening compared with closure has previously been observed (Xiong *et al*., 2018; Deans *et al*., 2019).

Counter to ferns and lycophytes, *Z. mays* exhibited a much faster stomatal closure response than opening. This is likely due to the dry and arid conditions in which *Z. mays* has become adapted to. In such conditions, WUE is likely a highly desirable trait. As such, the ability to close stomata after a period of high light would be highly important to limit superfluous water loss through open stomata for very little carbon gain. Interestingly, *A. thaliana* displayed faster closure than opening. While this species was included as shade adapted due to its relatively low growth light requirement, it behaved oppositely to the other shade adapted species. This may indicate that the asymmetric response favouring rapid stomatal opening

seen in the fern and lycophytes may be lineage specific; however, more species would have to be examined to make this conclusion.

It has previously been suggested that one of the advantages of dumbbell shaped stomata, and some kidney stomata, is the presence of subsidiary cells. Through proving a pool of solutes that facilitates rapid changes in internal guard cell turgor and by providing a source of mechanical advantage that can improve control of the stomatal pore, subsidiary cells are thought to improve stomatal response speeds (Edwards *et al*., 1976; Majorie *et al*., 2002; Franks and Farquhar, 2007). Using the *B. distachyon* mutant lacking subsidiary cells, *B. distachyon* (SID), the role of subsidiary cells in facilitating a stomatal response can be further elucidated, at least for dumbbell shaped guard cells (Raissig *et al*., 2017). *B. distachyon* (SID) plants had consistently slower stomata than *B. distachyon* and a reduced dynamic range during opening and closure. Although some of this difference in rate of change of g_s may be due to the reduced density of *B. distachyon* (SID), the longer opening and closure times indicate altered stomatal dynamics. The opening and closing speeds achieved by *B. distachyon* (SID) were far more similar to the slowest species with kidney shaped guard cells than any of the grasses with dumbbell shaped guard cells.

3.3.4. Stomatal size and density does not impact stomatal speed across a broad range of species

The importance of stomatal size on the speed of response remains an elusive issue, with contradictory evidence (Drake *et al*., 2013; Lawson and Blatt, 2014; McAusland *et al*., 2016; Elliot-Kingsotn *et al*., 2016; Kardiman and Ræbild, 2017; Deans *et al*., 2019). Here, there was no relationship between stomatal complex area and any metric associated with quantifying the speed of stomatal response. It is likely that when considering closely related species, or those which occupy a single niche, the size of stomata may be important. The wide range of species, which span multiple ecological niches studied here, do not support the hypothesis that size of stomata is an important determinant of the speed of the stomatal response. The results presented here, in part, support conclusions by Dean *et al*. (2019) who suggest that light fleck theory is a likely driver explanation for stomatal speed as ferns with larger stomata showed similar, or shorter, k_{op} than smaller kidney species.

3.3.4. Limitations and future work

The use of IRGAs in this study provides an excellent tool for real-time estimates of gas exchange to provide insight into the stomatal responses of species. However, the inevitably low-throughput nature of such a tool has limited the number of species that were able to be analysed. It would be useful to include more species that span not only the land plant phylogeny, but also broad ecological niche. Including species from the same clade, but that occupy distinctly different niches, such as contrasting light and water availability, might further elucidate the role of the environment in driving different stomatal responses. Furthermore, bolstering the species sampled with more than one genotype from each species would strengthen any relationships found between stomatal anatomical traits, evolution and response speed. As has been demonstrated by Zhang *et al*., (2022), genotypes within a species can display different stomatal response speeds to change in PPFD.

Additionally, many of the species in this study are crops, which have not only gone through the process of artificial selection, but often, by nature, occupy an annual rather than perennial growth habit. This may impact the life strategy of these species and hence gas-exchange optimisation. It would be an interesting avenue of research to address the role of life history traits on gas exchange and stomatal response speeds. Additionally, any crop species that are included may have been bred for higher gas exchange rates, due to the effects this may have on photosynthesis. This may impact the speed of stomatal response, in particular SI_{max} which is a function of time and the magnitude of change in g_s.

Across this study plants were grown under different conditions to ensure plants were not stressed before measurements were taken as this would inevitably impact gas exchange response. It is worth noting that these different conditions will also impact gas-exchange. As has been documented, surrounding light (intensity and quality), humidity and CO_2 (among others) can impact not only stomatal development but also stomatal responses (Casson and Gray, 2008; Hõrak *et al*., 2017).

Chapter 4. The impacts of stomatal response speed on biomass acquisition and water use under dynamic light conditions

4.1.1 Introduction

Photosynthesis, which is the ability to convert light into biomass, is the primary determinant of crop yields (Sinclair and Muchow, 1999). With a rapidly growing global population, agronomic output is at the centre of much scientific research. Growing competition for land between food, biofuel and the provision of ecological services adds additional stress to our agricultural system (Edgerton, 2009). The need to improve yields while limiting water use during crop growth remains an essential problem, with drought stress already thought to be the cause of 10% losses in cereal production from 1964 to 2007 (Ort and Long, 2014; Leak *et al*., 2016). Currently, 70-90% of available freshwater is used in agriculture globally which will not be sustainable for a growing population (Morrison *et al*., 2008).

It has been suggested that a faster stomatal aperture response could improve both carbon acquisition and WUE under a dynamic light regime. Adjustment of stomatal apertures often take tens of minutes and can be an order of magnitude slower than adjustments of *A,* leading to a limitation on carbon acquisition and superfluous water loss under dynamic field conditions (Knapp and Smith, 1989; Lawson and Blatt, 2014; McAusland *et al*., 2016; De Souza *et al*., 2020).

Central to the understanding of the importance of an active regulation of the stomatal pore, is the notion that more rapid stomatal responses are more efficient (Lawson and Vialet-Chabrand, 2019; Papanatsiou *et al*., 2019; Kimurara *et al*., 2020). Rapid stomatal responses have been cited as one of the advantages that have enabled grasses to colonise dry and arid environments, and understory species such as ferns and lycophytes to maximise sunflecks in an otherwise low PPFD environment (Grantz and Assman, 1991; Hetherington and Woodward, 2003; Chen *et al*., 2017; Deans *et al*., 2019). Interestingly, when growing different species in constant and fluctuating PPFD, Watling *et al*. (1997) reported inconsistent responses. Across four species, biomass acquisition was reduced in fluctuating PPFD compared to constant PPFD in two species, remained relatively unchanged in one species and

was greater in one species, despite the same net daily PPFD. However, no data was collected regarding stomatal response speeds of these species but, *A* under saturating light was not significantly different between these species (Watling *et al*., 1997).

Attempts to engineer *A. thaliana* plants with faster stomatal responses have yielded encouraging data, generally reporting an increase in WUE and biomass acquisition in plants with faster stomata responses under dynamic PPFD condition (Papanatsiou *et al*., 2019; Kimurara *et al*., 2020). It is worth noting that the majority of these studies focus on mutants with not only enhanced response speeds but also altered maximum and minimum g_s, which likely impacts both WUE and biomass acquisition. This makes it difficult to disentangle the benefits achieved through altered stomatal dynamics and those achieved through altered gas exchange capacity. Additionally, the majority of the studies focus on short intermittent light-darkness cycles that are poor replications of real field conditions (Papanatsiou *et al*., 2019; Kimurara *et al*., 2020). Efforts to translate these concepts into rice in the field have yielded positive results. Rice plants overexpressing the Na^+/H^+ antiporter *OsNHX1* had faster stomatal responses and showed an increase in biomass under drought conditions (Qu *et al*., 2020). Interestingly, rice plants without a functional *OsNHX1* did not show any difference in stomatal speed under well-watered conditions compared to the wild type but were significantly slower under drought conditions. It seems that while stomatal speed may play an important role in plant WUE and productivity in dynamic PPFD conditions, the surrounding environmental context is important.

4.1.2. Carbon isotope discrimination as a proxy for WUE

In addition to water loss and dry mass acquisition, WUE over the lifetime of tissue can be estimated using carbon isotope analysis (Adams and Grierson, 2001). Rubisco favourably carboxylates ^{12}C over ^{13}C (Farquhar and Sharkey, 1982; Adams and Grierson, 2001). A lower internal CO_2 concentration leads to higher ^{13}C carboxylation rates as discrimination is less possible and hence a higher ratio of ^{13}C : ^{12}C in tissue ($\Delta^{13}C$). Internal CO_2 is intrinsically linked to g_s and thus, reduced g_s leads to a higher $\Delta^{13}C$. This technique has often been used to estimate WUE of plants, with reduced discrimination indicating of a higher WUE (Seibt *et al*., 2008; Rajabi *et al*., 2009; Centritto *et al*., 2009).

4.1.3. Aims

The aim of the work in this chapter was to investigate the hypothesis that speed of stomatal response plays an important role in determining plant productivity and water use efficiency in a dynamic PPFD environment (similar to field conditions). Utilising species which display a spectrum of stomatal opening and closing speeds in response to PPFD (identified in Chapter 3), various metrics of plant WUE and photosynthetic output were compared between plants grown under typical lab conditions of constant daytime PPFD, and those grown under a fluctuating PPFD environment. If the hypothesis is correct, then it is expected that species with faster stomatal-responses will share similar photosynthetic and water-use values between light conditions, and that these will be superior to those plants with a slower stomata response under these different conditions.

4.2. Results

4.2.1. Plants were sampled which span a range of stomatal response speeds

To understand the importance of a rapid stomatal response in a dynamic environment, species were placed in either a constant PPFD chamber or a fluctuating PPFD chamber (**Figure 2.2**). Hereafter, constant light refers to a constant daytime PPFD. These either replicated typical growth chamber constant daytime PPFD conditions (400 µmol $m^{-2}s^{-1}$) or replicated real-world dynamic PPFD conditions taken from three days in June 2021 at the Arthur Willis Controlled Environment Centre, Sheffield, UK. This light regime accurately replicates the typical sun-shade pattern that might be expected from intermittent cloud cover – realistic conditions that these species might experience in the field in the UK. These real-world light regimes were adjusted so that the day length was the same as the constant PPFD chamber and that the maximum PPFD did not exceed 1000 µmol m^{-2} s^{-1}. The net daily PPFD flux across both chambers was the same. As the speed of stomatal response is central to the questions being asked, a range of species were selected, as determined in the previous chapter (**Chapter 3**). Species were chosen based on their *k* and SI_{max} during stomatal opening and closure to span a range of opening and closure times, but that could also be grown together. In order to isolate the impact of differences in stomatal response speed where possible, species were selected that were closely related to minimise inherent interspecies effects. For this reason,

Triticum species were heavily sampled due to their relatedness and natural differences in stomatal response characteristics. *B. distachyon* (SID) mutant was included due to its defective stomatal response with *B. distachyon* as a wild-type control. As all of these species had dumbbell shaped stomata, *G. max* and *S. lycopersicum* were included as representatives with kidney shaped stomata.

In this Chapter, species are arranged from lowest to highest $Sl_{max\ op}$ on all figures showing speed and plant growth/water use responses as determined in chapter 3. Excluding the mutant line *B. distachyon* (SID) there was a 5-fold difference between the $Sl_{max\ op}$ of the fastest (*T. boeoticum*) and slowest species (*G. max*) included (**Figures 4.1-4.2**). Likewise for stomatal closure, the same species achieved the highest and lowest $Sl_{max\ cls}$, with a 2 fold difference between the fastest and slowest. Compared to the other *Triticeae*, *T. boeoticum* consistently displayed the fastest stomatal response. This is shown by a more than 2-fold greater Sl_{max} during opening and a 1.5-fold greater Sl_{max} during closing than the slowest *Triticeae*, *T. araraticum*. *T. durum* and *T. aestivum* showed intermediate responses.

For *k*, *T. beoeticum* displayed the shortest response time of the *Triticeae*, less than half that of *T. araraticum* during opening and 3 minutes less during closure. Again *T. aestivum* and *T. durum* showed intermediate response times. The species with kidney shaped stomata, *G. max* and *S. lycopersicum*, typically achieved slow k_{op}, but *S. lycopersicum* achieved the shortest k_{cls} of any species included. The mutant *B. distachyon* (SID) displayed a consistently low Sl_{max} and longer *k* than any other species during both opening and closure (**Figures 4.1-4.2**).

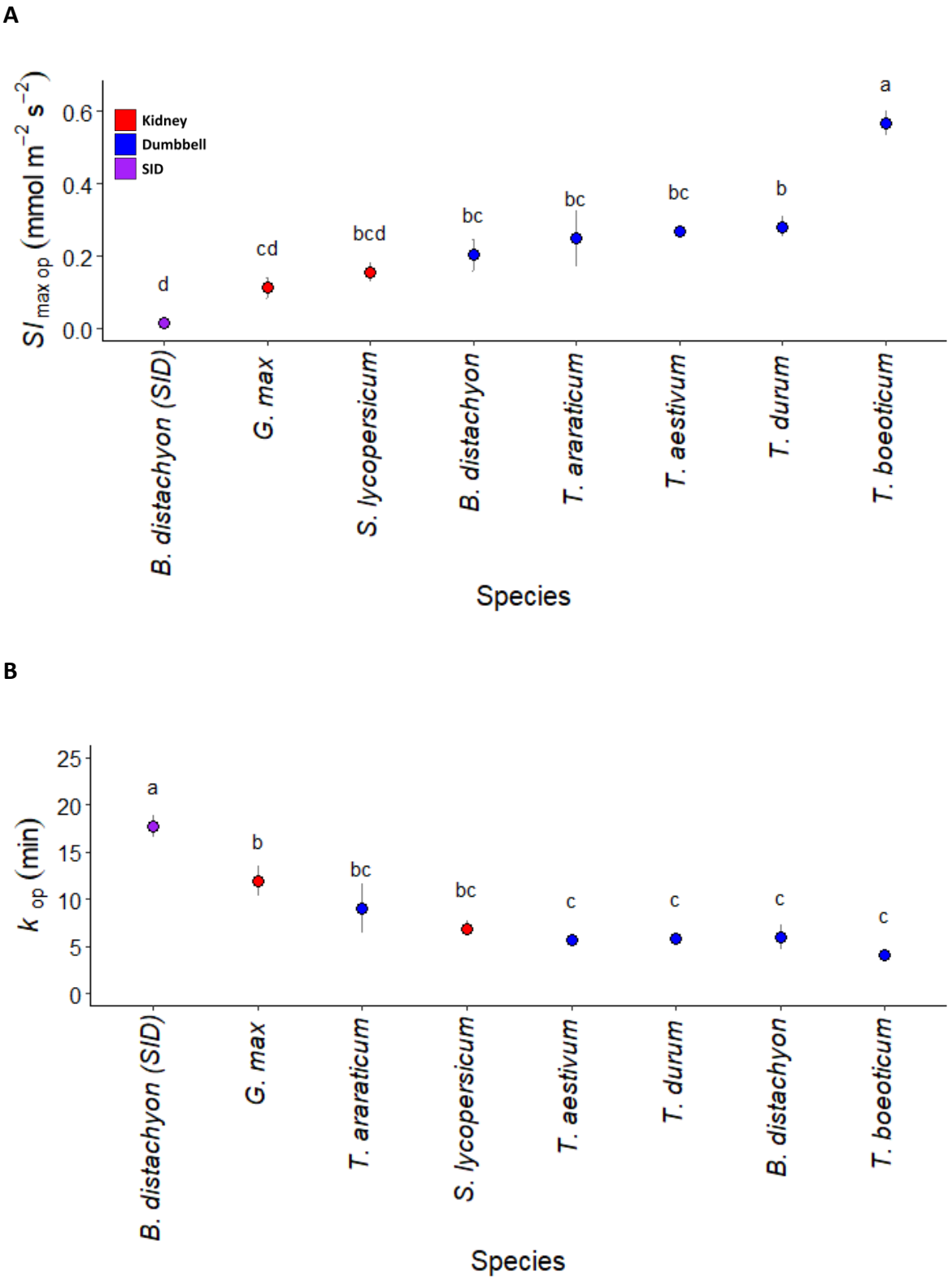

Figure 4.1. There is variation in stomatal opening speed between species
A) $SI_{max\ op}$ and **B)** k_{op} in response to a step change in PPFD across dumbbell species (blue), kidney species (red) and stomatal mutant *B. distachyon* (SID; purple) Letters indicate significant differences (p=<0.05). Tukey HSD one-way anova. Data shown are the mean ± SE (n = 3-7).

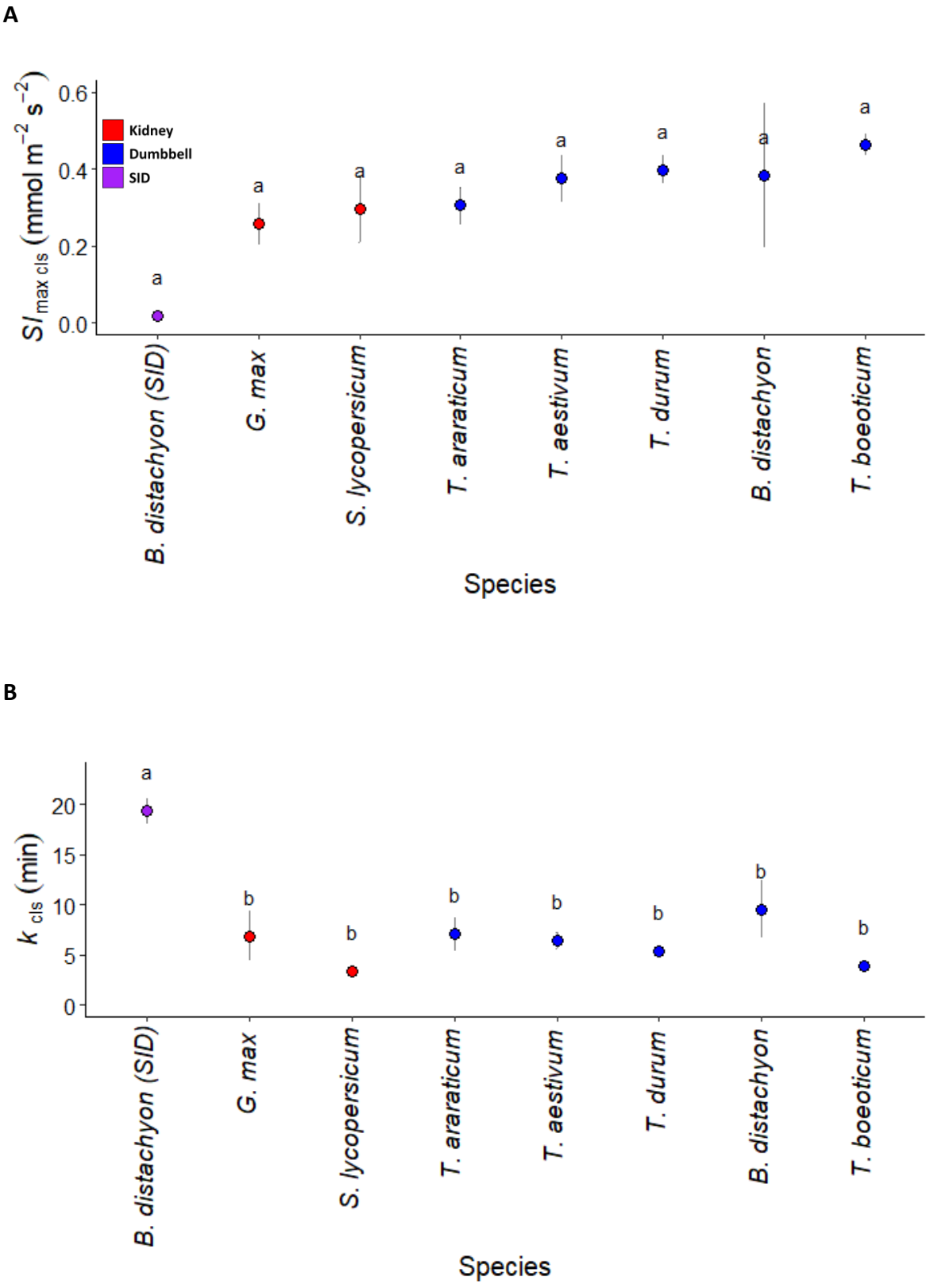

Figure 4.2. There is variation in stomatal closing speed between species
A) $SI_{max\ cls}$ and **B)** k_{cls} in response to a step change in PPFD across dumbbell species (blue), kidney species (red) and stomatal mutant *B. distachyon* (SID; purple). Letters indicate significant differences (p=<0.05). Tukey HSD one-way anova. Data shown are the mean ± SE (n = 3-7).

4.2.2. Plants grown in a dynamic light environment show no difference in plant growth or water-use metrics under well-watered conditions.

In order to understand whether growth in a fluctuating PPFD environment impacts stomatal development on leaves, stomatal density was calculated for the species used in these experiments (**Figure 4.3A**). There was found to be no difference in stomatal density between plants grown at a constant daytime PPFD and plants grown under fluctuating PPFD for any species tested (*t* test, $P > 0.05$; **Table 4.1**).

To examine the impact of a dynamic environment on transpiration, pots were weighed and watered to a given mass every day to determine water loss (**Figure 4.3B**). There was found to be no significant difference in water lost through transpiration between plants grown at constant or fluctuating PPFD for any of the species examined except *B. distachyon* (*t* test, $P > 0.05$; **Table 4.1**). *B. distachyon* lost more water in the fluctuating PPFD environment than the constant PPFD environment (*t* test, t statistic = -4.022, $P < 0.01$) however the SID mutant showed no significant difference.

To examine the impact of a dynamic environment on plant biomass acquisition, plants were harvested, and their dry biomass was measured after 7 weeks of growth (**Figure 4.4A**). There was found to be no significant difference in plant biomass gained between species grown at constant PPFD and those grown under fluctuating PPFD (*t* test, $P > 0.05$; **Table 4.1**).

In order to determine the light harvesting capacity of leaves grown under different light regimes a SPAD meter was used to estimate leaf chlorophyll content (**Figure 4.4B**). Only *G. max*, *S. lycopersicum, T. aestivum* and *T. durum* were measured as they filled the SPAD meter chamber aperture. There was found to be no significant difference in leaf relative chlorophyll content between *G. max, S. lycoersicum* and *T. durum* grown under a constant daily PPFD regime and those grown under a dynamic PPFD regime (*t* test, $P > 0.05$; **Table 4.1**). However, *T. aestivum* leaves had significantly less relative chlorophyll content when grown under fluctuating PPFD (*t* test, $P < 0.05$; **Table 4.1).**

In order to investigate any differences in the water use efficiency of plants between the two light environments, carbon isotope discrimination analysis of leaves was conducted (**Figure 4.5B**). This proxy measurement allows a comparison of WUE across the lifetime of the tissue. There was found to be no significant difference in leaf carbon isotope discrimination between

plants grown under a constant PPFD regime and those grown under a dynamic PPFD regime (*t* test, $P > 0.05$; **Table 4.1**), with the exception of *G. max*. This species, which had the slowest stomatal opening and closing Sl_{max} (excluding *B. distachyon* (SID)), showed significantly lower $\Delta^{13}C$ when grown under the constant PPFD environment indicating a higher WUE (*t* test, t statistic = 3.100, $P < 0.01$). *S. lycopersicum* and three of the *Triticeae* species showed remarkably little variation in carbon isotope ratios across and within the PPFD conditions.

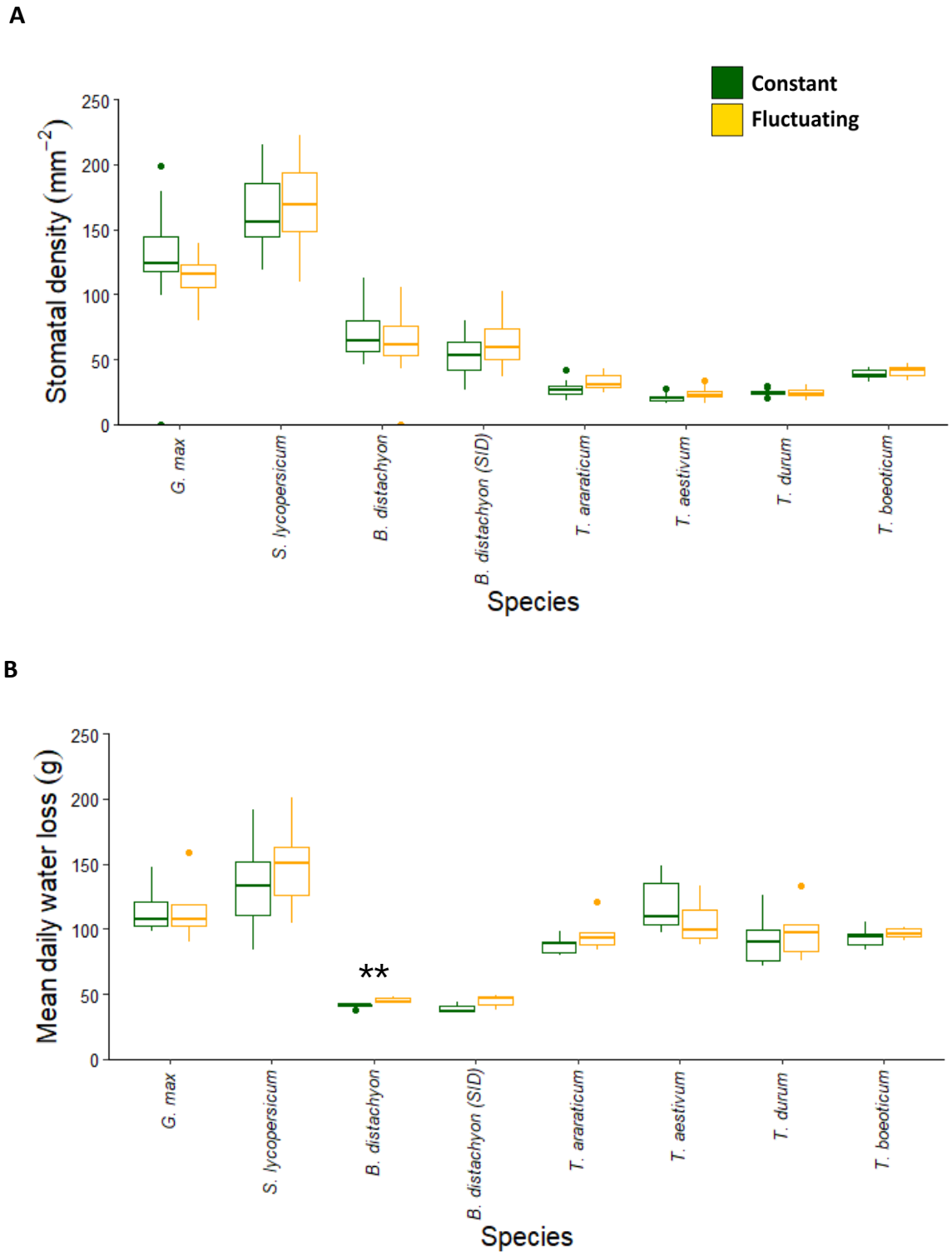

Figure 4.3. There is no difference in stomatal density or mean water loss between plants grown at constant PPFD or fluctuating PPFD in well-watered conditions.
A) Mean abaxial stomatal density across species. **B)** Mean daily water loss over 5 days. Plants were grown under constant (green) and fluctuating (gold) PPFD. Data shown are the mean ± SE. n = minimum of 5 per species (* indicates p=<0.05, ** indicates p=<0.01 , *** indicates p=<0.001)

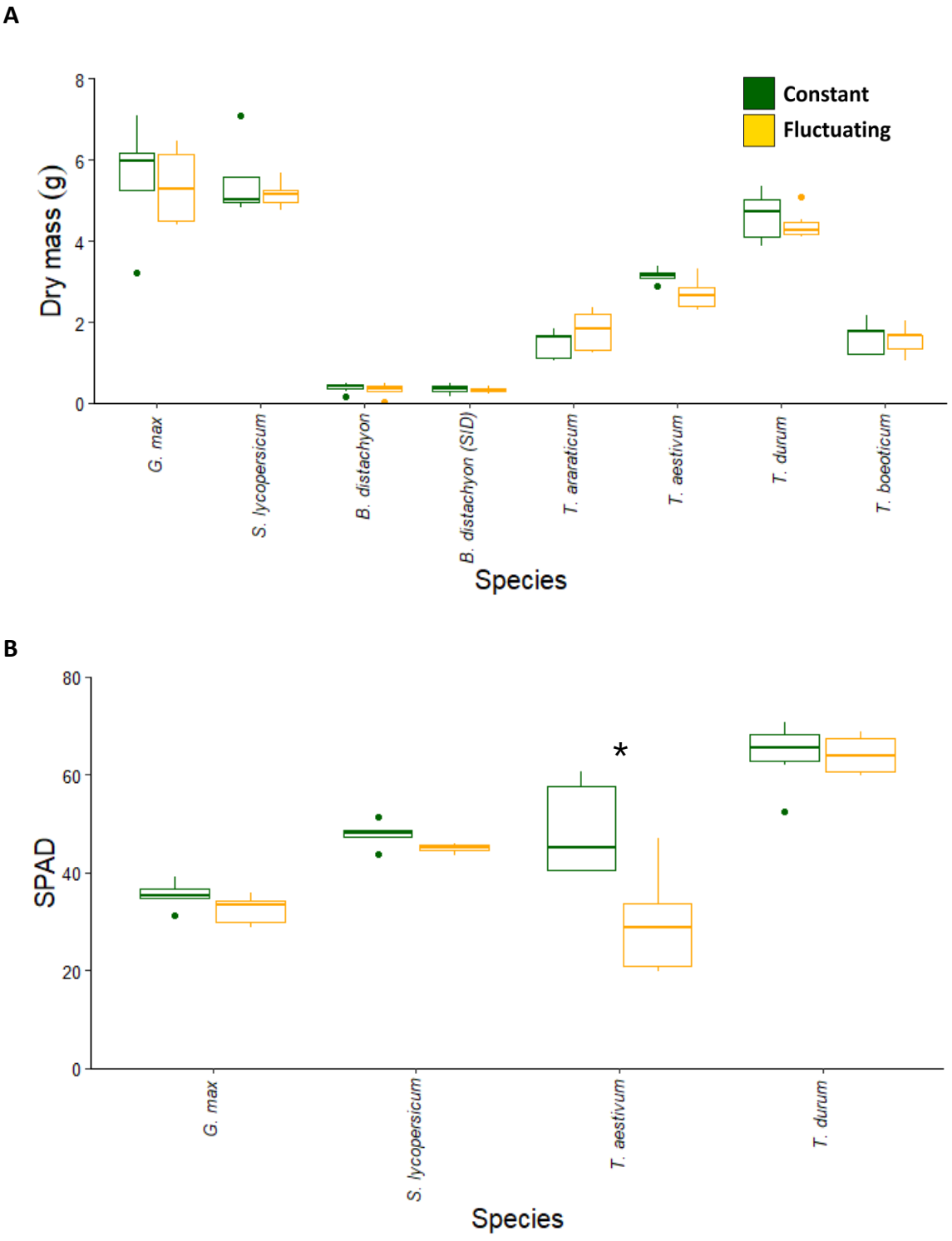

Figure 4.4. There is a difference in relative chlorophyll content between plants grown at constant PPFD or fluctuating PPFD in well-watered conditions in some species, but not dry mass.
A) Mean dry mass after 7 weeks of growth across species. **B)** Mean relative chlorophyll of leaf 6. Plants were grown under constant (green) and fluctuating (gold) PPFD. Data shown are the mean ± SE. n = minimum of 5 per species (* indicates *p*=<0.05, ** indicates *p*=<0.01 , *** indicates *p*=<0.001).

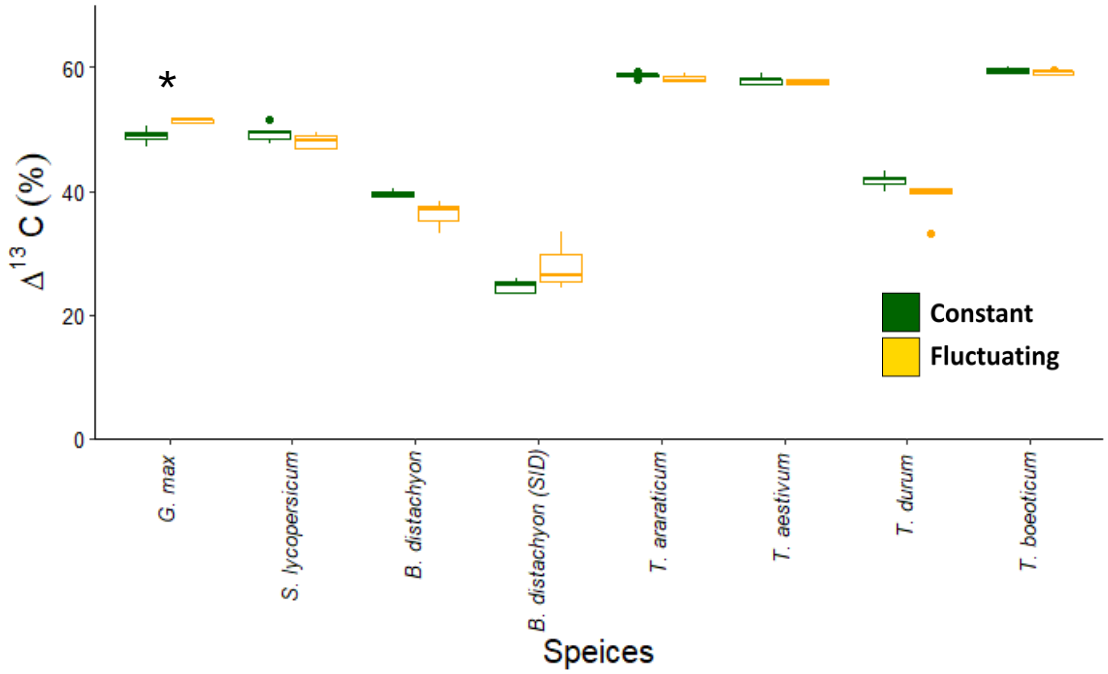

Figure 4.5. Most species show no difference in carbon isotope discrimination between plants grown at constant PPFD or fluctuating PPFD in well-watered conditions.
Mean carbon isotope discrimination between plants grown under constant (green) and fluctuating (gold) PPFD. Data shown are the mean ± SE. n = minimum of 5 per species (* indicates p=<0.05, ** indicates p=<0.01 , *** indicates p=<0.001).

Table 4.1. *t-test* significance values by parameter for well-watered plants
Each row indicates a *t-test* significance value between plants grown in a constant or dynamic light environment. Asterisks indicate significant differences (* indicates *p*=<0.05, ** indicates *p*=<0.01 , *** indicates *p*=<0.001).

Parameter	Species	Mean (C:F)	SE (C:F)	T statistic	P value
Stomatal density	*B. distachyon*	69.1 : 61.8	2.61 : 3.80	0.8344	0.419
	B. distachyon (SID)	52.8 : 62.2	2.38 : 3.48	-1.3242	0.223
	T. boeoticum	38.7 : 41.2	0.75 : 0.92	-1.7431	0.120
	T. araraticum	27.1 : 32.0	1.17 : 1.28	-1.5718	0.155
	T. durum	24.5 : 24.3	0.51 : 0.70	0.2514	0.808
	T. aestivum	20.8 : 24.3	0.79 : 1.18	-1.3135	0.238
	G. max	128 : 113	8.84 : 3.39	1.09915	0.327
	S. lycopersicum	164 : 171	6.45 : 6.59	-0.4073	0.695
Daily water loss	*B. distachyon*	41.1 : 45.4	0.70 : 0.82	-4.02245	0.0040**
	B. distachyon (SID)	39.0 : 44.9	1.42 : 2.09	-2.35587	0.05040
	T. boeoticum	93.5 : 96.8	3.72 : 1.94	-0.79623	0.45600
	T. araraticum	88.0 : 96.96	3.21 : 6.38	-1.24543	0.26000
	T. durum	92.8 : 98.5	9.64 : 10.0	-0.40757	0.69400
	T. aestivum	118.6 : 105.8	9.92 : 8.14	1.00626	0.34500
	G. max	115.5 : 115.6	8.95 : 11.9	-0.00538	0.99600
	S. lycopersicum	134.5 : 148.9	18.3 : 16.5	-0.5846	0.52750
Dry mass	*B. distachyon*	0.39 : 0.35	0.03 : 0.04	0.82346	0.4220
	B. distachyon (SID)	0.34 : 0.31	0.03 : 0.02	0.82151	0.4230
	T. boeoticum	1.63 : 1.54	0.19 : 0.17	0.34394	0.7400
	T. araraticum	1.46 : 1.79	0.16 : 0.23	-1.19964	0.2680
	T. durum	4.62 : 4.40	0.25 : 0.15	0.754845	0.4710
	T. aestivum	3.14 : 2.70	0.08 : 0.18	2.220871	0.0715
	G. max	5.54 : 5.36	0.64 : 0.52	0.22218	0.8310

	S. lycopersicum	5.48 : 5.16	0.41 : 0.16	0.714919	0.5060
SPAD	*T. aestivum*	48.9 : 30.1	4.31 : 4.94	2.87064	0.0212 *
	T. durum	64.2 : 64.1	2.66 : 1.59	0.00244	0.9810
	G. max	35.4 : 32.4	1.30 : 1.34	1.61154	0.1460
	S. lycopersicum	47.8 : 45.0	1.22 : 0.44	2.2421	0.0743
$\Delta\ ^{13}C$ %	*B. distachyon*	39.6 : 36.2	0.22 : 1.50	2.2323	0.1500
	B. distachyon (SID)	24.6 : 28	0.46 : 2.79	-1.2033	0.3470
	T. boeoticum	59.4 : 59.1	0.20 : 1.78	0.9573	0.3670
	T. araraticum	58.7 : 58.1	0.23 : 0.29	1.6711	0.1350
	T. durum	41.7 : 38.9	0.48 : 1.16	2.2992	0.0569
	T. aestivum	57.9 : 57.6	0.32 : 0.18	0.9142	0.3940
	G. max	48.9 : 51.3	0.56 : 0.21	-3.9999	0.0099 *
	S. lycopersicum	49.4 : 48.1	0.64 : 0.52	1.4947	0.1750

4.2.3. Droughted plants grown under fluctuating light show a penalty in biomass accumulation

The experiments described above, revealed an overall lack of differences in either water-use or plant biomass acquisition between plants grown at constant or fluctuating light conditions. This raised the question of whether stomatal speed is important to plant growth. To investigate further, the experiments were repeated with the three *Triticeae* species which showed large variation in stomatal response speeds (*T. boeoticum, araraticum* and *durum*), under water stress conditions. In this second experiment plants were grown under constant or fluctuating light conditions and drought stress was imposed from 3 weeks after sowing. The aim was to investigate whether the speed of stomatal response might be more important for plants growing under conditions where water is limiting.

To understand the relationship between water-use and stomatal speed, the difference in water loss between plants grown under constant and fluctuating light during drought was examined (**Figure 4.6A**). There was found to be no significant difference in pot water lost between plants grown at constant or fluctuating light for any of the species examined when plants were droughted (*t* test, $P > 0.05$; **Table 4.2**).

In order to compare the WUE of plants, carbon isotope discrimination of leaves was analysed after the plants had been grown under water restricted conditions for a further 2 weeks (**Figure 4.6B**). In this experiment, there was also found to be a significant difference in leaf carbon isotope discrimination between plants grown under a constant light regime and those grown under a dynamic light regime (*t* test, $P > 0.05$; **Table 4.2**). All three species grown under fluctuating light were found to have a higher carbon isotope discrimination than when grown under constant light.

To examine the impact of a dynamic environment on the photosynthetic capacity during drought, relative chlorophyll content of the leaves was estimated using a SPAD meter (**Figure 4.7A**). Regrettably there was a technical problem with the equipment and the readings for two species were not correctly taken but in the third species *T. durum,* a significant difference was found between constant light and fluctuating light (*t* test, $P < 0.05$; **Table 4.2**). *T. durum* plants had significantly less relative chlorophyll when grown under fluctuating light.

To examine the impact of a dynamic light environment on plant biomass acquisition during drought, plants were harvested, and their dry biomass was measured (**Figure 4.7B**). There was found to be a statistically significant difference in plant biomass gained between species grown at constant light and those grown under fluctuating light (*t* test, $P < 0.05$; **Table 4.2**). In all 3 species, plants accumulated substantially less dry biomass when grown under fluctuating light and drought conditions, with plants achieving on average 46.4% less biomass.

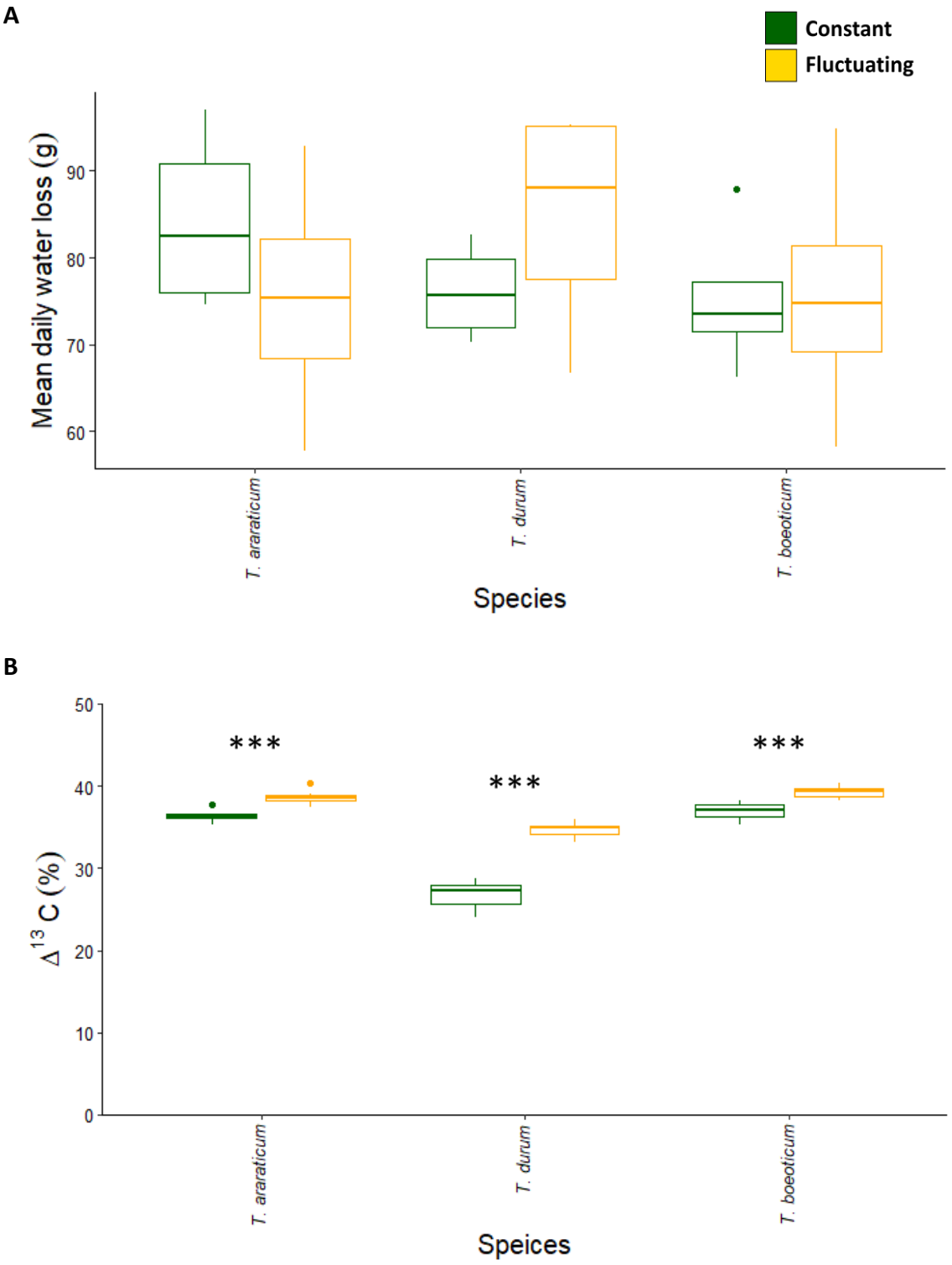

Figure 4.6. There is no difference in mean water loss between plants grown at constant light or fluctuating light in drought conditions, but plants grown under fluctuating light are less water use efficient
A) A) Mean daily water loss over 7 days across species. **B)** Mean carbon isotope discrimination between species. Plants were grown under constant (green) and fluctuating (gold) light. Asterisks indicate significant differences (* indicates *p*=<0.05, *** indicates *p*=<0.001). Data shown are the mean ± SE. n = minimum of 6 per species.

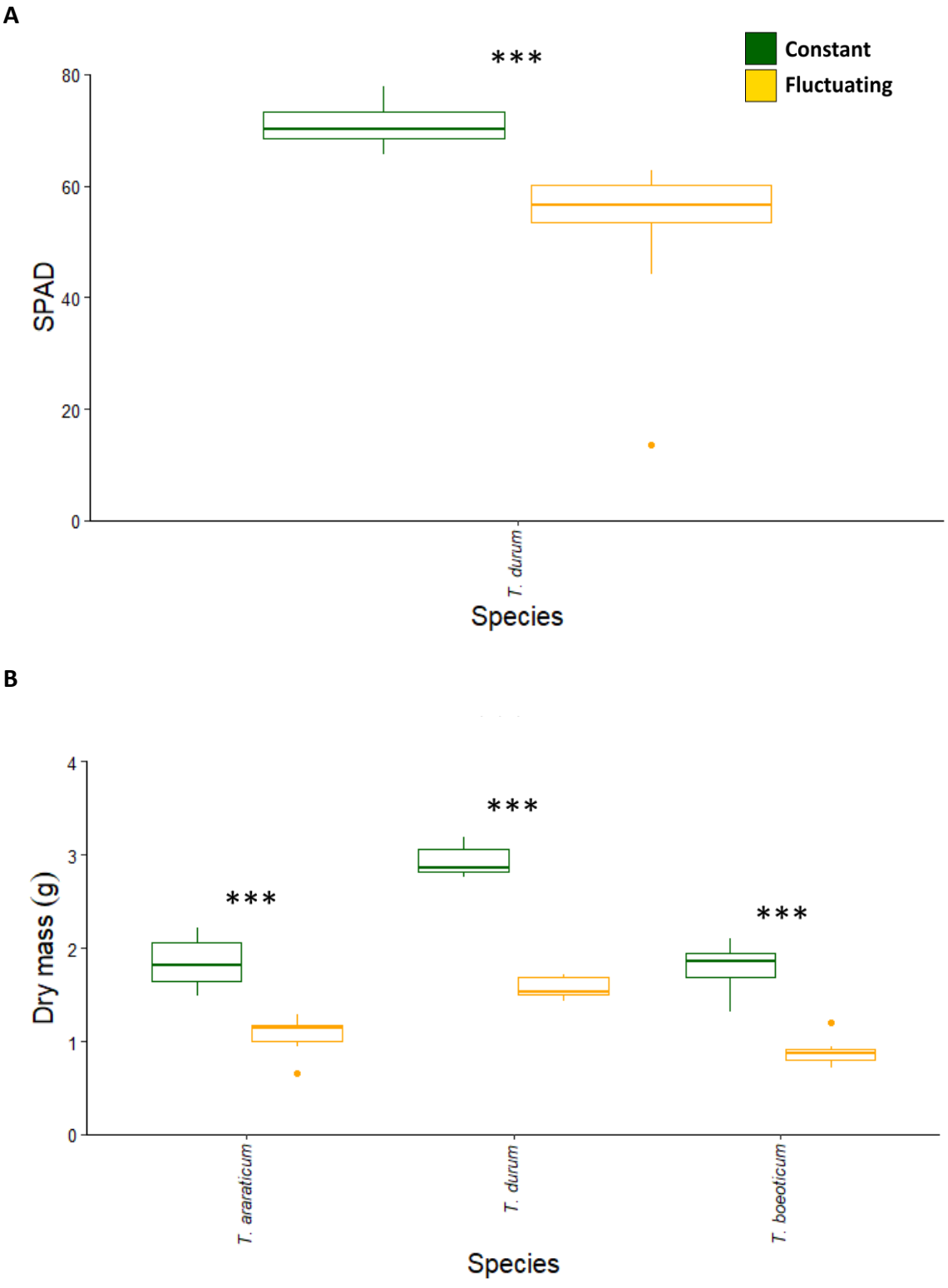

Figure 4.7. There is variation in dry mass acquisition and leaf chlorophyll between plants grown at constant light and fluctuating light while droughted.
A) Mean relative chlorophyll of leaf 6 and **B)** mean 7 week old dry mass plants were grown under constant (green) and fluctuating (gold) light. Asterisks indicate significant differences (* indicates p=<0.05, ** indicates p=<0.01 *** indicates p=<0.001). Data shown are the mean ± SE. n = minimum of 6 per species.

Table 4.2. *t-test* significance values by parameter for droughted plants
Each row indicates a *t-test* significance value between plants grown in a constant or dynamic light environment. Asterisks indicate significant differences (* indicates *p*=<0.05, ** indicates *p*=<0.01, *** indicates *p*=<0.001)

Parameter	Species	Mean (C:F)	SE (C:F)	T statistic	P value
Daily water loss	*T. boeoticum*	75.3 : 75.7	4.54 : 7.55	-0.04781	0.964
	T. araraticum	84.2 : 75.3	5.30 : 7.30	0.98233	0.367
	T. durum	76.1 : 84.5	2.86 : 6.80	-1.1478	0.315
Dry mass	*T. boeoticum*	1.79 : 0.89	0.10 : 0.06	7.53164	0.000004 ***
	T. araraticum	1.85 : 1.06	0.10 : 0.08	6.01664	0.000008 ***
	T. durum	2.94 : 1.58	0.06 : 0.04	17.8900	0.00001 ***
SPAD	*T. durum*	3.24 : 10.8	0.72 : 2.35	6.85139	0.00001 ***
ΔC^{13}	*T. boeoticum*	36.9 : 39.2	0.43 : 0.29	-4.46217	0.00005 ***
	T. araraticum	36.4 : 38.7	0.28 : 0.36	-5.07166	0.0011 ***
	T. durum	26.7 : 34.7	0.67 : 0.35	-10.5052	0.000006 ***

4.2.4. Plant traits associated with carbon capture and water use efficiency show no correlation with stomatal speed metrics under well-watered conditions.

To investigate whether this is a relationship between stomatal response speed and other parameters, such as plant growth, a correlation analysis was performed. To remove any impact that differences in species size might have on the results, percentage changes in plant growth and water-use metrics between constant and fluctuating light were used (**Figure 4.8A**). In the well-watered experiment, it was found that there was a strong statistically significant correlation between k_{op} and k_{cls} (Pearson correlation, $r^2 = 0.92$, $P < 0.05$). There was also found to be a strong statistically significant correlation between Sl_{max} during opening and closure (Pearson correlation, $r^2 = 0.83$, $P < 0.001$). There was also a statistically significant strong negative correlation between Sl_{max} and t during opening and closure (Pearson correlation, $r^2 = -0.78$, $P < 0.05$; Pearson correlation, $r^2 = -0.90$, $P < 0.05$, respectively).

There was found to be no significant correlation between any of the stomatal speed metrics (Sl_{max} and k) and any of the measures of plant growth ($\Delta^{13}C$, biomass accumulation and water loss) under well-watered conditions (Pearsons correlation, $P > 0.05$; **Figure 4.8A**). Under drought conditions, there was found to be a significant correlation between stomatal closure metrics (Sl_{max} and k) and water loss, with $Sl_{max\ cls}$ positively correlated and k_{cls} negatively correlated with pot water loss under drought (Pearsons correlation, $P < 0.05$; **Figure 4.8B**). Neither biomass accumulation or carbon isotope discrimination were correlated with metrics of stomatal response speed (Pearsons correlation, $P > 0.05$) under drought.

A

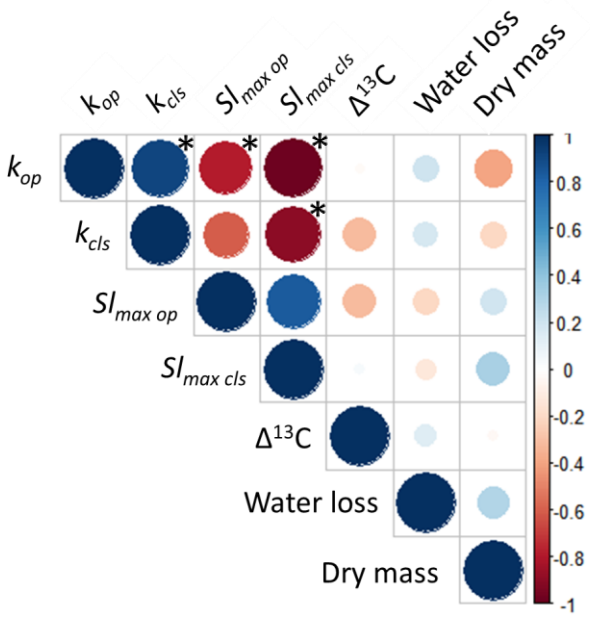

B

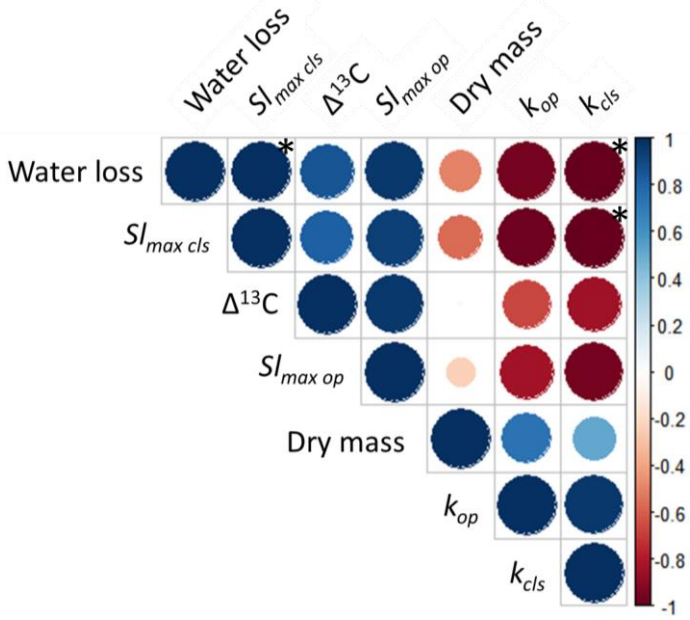

Figure 4.8. There is a strong correlation between opening and closing parameters, but no correlation between stomatal response speed and biomass acquisition or water use

A) Correlation plot between stomatal response metrics and measures of plant health and water use under well-watered conditions and **B)** drought conditions. Well-watered plot represents data from all 8 species, and the drought plot represents data from 3 *Triticeae* species. Positive correlations are shown in blue, negative correlations are shown in red. * indicate significant relationships ($P < 0.05$).

4.2.5. *T. aestivum* grown under dynamic light shows no difference in stomatal response speed

To test whether the growth light environment has an impact on the ability of stomata to respond to a change in light intensity, *T. aestivum* plants were grown at either constant or fluctuating light for 4 weeks and then were subjected to a light shift in an IRGA chamber (outlined in Chapter 3, methods). *T. aestivum* was selected due to its importance globally as a crop plant. *T. aestivum* plants responded to an increase in light intensity by rapidly increasing *A*, and more slowly increasing $g_{s,}$ as expected (**Figure 4.9A-B)**. Although the graphs in **Figure 4.11** appear to show that plants had higher gas exchange capacity following growth under fluctuating light there were no statistically significant differences in steady state g_s at high light (after 85 minutes at 1000 µmol $m^{-2}s^{-1}$) between plants previously grown under a constant daytime light or those grown at fluctuating light (*gs* = 0.48 and 0.52 µmol $m^{-2}s^{-1}$ respectively; unpaired *t* test, $t_{(8)}$ = -0.398, *P* = 0.318). Likewise, at low light (100 µmol $m^{-2}s^{-1}$) there was found to be no statistically significant difference in steady state g_s between plants grown previously under a constant daytime light or those grown at fluctuating light (0.192 and 0.202 µmol $m^{-2}s^{-1}$ respectively; unpaired *t* test, $t_{(8)}$ = -1.065, *P* = 0.700). There was found to be no significant difference in steady state *A* at high light between the constant or fluctuating light treatments (unpaired *t* test, $t_{(8)}$ = -0.549, *P* = 0.598). Again, at low light there was no significant difference in *A* between plants grown at constant light or fluctuating light (unpaired *t* test, $t_{(8)}$ = -0.209, *P* = 0.840).

There was found to be no significant difference in $Sl_{max\ op}$ between *T. aestivum* grown under constant or fluctuating light (unpaired *t* test, $t_{(8)}$ = 0.4227, *P* = 0.6837; **Figure 4.10B**). $Sl_{max\ cls}$ also showed no significant difference during close between *T. aestivum* grown under constant or fluctuating light (unpaired *t* test, $t_{(8)}$ = -0.09213, *P* = 0.9293; **Figure 4.11B**). There was found to be no significant difference in k_{op} between *T. aestivum* grown under constant or fluctuating light during opening in response to a step change in light (unpaired *t* test, $t_{(8)}$ = -1.289, *P* = 0.2534; **Figure 4.10A**). k_{cls} during closing also showed no significant difference during close between *T. aestivum* grown under constant or fluctuating light (unpaired *t* test, $t_{(8)}$ = -0.3468, *P* = 0.7378; **Figure 4.11B**).

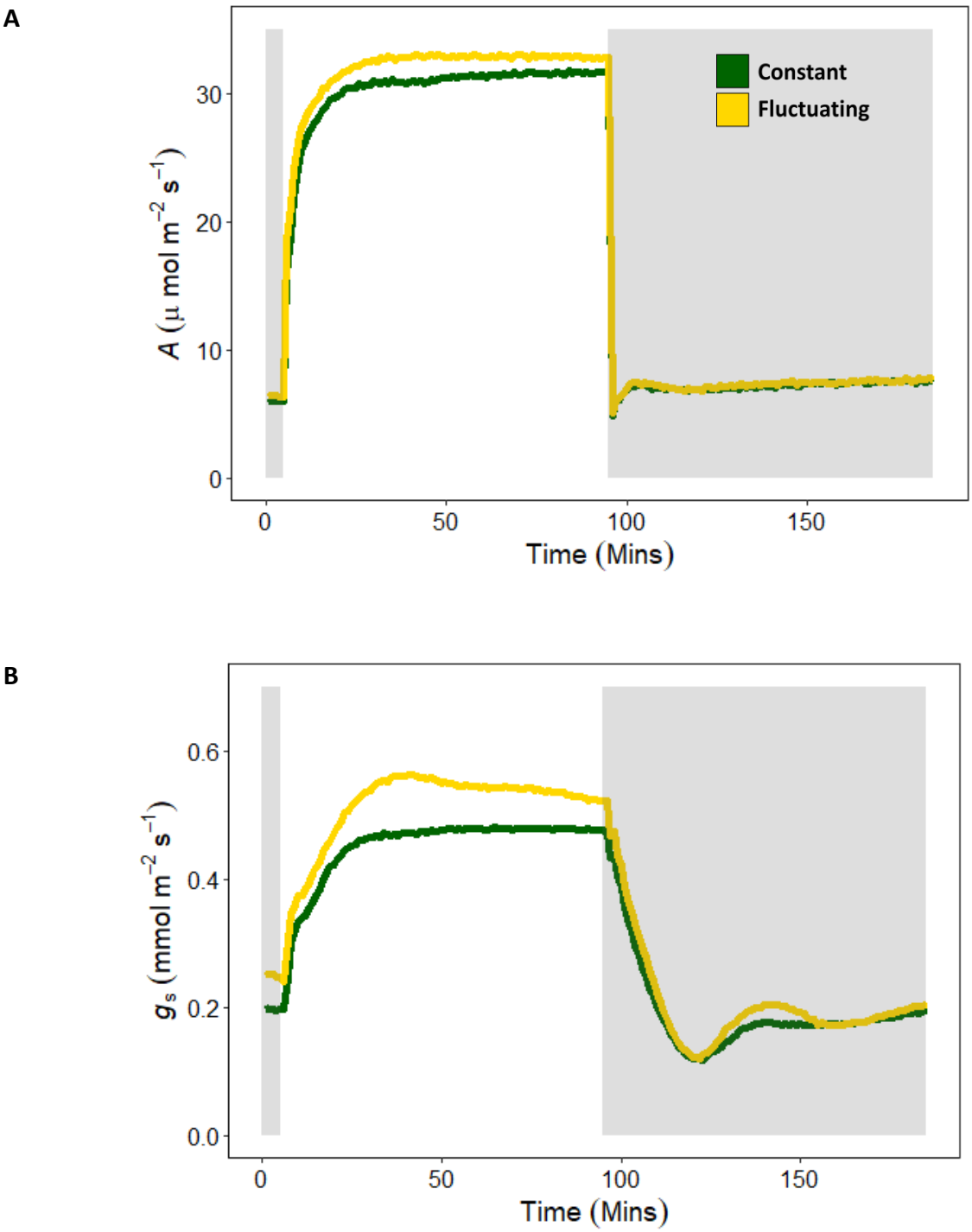

Figure 4.9. Temporal responses of *A* and g_s of plants previously grown under constant and fluctuating light. **A)** Response of carbon assimilation and **B)** stomatal conductance to a change in light intensity from 5 minutes at 100 µmol $m^{-2}s^{-1}$ (shaded area) to 1000 µmol m^{-2} s^{-1} for 90 minutes, followed by a decrease to 100 µmol $m^{-2}s^{-1}$ for 90 minutes. Colours represent plants grown under constant light (green) and fluctuating light (gold). Data shown are the mean (n = 4).

A

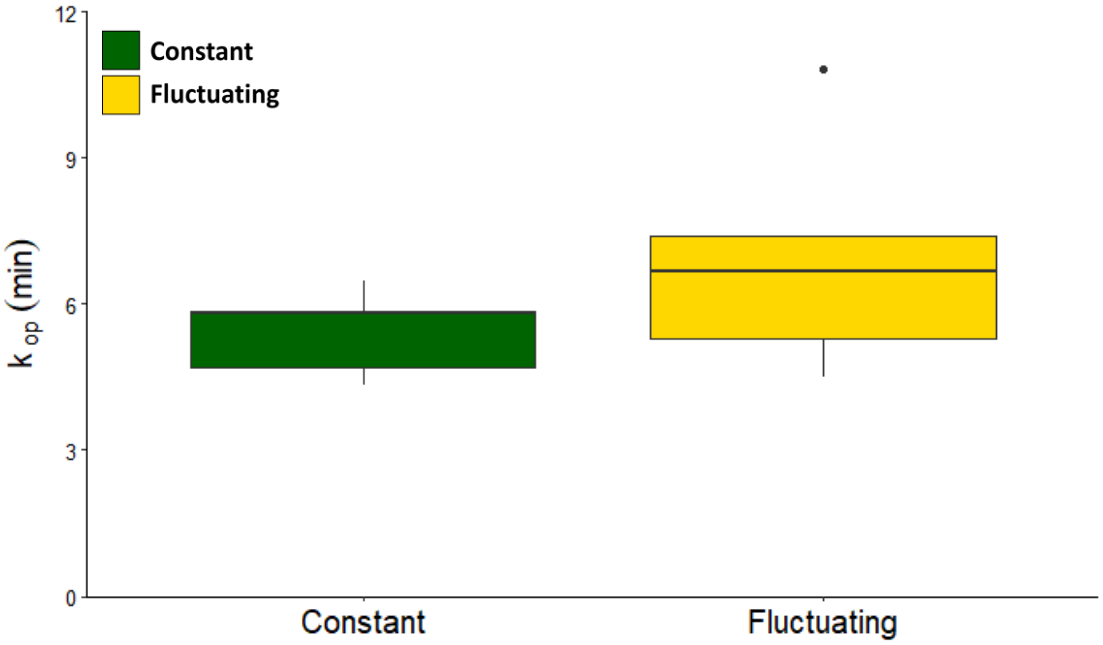

B

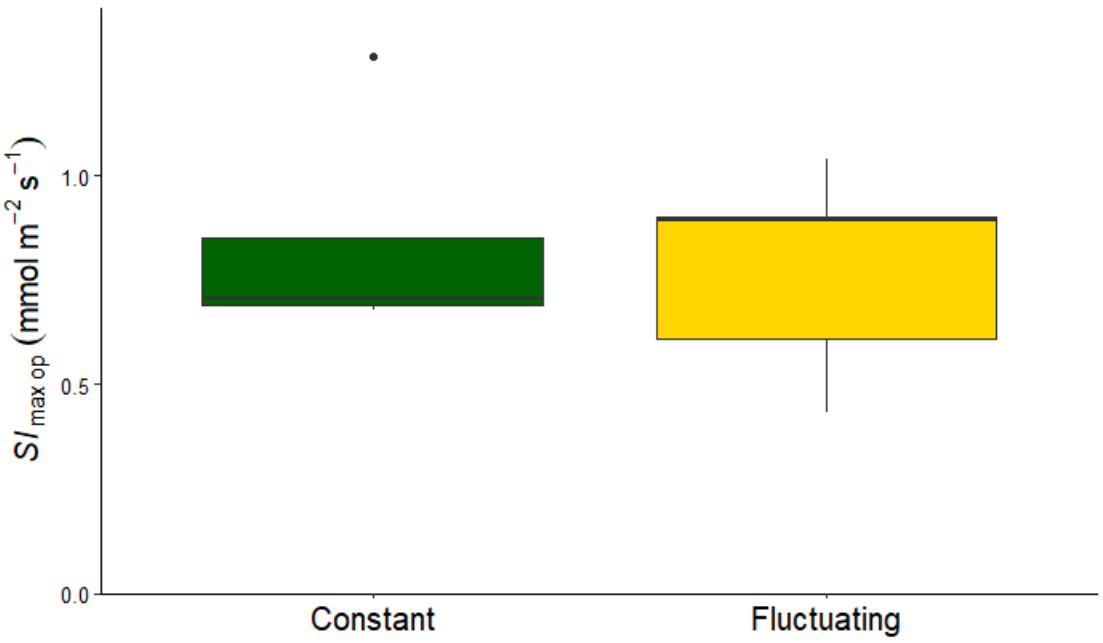

Figure 4.10. Stomatal opening parameters in response to a step change in light show no difference between plants grown under constant light or fluctuating light

A) Mean time constant and **B)** Sl_{max} during stomatal opening for plants grown under constant (green) and fluctuating (gold) light. Data shown are the mean ± SE (n = 4).

A

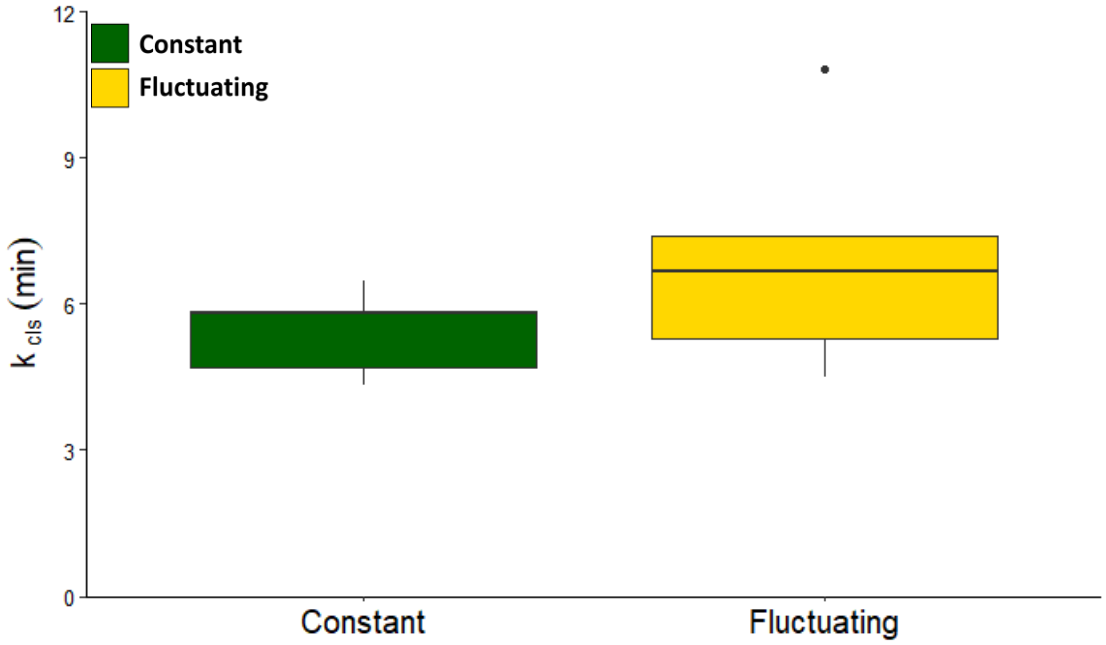

B

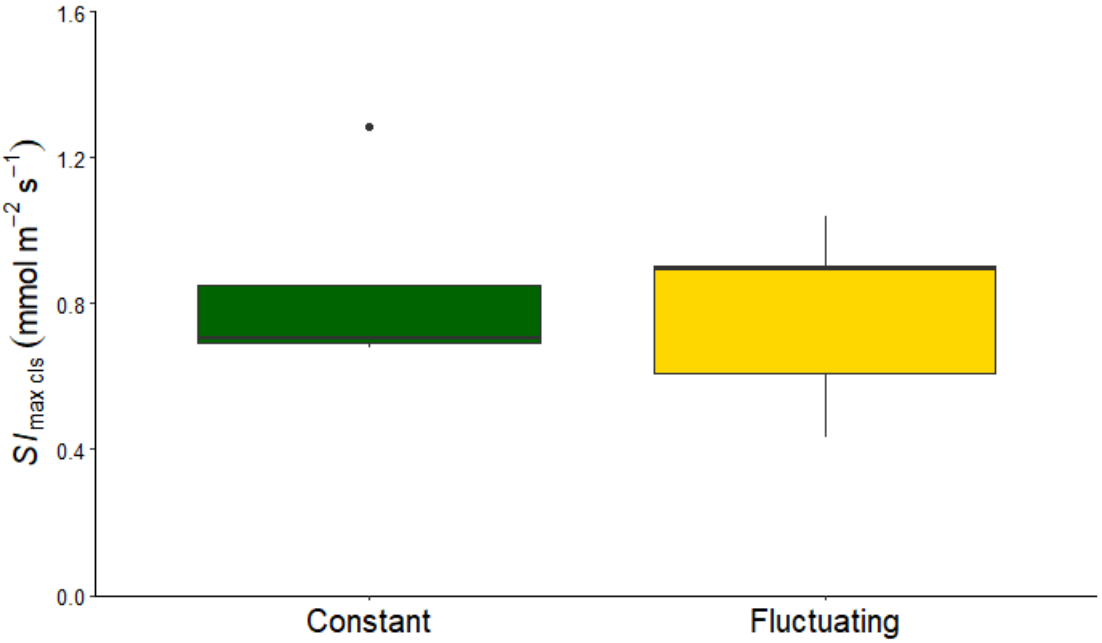

Figure 4.11. Stomatal closing parameters in response to a step change in light show no difference between plants grown under constant light or fluctuating light

A) Mean time constant and **B)** Sl_{max} during stomatal closure for plants grown under constant (green) and fluctuating (gold) light. Data shown are the mean ± SE (n = 4).

4.3. Discussion

It has been suggested that in a dynamic environment, particularly fluctuating light, faster stomatal responses should convey an advantage. By allowing plants to quickly maximise the photosynthetic potential of sudden increases in incident light on the leaf surface, rapid stomatal opening is thought to improve photosynthetic output. Fast stomatal closure is thought to improve water use efficiency by quickly closing stomata during rapid onset of periods of low light intensity, limiting superfluous water loss as assimilation rate rapidly decreases. This chapter aimed to explore the importance of a rapid stomatal response by utilising natural variation in stomatal response speeds from a variety of species and a light regime replicating real world conditions.

4.3.1. Plants grown in a dynamic light environment show no penalty in carbon acquisition and WUE in well-watered conditions

The importance of stomata in responding to environmental conditions has long been documented, however the vast majority of studies examining plant gas exchange have been done in static conditions (Gay and Hurd., 1975; Terashima *et al*., 2006; Lawson and Blatt, 2014). Typically, light has simply been turned on and off to replicate day/night cycles. These conditions do not accurately represent the dynamic environment in which plants exist and in which modulation of the stomatal aperture is thought to be most important (Pearcy *et al*., 1990; Slattery *et al*., 2018). Consequently, there has been increasing interest in understanding how plants respond in more variable conditions that more accurately represent field conditions.

The growth light environment has been documented to impact plants, with those grown under high light tending to have more Rubisco and an altered ratio of photosystem I and II (Bailey *et al*., 2001). *A. thaliana* plants grown under fluctuating conditions have been shown to have no difference in Rubisco per leaf area, but develop thinner leaves compared to constant light conditions (Vialet-Chabrand *et al*., 2017). This suggests a higher Rubisco content per cell. Interestingly plants from the same study achieved a slower initial growth rate and reduced biomass when grown under fluctuating light. Additionally, *A. thaliana* plants, and each of the species examined here, have been shown to not vary in stomatal density between constant and fluctuating light (Matthews *et al*., 2018).

The data presented here provide evidence of the role of environmental context when considering the importance of a rapid stomatal response upon plant success. When plants had access to ample water (70% field capacity soil hydration) there was found to be no difference in the amount of water used, nor the biomass accumulated between constant and fluctuating light environments. It was expected that those plants with faster stomata would lose less water, and see less of a yield penalty, in the dynamic conditions as their faster stomata would enable them to minimise water loss and maximise photosynthesis during repeated stomatal opening and closing throughout the day (Lawson and Vialet Chabrand, 2019). The lower chlorophyll content shown by SPAD readings in *T. aestivum* in fluctuating light are in line with previous observations that protein components associated with light harvesting and electron transport are also decreased in *A. thaliana* plants grown under fluctuating light (Vialet-Chabrand *et al*., 2017). The results for *G. max* and *S. lycopersicum* reported in this chapter showed a similar trend toward lower chlorophyll content but the differences were not statistically significant. While not measured here, the study by Vialet-Chabrand *et al*. (2017) found no difference in the levels of Calvin cycle associated proteins but did find an increase in maximum electron transport rate in *A. thaliana* plants grown under constant daytime light. This could explain the lack of differences in biomass observed here. If the differences in chlorophyll (and potentially electron transport, although not directly measured here) is not matched by an increase in Calvin cycle activity, it might be expected there will be no difference in biomass acquisition between growth light environments, as was observed across all species under well-watered conditions in this study. However, Calvin cycle associated proteins were not directly measured here.

The lack of difference in biomass indicated that, for the conditions in which these plants were measured, stomatal response speed appeared to have no impact on biomass gain. This is possibly due to the high-water availability in the soil. Under well-watered conditions, plants have been documented to maintain g_s above what is necessary at lower light levels, in order to maximise assimilation upon a rapid increase in light (McAusland *et al*., 2016). It might be expected that plants under well-watered and fluctuating light conditions maintain a higher g_s in order to maximise assimilation during constantly changing light. It has previously been suggested that under fluctuating light conditions, plants will maintain open stomata to reduce the limitation of g_s upon A (Ooba and Takahashi, 2003). However, this would inevitably come

at the cost of increased water use. Neither water loss through pot weighing, nor WUE measured through carbon isotope discrimination, indicated any difference in WUE between well-watered plants grown under constant and fluctuating light. Thus, simply maintaining a higher g_s seems unlikely, unless plants were able to quickly close stomata under low light, leading to brief periods of high WUE. No difference in stomatal density was observed between the light environments, indicating no difference in gas exchange potential.

Overall, these results are contrary to previous observations made utilising *A. thaliana* mutants with altered stomatal response speed (Papanatsiou *et al*., 2019; Kimura *et al*., 2020). However, the findings of Watling *et al*. (1997) suggest large, species-specific differences in biomass acquisition responses to fluctuating and constant light. The lack of observed differences reported here may be due to the magnitude of differences in response speed between species used in this study.

4.3.2. Light environment impacts plant biomass acquisition under drought conditions

To further understand the importance of stomatal speeds in dynamic light conditions, plants were subjected to drought conditions (30% field capacity) and various measurements of carbon acquisition and WUE were taken. It was expected that under drought conditions the speed of stomatal response would be more important than in well-watered conditions and therefore, play a more important role in determining plant performance under a fluctuating light regime. It has previously shown that drought in rice, soybean and tomato severely limits the magnitude of stomatal response, although droughted plants did reach steady state values of g_s quicker in tomato compared to plants grown under well-watered conditions (Sakoda *et al*., 2022; Sun *et al*., 2023). Unlike under well-watered conditions, droughted plants accumulated significantly lower biomass under fluctuating light than under constant light conditions. This may be due to the drought imposing a limitation on stomatal pore width and thus capping maximum g_s, as has previously been observed in crop species (Chaves *et al*., 2009; Sakoda *et al*., 2022; Sun *et al*., 2023). This limitation has previously been shown to limit *A,* and consequently plant growth (Pinheiro and Chaves, 2011). Under drought conditions in which maximal stomatal pore area is limited, it is unlikely that droughted plants could maximise the potential photosynthetic output at the high light intensities a fluctuating environment might offer (Grieco *et al*., 2020). Consequently, part of the daily PPFD becomes

unusable by the plant, unlike in the constant light chamber, resulting in reduced biomass. This has previously been observed in tomato, where drought stress has been shown to increase the loss of carbon gain for plants grown under fluctuating light (Sun *et al*., 2023). Further, while drought is well documented to decrease photosynthetic output, the increased stress associated with dissipating excess energy through non-photochemical quenching is likely higher in plants in the fluctuating light environment due to the much higher maximum PPFD (Sakoda *et al*., 2022). *A. thaliana* plants have been shown to increase NPQ during sunflecks, such that the use of additional light during short sunflecks (6-12 minutes) for assimilation is limited (Alter *et al*., 2012). Additionally, wheat plants have been shown to increase NPQ during drought stress (Greico *et al*., 2020). If the reducing power built up by the electron transport chain is not consumed by the Calvin cycle, reactive oxygen species (ROS) can be generated (Lawlor and Tezara, 2009). Indeed, under fluctuating light, droughted wheat plants have previously been shown to be more susceptible to photodamage than well-watered plants (Grieco *et al*., 2020). Interestingly, plants grown under fluctuating conditions showed significantly decreased relative chlorophyll levels in the leaves, potentially due to the limitation on photosynthetic capacity of both the drought and excess light. The combination of decreased photosynthetic capacity (through decreased g_s) and increased NPQ likely results in lower levels of photosynthetic pigments to reduce the risk of oxidative damage (Chaves *et al*., 2009). Thus, decreased chlorophyll as determined by SPAD measurements under drought (and associated photosynthetic proteins not directly measured here) may be an adaptation to limiting damage under water stress. However, these results need repeating with additional species due to technical issues. Plants grown under fluctuating light and drought were shown be less water-use efficient (through carbon isotope discrimination) than those grown under constant light conditions. This is likely due to a reduction in *A,* rather than a decrease in water-use, as no difference in daily water loss could be detected.

Despite the differences observed between constant and fluctuating light environments under drought conditions, there appears to be no relationship between stomatal response speed and CI discrimination or biomass accumulation. This contradicts the theory that faster stomatal responses are beneficial to carbon acquisition in a dynamic environment. There was however, a significant relationship between loss during drought and $SI_{max\ cls}\ k_{cls}$. This supports the theory that fast stomatal closing responses are beneficial for preventing excessive water

loss. It would be interesting to see if this reduced biomass under fluctuating PPFD and drought continued throughout the life of the plant and extended to the final seed mass produced. However, this was not investigated due to time constraints.

It is worth noting that all of the *Triticum* species examined were grown in pots of the same size. The pots were weighed and measured to the same field capacity, so it is possible that the larger species (*T. araraticum*) used up their water more quickly and had a higher relative drought stress. Additionally, repeating these measurements with additional species, with more different stomatal response speeds might provide further insight into the role of a rapid stomatal response under fluctuating PPFD.

4.3.3. Plants grown under a dynamic light environment show no difference in stomatal response speeds

Given the plasticity of plant development in response to environmental conditions, it might be expected that growth under a dynamic light environment would produce plants with more rapid stomatal responses. Therefore, the light responses measurements outlined in chapter 3 were repeated with plants grown at either constant or fluctuating light. There was no difference seen in any of the speed metrics between plants grown at constant or fluctuating light. This is partially in contrast to results observed in *A. thaliana*. In the study by Matthews *et al*. (2018), plants grown at constant or fluctuating light only showing differences in stomatal response speed when measured in the morning. The same experiments carried out later in the day showed no difference in stomatal response between growth conditions (Matthews *et al*., 2018). Woody plants grown under sun and shade conditions (1000 and 100 respectively µmol $m^{-2}s^{-1}$) showed on difference in time taken to respond to a change in light intensity suggesting low plasticity in these responses based on growth conditions (Freitas *et al*., 2023). Interestingly, more variation was observed in stomatal response time across genotypes of the same species in the study by Zhang *et al*. (2022), than seems to be observed based on growth conditions. This potentially suggests that a genetic component underpinning stomatal characteristics is more important that growth conditions.

Interestingly the *T. aestivum* plants showed slight difference in steady state g_s between the light conditions, with plants grown under fluctuating light tending toward having higher steady state g_s at 100 and 1000 µmol $m^{-2}s^{-1}$. This was not matched with higher *A*. This may

be an adaptation to fluctuating light, with plants keeping their stomata slightly more open to anticipate changes in PPFD. The rapid increase in PPFD upon transition from 100 to 1000 μmol $m^{-2}s^{-1}$ likely indicates that g_s under both conditions is above the requirement, as *A* is able to rapidly increase, as has been noted in previous studies (McAusland *et al*., 2016).

Chapter 5. Variation in guard cell wall composition across plant lineages

5.1. Introduction

5.1.1. Guard cell wall

The guard cells of vascular plants must be able to undergo reversible deformation of their cell walls in order to open and close stomata. To facilitate this, guard cells have distinct cell wall compositions, that achieve a strong and flexible structure (Wu and Sharpe, 1979; Amsbury *et al*., 2016; Carter *et al*.,2017; Shtein *et al*., 2017; Woolfenden *et al*., 2017; Rui *et al.,* 2018; Chen *et al*., 2021; Carroll *et al*., 2022; Durney *et al*., 2023). The composition and distribution of plant cell wall polysaccharides have been shown to be important for guard cell function. The composition of cell walls can be analysed and imaged using immunohistochemical techniques with antibodies that bind to specific epitopes. However, the majority of studies investigating guard cell wall composition have only focussed on a few species or a limited number of polysaccharides (Merced and Renzaglia, 2014; Amsbury *et al*., 2016; Carter *et al*.,2017; Shtein *et al*., 2017; Rui *et al.,* 2018; Chen *et al*., 2021; Carroll *et al*., 2022). Whilst these have shown that different species can have different guard cell wall compositions, the diversity of guard cell walls that exists across a broad range of species, spanning multiple clades has not previously been reported. Nor has a comparison between stomatal speed and guard cell wall composition across the land plant phylogeny been previously attempted.

5.1.2. Immunohistochemical approaches to study plant cell wall composition

An extensive collection of monoclonal antibodies specific for particular cell wall epitopes was assembled by the group led by Professor Paul Knox at the John Innes Institute and subsequently at the University of Leeds (JIM and LM antibodies, **Table 2.2**). These have proven useful tools to study plant cell wall components, particularly regarding the spatial distribution of cell wall polysaccharides by immunoloclisation (Jones *et al*., 2003; Amsbury *et al*., 2016; Chen *et al*., 2021; Carroll *et al*., 2022). The immunolabeling technique typically consists of a primary antibody that is specific to a defined epitope bound to a tissue section, and then a fluorescent secondary antibody is then bound that contains a fluorophore that allows visualisation at cellular resolution using a microscope. While such epifluorescence

techniques are useful for visualising tissue sections, quantification of cell wall components can also be done in tissue extracts using systems such as enzyme linked immunosorbent assays (ELISAs). However, while quantitative, ELISA techniques do not provide the same spatial resolution and are therefore less useful to study cell specific patterns.

5.1.3. Aims

Guard cell wall composition remains an area of stomatal biology that is not well understood, particularly outside of the model plant *A. thaliana*. This chapter aims to investigate the diversity of guard cell wall composition across a panel of species with kidney shaped guard cells, utilising a range of antibodies that recognise pectin and hemicellulose. Combining this data with that outlined in previous chapters concerning stomatal speeds, links between cell wall composition and function between species will be investigated. This data will help to determine the cell wall requirements for a functioning stomata, and potential evolutionary trends in guard cell wall composition.

5.2. Results

5.2.1. Kidney-shaped guard cell walls are rich in methyl-esterified HGA

To understand the diversity of guard cell wall composition an immunolabeling screen was carried out on major cell wall components. For clarity, when used here, epidermal cells refer to pavement cells, subsidiary cells and guard cells. Focussing first on pectins, leaf cross-sections were incubated with three antibodies that detect distinct pectin variants: JIM7 (which recognises HGA with a broad range of methyl-esterification patterns); LM19 (un-esterified HGA) and LM20 (methyl-esterified pectin) (see **Table 5.1**). The results are shown in a series of Figures (**Figure 5.1- 5.6**). Staining with calcofluor (blue) was included to indicate the positions of cell walls, and the immunolabelling signal (in green) showed the pattern for each antibody, as indicated. Species were arranged according to the phylogeny in Chapter 3 (**Figure 3.2**).

All species contained some detectable form of HGA in their guard cells with the notable exception of *G. biloba* (the only gymnosperm included in this study), which did not show any

binding from antibodies that recognise HGA in any of its methyl-esterification states (**Figures 5.2**). Signal in the adjacent pavement cells was observed, suggesting that the lack of signal in Ginkgo does not relate to an issue of, e.g., masking by other wall epitopes/structures.

In all other species examined, there was a strong JIM7 signal in the guard cells, suggesting that the guard cells of most plant species contain HGA. The LM19 antibody (un-esterified HGA) did not show any detectable signal in the guard cells of approximately half of the species. Only *A. filix femina*, *I. floridanum*, *M. grandiflora, Glycine. max* and *T. rubra* showed binding to this antibody and in most cases this signal was weak. In contrast, the LM20 antibody (highly methyl-esterified pectin) detected epitopes in the guard cells of all species (with the exception of *G. biloba, as noted above*). However, the signal intensity in guard cells relative to neighbouring cells varied across species. Notably, *O. regalis*, *S. lycopersicum* and *G. soja* had reduced signal in guard cells relative to surrounding cells, whereas *P. americana* showed a binding pattern unique in this data set with a strong guard cell specific LM20 pattern, with little signal in the surrounding cells. Overall, it appears that the strong JIM7 signal that was observed in the guard cells of almost all species reflects a combination of methyl-esterification states of HGA, with a trend for more methyl-esterified HGA in guard cells across evolutionary space. The patterns of HGA and other pectin epitopes in guard cells across these species are summarised in **Table 5.1**.

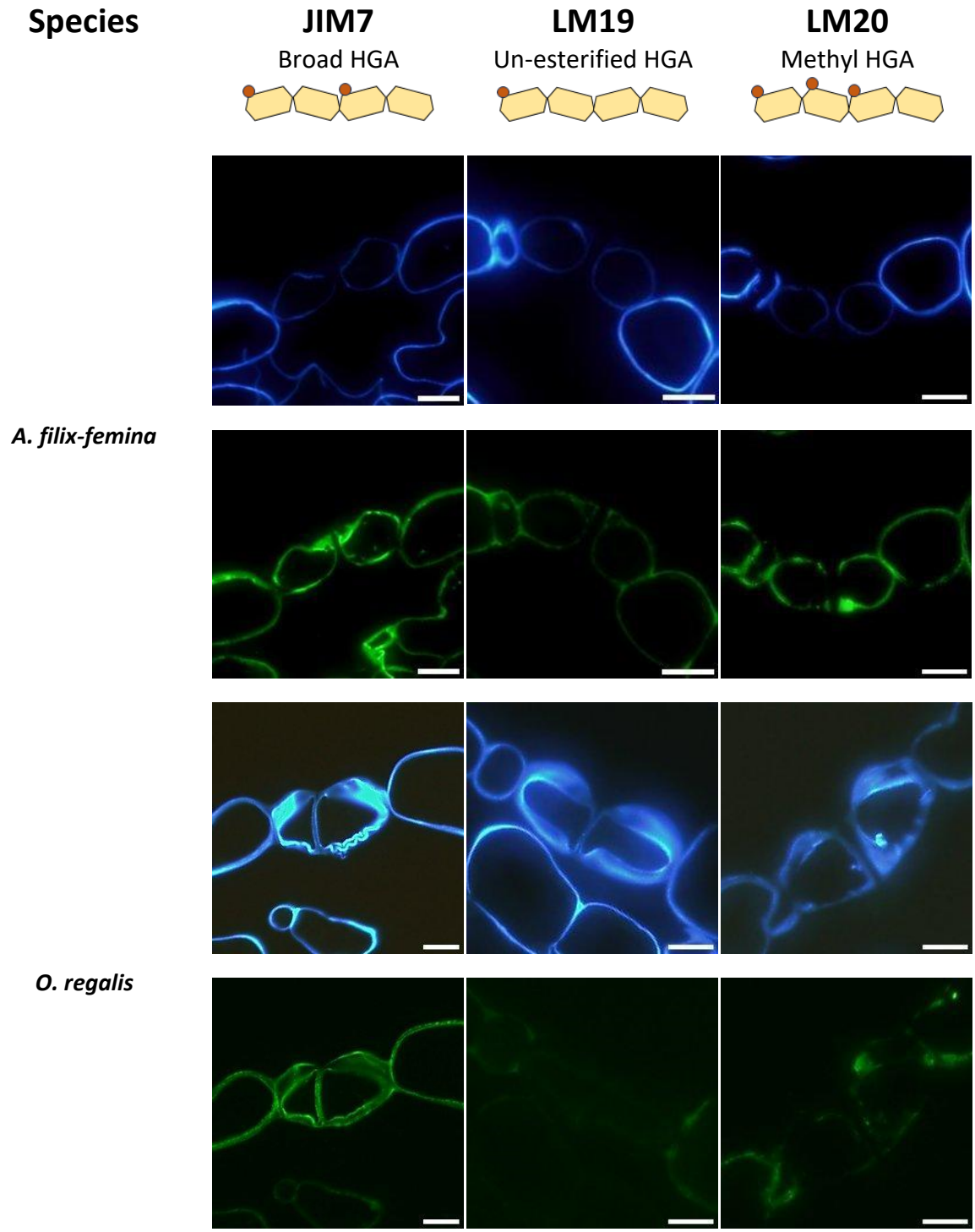

Figure 5.1. Homogalacturonan distribution and methyl-esterification across guard cells of *Athyrium filix-femina* and *Osmunda regalis*.
Cross-sections of epidermal layer of leaf tissue from *A. filix-femina* and *O. regalis* probed with antibodies (as indicated). For each section, the cell wall is indicated by calcofluor staining (blue signal) with the regions of antibody binding indicated in green in the images below. JIM7 binds HGA in a range of methyl-esterification states, LM19 demethy-esterified HGA and LM20 recognises highly methyl-esterified HGA. JIM7 binds to the guard cells of both species. LM19 shows weak binding in the guard cells of A. filix-femina and no binding in the guard cells of *O. regalis*. LM20 showed strong binding in the guard cells of A. filix-femina and weak binding in *O. regalis*. Scale bars = 10 µm. Images are representative of at least 2 biological reps.

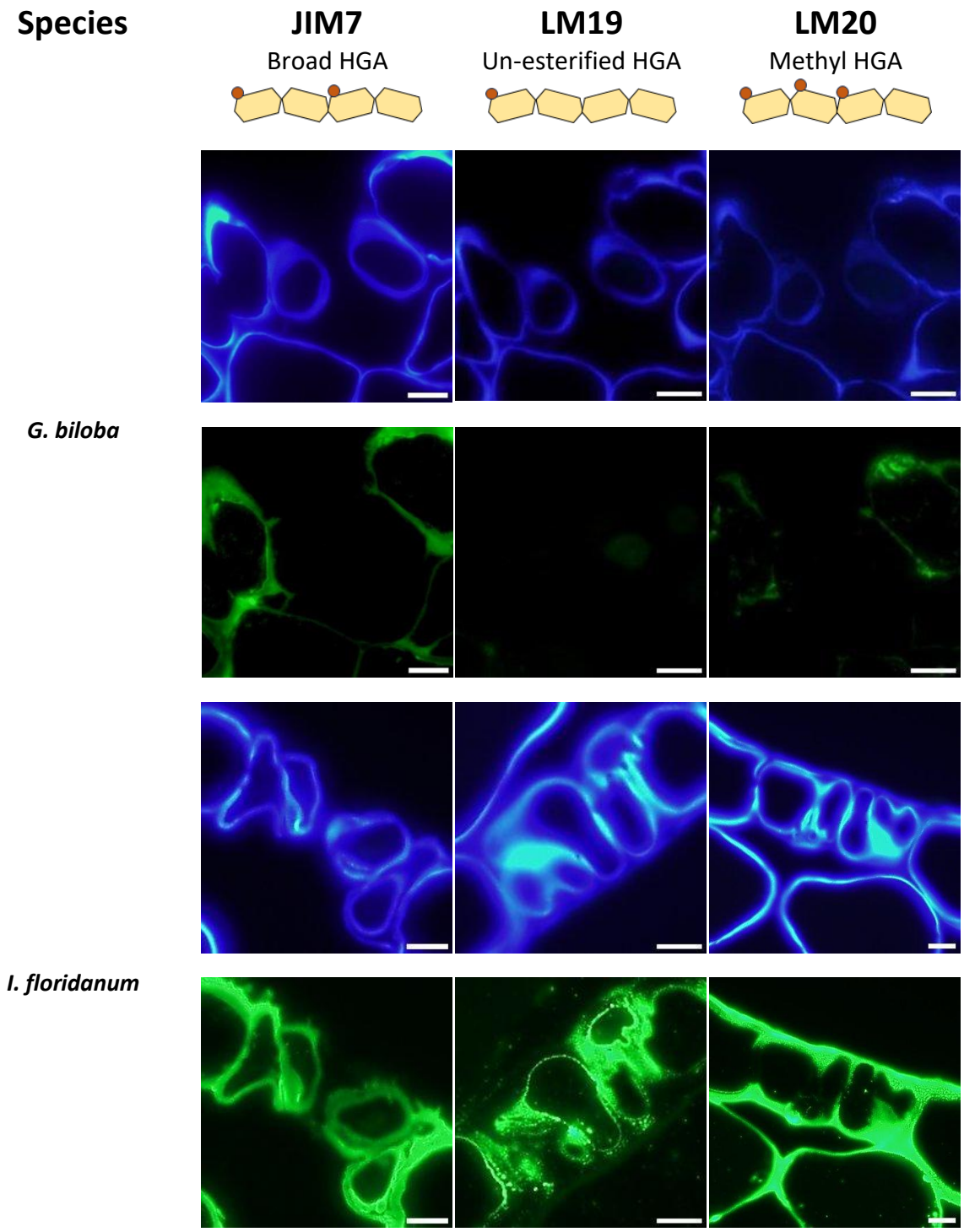

Figure 5.2. Homogalacturonan distribution and methyl-esterification across guard cells of *Ginkgo biloba* and *Illicium floridanum*.
Cross-sections of epidermal layer of leaf tissue from *G. biloba* and *I. floridanum* probed with antibodies (as indicated). For each section, the cell wall is indicated by calcofluor staining (blue signal) with the regions of antibody binding indicated in green in the images below. JIM7 binds to the guard cells of *I. floridanum*, but not *G. biloba*. LM19 shows strong binding in the guard cells of *I. floridanum* and no binding in the guard cells of *G. biloba*. LM20 showed strong binding in the guard cells of *I. floridanum* and no binding in *G. biloba*. Scale bars = 10 µm. Images are representative of at least 2 biological reps.

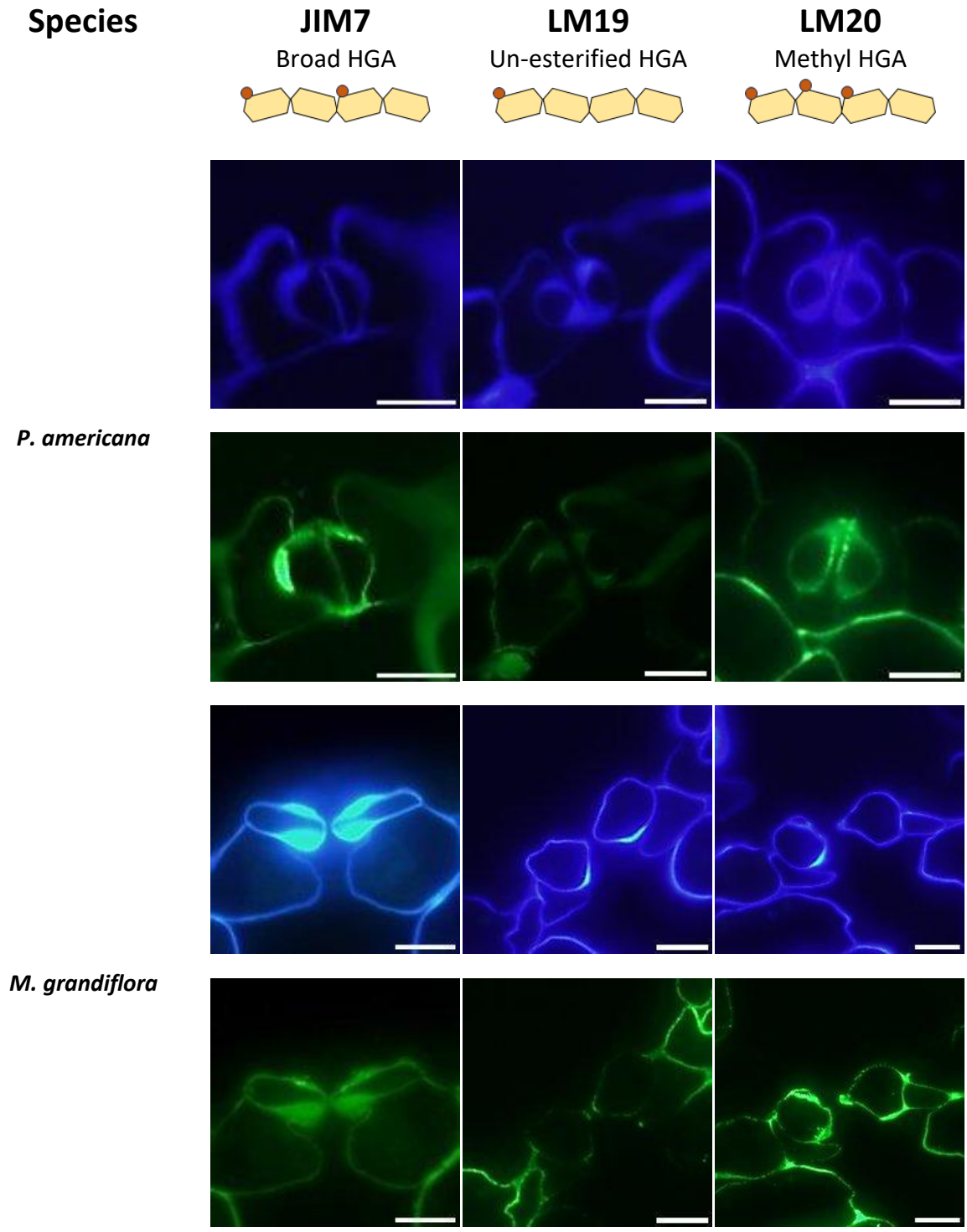

Figure 5.3. Homogalacturonan distribution and methyl-esterification across guard cells of *Persea americana* and *Magnolia grandiflora*.
Cross-sections of epidermal layer of leaf tissue from (name of species) probed with antibodies (as indicated). For each section, the cell wall is indicated by calcofluor staining (blue signal) with the regions of antibody binding indicated in green in the images below. JIM7 binds to the guard cells of both species. LM19 shows weak binding in the guard cells of *P. americana* and *M. grandiflora*. LM20 showed strong binding in the guard cells of *P. americana* and *M. grandiflora*. Scale bars = 10 µm. Images are representative of at least 2 biological reps.

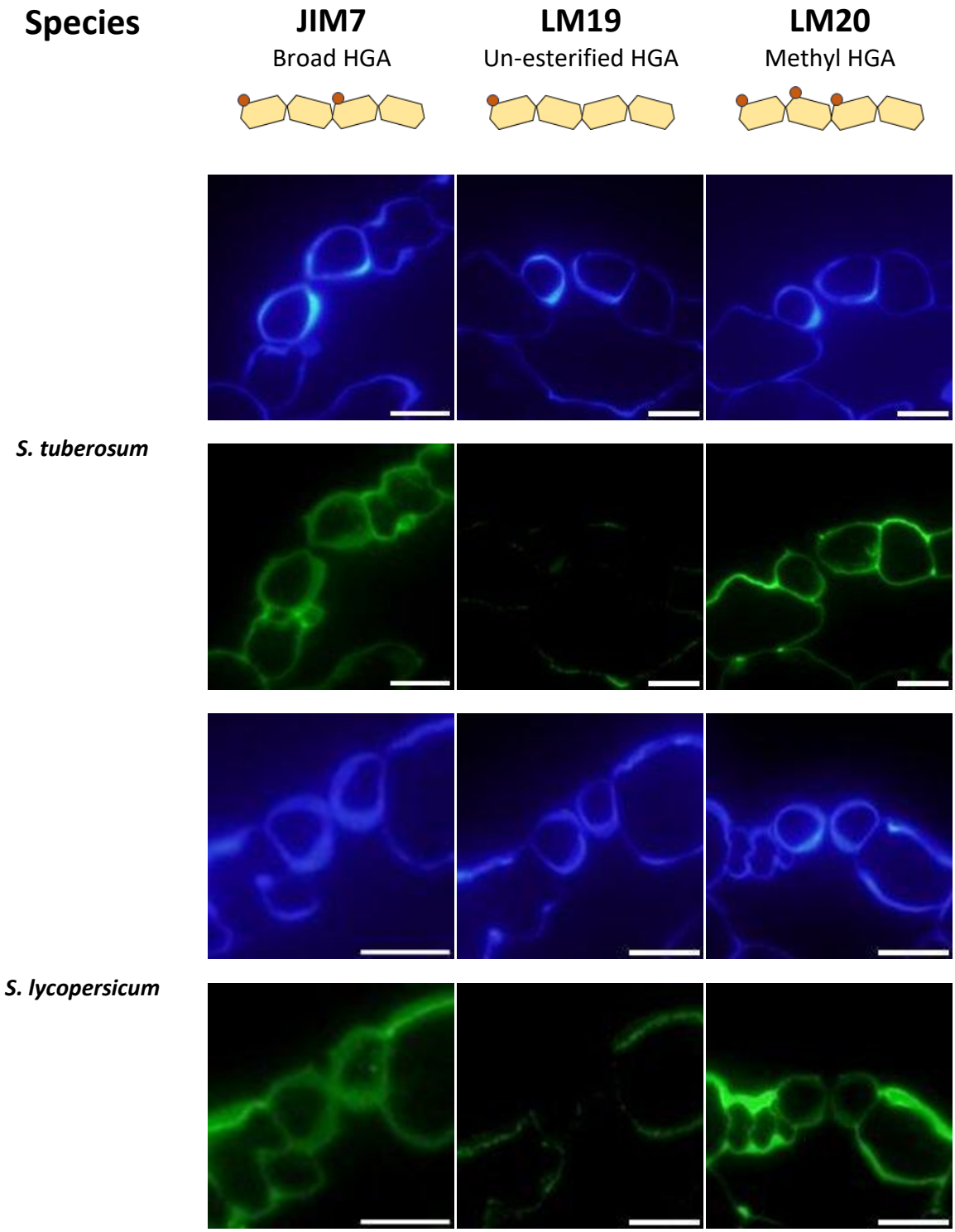

Figure 5.4. Homogalacturonan distribution and methyl-esterification across guard cells of *Solanum tuberosum* and *Solanum lycopersiucm*.
Cross-sections of epidermal layer of leaf tissue from (name of species) probed with antibodies (as indicated). For each section, the cell wall is indicated by calcofluor staining (blue signal) with the regions of antibody binding indicated in green in the images below. JIM7 binds HGA in a range of methyl-esterification states, LM19 demethy-esterified HGA and LM20 recognises highly methyl-esterified HGA. JIM7 binds to the guard cells of both species. LM19 shows no binding in the guard cells of either species. LM20 showed strong binding in the guard cells of *S. tuberosum* and moderate binding in *S. lycopersicum*. Scale bars = 10 µm. Images are representative of at least 2 biological reps.

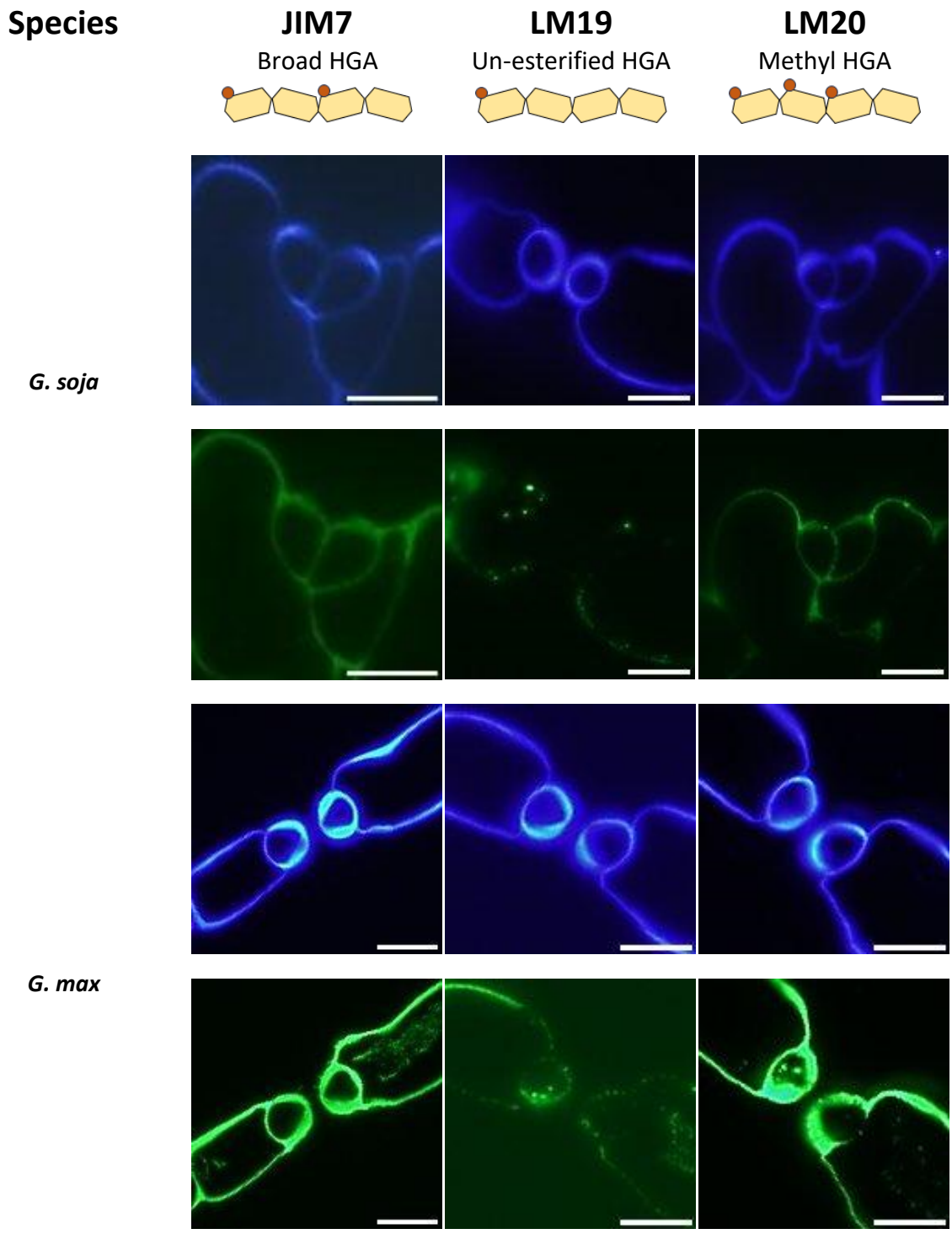

Figure 5.5. Homogalacturonan distribution and methyl-esterification across guard cells of *Glycine soja* and *Glycine max*.

Cross-sections of epidermal layer of leaf tissue from (name of species) probed with antibodies (as indicated). For each section, the cell wall is indicated by calcofluor staining (blue signal) with the regions of antibody binding indicated in green in the images below. JIM7 binds HGA in a range of methyl-esterification states, LM19 demethy-esterified HGA and LM20 recognises highly methyl-esterified HGA. JIM7 binds to the guard cells of both species. LM19 shows weak binding in the guard cells of *G. max* and no binding in the guard cells of *G. soja*. LM20 showed strong binding in the guard cells of *G. max* and weak binding in *G. soja*. Scale bars = 10 µm. Images are representative of at least 2 biological reps.

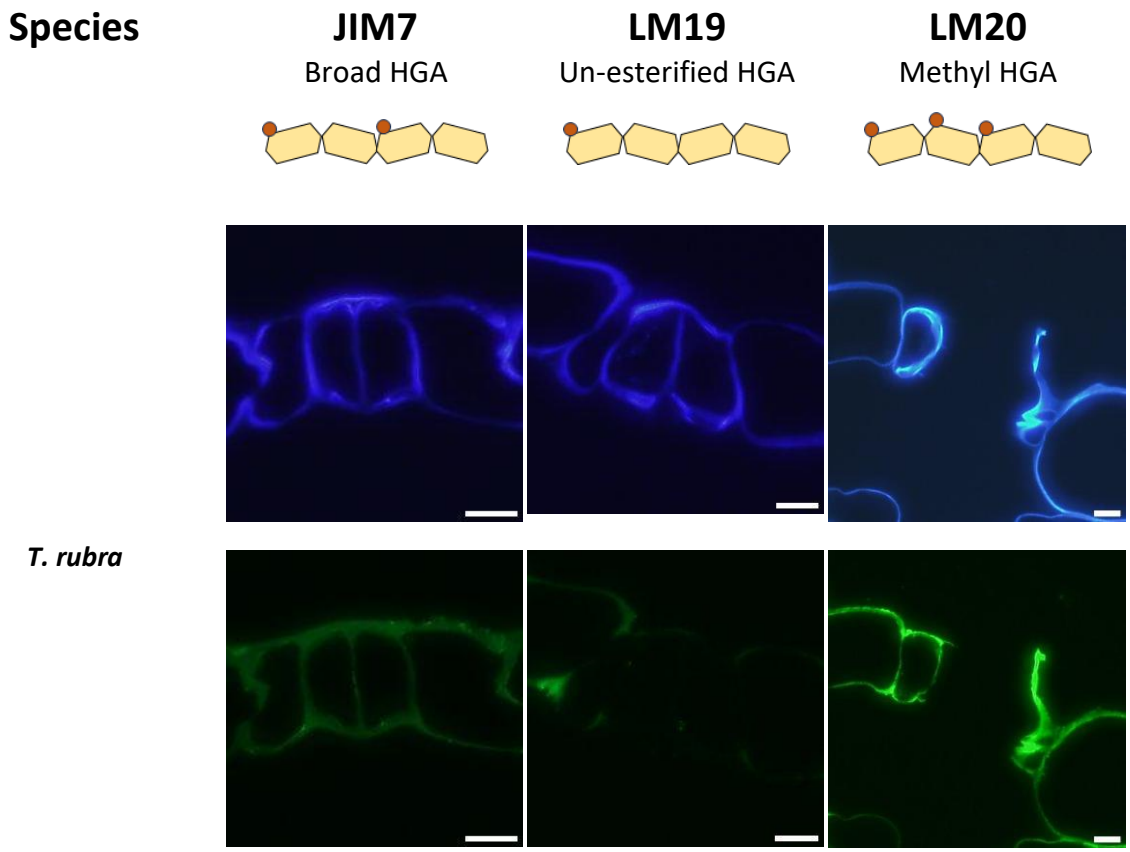

Figure 5.6. Homogalacturonan distribution and methyl-esterification across guard cells of *Tradescantia rubra*. Cross-sections of epidermal layer of leaf tissue from (name of species) probed with antibodies (as indicated). For each section, the cell wall is indicated by calcofluor staining (blue signal) with the regions of antibody binding indicated in green in the images below. JIM7 binds HGA in a range of methyl-esterification states, LM19 demethy-esterified HGA and LM20 recognises highly methyl-esterified HGA. JIM7 bound uniformly to the epidermal cells of *T. rubra*, as did LM20. LM19 bound to pavement cells, but signal was excluded from the guard cells of *T. rubra*. Scale bars = 10 µm. Images are representative of at least 2 biological reps.

5.2.2. Guard cell specific patterns of cell wall pectin are not conserved across species

In addition to methylation/demethylation, pectin can be decorated by extremely complex patterns of sugar moieties, as exemplified in Rhamnogalacturonan I and Rhamnogalacturonan II. To investigate whether there were conserved patterns of epitopes associated with these pectin components, I performed immunolabeling experiments on sections from the same 14 species described above using antibodies which detected some of these epitopes associated with pectin beyond HGA.

LM6M (which binds to short chains of arabinan) was generally not present in epidermal cells with the exception of *Glycine max* where there was a clear guard cell specific signal (**Fig. 5.7**). The wild progenitor species of this crop, *G. soja* displayed a weak signal with this antibody as did all the epidermal cells (including guard cells) in *T. rubra* (**Fig. 5.7**). For clarity, the contrast of the images of *G. soja* and *M. grandiflora* has been altered to enhance the weak signal. Linear arabinan decorations of cell wall polymers can also occur and are recognised by the LM13 antibody). Signal was not observed in any epidermal cells of any species, with the exception of *M. grandiflora*, which showed weak binding across all epidermal cells (**Figure 5.8**).

A guard cell specific signal was observed in the binding of LM5 (which recognised the non-reducing end of galactan) in the fern *O. regalis* (**Fig 5.10**), whereas, both *M. grandiflora* and *P. americana* showed strong binding of this antibody to epidermal cells with the exception of the guard cells (**Fig 5.10**). In contrast, LM26 (which binds to branched galactans decorations of pectin) only showed signal in *O. regalis*, and this was across all epidermal cells with no guard cell specificity or exclusion (**Fig. 5.9**).

For brevity, the immunolocalization results for species that showed no binding have been included in the figures and a summary of all results, comparing the relative intensity of binding to the different guard cell wall components, is shown in **Table 5.1**.

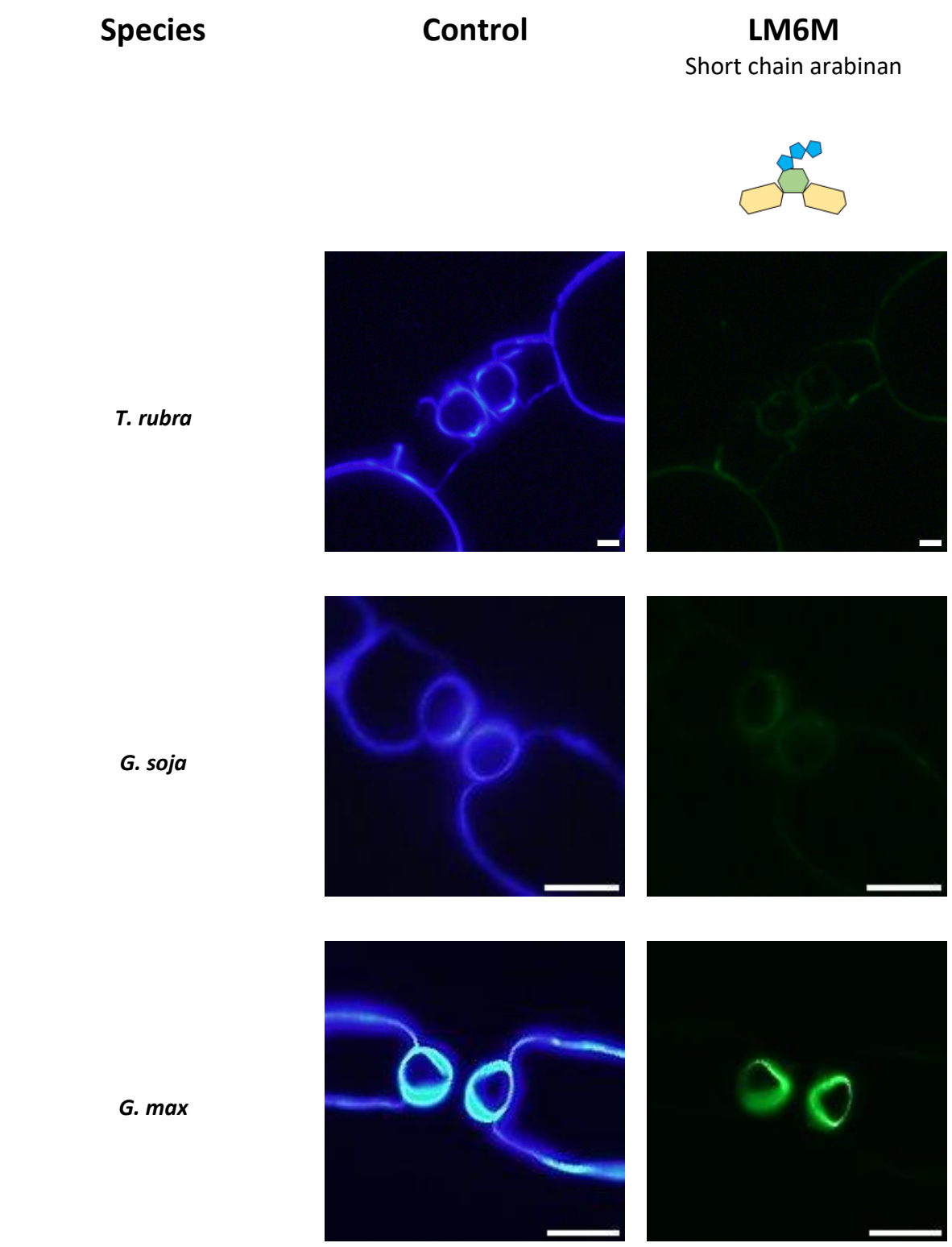

Figure 5.7. Short linear arabinan distribution across guard cells of *Glycine soja* and *Glycine max*. Cross-sections of epidermal layer of leaf tissue from (name of species) probed with antibodies (as indicated). For each section, the cell wall is indicated by calcofluor staining (blue signal) with the regions of antibody binding indicated in green in the images below. LM6M binds to short linear chains of arabinan. LM6M binds weakly across the epidermis of *T. rubra*. Binding in *G. max* appears to be strongly localised to the guard cells and weaky in *G. soja*. Scale bars = 10 µm. Images are representative of at least 2 biological reps.

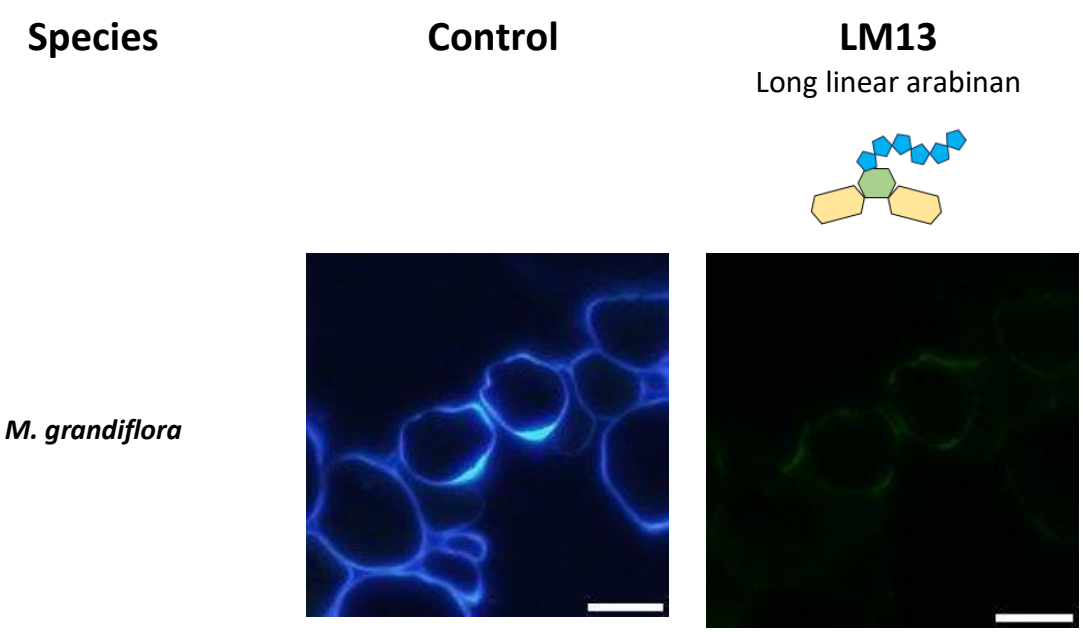

Figure 5.8. Long linear arabinan distribution across guard cells.
Cross-sections of epidermal layer of leaf tissue from (name of species) probed with antibodies (as indicated). For each section, the cell wall is indicated by calcofluor staining (blue signal) with the regions of antibody binding indicated in green in the images below. Blue images show counter staining with counterstain (left). Green images show antibody binding (right). LM13 binds to long linear chains of arabinan. The epidermis of *M. grandiflora* shows weak binding of LM13. Scale bars = 10 µm. Images are representative of at least 2 biological reps.

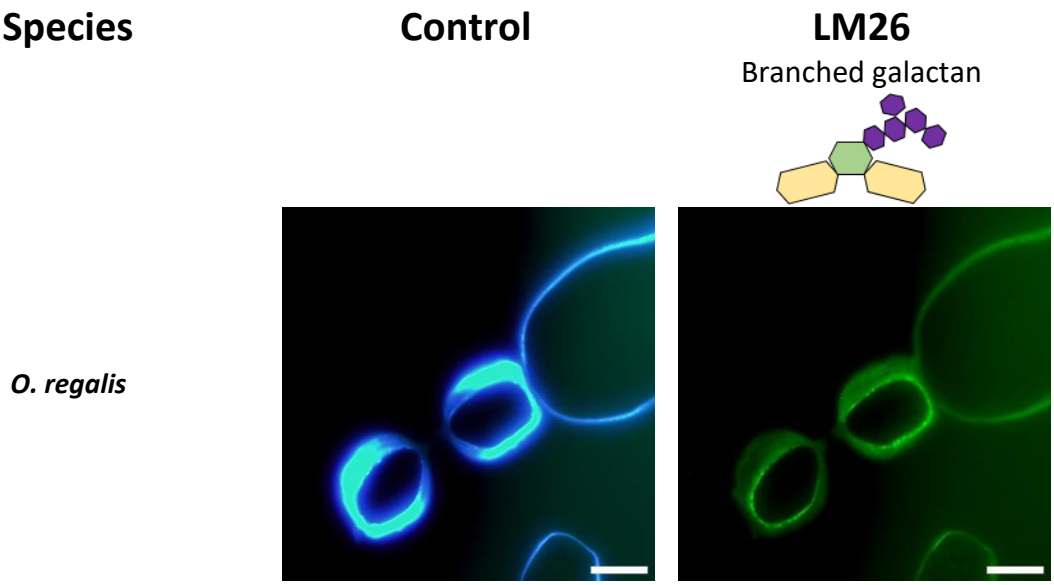

Figure 5.9. Branched galactan distribution across guard cells.
Cross-sections of epidermal layer of leaf tissue from (name of species) probed with antibodies (as indicated). For each section, the cell wall is indicated by calcofluor staining (blue signal) with the regions of antibody binding indicated in green in the images below. LM26 binds to branched galactan. The epidermis of *O. regalis* shows strong binding of LM26. Scale bars = 10 µm. Images are representative of at least 2 biological reps.

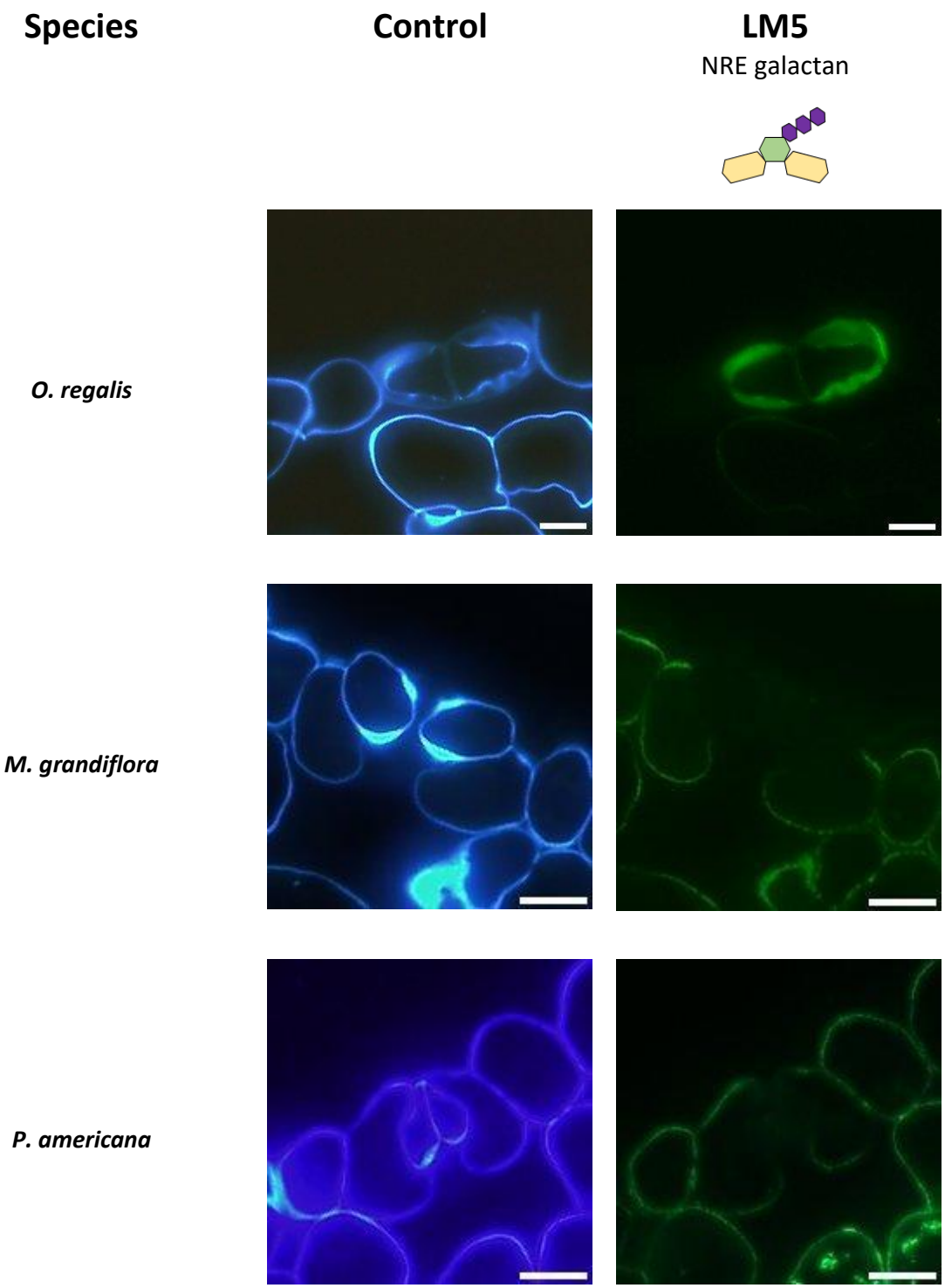

Figure 5.10. Non-reducing end of pectin galactan distribution across guard cells.
Cross-sections of epidermal layer of leaf tissue from (name of species) probed with antibodies (as indicated). For each section, the cell wall is indicated by calcofluor staining (blue signal) with the regions of antibody binding indicated in green in the images below. LM5 binds to the non-reducing end of pectic galactan side chains. The guard of *O. regalis* shows strong binding of LM26 in contrast to surrounding epidermal cells. In contrast, both *M. grandiflora* and *P. americana* have epidermal cells with strong signal for LM5, except the guard cells. Scale bars = 10 µm. Images are representative of at least 2 biological reps

Table 5.1. Guard cell wall pectin content across species.

Summary of guard cell wall pectin from immunolabeling data. Scores for binding intensity were estimated by eye. 1- no signal, 2 - weak signal, 3 = moderate signal and 4 = strong signal in guard cells. * indicate where surrounding epidermal cells show strong signal but not in the guard cell.

Species	JIM7	LM19	LM20	LM6M	LM13	LM5	LM26
A. filix-femina	4	1	2	1	1	4	4
O. regalis	4	2	3	1	1	1	1
G. biloba	1	1	1	1	1	1	1
I. floridanum	3	4	4	1	1	1	1
P. americana	4	3	4	1	1	1	1*
M. grandiflora	3	2	4	2	2	1	1*
S. tuberosum	3	1*	3	1	1	1	1
S. lycopersicum	3	1*	3	1	1	1	1
G. soja	4	2*	3	3	1	1	1
G. max	4	2	4	4	1	1	1
T. rubra	3	1*	4	1	1	1	1

5.2.3. Kidney-shaped guard cells show diverse patterning of xyloglucan

In addition to pectins, cell walls generally contain high levels of xyloglucan, the major hemicellulose of dicots. To describe the diversity in xyloglucan distribution in stomata across species, immunolabelling was carried out on the species described in **Table 5.3** using three antibodies with differing affinity for alternative xyloglucan structures: LM25 binds broadly to xyloglucan with a range of motifs (XXXG, XXLG, XLLG where G is an undecorated glucose, X is a xylose residue, L is a galactose residue and F is a fucose residue), whereas LM15 and LM24 bind more specifically to XXXG and galactosylated motifs, respectively (Pedersen *et al*., 2012). The results are shown in **Figures 5.11- 5.16**).

LM25 bound to all species with the notable exception of the fern *A. filix-femina*, which showed no signal for any of the antibodies against this major class of hemicellulose (**Fig. 5.11**). In other species, although the signal intensity varied slightly, in general there was strong binding of the LM25 antibody in all epidermal cells.

With respect to XXXG motifs, binding of LM15 showed a range of patterns across species. *S. lycopersicum* and *S. tuberosum* showed no detectable signal (**Fig. 5.14**), whereas in *O. regalis, Glycine soja, Glycine max* and *T. rubra* LM15 bound in a guard cell specific pattern (**Figs. 5.11, 15 and 16**). This pattern was extended to include the neighbouring subsidiary cells in *M. grandiflora* but excluded the pavement cells (**Fig. 5.13**). The gymnosperm *G. biloba* showed a reverse pattern of LM15 binding to *M. grandiflora*, with no signal in the guard cells but strong signal in the surrounding epidermal cells (**Fig. 5.13**). In contrast, *I. floridanum* and *P. americana* showed strong binding of LM15 in all epidermal cells (**Fig. 5.12, 13**). With respect to galactosylated motifs, LM24 generally showed weaker signal in epidermal cells than either LM25 or LM15, but there was a guard cell enriched pattern of binding in *I. floridanum* and *P. americana* (and to a lesser extent *T. rubra, G. biloba* and *M. grandiflora*) (**Fig. 5.12, 13 and 16**). The patterns of hemicellulose epitopes in guard cells across these species are summarised in **Table 5.2**.

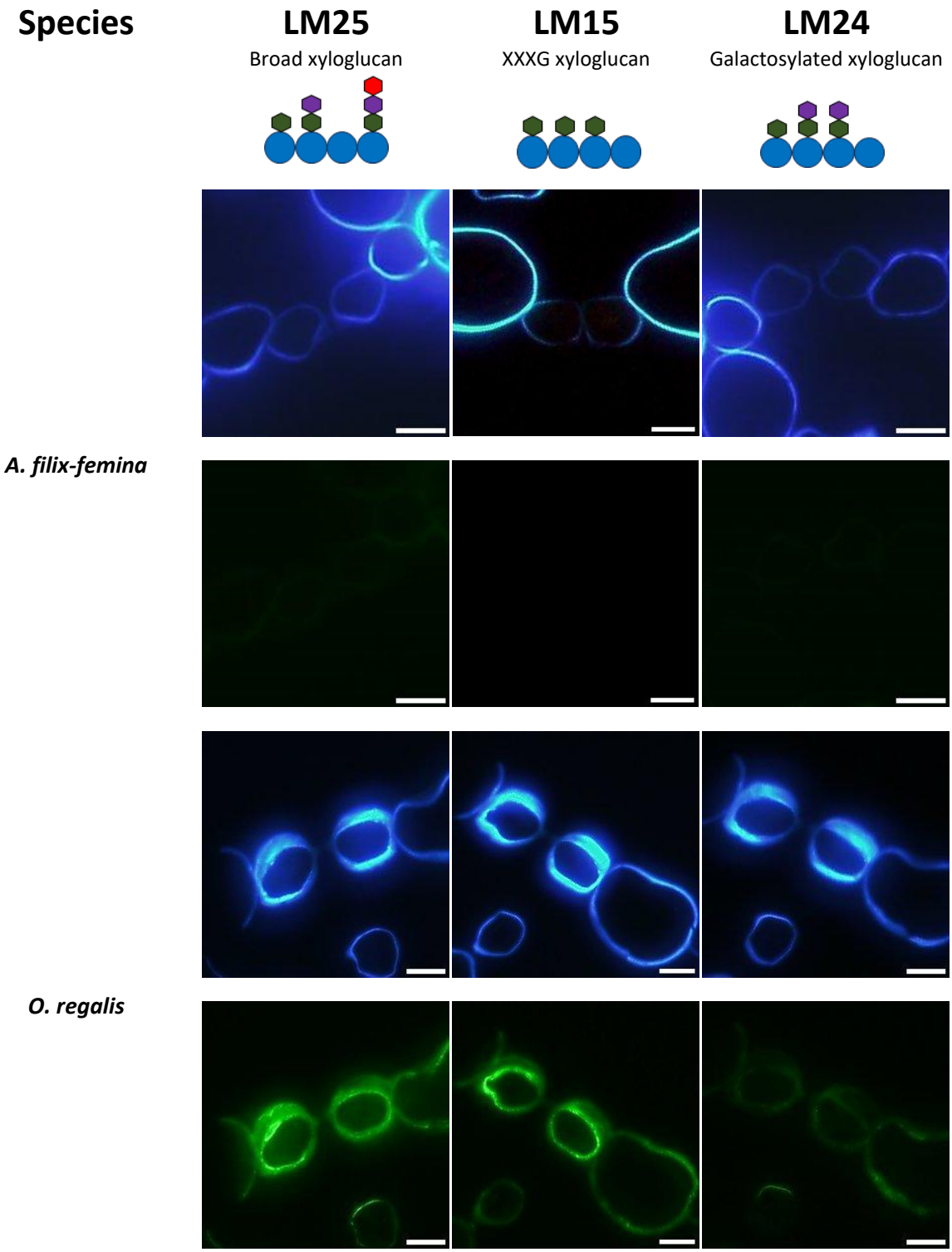

Figure 5.11. Xyloglucan distribution in guard cells of *Athyrium filix-femina* and *Osmunda regalis*.
Cross-sections of epidermal layer of leaf tissue from (name of species) probed with antibodies (as indicated). For each section, the cell wall is indicated by calcofluor staining (blue signal) with the regions of antibody binding indicated in green in the images below. LM25 binds a broad range of xyloglucan compositions, LM15 recognises the XXXG motif and LM24 recognises galactosylated xyloglucan respectively. *A. filix femina* did not show signal from LM25, LM15 or LM24. LM25 and LM24 bind strongly across the epidermis of *O. regalis*. LM24 showed weaker binding across the epidermis of *O. regalis*. Scale bars = 10 µm. Images are representative of at least 2 biological reps.

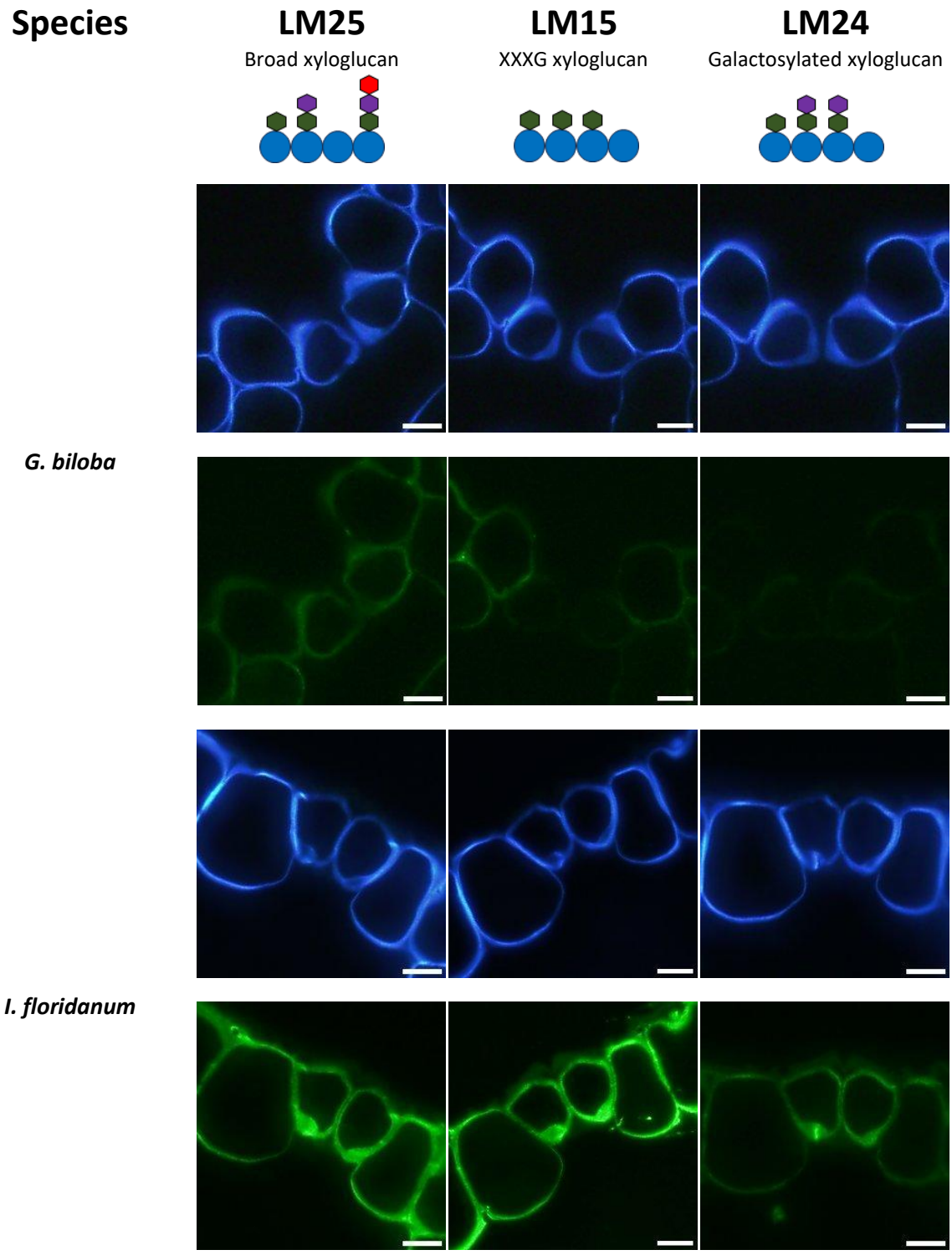

Figure 5.12. Xyloglucan distribution in guard cells of *Ginkgo biloba* and *Illicium floridanum*.
Cross-sections of epidermal layer of leaf tissue from (name of species) probed with antibodies (as indicated). The cell wall is indicated by calcofluor staining (blue signal) with the regions of antibody binding indicated in green in the images below. LM25 binds a broad range of xyloglucan compositions, LM15 recognises the XXXG motif and LM24 recognises galactosylated xyloglucan respectively. LM25 binds strongly across the epidermis of *G. biloba* and *I. floridanum*. LM15 binds strongly across the epidermis of *I. floridanum* and *G. biloba*, except the guard cells in *G. biloba*. LM24 showed weak binding only in the guard cells of *G. biloba*, and medium binding across the epidermis of *I. floridanum*. Scale bars = 10 µm. Images are representative of at least 2 biological reps.

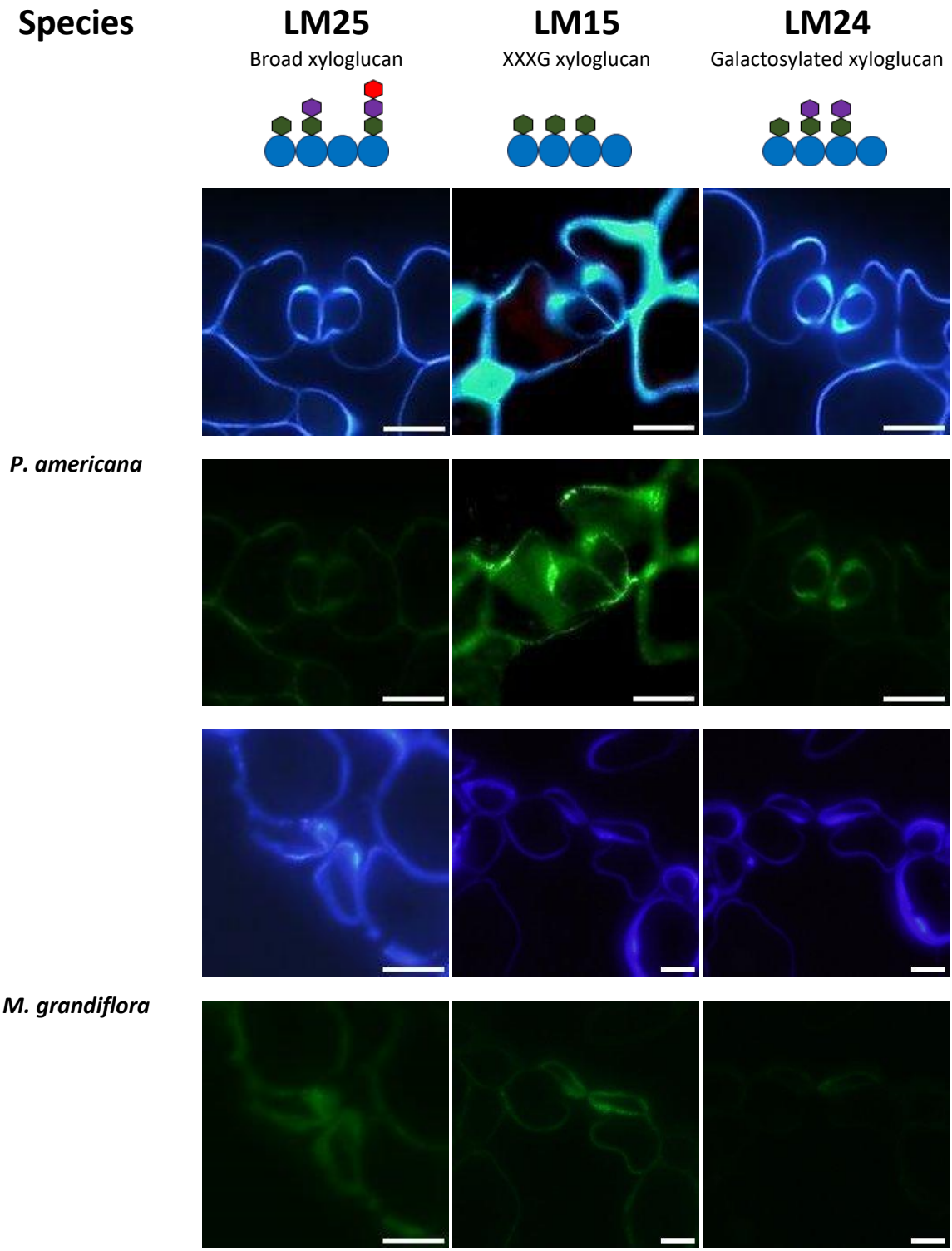

Figure 5.13. Xyloglucan distribution in guard cells of *Persea americana* and *Magnolia grandiflora*.
Cross-sections of epidermal layer of leaf tissue from (name of species) probed with antibodies (as indicated). For each section, the cell wall is indicated by calcofluor staining (blue signal) with the regions of antibody binding indicated in green in the images below. LM25 binds a broad range of xyloglucan compositions, LM15 recognises the XXXG motif and LM24 recognises galactosylated xyloglucan respectively. LM25 and LM15 bind across all epidermal cells of *P. americana* and *M. grandiflora*. LM24 showed strong binding exclusively in the guard cells of *P. americana* and *M. grandiflora*. Scale bars = 10 µm. Images are representative of at least 2 biological reps.

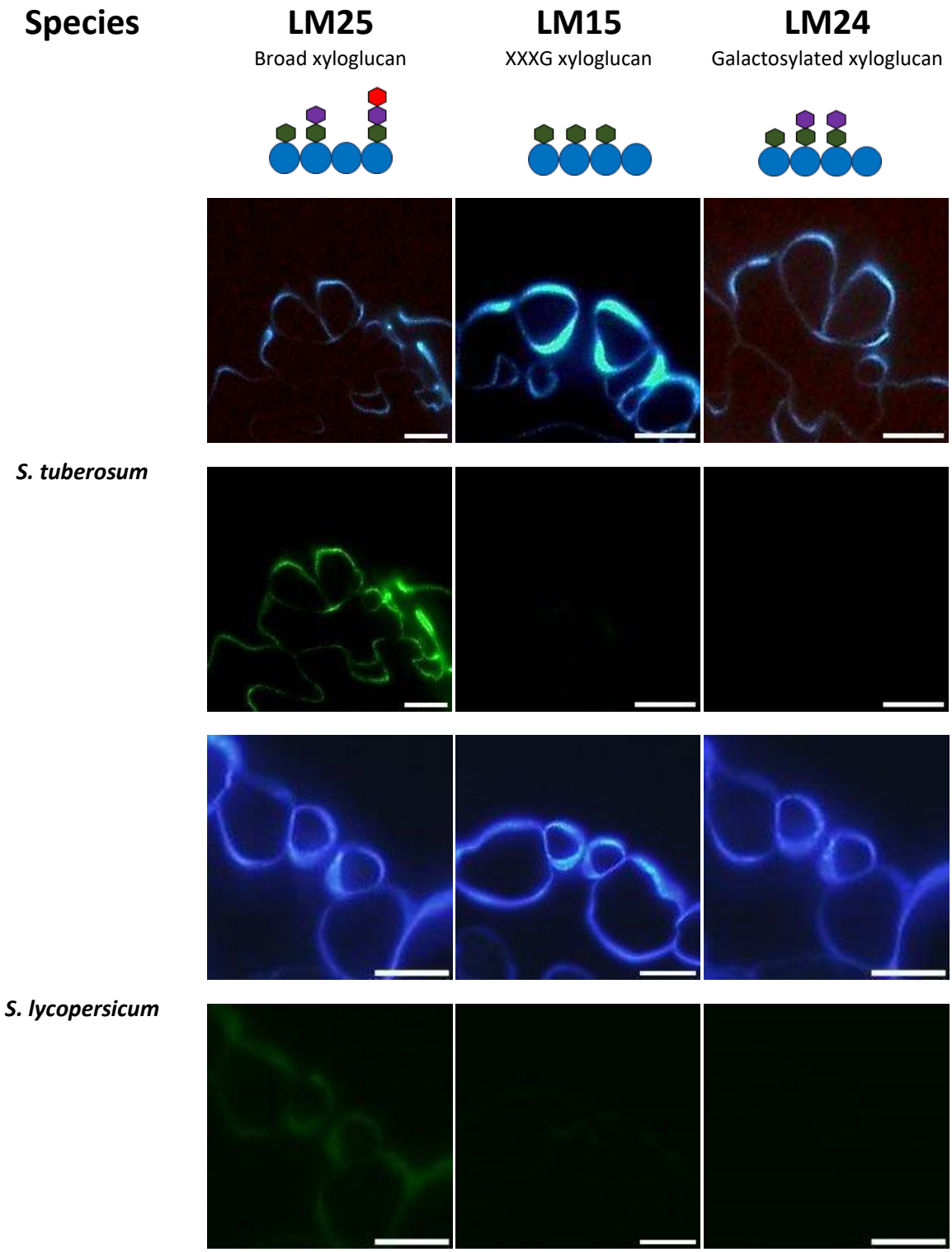

Figure 5.14. Xyloglucan distribution in guard cells *Solanum tuberosum* and *Solanum lycopersiucm*.
Cross-sections of epidermal layer of leaf tissue from (name of species) probed with antibodies (as indicated). For each section, the cell wall is indicated by calcofluor staining (blue signal) with the regions of antibody binding indicated in green in the images below. LM25 binds a broad range of xyloglucan compositions, LM15 recognises the XXXG motif and LM24 recognises galactosylated xyloglucan respectively. LM25 binds strongly across the epidermis of *S. tuberosum* and *S. lycopersicum*. LM15 and LM24 showed little or no signal in the epidermal cells of *S. tuberosum* and *S. lycopersicum*. Scale bars = 10 µm. Images are representative of at least 1-2 biological reps.

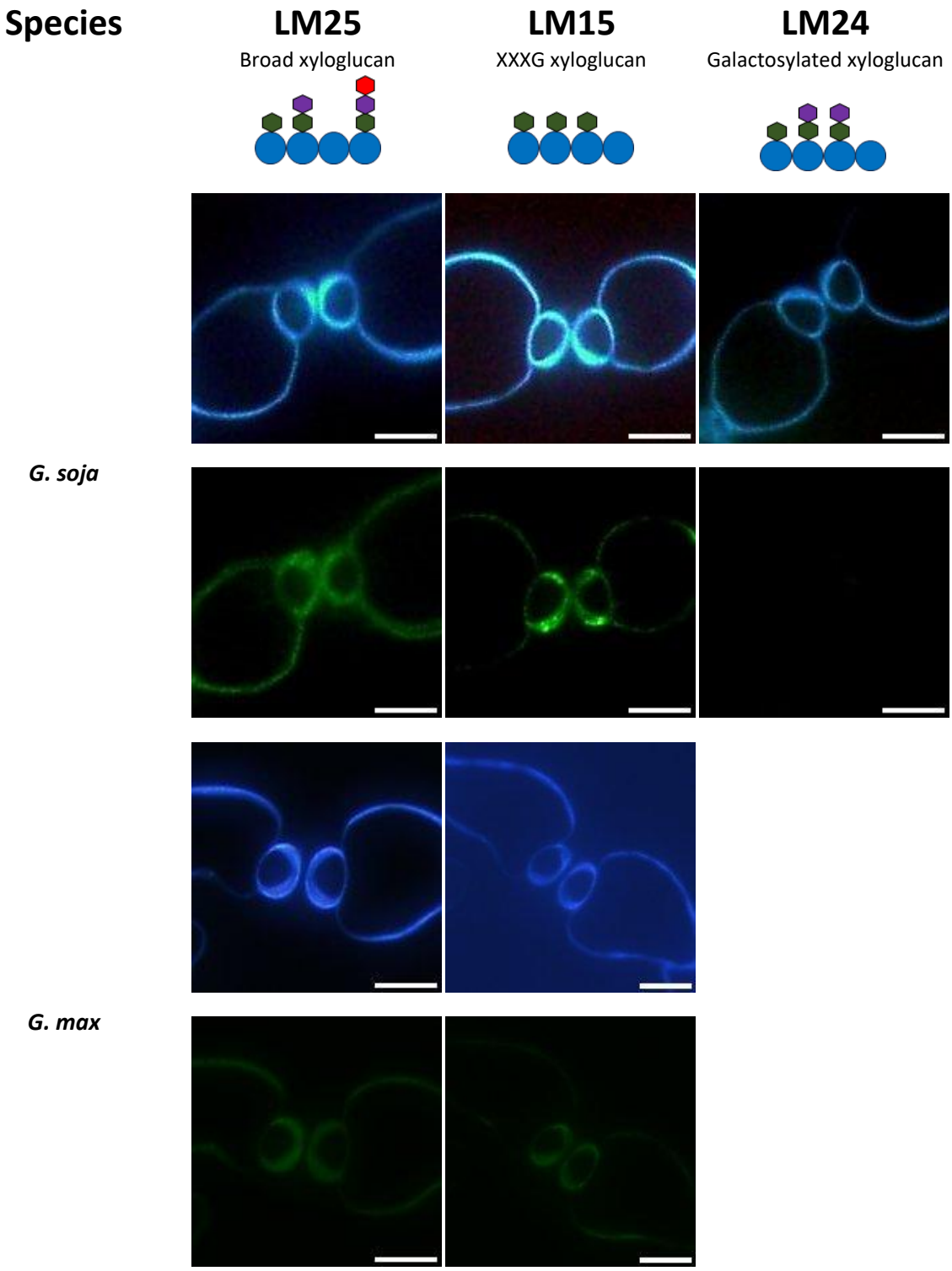

Figure 5.15. Xyloglucan distribution in guard cells of *Glycine soja* and *Glycine max*.
Cross-sections of epidermal layer of leaf tissue from (name of species) probed with antibodies (as indicated). For each section, the cell wall is indicated by calcofluor staining (blue signal) with the regions of antibody binding indicated in green in the images below. LM25 binds a broad range of xyloglucan compositions, LM15 recognises the XXXG motif and LM24 recognises galactosylated xyloglucan respectively. LM25 bound strongly across the epidermis of *G. max* and *G. soja*. LM15 signal was strongly enriched in the guard cells of *G. max* and *G. soja*. LM24 did not show binding on either species. Scale bars = 10 µm. Images are representative of at least 1-2 biological reps.

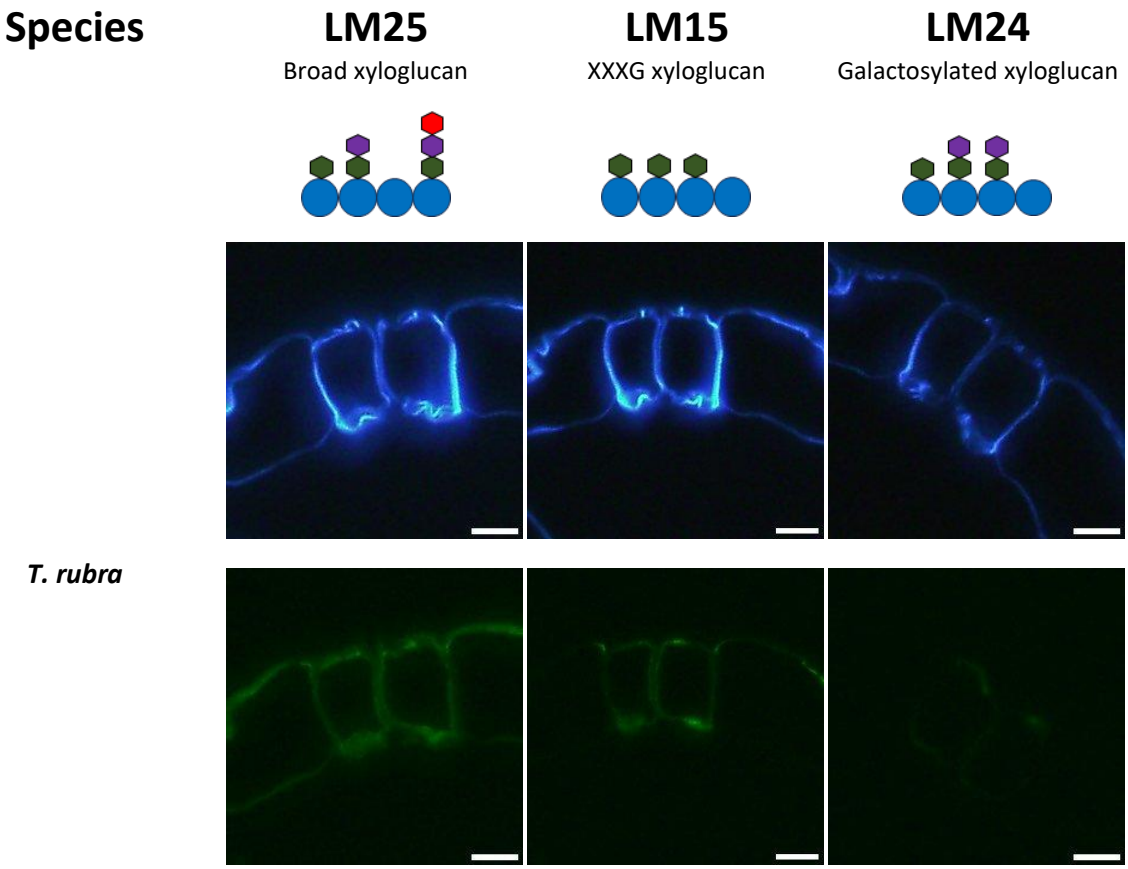

Figure 5.16. Xyloglucan distribution in guard cells of *Tradescantia rubra*.
Cross-sections of epidermal layer of leaf tissue from (name of species) probed with antibodies (as indicated). For each section, the cell wall is indicated by calcofluor staining (blue signal) with the regions of antibody binding indicated in green in the images below. LM25 binds a broad range of xyloglucan compositions, LM15 recognises the XXXG motif and LM24 recognises galactosylated xyloglucan respectively. LM25 bound strongly across the epidermis of *T. rubra*. LM15 signal was strongly enriched in the guard cells of *T. rubra*. LM24 showed weak binding in a guard cell specific pattern. Scale bars = 10 µm. Images are representative of at least 2 biological reps.

5.2.4. Kidney shaped guard cells show diverse patterning of xylan and mannan

Hemicellulose can also contain polymers of xylan and mannan. To investigate the pattern of these polymers in guard cells, a series of immunolabelling experiments were performed. The LM10 antibody recognises the non-reducing end of cell wall xylan. This polysaccharide was not detected in the epidermal cells of most species but both *O. regalis* and *G. biloba* displayed weak guard cell specific binding of LM10 (**Figure 5.17**). *M. grandiflora* showed the reverse pattern, with no signal in the guard and subsidiary cells but signal was present in the surrounding pavement cells. LM11 antibody (which recognises low-substituted xylan) showed a similar pattern for *O. regalis*, *G. biloba* and *M. grandiflora* as for LM10 (**Figure 5.18**). The signal for LM11 was stronger than that of LM10 across these three species. LM21 binds to cell wall mannan. The only species which showed binding of this antibody was *G. biloba*, which interestingly displayed strong binding only in the guard cells (**Figure 5.19**).

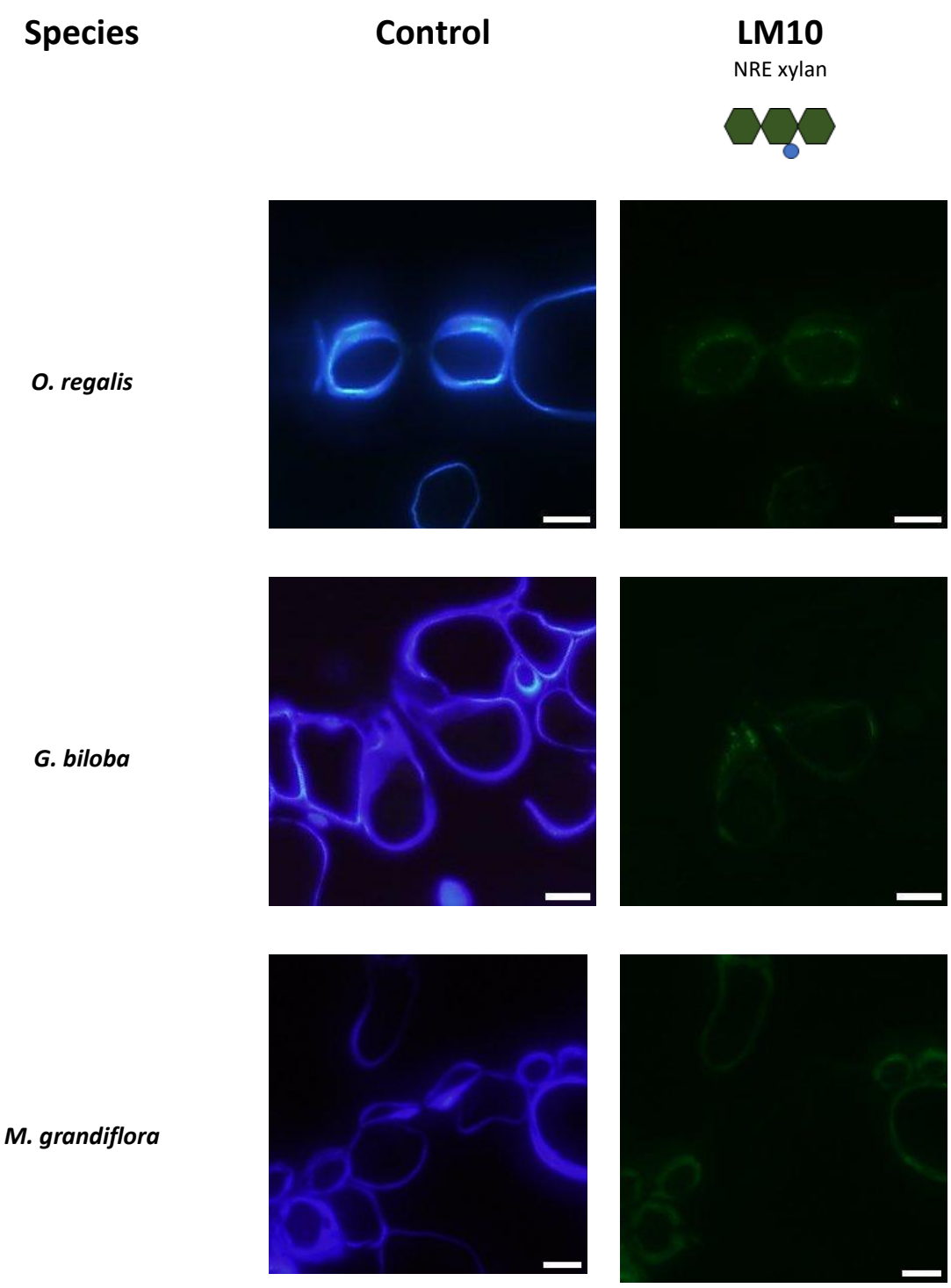

Figure 5.17. Non-reducing end of xylan distribution across guard cells.
Cross-sections of epidermal layer of leaf tissue from (name of species) probed with antibodies (as indicated). For each section, the cell wall is indicated by calcofluor staining (blue signal) with the regions of antibody binding indicated in green in the images below. LM10 binds to the non-reducing end of cell wall xylan. The guard of *O. regalis* and *G. biloba* shows weak binding of LM10 in contrast to surrounding epidermal cells which show no signal. *M. grandiflora* shows weak binding in the epidermal but not in guard cells. Scale bars = 10 µm. Images are representative of at least 2 biological reps.

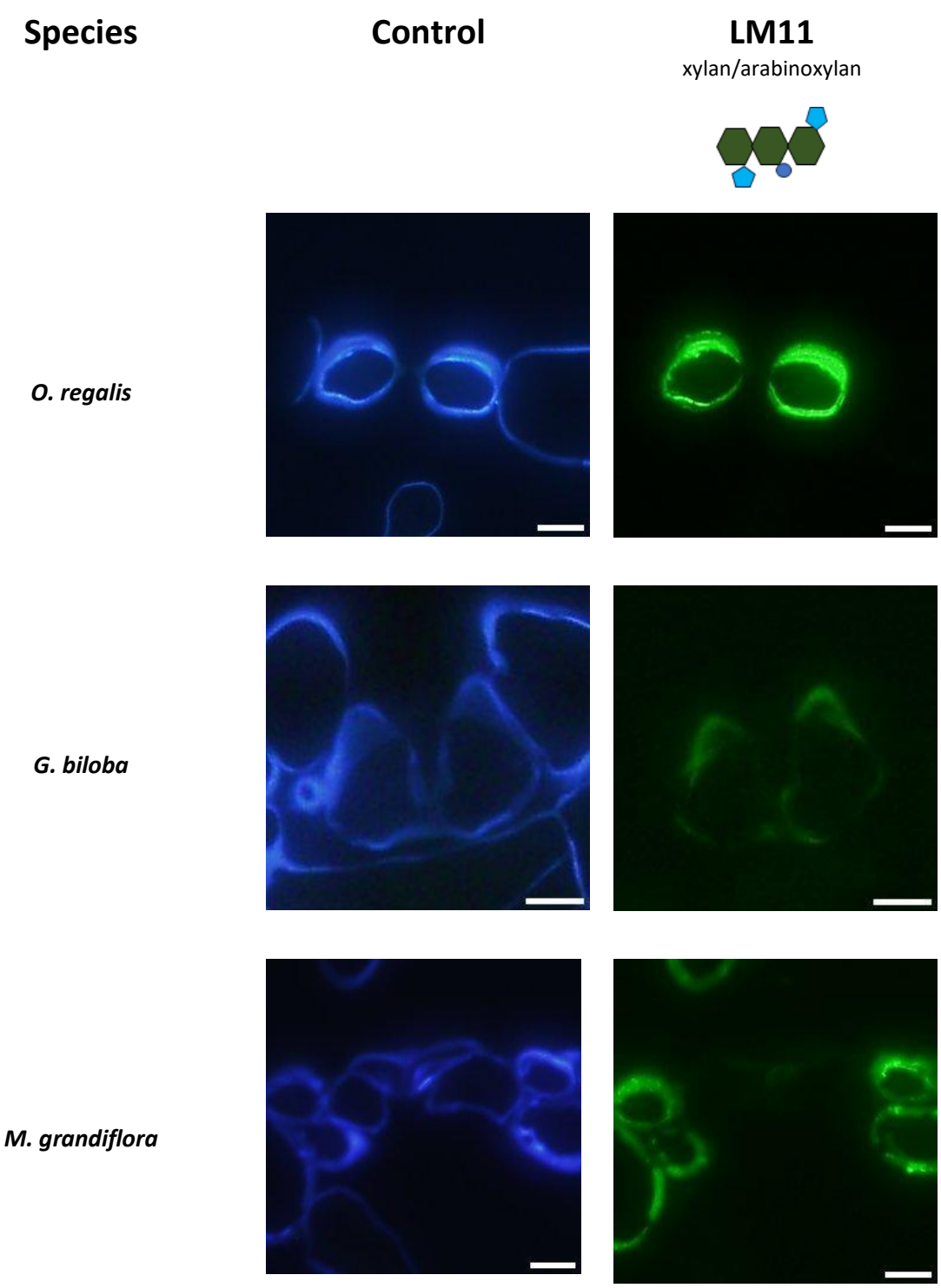

Figure 5.18. Low substituted xylan distribution across guard cells.
Cross-sections of epidermal layer of leaf tissue from (name of species) probed with antibodies (as indicated). For each section, the cell wall is indicated by calcofluor staining (blue signal) with the regions of antibody binding indicated in green in the images below.. LM11 binds to low substituted cell wall xylan. The guard cells of *O. regalis* and *G. biloba* show strong binding of LM11 in contrast to surrounding epidermal cells which show no signal. *M. grandiflora* shows weak binding in the epidermal but not in guard cells. Scale bars = 10 µm. Images are representative of at least 2 biological reps.

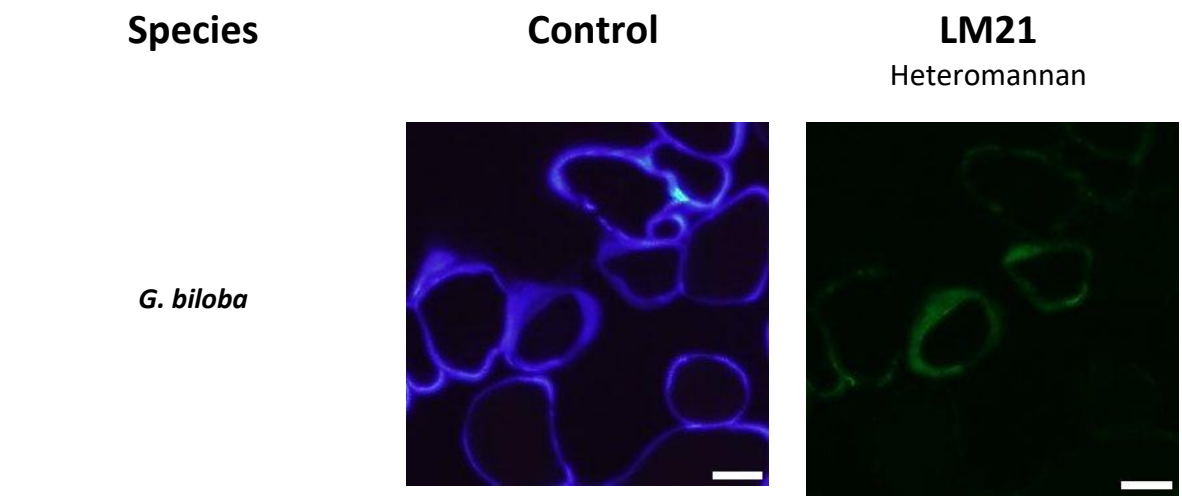

Figure 5.19. Mannan distribution across guard cells.
Cross-sections of epidermal layer of leaf tissue from (name of species) probed with antibodies (as indicated). For each section, the cell wall is indicated by calcofluor staining (blue signal) with the regions of antibody binding indicated in green in the images below.. LM21 binds to mannan. The guard cells of *G. biloba* show strong binding of LM21 in contrast to surrounding epidermal cells which show little or no signal. Scale bars = 10 µm. Images are representative of at least 2 biological reps.

Table 5.2. Guard cell hemicellulose content across species.

Summary of guard cell wall hemicellulose from immunolabeling data. Scores were estimated by eye. 1- no signal, 2 - weak signal, 3 = moderate signal and 4 = strong signal in guard cells. * indicate surrounding epidermal cells show strong signal but not in the guard cell.

Species	LM25	LM15	LM24	LM10	LM11	LM21
A. filix-femina	1	1	1	1	1	1
O. regalis	1	1	1	3	4	1
G. biloba	1	1*	1	2	1	3
I. floridanum	4	4	3	1	3	1
P. americana	3	3	3	1	1	1
M. grandiflora	4	4	3	1	1*	1
S. tuberosum	3	1	1	1	1	1
S. lycopersiucm	4	1	1	1	1	1
G. soja	2	4	1	1	1	1
G. max	3	3		1	1	1
T. rubra	3	3	1	1	1	1

5.2.5. Guard cell wall composition does not correlate with stomatal response speed across species

To understand the relationship between plant cell wall composition and stomatal response speeds, a correlation analysis was carried out including the measurements of stomata speed measured by infra red gas analysis in Chapter 3. As metrics of speed, SI_{max}, t and the Δ_{gs} during opening were used. Plant cell wall pectin and hemicellulose components were used from **Table 5.1-2**. None of the antibody signal intensities were significantly correlated with the measurements defining the stomatal response **Figure 5.20**.

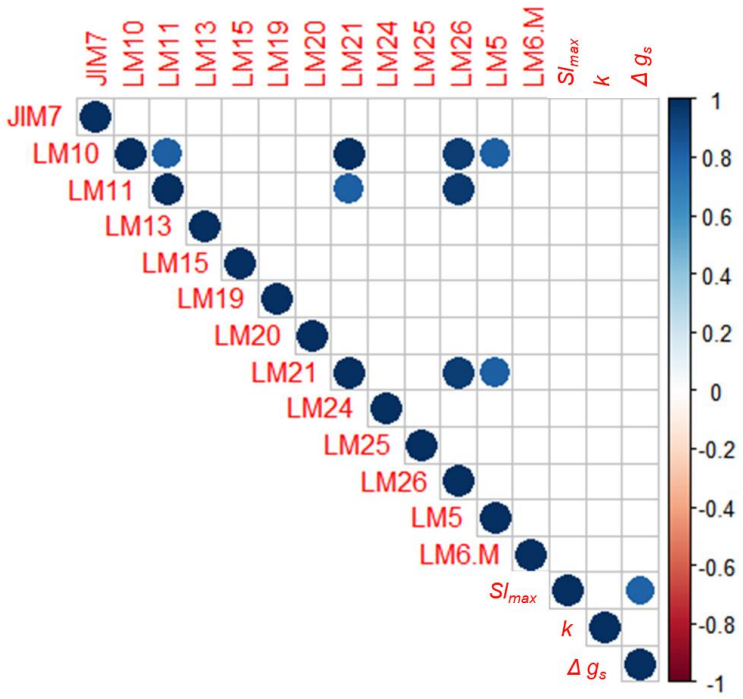

Figure 5.20. Correlation analysis of stomatal response traits and cell wall composition.
Statistically significant correlations are shown, non-significant correlations are left blank ($P < 0.05$). Blue indicates a positive correlation. For antibody specificities refer to **Table 2.2**. For speed metrics refer to **Figure 3.1**.

5.2.6. When present, guard cell wall arabinan is important for stomatal function

Short chains of arabinan (recognised by LM6M) were found only in the guard cells of some of dicotyledonous angiosperms tested i.e., *G. max*, *G. soja* and to a lesser extent, *M. grandiflora*. To understand the functional role of arabinan in the cell wall of *G. max*, a stomatal response bioassay was performed on tissue treated with arabinase which digests arabinans (**Figure 5.21**). Also included in this assay were leaf sections of *S. tuberosum* as a control which did not contain any detectable arabinan in the immunolabeling screen, and samples incubated similarly but with no arabinase enzyme added. In the no enzyme treatment, both *S. tuberosum* and *G. max* were able to open their stomata in response to fusicoccin (a fungal toxin that activates proton ATPase activity and stomatal opening) and close in response to the drought stress hormone ABA. *S. tuberosum* did not show any significant differences in opening or closing responses between tissue treated or not treated with arabinase. When treated with arabinase, *G. max* showed a lack of ability to close stomata in response to ABA compared to the no enzyme control (ANOVA, $F_{(1,32)} = 7.57$, $P < 0.05$). Interestingly, there was no difference between arabinase and no enzyme treated *G. max*, when incubated with the fusicoccin stomatal opening stimulus. Together these results indicate a reduced dynamic range of *G. max* stomata when treated with arabinase, specifically in the closing response. This suggests that guard cell arabinan is involved in regulating the extent of flexibility in *G. max* but not in *S. tuberosum* guard cell walls.

A *S. tuberosum*

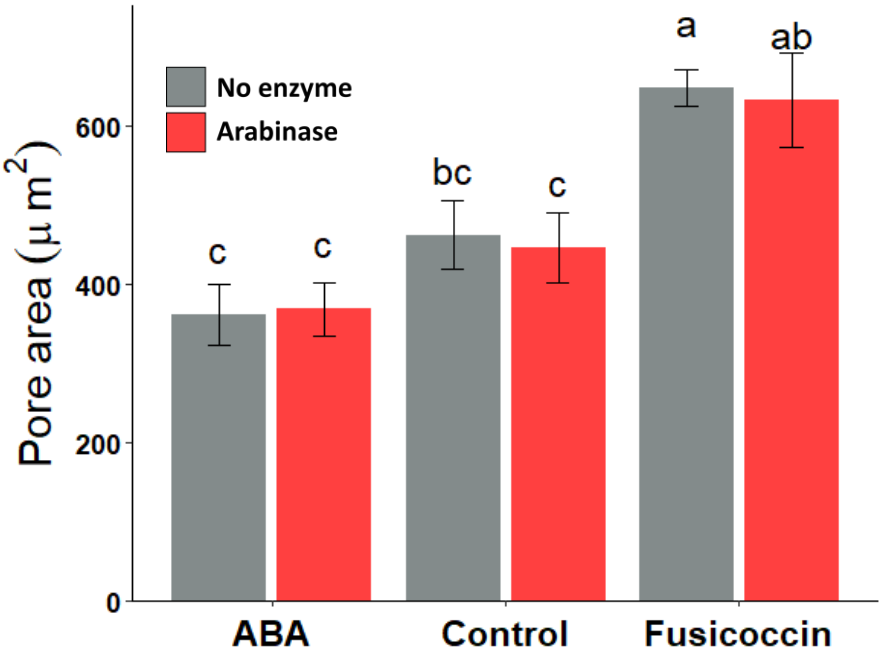

B *G. max*

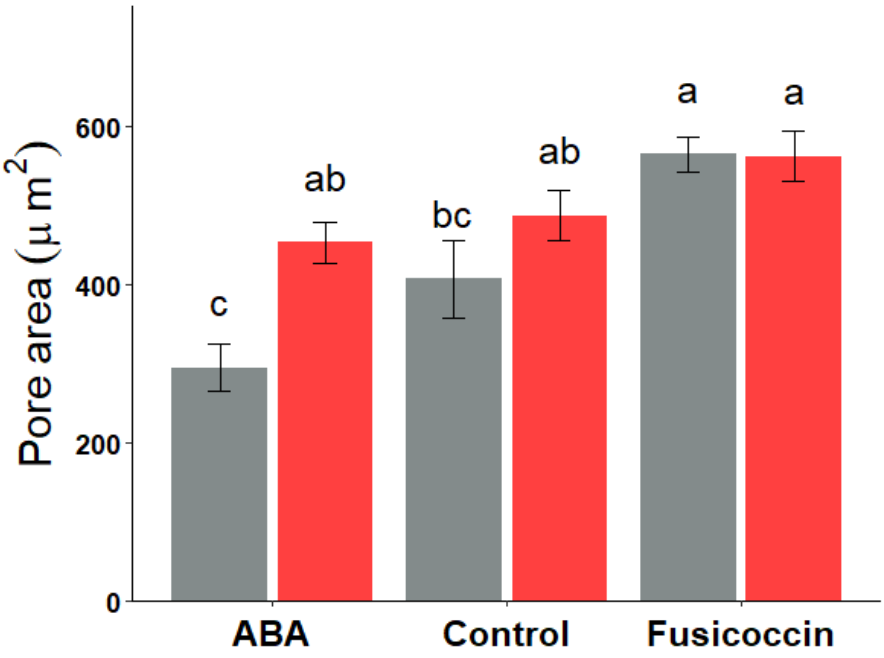

Figure 5.21. Stomatal function bioassay with and without pre-treatment with arabinase.
Excised leaf tissue of *S. tuberosum* (A) and *G. max* (B) was either treated with (red) or without (grey) arabinase. Stomata were either opened with fusicoccin, closed with ABA or leaf with an ambient air control. Treatments that cannot be distinguished from each other at 0.05 confidence limit are indicated by different letters as determined by ANOVA with a Tukey HSD (n = 6, 84 stomata per bar from 6 plants).

5.3. Discussion

Guard cells are highly specialised in their ability to expand and contract throughout the diurnal cycle, and on sensing environmental stress, and have been shown to exhibit distinct cell walls compared to neighbouring epidermal pavement cells (Wu and Sharpe, 1979; Verherbruggen et al., 2009b; Merced and Renzaglia, 2014; Amsbury *et al*., 2016; Carter *et al*.,2017; Shtein *et al.*, 2017; Woolfenden *et al*., 2017; Rui *et al*., 2018; Chen *et al*., 2021; Carroll *et al*., 2022). However, these analyses have been performed on only a few species, with a recent focus on the model plant Arabidopsis. There is thus limited information on the diversity of guard cell wall composition across different species and whether this has changed across evolutionary time. It has been shown that stomata with kidney shaped guard cells possess radially arranged cellulose microfibrils, but show distinct differences in areas of cellulose crystallinity based on lineage (Shtein *et al*., 2017). Dumbbell shaped guard cells have longitudinally arranged cellulose microfibrils (Shtein *et al*., 2017; Durney *et al*., 2023) However, it is largely unknown what diversity exists in pectin and hemicellulose composition across guard cell walls.

To date, the vast majority of studies investigating pectin and hemicellulose guard cell wall composition have been conducted on *A. thaliana* and a handful of other species albeit in less depth. While *A. thaliana* is a useful tool to study guard cell wall composition and mechanics due the abundance of genetic resources available, it is likely that there exists a large diversity in guard cell walls across plantae. This chapter primarily focused on an immunohistochemical localisation approach to study the cell wall composition of guard cells, and neighbouring epidermal cells across a diverse range of species. Using a broad spectrum of antibodies raised against specific cell wall polysaccharides, new trends in guard cell wall composition have been uncovered, revealing an unexpected variability in guard cell wall pectin and hemicellulose composition.

5.3.1. HGA is largely conserved across kidney shaped guard cell walls, but with differing methyl-esterification states

Type I cell walls are often characterised by an abundance of pectin (Carpita & Gibeaut, 1993), which can be observed by the presence of HGA in the epidermal cells of all species included in this study. Characterised by a linear backbone of galacturonic acid, HGA is often cited as

the most abundant pectin in cell walls (Mohnen, 2008) and was present in all guard cells, with the clear exception of the gymnosperm *G. biloba*. The high abundance of HGA in guard cells is consistent with other studies investigating the guard cell walls of *A. thaliana* (Amsbury *et al.*, 2016; Chen *et al.*, 2021). While it cannot be conclusively stated that guard cells of *G. biloba* do not contain any HGA, it was not detectable by any of the three antibodies (JIM7, LM19 and LM20) which detect a range of methyl esterification states of HGA. This binding pattern may be due to the functional role of the sunken nature of these guard cells, a feature unique to this species within this study. This may alter the mechanics of these guard cells and consequently the requirements of the guard cell wall (Gray *et al*., 2020). As such it is likely that the subsidiary cells may play an important role in modulating the gas exchange of this species. Interestingly *G. biloba* subsidiary cells did display abundant HGA. *G. biloba* was identified as a particularly slow species in chapter 3. It would be interesting to investigate further if the lack of HGA in guard cells is a common feature of gymnosperms, or species with sunken stomata.

It has been suggested that modifications to HGA, in the form of removal of methyl groups, can impact cell wall stiffness and consequently guard cell function. Again in *A. thaliana*, it has been shown that for proper guard cell function HGA must be un-esterified, and that the spatial deposition varies across the guard cell (Amsbury *et al.*, 2016; Carter et al., 2017; Chen *et al.*, 2021). However, when looking at the pectin methyl-esterification status of HGA across a broad range of species this pattern was not consistent. The results in this Chapter revealed a spectrum of HGA methyl-esterification patterns, however most species showed a contrasting methyl esterification pattern to *A. thaliana*, i.e., their guard cell walls were more methyl-esterified than the surrounding cells. While it is likely that alteration of cell wall stiffness through HGA methyl group removal is necessary for stomatal function in most species, individual guard cell wall requirements of each species likely differ. A clear example of this can be seen in monocotyledonous angiosperm stomata, which possess a unique dumbbell guard cell morphology, likely aided by different pectin and hemicellulose proportions, as well as alternatively arranged crystalline cellulose microfibrils (Carpita & Gibeaut, 1993; Carpita, 1996; Vogel, 2008; Shtein *et al.*, 2017). While general trends can be observed between dicots and monocots, there are likely different guard cell wall needs between species based on gas exchange capacity (and requirement), stomatal size, shape and

location, that necessitate individual species to specialise guard cell walls in subtly different ways. All sections taken for this study were transverse, precluding observations on the spatial distribution of methyl-esterified HGA across the guard cell as has been previously reported (Carter *et al.*, 2017). It is possible that, using paradermal sections, differing spatial distributions of these pectic polysaccharides may appear, however this was beyond the scope of this thesis. Irrespective of modification, it appears that HGA is a largely conserved component across kidney shaped guard cells with the possible exception of the gymnosperms. HGA has been detected in the guard cells of extant moss, despite the disputed functionality of their stomata (Merced and Renzaglia, 2014). Further, guard cell walls enriched in methyl-esterified HGA appear to be common.

5.3.2. Guard call arabinan is not essential to all stomata for guard cell function

Rhamnogalacturonan I is a major cell wall pectin component, characterised by a backbone of alternating galacturonic acid and rhamnose. This backbone can be decorated with side chains that are thought to alter the mechanical properties of the cell wall matrix (Jones *et al*., 2003; 2005; Moore *et al*., 2008; Moore *et al.*, 2013). One of the pectic guard cell wall components that has received particular attention is arabinan, a side chain associated with RG1. This RGI side chain has been suggested to act to separate pectin molecules in situations where flexibility is essential, such as in desiccation resistant plants and guard cells (Jones *et al*., 2003; 2005; Moore *et al.*, 2008; Moore *et al*., 2013). In earlier studies, *Commelina communis*, *Vicia faba* and *Zea mays* were shown to be rich in arabinan and enzymatic digestion with arabinase restricted stomatal opening and closure (Jones *et al*., 2003; 2005). More recently, *A. thaliana* mutants deficient in the arabinan synthesis gene ARABINAN DEFICIENT 1 (ARAD1) displayed reduced stomatal aperture responses (Carroll *et al*., 2022).

Despite the seeming widespread abundance of this arabinan across guard cells in the few species previously analysed, the vast majority of species included in this study did not contain any detectable cell wall arabinan that was detectable with either the LM6M or LM13 antibody. There were three notable exceptions, with *G. max* seemingly possessing guard cells particularly enriched in short chains of arabinan (recognised by LM6M). Enzymatic digestion of arabinan appears to disrupt the function of stomata in *G. max* in a similar but distinctly different way compared to the observations from Carroll *et al*. (2022) in *A. thaliana*. While

both species displayed a reduced range of pore area after digestion with arabinase, the treated stomata of *A. thaliana* tended towards a more closed orientation, whereas *G. max* tended towards open stomata that were unable to close. This is likely explained by the differences in the composition of other cell wall components. The guard cell walls of *A. thaliana* are characterised by a high abundance of unesterified HGA and relatively little highly methyl-esterified HGA (Amsbury *et al*., 2016). Here, it was shown that the guard cell walls of *G. max* show the reverse pattern of HGA methyl-esterification. As mentioned above, numerous studies have implicated HGA methyl-esterification in contributing to cell wall flexibility. It has been suggested that pectin side chains such as arabinan play a role in governing formation of calcium cross links between adjacent HGA molecules (Jones *et al*., 2013). Therefore, it is likely that when considering species with differing HGA methyl-esterification states, manipulation of another cell wall component that has been associated with governance of cell wall flexibility (such as arabinan) may produce different results.

5.3.3. Hemicelluloses in kidney shaped guard cell walls

Xyloglucan appears to be a largely conserved epidermal cell wall component across kidney shaped guard cell walls, with the exception of *A. filix-femina* which did not contain any detectable hemicelluloses. This largely conserved role of xyloglucan appears to agree with previous observations that xyloglucan is essential for correct stomatal pore opening (Rui and Anderson, 2016). Using oligosaccharide data and the binding patterns of LM25, LM15 and LM24, additional information about the structure of xyloglucan can be inferred. These microarray data sets are gathered by using synthesised oligosaccharides and testing antibody binding affinity for each well-defined synthesised oligosaccharide. This enables a deeper understanding of the structures to which each antibody may bind. While oligosaccharide microarrays are useful for understanding antibody binding patterns, they do not contain a completely exhaustive list of cell wall components. Consequently, it cannot be conclusively stated that these structures are present, only that it is highly likely. Despite this they remain a useful tool. Using the published glycome microarray by Pedersen *et al*., (2012) inferences about the xyloglucan content of the guard cells of some species can be made, based on the pattern of binding across the 3 antibodies (LM25, LM15, LM24). For example, the guard cells of both *S. lycopersicum* and *S. tuberosum* showed strong binding of LM25, but not LM15 or LM24. This same pattern was seen in the guard cells of *G. biloba*, while the rest of the

epidermis of this species also showed strong LM15 signal. This indicates that the cells are enriched in xyloglucan composed mostly of longer sequential XXXG oligosaccharides. In other studies, species from the Solanales family have been shown to display distinct leaf cell wall xyloglucan compared to other dicots. In the data presented here, they were enriched in longer stretches of XXXG xyloglucan rather than XXGG chains (Pauly and Keegstra, 2016). However, the glycome microarray used to verify the specificity of these antibodies did not include XXGG oligosaccharide. Most other species showed guard cell signal for both LM25 and LM15 antibodies, indicating an abundance of single XXXG oligosaccharides. Interestingly, few species showed binding of LM25, LM15 and LM24 which implies enrichment of the XLXG motif (galactosylated xyloglucan) in these species.

Unlike xyloglucan, the results reported in this Chapter indicated that xylan is enriched in the guard cells of the fern *O. regalis* and the gymnosperm *G. biloba* but notably absent in the majority of species. Interestingly, the early angiosperm *M. grandiflora* displayed the opposite trend with only the pavement cells enriched in xylan. Here, two xylan specific antibodies revealed differing binding affinities for different cell wall xylan compositions. While both LM10 and LM11 showed a similar binding pattern, they showed a difference in signal intensity. All species showed a much stronger signal from LM11. This potentially indicates that there is a high content of arabinose substituted xylan or glucuronic acid side chains (Pedersen *et al*., 2012; Ruprecht *et al.*, 2017). Overall, the apparent reduced abundance of cell wall xylan is in keeping with typical observations of the composition of type I cell walls.

Interestingly, the only species that clearly displayed observable mannan signal was *G. biloba*. Gymnosperms have been noted for the high abundance of mannan in their cell walls (Sarkar *et al*., 2009). However, this has not been reported exclusively in the guard cells as has been observed here. The mannan patterning in *G. biloba* is in direct contrast to the patterns observed for HGA, which was unusually absent for this species. The sole instance of detectable mannan in this species may indicate an alternative stomatal composition in Gingko or across gymnosperms, in which this mannan is compensating for the lack of HGA; however, determining this was beyond the scope of this thesis.

5.3.4. Guard cell wall composition is diverse across species and does not correlate with stomatal response speed

Across the diverse species used in this study guard cell wall composition appears to vary greatly. Although the main cell wall components, such as HGA and xyloglucan, are present in the majority of guard cell walls tested, their exact composition appears to vary greatly across species. Further, the presence of typically less common cell wall components appears in specific species, sometimes in a guard cell specific manner. For example, the presence of arabinan side chains in guard cell walls is not widespread, at least in the species included in this study. The observation that guard cells of *S. tuberosum* do not seem to contain any cell wall arabinan (supported by the lack of any altered stomatal response in bioassays after arabinase treatment) implies that functioning guard cells can be made with a diverse composition of cell wall polysaccharides in relatively closely related species. This observation is supported by highly guard cell-enriched patterns of galactan side chains in the fern *O. regali*s that are rin contrast with those seen in the angiosperms *P. americana* and *M. grandiflora*. All three of these species have been shown to possess functional stomata (Chapter 3) and yet have mirrored guard cell wall patterns for this epitope. Understanding the functional role of galactan in the guard cells of these species is beyond the scope of this thesis, however it does seem that the role of guard cell wall composition in facilitating a successful stomatal opening and closing response might be highly species-specific. Previous studies on *A. thaliana* demonstrated that the specific HGA methyl-esterification status of guard cells wall is essential for an efficient stomatal aperture stomatal response (Amsbury *et al*., 2016; Chen *et al*., 2021). However, this is far from universal across species. To try and understand the contribution of various cell wall components on stomatal speed a correlation analysis was conducted using these parameters, however the results did not indicate a trend of any specific cell wall components as key to a fast stomatal response. Thus, as is often the case in plant cell wall studies, the picture is complicated, and it is probable that multiple components could be utilised to achieve the flexibility required for stomatal opening and closing responses.

5.3.5 Limitations of immunolabeling

Immunolabeling has allowed the characterization of cell wall composition by providing spatial data across leaf sections and elucidated cell specific patterns of cell wall composition. However, to appropriately interpret this data the limitations must be considered. Due to the

nature of the immunolabeling process, replication levels are low and quantification of the results may be inaccurate. Differences in antibody binding levels mean that comparisons between epitope levels are not accurate. Although the results shown here were observed in more than one sample, any attempts at quantification must be viewed in the context that fluorescence is subject to various conditions outside of the binding of the antibody itself. For example, secondary antibody fluorescence decays over time, as does the intensity of mercury or xenon arc bulbs used to visualise fluorescence. For these reasons quantification of the cell wall was only attempted at a comparative level, attempting to avoid drawing erroneous conclusions upon fluorescence intensity. Instead, a more simple distinction between strong and weak binding has been attempted (Brennan *et al*., 2019).

Another limitation of the immunolabeling technique is the spectrum of antibodies available. Although over 200 monoclonal antibodies exist that bind to plant cell wall polysaccharides, there are many specific epitope patterns for which antibodies do not exist (Ruprecht *et al*., 2017). Further, while the broad target of antibodies may be known, the exact structure of the polysaccharide epitope may be unknown or the antibody may be known to bind to multiple arrangements of a polysaccharide component (Verhertbruggen *et al*., 2009; Pederson e*t al*., 2012). Therefore, care must be taken concerning the various causes of any observed binding patterns. There exists the potential for masking of cell wall components, notably when HGA is highly abundant as has been observed for the majority of species probed in this study (Marcus *et al*., 2008; 2010). To address this here, pectin was digested prior to probing with antibodies that recognise hemicellulose, to minimise the possibility of masking of these components.

Care must be taken when taking immunolabelling data and applying observations ubiquitously across plants of a species. While the process is robust for detecting cell wall polysaccharides, it can only detect what is there. Therefore, this process does not account for the impact of growth conditions on cell wall composition. For example, it has been demonstrated that when challenged with salt stress, Ca^{2+} cross linking between HGA can be disrupted (Feng *et al*.,2018). It would be interesting to repeat this process with plants growth under different daily PPFD or fertilisation regimes. Recently, is has been shown that cell wall composition, in particular the HGA methyl-esterification status, may be actively changed during stomatal opening and closure (Gkolemis *et al*., 2023).

Finally, the process of immunolabeling requires semi-thin sections of fixed tissue. In an attempt to make this method more high throughput, sections were taken in the transverse orientation (as opposed to paradermal). While this provides clear cross sections of guard cells, the location along the guard cell at which the section has been taken is difficult to determine. Therefore, any spatial patterns of cell wall distribution across the guard cell itself cannot be determined.

Chapter 6. General discussion

Stomata were a key innovation allowing plant survival in a dynamic terrestrial environment and are widely believed to have been important for the greening of the earth around 400 million years ago. By regulating gas exchange these pores control both carbon uptake and water loss in constantly changing conditions. The size and density of stomata and also the rapidity at which they respond to a changing environment governs plant gas exchange. The experiments described in this thesis investigated the diversity in stomatal response speeds from species spanning a broad range of evolutionary groups and stomatal morphological traits, as well as the diversity that exists in guard cell wall composition to facilitate the active adjustment of the stomatal pore.

In Chapter 3, the diversity of stomatal size, density, distribution and the magnitude and speed of response to a change in light intensity was investigated across species from diverse evolutionary lineages. When arranged by phylogeny, from earliest to latest diverging, these metrics revealed insights into the diversity of stomata across land plants. One of the most striking observations was a significant increase in leaf stomatal density on the adaxial surface of the leaf, due to the evolution of amphistomaty (stomata on both leaf surfaces) in the angiosperms. Species from the Asterid, Rosid and Monocot clades of the angiosperm lineage displayed hypostomatous leaves, whereas the more basal lycophyte and fern lineages were ubiquitously hypostomatous. This coincides well with both modelled optimal stomatal distributions and empirical measurements across a broad range of plant lineages (Muir *et al*., 2014; Muir, 2015; Haworth *et al*., 2018). As predicted by models (Muir *et al*., 2015) these later evolving, amphistomatous, species are mostly fast-growing annuals, with the distribution of stomata seemingly increasing gas exchange potential as observed experimentally under high light in this study. It is noteworthy that, while the well-studied *A. thaliana* has a typical stomatal distribution for its clade (Rosid) it is not representative of all major land plant clades.

The leaves of all species investigated showed a rapid increase in stomatal conductance in response to a step increase in light suggesting active regulation of the stomatal pore. The more rapid response of stomata with dumbbell-shaped rather than kidney-shaped guard cells was confirmed with grass species achieving faster maximum rates of both stomatal opening and closure (Raven, 2002; Hetherington and Woodward., 2003; Vico *et al*., 2011; McAusland

et al., 2016; Elliot -Kingston *et al*., 2016; Haworth *et al*., 2018). However, species with dumbbell guard cell used here were all grasses, making it difficult to distinguish if the superior performance is due to the species being grasses or because of the unique morphology. Including sedges in future work, which belong to the graminoid family, but possess kidney-shaped guard cells could help to further understand the source of this superior performance.

Although species with dumbbell-shaped guard cells consistently opened and closed in less time than kidney-shaped guard cells, this difference was not significant, instead it seems that the higher maximum rate of change in the dumbbell species is also due to their greater dynamic range, rather than speed of opening and closure alone. When considering time of opening and closure alone, species often demonstrated asymmetric response times. In particular, the suggestion that lycophytes, ferns and other shade adapted species open their stomata more quickly than they close was confirmed (Xiong *et al*., 2018; Deans *et al*., 2019). This is likely an adaptation to maximise the rare transient light flecks that make up a significant proportion of PPFD in understory environments, coupled with a reduced need to limit water loss (Knapp and Smith, 1987; Xiong *et al*., 2018; Deans *et al*., 2019). The commonly held notion that ferns and lycophytes possess stomata that adjust slowly may have been perpetuated by studies only focussing on stomatal closure, or studies measuring rate of change rather than time (Elliot-Kingston *et al*., 2016; Haworth *et al*., 2018). However, the slow closure response of ferns does seem to be ubiquitous across studies (Elliot-Kingston *et al*., 2016; Haworth *et al*., 2018; Xiong *et al*., 2018; Deans *et al*., 2019).

In Chapter 4, the relationship between stomatal response speed and plant growth was investigated in a dynamic light environment. It has been suggested for some time that faster stomatal responses convey an advantage to plants, particularly those growing in more arid environments (Raven 2002; Hetherington and Woodward, 2003; Lawson and Blatt, 2014). By opening and closing stomata more quickly, the plants are able to capitalise on rapid increases in light intensity and limit water loss through open stomata after a period of increased irradiance. These theories have been backed up by empirical measurements taken from genetically altered plants with altered stomatal dynamics, albeit usually accompanied by an altered dynamic range of g_s (Papanatsiou *et al*., 2019; Kimurara *et al*., 2020). However, when

using a panel of species with a spectrum of stomatal responses, there was generally found to be no significant difference in biomass acquisition, water loss or carbon isotope discrimination between plants of the same species grown at constant or fluctuating daytime light. When a subset of the cereal plants were grown under the same light conditions but also under drought, differences between the light conditions became apparent. Plants of all three species grown under fluctuating light gained less biomass when grown under drought in comparison to those grown under constant daytime light. However, no consistent impact of stomatal speed upon plant growth and water use could be seen. It would be interesting to experiment further with vapour pressure deficit (VPD) and the role this may play in governing stomatal dynamics under fluctuating light, due to the shared signalling pathway with the typical ABA drought response (Zhang *et al*., 2023).

Chapter 5 explored the diversity in stomatal cell wall composition across species with kidney-shaped guard cells from diverse evolutionary lineages. Using this analysis and data gathered in Chapter 3, any correlation between cell wall composition and stomatal speed was investigated. Given the limited number of species that have had guards cell wall composition examined in depth it is not surprising the previously held notions of the composition of guard cell walls were not held to be consistent across the diverse species screened in this chapter (Amsbury *et al*., 2016; Carter *et al*.,2017; Shtein *et al*., 2017; Woolfenden *et al*., 2017; Rui *et al.,* 2018; Chen *et al*., 2021; Carroll *et al*., 2022; Durney *et al*., 2023). Of particular note is the variety of HGA methyl-esterification patterns that have emerged. The majority of studies looking in depth at guard cell wall composition have focused, with good reason, on *A. thaliana* (Amsbury *et al*., 2016; Carter *et al*., 2017; Woolfenden *et al*., 2017; Rui *et al.,* 2018; Chen *et al*., 2021; Carroll *et al*., 2022). The range of genetic resources studied here have enabled more in depth characterisation of the functional role of guard cell wall components than would otherwise be possible. However, this work demonstrated that the previously observed abundance of de-methylesterifed HGA in *A. thaliana* is far from widespread. This cell wall component in *A.thaliana* has been shown to be essential for a complete stomatal response (Amsbury *et al*., 2016). Thus, the sparse distribution of demethyl-esterified HGA in the guard cell wall of species included in this screen indicates overlapping roles of cell wall components in facilitating a stomatal response. In particular, the potential for guard cells to be composed

of differing proportions of cell wall polysaccharides that are capable of fulfilling the same function.

This concept is demonstrated by immunolocalisation of antibodies raised against arabinan side chains and stomatal response bioassays. The digestion of arabinans with arabinase enzyme in *G. max* (shown to contain arabinan) and *S. tuberosum* (shown to contain no detectable arabinan) resulted in different results. Digestion of arabinans reduced stomatal function in *G. max* but not *S. tuberosum* indicating that efficient stomatal functioning can be achieved by different cell wall components. This observation, once again, points to the limited conclusions that can be drawn from only focusing on *A. thaliana*. This model species also has guard cells rich in arabinan, but from the species included in the panel presented in this chapter this is more the exception than the rule (Jones *et al*., 2003; Carroll *et al*., 2022).

With these observations in mind, it does not seem surprising that there was found to be no obvious relationship between dynamic stomatal response metrics and guard cell wall composition. It is likely that multiple combinations of guard cell wall components can achieve the same result across different species and hence simple visualisation by immunolabeling is insufficient to tease apart any links between guard cell wall composition and stomatal response speed. The role of growth conditions on guard cell wall composition remains a poorly understood topic, throughout this thesis plants were, by necessity grown under their ideal conditions to minimise stress throughout growth. Active modifications to plant cell wall pectin under heat stress have been documented (Wu *et al*., 2018). Therefore, the possibility exists that the diverse growth conditions used may impact guard cell wall composition however, this is beyond the scope of this thesis.

Overall, this thesis has confirmed the hypothesis that dumbbell guard cells are more able to rapidly adjust g_s, but that large diversity exists across guard cell geometries. While all species with dumbbell-shaped guard cells responded quukcly, some species with kidney-shaped guard cells were able to achieve similar response speeds as dumbbell species. One of the keys to the success of the dumbbell-shaped guard cell lies in the accompanying subsidiary cells. *B. distachyon* mutants lacking subsidiary cells opened and closed their stomata in a manner far more similar to the slower kidney shaped species, despite resembling the dumbbell geometry.

In general, the results presented here suggest that guard cell geometry is more important in determining a stomatal response speed than cell wall composition.

6.2. Further work

The outcomes of experiments described across the previous three chapters have raised some interesting potential avenues for further research, with key questions posed below.

Is the rapid stomatal opening response of ferns and lycophytes a general feature of shade-tolerant plants that can be extended to under-story species of other clades?

One of the key findings of this work was the relatively short time taken for ferns and lycophytes to open their stomata. While the rapid response of members of these lineages has previously been suggested, empirical measurements have only been carried out on a handful of species (Knapp and Smith, 1987; Xiong *et al*., 2018; Deans *et al*., 2019). Investigating whether this asymmetric stomatal response is a trait of ferns and lycophytes or understory plants in general could be done by including more angiosperms that are adapted to these lower light environments.

Can stomatal response times be attributed to habit environment rather than evolutionary history?

Despite the clear trend for the grasses to display faster rates of stomatal opening and closure, the role of surrounding environment upon stomatal closure requires further research. The importance of stomatal response speed in different environments has been discussed above. But focussing on fewer clades, but with more individuals that span a range of ecological niches, the role of environment on stomatal response speed could be further elucidated. **Is stomatal response speed important for determining other metrics of plant growth or under a different fluctuating light regime?**

One of the most unexpected results in this thesis was the apparent lack of impact of stomatal response speeds on plant growth in well-watered conditions. The relationship between stomatal response speeds, plant growth and WUE is central to much work aimed at engineering more efficient crops (Qu *et al*., 2020; Horaruang *et al*., 2022). Thus, investigating

the extent to which stomatal response speeds are important under dynamic conditions may help to guide efforts to engineer these crops. In particular, the data presented here suggest that drought is a key environmental condition under which the light environment becomes more important. Repeating these experiments under drought with additional species, particularly *B. distachyon* and *B. distachyon* (SID) with their severe stomatal response phenotype may further shed light on this.

Does the rapid stomatal response speed of grasses play a role other than adjusting gaseous exchange. For example, a defence response to block pathogen entry?

It has been suggested that the rapid stomatal responses of grasses, facilitated by their distinct dumbbell guard cell morphology have been key to their success in colonising dry arid environments (Hetherington and Woodward, 2002). At the same grasses are characterised by amphistomatous leaves with high stomatal density, which present additional more accessible sites of pathogen entry (McKown *et al*., 2014; Drake *et al*., 2018). Research into an alternative role of rapid stomatal response in preventing pathogen entry could aid in the understanding of plant-pathogen interactions and engineering of new resistant crops.

Are cell wall components distributed evenly across guard cell walls, or is there a spatial pattern?

While immunolabelling is a useful tool for visualising the plant cell wall, the spatial data gained is only in one 2D plane. This makes it difficult to make conclusions about how guard cell wall composition may vary spatial in 3D. Development of smaller antibody fragments, coupled with quantum dots may provide an avenue for investigating guard cells in 3D and may further uncover the diversity that exists in guard cell walls components spatially across the guard cell.

References

Adams, M.A. and Grierson, P.F., 2001. Stable isotopes at natural abundance in terrestrial plant ecology and ecophysiology: an update. *Plant Biology*, *3*(04), pp.299-310.

Alter, P., Dreissen, A., Luo, F.L. and Matsubara, S., 2012. Acclimatory responses of Arabidopsis to fluctuating light environment: comparison of different sunfleck regimes and accessions. *Photosynthesis research*, *113*, pp.221-237.

Amsbury, S., Hunt, L., Elhaddad, N., Baillie, A., Lundgren, M., Verhertbruggen, Y., Scheller, H.V., Knox, J.P., Fleming, A.J. and Gray, J.E., 2016. Stomatal function requires pectin de-methyl-esterification of the guard cell wall. *Current Biology*, *26*(21), pp.2899-2906.

Andrés, Z., Pérez-Hormaeche, J., Leidi, E.O., Schlücking, K., Steinhorst, L., McLachlan, D.H., Schumacher, K., Hetherington, A.M., Kudla, J., Cubero, B. and Pardo, J.M., 2014. Control of vacuolar dynamics and regulation of stomatal aperture by tonoplast potassium uptake. *Proceedings of the National Academy of Sciences*, *111*(17), pp.E1806-E1814.

Aro, E.M., Suorsa, M., Rokka, A., Allahverdiyeva, Y., Paakkarinen, V., Saleem, A., Battchikova, N. and Rintamäki, E., 2005. Dynamics of photosystem II: a proteomic approach to thylakoid protein complexes. *Journal of experimental botany*, *56*(411), pp.347-356.

Assmann, S.M. and Jegla, T., 2016. Guard cell sensory systems: recent insights on stomatal responses to light, abscisic acid, and CO2. *Current opinion in plant biology*, *33*, pp.157-167.

Assmann, S.M., Simoncini, L. and Schroeder, J.I., 1985. Blue light activates electrogenic ion pumping in guard cell protoplasts of Vicia faba. *Nature*, *318*(6043), pp.285-287.

Atmodjo, M.A., Hao, Z. and Mohnen, D., 2013. Evolving views of pectin biosynthesis. *Annual review of plant biology*, *64*, pp.747-779.

Bailey, S., Walters, R.G., Jansson, S. and Horton, P., 2001. Acclimation of Arabidopsis thaliana to the light environment: the existence of separate low light and high light responses. *Planta*, *213*, pp.794-801.

Baker, N.R., 2008. Chlorophyll fluorescence: a probe of photosynthesis in vivo. *Annu. Rev. Plant Biol.*, *59*, pp.89-113.

Bergmann, D.C. and Sack, F.D., 2007. Stomatal development. *Annu. Rev. Plant Biol.*, *58*, pp.163-181.

Bertolino, L.T., Caine, R.S. and Gray, J.E., 2019. Impact of stomatal density and morphology on water-use efficiency in a changing world. *Frontiers in plant science*, *10*, p.225.

Blatt, M.R. and Gradmann, D., 1997. K+-sensitive gating of the K+ outward rectifier in Vicia guard cells. The Journal of membrane biology, 158, pp.241-256.

Blatt, M.R., 1988. Potassium-dependent, bipolar gating of K+ channels in guard cells. The Journal of Membrane Biology, 102, pp.235-246.

Blatt, M.R., 2000. Cellular signaling and volume control in stomatal movements in plants. *Annual review of cell and developmental biology*, *16*(1), pp.221-241.

Blum, A., 2009. Effective use of water (EUW) and not water-use efficiency (WUE) is the target of crop yield improvement under drought stress. *Field crops research*, *112*(2-3), pp.119-123.

Brearley, J., Venis, M.A. and Blatt, M.R., 1997. The effect of elevated CO 2 concentrations on K+ and anion channels of Vicia faba L. guard cells. *Planta*, *203*, pp.145-154.

Brennan, M., Fakharuzi, D. and Harris, P.J., 2019. Occurrence of fucosylated and non-fucosylated xyloglucans in the cell walls of monocotyledons: an immunofluorescence study. *Plant Physiology and Biochemistry*, *139*, pp.428-434.

Briggs, W.R. and Christie, J.M., 2002. Phototropins 1 and 2: versatile plant blue-light receptors. *Trends in plant science*, *7*(5), pp.204-210.

Brodribb, T.J. and McAdam, S.A., 2011. Passive origins of stomatal control in vascular plants. *Science*, *331*(6017), pp.582-585.

Cai, S., Huang, Y., Chen, F., Zhang, X., Sessa, E., Zhao, C., Marchant, D.B., Xue, D., Chen, G., Dai, F. and Leebens-Mack, J.H., 2021. Evolution of rapid blue-light response linked to explosive diversification of ferns in angiosperm forests. *New Phytologist*, *230*(3), pp.1201-1213.

Caine, R.S., Chater, C.C., Kamisugi, Y., Cuming, A.C., Beerling, D.J., Gray, J.E. and Fleming, A.J., 2016. An ancestral stomatal patterning module revealed in the non-vascular land plant Physcomitrella patens. *Development*, *143*(18), pp.3306-3314.

Caine, R.S., Yin, X., Sloan, J., Harrison, E.L., Mohammed, U., Fulton, T., Biswal, A.K., Dionora, J., Chater, C.C., Coe, R.A. and Bandyopadhyay, A., 2019. Rice with reduced stomatal density conserves water and has improved drought tolerance under future climate conditions. *New Phytologist*, *221*(1), pp.371-384.

Carpita, N.C. and Gibeaut, D.M., 1993. Structural models of primary cell walls in flowering plants: consistency of molecular structure with the physical properties of the walls during growth. *The Plant Journal*, *3*(1), pp.1-30.

Carpita, N.C., 1996. Structure and biogenesis of the cell walls of grasses. *Annual review of plant biology*, *47*(1), pp.445-476.

Carroll, S., Amsbury, S., Durney, C.H., Smith, R.S., Morris, R.J., Gray, J.E. and Fleming, A.J., 2022. Altering arabinans increases Arabidopsis guard cell flexibility and stomatal opening. *Current Biology*, *32*(14), pp.3170-3179.

Carter, R., Woolfenden, H., Baillie, A., Amsbury, S., Carroll, S., Healicon, E., Sovatzoglou, S., Braybrook, S., Gray, J.E., Hobbs, J. and Morris, R.J., 2017. Stomatal opening involves polar, not radial, stiffening of guard cells. *Current Biology*, *27*(19), pp.2974-2983.

Casson, S. and Gray, J.E., 2008. Influence of environmental factors on stomatal development. *New phytologist*, *178*(1), pp.9-23.

Cavalier, D.M., Lerouxel, O., Neumetzler, L., Yamauchi, K., Reinecke, A., Freshour, G., Zabotina, O.A., Hahn, M.G., Burgert, I., Pauly, M. and Raikhel, N.V., 2008. Disrupting two Arabidopsis thaliana xylosyltransferase genes results in plants deficient in xyloglucan, a major primary cell wall component. *The Plant Cell*, *20*(6), pp.1519-1537.

Centritto, M., Lauteri, M., Monteverdi, M.C. and Serraj, R., 2009. Leaf gas exchange, carbon isotope discrimination, and grain yield in contrasting rice genotypes subjected to water deficits during the reproductive stage. *Journal of experimental botany*, *60*(8), pp.2325-2339.

Chater, C., Kamisugi, Y., Movahedi, M., Fleming, A., Cuming, A.C., Gray, J.E. and Beerling, D.J., 2011. Regulatory mechanism controlling stomatal behavior conserved across 400 million years of land plant evolution. *Current Biology*, *21*(12), pp.1025-1029.

Chater, C.C., Caine, R.S., Tomek, M., Wallace, S., Kamisugi, Y., Cuming, A.C., Lang, D., MacAlister, C.A., Casson, S., Bergmann, D.C. and Decker, E.L., 2016. Origin and function of stomata in the moss Physcomitrella patens. *Nature plants*, *2*(12), pp.1-7.

Chaves, M.M., Flexas, J. and Pinheiro, C., 2009. Photosynthesis under drought and salt stress: regulation mechanisms from whole plant to cell. *Annals of botany*, *103*(4), pp.551-560.

Chazdon, R.L. and Pearcy, R.W., 1991. The importance of sunflecks for forest understory plants. *BioScience*, *41*(11), pp.760-766.

Chen, Y., Li, W., Turner, J.A. and Anderson, C.T., 2021. PECTATE LYASE LIKE12 patterns the guard cell wall to coordinate turgor pressure and wall mechanics for proper stomatal function in Arabidopsis. *The Plant Cell*, *33*(9), pp.3134-3150.

Chen, Z.H., Chen, G., Dai, F., Wang, Y., Hills, A., Ruan, Y.L., Zhang, G., Franks, P.J., Nevo, E. and Blatt, M.R., 2017. Molecular evolution of grass stomata. *Trends in Plant Science*, *22*(2), pp.124-139.

Christin, P.A., Spriggs, E., Osborne, C.P., Strömberg, C.A., Salamin, N. and Edwards, E.J., 2014. Molecular dating, evolutionary rates, and the age of the grasses. *Systematic biology*, *63*(2), pp.153-165.

Clark, J.W., Harris, B.J., Hetherington, A.J., Hurtado-Castano, N., Brench, R.A., Casson, S., Williams, T.A., Gray, J.E. and Hetherington, A.M., 2022. The origin and evolution of stomata. Current Biology, 32(11), pp.R539-R553.

Clarke, J.T., Warnock, R.C. and Donoghue, P.C., 2011. Establishing a time-scale for plant evolution. *New Phytologist*, *192*(1), pp.266-301.

Cockburn, W., 1983. Stomatal mechanism as the basis of the evolution of CAM and C4 photosynthesis. *Plant, Cell & Environment*, *6*(4), pp.275-279.

Cornuault, V., Buffetto, F., Marcus, S.E., Crépeau, M.J., Guillon, F., Ralet, M.C. and Knox, J.P., 2017. LM6-M: a high avidity rat monoclonal antibody to pectic α-1, 5-L-arabinan. *BioRxiv*, p.161604.

Cosgrove, D.J. and Jarvis, M.C., 2012. Comparative structure and biomechanics of plant primary and secondary cell walls. *Frontiers in plant science*, *3*, p.204.

De Angeli, A., Zhang, J., Meyer, S. and Martinoia, E., 2013. AtALMT9 is a malate-activated vacuolar chloride channel required for stomatal opening in Arabidopsis. *Nature communications*, *4*(1), p.1804.

de Boer, H.J., Price, C.A., Wagner-Cremer, F., Dekker, S.C., Franks, P.J. and Veneklaas, E.J., 2016. Optimal allocation of leaf epidermal area for gas exchange. *New Phytologist*, *210*(4), pp.1219-1228.

De Souza, A.P., Wang, Y., Orr, D.J., Carmo-Silva, E. and Long, S.P., 2020. Photosynthesis across African cassava germplasm is limited by Rubisco and mesophyll conductance at steady state, but by stomatal conductance in fluctuating light. *New Phytologist*, *225*(6), pp.2498-2512.

Deans, R.M., Brodribb, T.J., Busch, F.A. and Farquhar, G.D., 2019. Plant water-use strategy mediates stomatal effects on the light induction of photosynthesis. *New Phytologist*, *222*(1), pp.382-395.

Doheny-Adams, T., Hunt, L., Franks, P.J., Beerling, D.J. and Gray, J.E., 2012. Genetic manipulation of stomatal density influences stomatal size, plant growth and tolerance to restricted water supply across a growth carbon dioxide gradient. *Philosophical Transactions of the Royal Society B: Biological Sciences*, *367*(1588), pp.547-555.

Dow, G.J. and Bergmann, D.C., 2014a. Patterning and processes: how stomatal development defines physiological potential. *Current opinion in plant biology*, *21*, pp.67-74.

Dow, G.J., Bergmann, D.C. and Berry, J.A., 2014b. An integrated model of stomatal development and leaf physiology. *New Phytologist*, *201*(4), pp.1218-1226.

Drake, P.L., De Boer, H.J., Schymanski, S.J. and Veneklaas, E.J., 2019. Two sides to every leaf: water and CO 2 transport in hypostomatous and amphistomatous leaves. *New Phytologist*, *222*(3), pp.1179-1187.

Drake, P.L., Froend, R.H. and Franks, P.J., 2013. Smaller, faster stomata: scaling of stomatal size, rate of response, and stomatal conductance. *Journal of experimental botany*, *64*(2), pp.495-505.

Duckett, J.G., Pressel, S., P'ng, K.M. and Renzaglia, K.S., 2009. Exploding a myth: the capsule dehiscence mechanism and the function of pseudostomata in Sphagnum. *New Phytologist*, *183*(4), pp.1053-1063.

Dunn, J., Hunt, L., Afsharinafar, M., Meselmani, M.A., Mitchell, A., Howells, R., Wallington, E., Fleming, A.J. and Gray, J.E., 2019. Reduced stomatal density in bread wheat leads to increased water-use efficiency. *Journal of Experimental Botany*, *70*(18), pp.4737-4748.

Durney, C.H., Wilson, M.J., McGregor, S., Armand, J., Smith, R.S., Gray, J.E., Morris, R.J. and Fleming, A.J., 2023. Grasses exploit geometry to achieve improved guard cell dynamics. *Current Biology*.

Edgerton, M.D., 2009. Increasing crop productivity to meet global needs for feed, food, and fuel. *Plant physiology*, *149*(1), pp.7-13.

Edwards, D., Kerp, H. and Hass, H., 1998. Stomata in early land plants: an anatomical and ecophysiological approach. *Journal of Experimental Botany*, pp.255-278.

Edwards, M., Meidner, H. and Sheriff, D.W., 1976. Direct measurements of turgor pressure potentials of guard cells: II. The mechanical advantage of subsidiary cells, The spannunqsphase, and the optimum leaf water deficit. *Journal of Experimental Botany*, *27*(1), pp.163-171.

Elliott-Kingston, C., Haworth, M., Yearsley, J.M., Batke, S.P., Lawson, T. and McElwain, J.C., 2016. Does size matter? Atmospheric CO2 may be a stronger driver of stomatal closing rate than stomatal size in taxa that diversified under low CO2. *Frontiers in Plant Science*, *7*, p.1253.

Farquhar, G.D. and Sharkey, T.D., 1982. Stomatal conductance and photosynthesis. *Annual review of plant physiology*, *33*(1), pp.317-345.

Feng, W., Kita, D., Peaucelle, A., Cartwright, H.N., Doan, V., Duan, Q., Liu, M.C., Maman, J., Steinhorst, L., Schmitz-Thom, I. and Yvon, R., 2018. The FERONIA receptor kinase maintains cell-wall integrity during salt stress through Ca2+ signaling. Current Biology, 28(5), pp.666-675.

Flexas, J., Bota, J., Loreto, F., Cornic, G. and Sharkey, T.D., 2004. Diffusive and metabolic limitations to photosynthesis under drought and salinity in C3 plants. *Plant biology*, *6*(03), pp.269-279.

Flexas, J., Ribas-Carbó, M., Bota, J., Galmés, J., Henkle, M., Martínez-Cañellas, S. and Medrano, H., 2006. Decreased Rubisco activity during water stress is not induced by decreased relative water content but related to conditions of low stomatal conductance and chloroplast CO2 concentration. *New Phytologist*, *172*(1), pp.73-82.

Flütsch, S., Wang, Y., Takemiya, A., Vialet-Chabrand, S.R., Klejchová, M., Nigro, A., Hills, A., Lawson, T., Blatt, M.R. and Santelia, D., 2020. Guard cell starch degradation yields glucose for rapid stomatal opening in Arabidopsis. *The Plant Cell*, *32*(7), pp.2325-2344.

Franks, P.J. and Beerling, D.J., 2009. Maximum leaf conductance driven by CO2 effects on stomatal size and density over geologic time. *Proceedings of the National Academy of Sciences*, *106*(25), pp.10343-10347.

Franks, P.J. and Farquhar, G.D., 2001. The effect of exogenous abscisic acid on stomatal development, stomatal mechanics, and leaf gas exchange in Tradescantia virginiana. *Plant physiology*, *125*(2), pp.935-942.

Franks, P.J. and Farquhar, G.D., 2007. The mechanical diversity of stomata and its significance in gas-exchange control. *Plant physiology*, *143*(1), pp.78-87.

Franks, P.J., W. Doheny-Adams, T., Britton-Harper, Z.J. and Gray, J.E., 2015. Increasing water-use efficiency directly through genetic manipulation of stomatal density. *New Phytologist*, *207*(1), pp.188-195.

Freitas, R.S., Oliveira, L.A., McAdam, S.A., Lawson, T., DaMatta, F.M. and Cardoso, A.A., 2023. Woody species grown under sun and shade present similar stomatal speed. *Theoretical and Experimental Plant Physiology*, pp.1-12.

Garnett, T., Appleby, M.C., Balmford, A., Bateman, I.J., Benton, T.G., Bloomer, P., Burlingame, B., Dawkins, M., Dolan, L., Fraser, D. and Herrero, M., 2013. Sustainable intensification in agriculture: premises and policies. *Science*, *341*(6141), pp.33-34.

Gay, A.P. and Hurd, R.G., 1975. The influence of light on stomatal density in the tomato. *New Phytologist*, *75*(1), pp.37-46.

Geiger, D., Scherzer, S., Mumm, P., Stange, A., Marten, I., Bauer, H., Ache, P., Matschi, S., Liese, A., Al-Rasheid, K.A. and Romeis, T., 2009. Activity of guard cell anion channel SLAC1 is controlled by drought-stress signaling kinase-phosphatase pair. *Proceedings of the National Academy of Sciences*, *106*(50), pp.21425-21430.

Givnish, T.J., Evans, T.M., Zjhra, M.L., Patterson, T.B., Berry, P.E. and Sytsma, K.J., 2000. Molecular evolution, adaptive radiation, and geographic diversification in the amphiatlantic family Rapateaceae: evidence from ndhF sequences and morphology. *Evolution*, *54*(6), pp.1915-1937.

Gkolemis, K., Giannoutsou, E., Adamakis, I-D, S., Galatis, B. and Apostolakos, P., 2023. Cell wall anisotropy plays a key role in Zea mays stomatal complex movement: the possible role of the cell wall matrix. Plant Molecular Biology.

Goh, C.H., Kinoshita, T., Oku, T. and Shimazaki, K.I., 1996. Inhibition of blue light-dependent H+ pumping by abscisic acid in Vicia guard-cell protoplasts. *Plant Physiology*, *111*(2), pp.433-440.

Grantz, D.A. and Assmann, S.M., 1991. Stomatal response to blue light: water use efficiency in sugarcane and soybean. *Plant, Cell & Environment*, *14*(7), pp.683-690.

Gray, A., Liu, L. and Facette, M., 2020. Flanking support: how subsidiary cells contribute to stomatal form and function. *Frontiers in Plant Science*, *11*, p.881.

Grieco, M., Roustan, V., Dermendjiev, G., Rantala, S., Jain, A., Leonardelli, M., Neumann, K., Berger, V., Engelmeier, D., Bachmann, G. and Ebersberger, I., 2020. Adjustment of photosynthetic activity to drought and fluctuating light in wheat. *Plant, Cell & Environment*, *43*(6), pp.1484-1500.

Hara, K., Kajita, R., Torii, K.U., Bergmann, D.C. and Kakimoto, T., 2007. The secretory peptide gene EPF1 enforces the stomatal one-cell-spacing rule. *Genes & development*, *21*(14), pp.1720-1725.

Hara, K., Yokoo, T., Kajita, R., Onishi, T., Yahata, S., Peterson, K.M., Torii, K.U. and Kakimoto, T., 2009. Epidermal cell density is autoregulated via a secretory peptide, EPIDERMAL PATTERNING FACTOR 2 in Arabidopsis leaves. *Plant and Cell Physiology*, *50*(6), pp.1019-1031.

Harris, B.J., Harrison, C.J., Hetherington, A.M. and Williams, T.A., 2020. Phylogenomic evidence for the monophyly of bryophytes and the reductive evolution of stomata. *Current Biology*, *30*(11), pp.2001-2012.

Hashimoto, M., Negi, J., Young, J., Israelsson, M., Schroeder, J.I. and Iba, K., 2006. Arabidopsis HT1 kinase controls stomatal movements in response to CO2. *Nature cell biology*, *8*(4), pp.391-397.

Hatch, M.D., 1987. C4 photosynthesis: a unique elend of modified biochemistry, anatomy and ultrastructure. *Biochimica et Biophysica Acta (BBA)-Reviews on Bioenergetics*, *895*(2), pp.81-106.

Haworth, M., Scutt, C.P., Douthe, C., Marino, G., Gomes, M.T.G., Loreto, F., Flexas, J. and Centritto, M., 2018. Allocation of the epidermis to stomata relates to stomatal physiological control: stomatal factors involved in the evolutionary diversification of the angiosperms and development of amphistomaty. *Environmental and Experimental Botany*, *151*, pp.55-63.

Heath, O.V.S., 1938. An Experimental Investigation of the Mechanism of Stomatal Movement, with Some Preliminary Observations Upon the Response of the Guard Cells to" Shock". *The New Phytologist*, *37*(5), pp.385-395.

Hedges, S.B. and Kumar, S. eds., 2009. *The timetree of life*. OUP Oxford.

Hepworth, C., Caine, R.S., Harrison, E.L., Sloan, J. and Gray, J.E., 2018. Stomatal development: focusing on the grasses. *Current opinion in plant biology*, *41*, pp.1-7.

Hepworth, C., Doheny-Adams, T., Hunt, L., Cameron, D.D. and Gray, J.E., 2015. Manipulating stomatal density enhances drought tolerance without deleterious effect on nutrient uptake. *The New Phytologist*, *208*(2), p.336.

Hetherington, A.M. and Woodward, F.I., 2003. The role of stomata in sensing and driving environmental change. *Nature*, *424*(6951), pp.901-908.

Hill Jr, J.L., Hammudi, M.B. and Tien, M., 2014. The Arabidopsis cellulose synthase complex: a proposed hexamer of CESA trimers in an equimolar stoichiometry. *The Plant Cell*, *26*(12), pp.4834-4842.

Hocq, L., Pelloux, J. and Lefebvre, V., 2017. Connecting homogalacturonan-type pectin remodeling to acid growth. *Trends in Plant Science*, *22*(1), pp.20-29.

Hõrak, H., Kollist, H. and Merilo, E., 2017. Fern stomatal responses to ABA and CO2 depend on species and growth conditions. *Plant Physiology*, *174*(2), pp.672-679.

Horaruang, W., Klejchová, M., Carroll, W., Silva-Alvim, F.A., Waghmare, S., Papanatsiou, M., Amtmann, A., Hills, A., Alvim, J.C., Blatt, M.R. and Zhang, B., 2022. Engineering a K+ channel 'sensory antenna'enhances stomatal kinetics, water use efficiency and photosynthesis. *Nature Plants*, pp.1-13.

Horrer, D., Flütsch, S., Pazmino, D., Matthews, J.S., Thalmann, M., Nigro, A., Leonhardt, N., Lawson, T. and Santelia, D., 2016. Blue light induces a distinct starch degradation pathway in guard cells for stomatal opening. *Current Biology*, *26*(3), pp.362-370.

Hughes, J., Hepworth, C., Dutton, C., Dunn, J.A., Hunt, L., Stephens, J., Waugh, R., Cameron, D.D. and Gray, J.E., 2017. Reducing stomatal density in barley improves drought tolerance without impacting on yield. *Plant physiology*, *174*(2), pp.776-787.

Hughes, J., Hepworth, C., Dutton, C., Dunn, J.A., Hunt, L., Stephens, J., Waugh, R., Cameron, D.D. and Gray, J.E., 2017. Reducing stomatal density in barley improves drought tolerance without impacting on yield. *Plant physiology*, *174*(2), pp.776-787.

Hunt, L. and Gray, J.E., 2009. The signaling peptide EPF2 controls asymmetric cell divisions during stomatal development. *Current Biology*, *19*(10), pp.864-869.

Hunt, L., Bailey, K.J. and Gray, J.E., 2010. The signalling peptide EPFL9 is a positive regulator of stomatal development. *New Phytologist*, pp.609-614.

Inoue, S.I. and Kinoshita, T., 2017. Blue light regulation of stomatal opening and the plasma membrane H+-ATPase. *Plant Physiology*, *174*(2), pp.531-538.

Ishii, T. and Matsunaga, T., 1996. Isolation and characterization of a boron-rhamnogalacturonan-II complex from cell walls of sugar beet pulp. *Carbohydrate research*, *284*(1), pp.1-9.

Israel, W.K., Watson-Lazowski, A., Chen, Z.H. and Ghannoum, O., 2022. High intrinsic water use efficiency is underpinned by high stomatal aperture and guard cell potassium flux in C3 and

C4 grasses grown at glacial CO2 and low light. *Journal of Experimental Botany*, *73*(5), pp.1546-1565.

Jones, L., Milne, J.L., Ashford, D. and McQueen-Mason, S.J., 2003. Cell wall arabinan is essential for guard cell function. *Proceedings of the National Academy of Sciences*, *100*(20), pp.11783-11788.

Jones, L., Milne, J.L., Ashford, D., McCann, M.C. and McQueen-Mason, S.J., 2005. A conserved functional role of pectic polymers in stomatal guard cells from a range of plant species. *Planta*, *221*, pp.255-264.

Jones, L., Seymour, G.B. and Knox, J.P., 1997. Localization of pectic galactan in tomato cell walls using a monoclonal antibody specific to (1 [->] 4)-β-D-Galactan. *Plant physiology*, *113*(4), pp.1405-1412.

Jossier, M., Kroniewicz, L., Dalmas, F., Le Thiec, D., Ephritikhine, G., Thomine, S., Barbier-Brygoo, H., Vavasseur, A., Filleur, S. and Leonhardt, N., 2010. The Arabidopsis vacuolar anion transporter, AtCLCc, is involved in the regulation of stomatal movements and contributes to salt tolerance. *The Plant Journal*, *64*(4), pp.563-576.

Kanaoka, M.M., Pillitteri, L.J., Fujii, H., Yoshida, Y., Bogenschutz, N.L., Takabayashi, J., Zhu, J.K. and Torii, K.U., 2008. SCREAM/ICE1 and SCREAM2 specify three cell-state transitional steps leading to Arabidopsis stomatal differentiation. *The Plant Cell*, *20*(7), pp.1775-1785.

Kardiman, R. and Ræbild, A., 2018. Relationship between stomatal density, size and speed of opening in Sumatran rainforest species. *Tree physiology*, *38*(5), pp.696-705.

Kijne, J.W., Barker, R. and Molden, D.J. eds., 2003. *Water productivity in agriculture: limits and opportunities for improvement* (Vol. 1). Cabi.

Kim, T.H., Böhmer, M., Hu, H., Nishimura, N. and Schroeder, J.I., 2010. Guard cell signal transduction network: advances in understanding abscisic acid, CO2, and Ca2+ signaling. *Annual review of plant biology*, *61*, pp.561-591.

Kimura, H., Hashimoto-Sugimoto, M., Iba, K., Terashima, I. and Yamori, W., 2020. Improved stomatal opening enhances photosynthetic rate and biomass production in fluctuating light. *Journal of experimental botany*, *71*(7), pp.2339-2350.

Kinoshita, T. and Hayashi, Y., 2011. New insights into the regulation of stomatal opening by blue light and plasma membrane H+-ATPase. *International Review of Cell and Molecular Biology*, *289*, pp.89-115.

Knapp, A.K. and Smith, W.K., 1987. Stomatal and photosynthetic responses during sun/shade transitions in subalpine plants: influence on water use efficiency. *Oecologia*, pp.62-67.

Knapp, A.K. and Smith, W.K., 1989. Influence of growth from on ecophysiological responses to variable sunlight in subalpine plants. *Ecology*, *70*(4), pp.1069-1082.

Kollist, H., Nuhkat, M. and Roelfsema, M.R.G., 2014. Closing gaps: linking elements that control stomatal movement. *New Phytologist*, *203*(1), pp.44-62.

Krieger-Liszkay, A., 2005. Singlet oxygen production in photosynthesis. *Journal of experimental botany*, *56*(411), pp.337-346.

Kuiper, P.J., 1964. Dependence upon wavelength of stomatal movement in epidermal tissue of Senecio odoris. *Plant Physiology*, *39*(6), p.952.

Kumar, S., Suleski, M., Craig, J.M., Kasprowicz, A.E., Sanderford, M., Li, M., Stecher, G. and Hedges, S.B., 2022. TimeTree 5: an expanded resource for species divergence times. *Molecular Biology and Evolution*, *39*(8), p.msac174.

Lampard, G.R., Lukowitz, W., Ellis, B.E. and Bergmann, D.C., 2009. Novel and expanded roles for MAPK signaling in Arabidopsis stomatal cell fate revealed by cell type–specific manipulations. *The Plant Cell*, *21*(11), pp.3506-3517.

Lampard, G.R., MacAlister, C.A. and Bergmann, D.C., 2008. Arabidopsis stomatal initiation is controlled by MAPK-mediated regulation of the bHLH SPEECHLESS. *Science*, *322*(5904), pp.1113-1116.

Larkin, J.C., Marks, M.D., Nadeau, J. and Sack, F., 1997. Epidermal cell fate and patterning in leaves. *The Plant Cell*, *9*(7), p.1109.

Lawlor, D.W. and Tezara, W., 2009. Causes of decreased photosynthetic rate and metabolic capacity in water-deficient leaf cells: a critical evaluation of mechanisms and integration of processes. *Annals of botany*, *103*(4), pp.561-579.

Lawson, T. and Blatt, M.R., 2014. Stomatal size, speed, and responsiveness impact on photosynthesis and water use efficiency. *Plant physiology*, *164*(4), pp.1556-1570.

Lawson, T. and Vialet-Chabrand, S., 2019. Speedy stomata, photosynthesis and plant water use efficiency. *New Phytologist*, *221*(1), pp.93-98.

Lee, J.S., Hnilova, M., Maes, M., Lin, Y.C.L., Putarjunan, A., Han, S.K., Avila, J. and Torii, K.U., 2015. Competitive binding of antagonistic peptides fine-tunes stomatal patterning. *Nature*, *522*(7557), pp.439-443.

Lee, S.C., Lan, W., Buchanan, B.B. and Luan, S., 2009. A protein kinase-phosphatase pair interacts with an ion channel to regulate ABA signaling in plant guard cells. *Proceedings of the National Academy of Sciences*, *106*(50), pp.21419-21424.

Lesk, C., Rowhani, P. and Ramankutty, N., 2016. Influence of extreme weather disasters on global crop production. *Nature*, *529*(7584), pp.84-87.

Li, S., Bashline, L., Lei, L. and Gu, Y., 2014. Cellulose synthesis and its regulation. *The Arabidopsis Book/American Society of Plant Biologists*, *12*.

Lind, C., Dreyer, I., Lopez-Sanjurjo, E.J., von Meyer, K., Ishizaki, K., Kohchi, T., Lang, D., Zhao, Y., Kreuzer, I., Al-Rasheid, K.A. and Ronne, H., 2015. Stomatal guard cells co-opted an ancient ABA-dependent desiccation survival system to regulate stomatal closure. *Current Biology*, *25*(7), pp.928-935.

Liu, T., Ohashi-Ito, K. and Bergmann, D.C., 2009. Orthologs of Arabidopsis thaliana stomatal bHLH genes and regulation of stomatal development in grasses.

Long, S.P., Humphries, S. and Falkowski, P.G., 1994. Photoinhibition of photosynthesis in nature. *Annual review of plant biology*, *45*(1), pp.633-662.

Lundgren, M.R., Osborne, C.P. and Christin, P.A., 2014. Deconstructing Kranz anatomy to understand C4 evolution. *Journal of experimental botany*, *65*(13), pp.3357-3369.

MacAlister, C.A. and Bergmann, D.C., 2011. Sequence and function of basic helix–loop–helix proteins required for stomatal development in Arabidopsis are deeply conserved in land plants. *Evolution & development*, *13*(2), pp.182-192.

MacAlister, C.A., Ohashi-Ito, K. and Bergmann, D.C., 2007. Transcription factor control of asymmetric cell divisions that establish the stomatal lineage. *Nature*, *445*(7127), pp.537-540.

Magallón, S., Hilu, K.W. and Quandt, D., 2013. Land plant evolutionary timeline: gene effects are secondary to fossil constraints in relaxed clock estimation of age and substitution rates. *American Journal of Botany*, *100*(3), pp.556-573.

Majore, I., Wilhelm, B. and Marten, I., 2002. Identification of K+ channels in the plasma membrane of maize subsidiary cells. *Plant and cell physiology*, *43*(8), pp.844-852.

Marcus, S.E., Blake, A.W., Benians, T.A., Lee, K.J., Poyser, C., Donaldson, L., Leroux, O., Rogowski, A., Petersen, H.L., Boraston, A. and Gilbert, H.J., 2010. Restricted access of proteins to mannan polysaccharides in intact plant cell walls. *The Plant Journal*, *64*(2), pp.191-203.

Marcus, S.E., Verhertbruggen, Y., Hervé, C., Ordaz-Ortiz, J.J., Farkas, V., Pedersen, H.L., Willats, W.G. and Knox, J.P., 2008. Pectic homogalacturonan masks abundant sets of xyloglucan epitopes in plant cell walls. *BMC plant biology*, *8*, pp.1-12.

Matrosova, A., Bogireddi, H., Mateo-Peñas, A., Hashimoto-Sugimoto, M., Iba, K., Schroeder, J.I. and Israelsson-Nordström, M., 2015. The HT 1 protein kinase is essential for red light-induced stomatal opening and genetically interacts with OST 1 in red light and CO 2-induced stomatal movement responses. *New Phytologist*, *208*(4), pp.1126-1137.

Matthews, J.S., Vialet-Chabrand, S. and Lawson, T., 2018. Acclimation to fluctuating light impacts the rapidity of response and diurnal rhythm of stomatal conductance. *Plant Physiology*, *176*(3), pp.1939-1951.

Matthews, J.S., Vialet-Chabrand, S. and Lawson, T., 2020. Role of blue and red light in stomatal dynamic behaviour. *Journal of Experimental Botany*, *71*(7), pp.2253-2269.

Matthews, J.S., Vialet-Chabrand, S.R. and Lawson, T., 2017. Diurnal variation in gas exchange: the balance between carbon fixation and water loss. *Plant Physiology*, *174*(2), pp.614-623.

McAusland, L., Vialet-Chabrand, S., Davey, P., Baker, N.R., Brendel, O. and Lawson, T., 2016. Effects of kinetics of light-induced stomatal responses on photosynthesis and water-use efficiency. *New Phytologist*, *211*(4), pp.1209-1220.

McCartney, L., Marcus, S.E. and Knox, J.P., 2005. Monoclonal antibodies to plant cell wall xylans and arabinoxylans. *Journal of Histochemistry & Cytochemistry*, *53*(4), pp.543-546.

McElwain, J.C., Yiotis, C. and Lawson, T., 2016. Using modern plant trait relationships between observed and theoretical maximum stomatal conductance and vein density to examine patterns of plant macroevolution. *New Phytologist*, *209*(1), pp.94-103.

McGregor, S., 2021. Cell Wall Composition and Morphology in Grass Stomata (Issue December)

McKown, A.D., Guy, R.D., Quamme, L., Klápště, J., La Mantia, J., Constabel, C.P., El-Kassaby, Y.A., Hamelin, R.C., Zifkin, M. and Azam, M.S., 2014. Association genetics, geography and ecophysiology link stomatal patterning in P opulus trichocarpa with carbon gain and disease resistance trade-offs. *Molecular ecology*, *23*(23), pp.5771-5790.

McKown, K.H. and Bergmann, D.C., 2020. Stomatal development in the grasses: lessons from models and crops (and crop models). *New Phytologist*, *227*(6), pp.1636-1648.

Melis, A., 1999. Photosystem-II damage and repair cycle in chloroplasts: what modulates the rate of photodamage in vivo?. *Trends in plant science*, *4*(4), pp.130-135.

Mencuccini, M., Mambelli, S. and Comstock, J., 2000. Stomatal responsiveness to leaf water status in common bean (Phaseolus vulgaris L.) is a function of time of day. *Plant, cell & environment*, *23*(10), pp.1109-1118.

Merced, A. and Renzaglia, K., 2014. Developmental changes in guard cell wall structure and pectin composition in the moss Funaria: implications for function and evolution of stomata. *Annals of Botany*, *114*(5), pp.1001-1010.

Merced, A. and Renzaglia, K.S., 2013. Moss stomata in highly elaborated Oedipodium (Oedipodiaceae) and highly reduced Ephemerum (Pottiaceae) sporophytes are remarkably similar. *American Journal of Botany*, *100*(12), pp.2318-2327.

Merced, A. and Renzaglia, K.S., 2016. Patterning of stomata in the moss Funaria: a simple way to space guard cells. *Annals of Botany*, *117*(6), pp.985-994.

Messinger, S.M., Buckley, T.N. and Mott, K.A., 2006. Evidence for involvement of photosynthetic processes in the stomatal response to CO2. *Plant physiology*, *140*(2), pp.771-778.

Mizokami, Y., Noguchi, K.O., Kojima, M., Sakakibara, H. and Terashima, I., 2015. Mesophyll conductance decreases in the wild type but not in an ABA-deficient mutant (aba1) of Nicotiana plumbaginifolia under drought conditions. *Plant, Cell & Environment*, *38*(3), pp.388-398.

Mohnen, D., 2008. Pectin structure and biosynthesis. *Current opinion in plant biology*, *11*(3), pp.266-277.

Moore, J.P., Farrant, J.M. and Driouich, A., 2008. A role for pectin-associated arabinans in maintaining the flexibility of the plant cell wall during water deficit stress. *Plant Signaling & Behavior*, *3*(2), pp.102-104.

Moore, J.P., Nguema-Ona, E.E., Vicré-Gibouin, M., Sørensen, I., Willats, W.G., Driouich, A. and Farrant, J.M., 2013. Arabinose-rich polymers as an evolutionary strategy to plasticize resurrection plant cell walls against desiccation. *Planta*, *237*, pp.739-754.

Morison, J.I.L., Baker, N.R., Mullineaux, P.M. and Davies, W.J., 2008. Improving water use in crop production. *Philosophical Transactions of the Royal Society B: Biological Sciences*, *363*(1491), pp.639-658.

Mott, K.A., 1988. Do stomata respond to CO2 concentrations other than intercellular?. *Plant physiology*, *86*(1), pp.200-203.

Muir, C.D., 2015. Making pore choices: repeated regime shifts in stomatal ratio. *Proceedings of the Royal Society B: Biological Sciences*, *282*(1813), p.20151498.

Muir, C.D., Hangarter, R.P., Moyle, L.C. and Davis, P.A., 2014. Morphological and anatomical determinants of mesophyll conductance in wild relatives of tomato (Solanum sect. l ycopersicon, sect. l ycopersicoides; s olanaceae). *Plant, Cell & Environment*, *37*(6), pp.1415-1426.

Ohashi-Ito, K. and Bergmann, D.C., 2006. Arabidopsis FAMA controls the final proliferation/differentiation switch during stomatal development. *The Plant Cell*, *18*(10), pp.2493-2505.

Oikawa, A., Lund, C.H., Sakuragi, Y. and Scheller, H.V., 2013. Golgi-localized enzyme complexes for plant cell wall biosynthesis. *Trends in plant science*, *18*(1), pp.49-58.

Olsen, R.L., Pratt, R.B., Gump, P., Kemper, A. and Tallman, G., 2002. Red light activates a chloroplast-dependent ion uptake mechanism for stomatal opening under reduced CO2 concentrations in Vicia spp. *New Phytologist*, *153*(3), pp.497-508.

O'NEeill, M.A., Albersheim, P. and Darvill, A., 1990. The pectic polysaccharides of primary cell walls. In *Methods in plant biochemistry* (Vol. 2, pp. 415-441). Academic Press.

O'Neill, M.A., Ishii, T., Albersheim, P. and Darvill, A.G., 2004. Rhamnogalacturonan II: structure and function of a borate cross-linked cell wall pectic polysaccharide. *Annu. Rev. Plant Biol.*, *55*, pp.109-139.

Ooba, M. and Takahashi, H., 2003. Effect of asymmetric stomatal response on gas-exchange dynamics. *Ecological Modelling*, *164*(1), pp.65-82.

Ooba, M. and Takahashi, H., 2003. Effect of asymmetric stomatal response on gas-exchange dynamics. *Ecological Modelling*, *164*(1), pp.65-82.

Ort, D.R. and Long, S.P., 2014. Limits on yields in the corn belt. *Science*, *344*(6183), pp.484-485.

Osborne, C.P. and Sack, L., 2012. Evolution of C4 plants: a new hypothesis for an interaction of CO2 and water relations mediated by plant hydraulics. *Philosophical Transactions of the Royal Society B: Biological Sciences*, *367*(1588), pp.583-600.

Ozeki, K., Miyazawa, Y. and Sugiura, D., 2022. Rapid stomatal closure contributes to higher water use efficiency in major C4 compared to C3 Poaceae crops. *Plant physiology*, *189*(1), pp.188-203.

Papanatsiou, M., Petersen, J., Henderson, L., Wang, Y., Christie, J.M. and Blatt, M.R., 2019. Optogenetic manipulation of stomatal kinetics improves carbon assimilation, water use, and growth. *Science*, *363*(6434), pp.1456-1459.

Parfrey, L.W., Lahr, D.J., Knoll, A.H. and Katz, L.A., 2011. Estimating the timing of early eukaryotic diversification with multigene molecular clocks. *Proceedings of the National Academy of Sciences*, *108*(33), pp.13624-13629.

Pauly, M. and Keegstra, K., 2016. Biosynthesis of the plant cell wall matrix polysaccharide xyloglucan. *Annual review of plant biology*, *67*, pp.235-259.

Pearcy, R.W., 1990. Sunflecks and photosynthesis in plant canopies. *Annual review of plant biology*, *41*(1), pp.421-453.

Pearcy, R.W., Roden, J.S. and Gamon, J.A., 1990. Sunfleck dynamics in relation to canopy structure in a soybean (Glycine max (L.) Merr.) canopy. *Agricultural and Forest Meteorology*, *52*(3-4), pp.359-372.

Pedersen, H.L., Fangel, J.U., McCleary, B., Ruzanski, C., Rydahl, M.G., Ralet, M.C., Farkas, V., von Schantz, L., Marcus, S.E., Andersen, M.C. and Field, R., 2012. Versatile high resolution oligosaccharide microarrays for plant glycobiology and cell wall research. *Journal of Biological Chemistry*, *287*(47), pp.39429-39438.

Pemadasa, M.A., 1979. Movements of abaxial and adaxial stomata. *New Phytologist*, *82*(1), pp.69-80.

Pillitteri, L.J., Sloan, D.B., Bogenschutz, N.L. and Torii, K.U., 2007. Termination of asymmetric cell division and differentiation of stomata. *Nature*, *445*(7127), pp.501-505.

Pinheiro, C. and Chaves, M.M., 2011. Photosynthesis and drought: can we make metabolic connections from available data?. *Journal of experimental botany*, *62*(3), pp.869-882.

Plackett, A.R., Emms, D.M., Kelly, S., Hetherington, A.M. and Langdale, J.A., 2021. Conditional stomatal closure in a fern shares molecular features with flowering plant active stomatal responses. *Current Biology*, *31*(20), pp.4560-4570.

Qu, M., Essemine, J., Xu, J., Ablat, G., Perveen, S., Wang, H., Chen, K., Zhao, Y., Chen, G., Chu, C. and Zhu, X., 2020. Alterations in stomatal response to fluctuating light increase biomass and yield of rice under drought conditions. *The Plant Journal*, *104*(5), pp.1334-1347.

Raissig, M.T., Abrash, E., Bettadapur, A., Vogel, J.P. and Bergmann, D.C., 2016. Grasses use an alternatively wired bHLH transcription factor network to establish stomatal identity. *Proceedings of the National Academy of Sciences*, *113*(29), pp.8326-8331.

Raissig, M.T., Matos, J.L., Anleu Gil, M.X., Kornfeld, A., Bettadapur, A., Abrash, E., Allison, H.R., Badgley, G., Vogel, J.P., Berry, J.A. and Bergmann, D.C., 2017. Mobile MUTE specifies subsidiary cells to build physiologically improved grass stomata. *Science*, *355*(6330), pp.1215-1218.

Rajabi, A., Ober, E.S. and Griffiths, H., 2009. Genotypic variation for water use efficiency, carbon isotope discrimination, and potential surrogate measures in sugar beet. *Field Crops Research*, *112*(2-3), pp.172-181.

Ran, J.H., Shen, T.T., Liu, W.J. and Wang, X.Q., 2013. Evolution of the bHLH genes involved in stomatal development: implications for the expansion of developmental complexity of stomata in land plants. *PLoS One*, *8*(11), p.e78997.

Raven, J.A., 2002. Selection pressures on stomatal evolution. *New Phytologist*, *153*(3), pp.371-386.

Raven, J.A., 2014. Speedy small stomata?. *Journal of Experimental Botany*, *65*(6), pp.1415-1424.

Rennie, E.A. and Scheller, H.V., 2014. Xylan biosynthesis. *Current opinion in biotechnology*, *26*, pp.100-107.

Renzaglia, K.S., Browning, W.B. and Merced, A., 2020. With over 60 independent losses, stomata are expendable in mosses. *Frontiers in plant science*, *11*, p.567.

Roelfsema, M.R.G., Hanstein, S., Felle, H.H. and Hedrich, R., 2002. CO2 provides an intermediate link in the red light response of guard cells. *The Plant Journal*, *32*(1), pp.65-75.

Roelfsema, M.R.G., Steinmeyer, R., Staal, M. and Hedrich, R., 2001. Single guard cell recordings in intact plants: light-induced hyperpolarization of the plasma membrane. *The Plant Journal*, *26*(1), pp.1-13.

Rui, Y. and Anderson, C.T., 2016. Functional analysis of cellulose and xyloglucan in the walls of stomatal guard cells of Arabidopsis. *Plant Physiology*, *170*(3), pp.1398-1419.

Rui, Y., Chen, Y., Kandemir, B., Yi, H., Wang, J.Z., Puri, V.M. and Anderson, C.T., 2018. Balancing strength and flexibility: how the synthesis, organization, and modification of guard cell walls govern stomatal development and dynamics. *Frontiers in plant science*, *9*, p.1202.

Ruprecht, C., Bartetzko, M.P., Senf, D., Dallabernadina, P., Boos, I., Andersen, M.C., Kotake, T., Knox, J.P., Hahn, M.G., Clausen, M.H. and Pfrengle, F., 2017. A synthetic glycan microarray enables epitope mapping of plant cell wall glycan-directed antibodies. *Plant physiology*, *175*(3), pp.1094-1104.

Russo, S.E., Cannon, W.L., Elowsky, C., Tan, S. and Davies, S.J., 2010. Variation in leaf stomatal traits of 28 tree species in relation to gas exchange along an edaphic gradient in a Bornean rain forest. *American journal of botany*, *97*(7), pp.1109-1120.

Ruszala, E.M., Beerling, D.J., Franks, P.J., Chater, C., Casson, S.A., Gray, J.E. and Hetherington, A.M., 2011. Land plants acquired active stomatal control early in their evolutionary history. *Current biology*, *21*(12), pp.1030-1035.

Sack, F.D. and Paolillo Jr, D.J., 1985. Incomplete cytokinesis in Funaria stomata. *American Journal of Botany*, *72*(9), pp.1325-1333.

Sage, R.F., Christin, P.A. and Edwards, E.J., 2011. The C4 plant lineages of planet Earth. *Journal of experimental botany*, *62*(9), pp.3155-3169.

Sakoda, K., Taniyoshi, K., Yamori, W. and Tanaka, Y., 2022. Drought stress reduces crop carbon gain due to delayed photosynthetic induction under fluctuating light conditions. *Physiologia Plantarum*, *174*(1), p.e13603.

Salamon, M.A., Gerrienne, P., Steemans, P., Gorzelak, P., Filipiak, P., Le Hérissé, A., Paris, F., Cascales-Miñana, B., Brachaniec, T., Misz-Kennan, M. and Niedźwiedzki, R., 2018. Putative late Ordovician land plants. *New Phytologist*, *218*(4), pp.1305-1309.

Sarkar, P., Bosneaga, E. and Auer, M., 2009. Plant cell walls throughout evolution: towards a molecular understanding of their design principles. *Journal of experimental botany*, *60*(13), pp.3615-3635.

Scheller, H.V. and Ulvskov, P., 2010. Hemicelluloses. *Annual review of plant biology*, *61*, pp.263-289.

Seibt, U., Rajabi, A., Griffiths, H. and Berry, J.A., 2008. Carbon isotopes and water use efficiency: sense and sensitivity. *Oecologia*, *155*, pp.441-454.

Sharkey, T.D. and Raschke, K., 1981. Separation and measurement of direct and indirect effects of light on stomata. *Plant physiology*, *68*(1), pp.33-40.

Shpak, E.D., McAbee, J.M., Pillitteri, L.J. and Torii, K.U., 2005. Stomatal patterning and differentiation by synergistic interactions of receptor kinases. *Science*, *309*(5732), pp.290-293.

Shtein, I., Shelef, Y., Marom, Z., Zelinger, E., Schwartz, A., Popper, Z.A., Bar-On, B. and Harpaz-Saad, S., 2017. Stomatal cell wall composition: distinctive structural patterns associated with different phylogenetic groups. *Annals of Botany*, *119*(6), pp.1021-1033.

Sinclair, T.R. and Muchow, R.C., 1999. Radiation use efficiency. *Advances in agronomy*, *65*, pp.215-265.

Slattery, R.A., Walker, B.J., Weber, A.P. and Ort, D.R., 2018. The impacts of fluctuating light on crop performance. *Plant physiology*, *176*(2), pp.990-1003.

Sun, H., Shi, Q., Liu, N.Y., Zhang, S.B. and Huang, W., 2023. Drought stress delays photosynthetic induction and accelerates photoinhibition under short-term fluctuating light in tomato. *Plant Physiology and Biochemistry*, *196*, pp.152-161.

Takahashi, S. and Badger, M.R., 2011. Photoprotection in plants: a new light on photosystem II damage. *Trends in plant science*, *16*(1), pp.53-60.

Takemiya, A., Sugiyama, N., Fujimoto, H., Tsutsumi, T., Yamauchi, S., Hiyama, A., Tada, Y., Christie, J.M. and Shimazaki, K.I., 2013. Phosphorylation of BLUS1 kinase by phototropins is a primary step in stomatal opening. *Nature communications*, *4*(1), p.2094.

Terashima, I., Hanba, Y.T., Tazoe, Y., Vyas, P. and Yano, S., 2006. Irradiance and phenotype: comparative eco-development of sun and shade leaves in relation to photosynthetic CO2 diffusion. *Journal of experimental botany*, *57*(2), pp.343-354.

Torii, K.U., Mitsukawa, N., Oosumi, T., Matsuura, Y., Yokoyama, R., Whittier, R.F. and Komeda, Y., 1996. The Arabidopsis ERECTA gene encodes a putative receptor protein kinase with extracellular leucine-rich repeats. *The Plant Cell*, *8*(4), pp.735-746.

Torode, T.A., O'Neill, R., Marcus, S.E., Cornuault, V., Pose, S., Lauder, R.P., Kračun, S.K., Rydahl, M.G., Andersen, M.C., Willats, W.G. and Braybrook, S.A., 2018. Branched pectic galactan in phloem-sieve-element cell walls: implications for cell mechanics. *Plant physiology*, *176*(2), pp.1547-1558.

Turner, N.C. and Graniti, A., 1969. Fusicoccin: a fungal toxin that opens stomata. *Nature*, *223*(5210), pp.1070-1071.

Vahisalu, T., Kollist, H., Wang, Y.F., Nishimura, N., Chan, W.Y., Valerio, G., Lamminmäki, A., Brosché, M., Moldau, H., Desikan, R. and Schroeder, J.I., 2008. SLAC1 is required for plant guard cell S-type anion channel function in stomatal signalling. *Nature*, *452*(7186), pp.487-491.

Verhertbruggen, Y., Marcus, S.E., Haeger, A., Ordaz-Ortiz, J.J. and Knox, J.P., 2009. An extended set of monoclonal antibodies to pectic homogalacturonan. *Carbohydrate research*, *344*(14), pp.1858-1862.

Verhertbruggen, Y., Marcus, S.E., Haeger, A., Verhoef, R., Schols, H.A., McCleary, B.V., McKee, L., Gilbert, H.J. and Paul Knox, J., 2009b. Developmental complexity of arabinan polysaccharides and their processing in plant cell walls. *The Plant Journal*, *59*(3), pp.413-425.

Vialet-Chabrand, S., Matthews, J.S., Simkin, A.J., Raines, C.A. and Lawson, T., 2017. Importance of fluctuations in light on plant photosynthetic acclimation. *Plant physiology*, *173*(4), pp.2163-2179.

Vialet-Chabrand, S.R., Matthews, J.S., McAusland, L., Blatt, M.R., Griffiths, H. and Lawson, T., 2017. Temporal dynamics of stomatal behavior: modeling and implications for photosynthesis and water use. *Plant physiology*, *174*(2), pp.603-613.

Vico, G., Manzoni, S., Palmroth, S. and Katul, G., 2011. Effects of stomatal delays on the economics of leaf gas exchange under intermittent light regimes. *New Phytologist*, *192*(3), pp.640-652.

Vogel, J., 2008. Unique aspects of the grass cell wall. *Current opinion in plant biology*, *11*(3), pp.301-307.

Voiniciuc, C., Pauly, M. and Usadel, B., 2018. Monitoring polysaccharide dynamics in the plant cell wall. *Plant physiology*, *176*(4), pp.2590-2600.

von Caemmerer, S. and Furbank, R.T., 2003. The C 4 pathway: an efficient CO 2 pump. *Photosynthesis research*, *77*, pp.191-207.

von Caemmerer, S., Lawson, T., Oxborough, K., Baker, N.R., Andrews, T.J. and Raines, C.A., 2004. Stomatal conductance does not correlate with photosynthetic capacity in transgenic tobacco with reduced amounts of Rubisco. *Journal of experimental botany*, *55*(400), pp.1157-1166.

Wall, S., Vialet-Chabrand, S., Davey, P., Van Rie, J., Galle, A., Cockram, J. and Lawson, T., 2022. Stomata on the abaxial and adaxial leaf surfaces contribute differently to leaf gas exchange and photosynthesis in wheat. *New Phytologist*, *235*(5), pp.1743-1756.

Watling, J.R., Ball, M.C. and Woodrow, I.E., 1997. The utilization of lightflecks for growth in four Australian rain-forest species. *Functional Ecology*, *11*(2), pp.231-239.

Wheeler, T. and Von Braun, J., 2013. Climate change impacts on global food security. *Science*, *341*(6145), pp.508-513.

Wikström, N. and Kenrick, P., 2001. Evolution of Lycopodiaceae (Lycopsida): estimating divergence times from rbcL gene sequences by use of nonparametric rate smoothing. *Molecular phylogenetics and evolution*, *19*(2), pp.177-186.

Wolf, S., Mouille, G. and Pelloux, J., 2009. Homogalacturonan methyl-esterification and plant development. *Molecular plant*, *2*(5), pp.851-860.

Wong, S.C., Cowan, I.R. and Farquhar, G.D., 1979. Stomatal conductance correlates with photosynthetic capacity. *Nature*, *282*(5737), pp.424-426.

Woods, D.B. and Turner, N.C., 1971. Stomatal response to changing light by four tree species of varying shade tolerance. *New Phytologist*, *70*(1), pp.77-84.

Woolfenden, H.C., Bourdais, G., Kopischke, M., Miedes, E., Molina, A., Robatzek, S. and Morris, R.J., 2017. A computational approach for inferring the cell wall properties that govern guard cell dynamics. *The Plant Journal*, *92*(1), pp.5-18.

Wu, H.C., Bulgakov, V.P. and Jinn, T.L., 2018. Pectin methylesterases: cell wall remodeling proteins are required for plant response to heat stress. Frontiers in plant science, 9, p.1612.

WU, H.I. and SHARPE, P.J., 1979. Stomatal mechanics II*: material properties of guard cell walls. *Plant, Cell & Environment*, *2*(3), pp.235-244.

Wu, Z.Q. and Ge, S., 2012. The phylogeny of the BEP clade in grasses revisited: evidence from the whole-genome sequences of chloroplasts. *Molecular Phylogenetics and Evolution*, *62*(1), pp.573-578.

Xiong, D. and Flexas, J., 2020. From one side to two sides: the effects of stomatal distribution on photosynthesis. *New Phytologist*, *228*(6), pp.1754-1766.

Xiong, D., Douthe, C. and Flexas, J., 2018. Differential coordination of stomatal conductance, mesophyll conductance, and leaf hydraulic conductance in response to changing light across species. *Plant, cell & environment*, *41*(2), pp.436-450.

Xue, S., Hu, H., Ries, A., Merilo, E., Kollist, H. and Schroeder, J.I., 2011. Central functions of bicarbonate in S-type anion channel activation and OST1 protein kinase in CO2 signal transduction in guard cell. *The EMBO journal*, *30*(8), pp.1645-1658.

Yamamoto, Y., Negi, J., Wang, C., Isogai, Y., Schroeder, J.I. and Iba, K., 2016. The transmembrane region of guard cell SLAC1 channels perceives CO2 signals via an ABA-independent pathway in Arabidopsis. *The Plant Cell*, *28*(2), pp.557-567.

Yamori, W., Irving, L.J., Adachi, S. and Busch, F., 2016. Strategies for optimizing photosynthesis with biotechnology to improve crop yield. *Handbook of photosynthesis*.

Yang, X., Yang, Y., Ji, C., Feng, T., Shi, Y., Lin, L., Ma, J. and He, J.S., 2014. Large-scale patterns of stomatal traits in Tibetan and Mongolian grassland species. Basic and Applied Ecology, 15(2), pp.122-132.

Yin, Q., Tian, T., Kou, M., Liu, P., Wang, L., Hao, Z. and Yue, M., 2020. The relationships between photosynthesis and stomatal traits on the Loess Plateau. *Global Ecology and Conservation*, *23*, p.e01146.

Yin, X., Biswal, A.K., Dionora, J., Perdigon, K.M., Balahadia, C.P., Mazumdar, S., Chater, C., Lin, H.C., Coe, R.A., Kretzschmar, T. and Gray, J.E., 2017. CRISPR-Cas9 and CRISPR-Cpf1 mediated targeting of a stomatal developmental gene EPFL9 in rice. *Plant cell reports*, *36*, pp.745-757.

Yuzawa, Y., Nishihara, H., Haraguchi, T., Masuda, S., Shimojima, M., Shimoyama, A., Yuasa, H., Okada, N. and Ohta, H., 2012. Phylogeny of galactolipid synthase homologs together with their enzymatic analyses revealed a possible origin and divergence time for photosynthetic membrane biogenesis. *DNA research*, *19*(1), pp.91-102.

Zandleven, J., Sørensen, S.O., Harholt, J., Beldman, G., Schols, H.A., Scheller, H.V. and Voragen, A.J., 2007. Xylogalacturonan exists in cell walls from various tissues of Arabidopsis thaliana. *Phytochemistry*, *68*(8), pp.1219-1226.

Zeiger, E. and Hepler, P.K., 1977. Light and stomatal function: blue light stimulates swelling of guard cell protoplasts. *Science*, *196*(4292), pp.887-889.

Zeiger, E., 1984. Blue light and stomatal function. *Blue light effects in biological systems*, pp.484-494.

Zeiger, E., Talbott, L.D., Frechilla, S., Srivastava, A. and Zhu, J., 2002. The guard cell chloroplast: a perspective for the twenty-first century. *New Phytologist*, *153*(3), pp.415-424.

Zhang, N., Berman, S.R., Joubert, D., Vialet-Chabrand, S., Marcelis, L.F. and Kaiser, E., 2022. Variation of photosynthetic induction in major horticultural crops is mostly driven by differences in stomatal traits. *Frontiers in Plant Science*, *13*, p.860229.

Zhang, N., Zeng, L., Shan, H. and Ma, H., 2012. Highly conserved low-copy nuclear genes as effective markers for phylogenetic analyses in angiosperms. *New Phytologist*, *195*(4), pp.923-937.

Zhang, Q., Peng, S. and Li, Y., 2019. Increase rate of light-induced stomatal conductance is related to stomatal size in the genus Oryza. *Journal of Experimental Botany*, *70*(19), pp.5259-5269.

Zhang, Q., Tang, W., Xiong, Z., Peng, S. and Li, Y., 2023. Stomatal conductance in rice leaves and panicles responds differently to abscisic acid and soil drought. Journal of Experimental Botany, 74(5), pp.1551-1563.

Zoulias, N., Harrison, E.L., Casson, S.A. and Gray, J.E., 2018. Molecular control of stomatal development. *Biochemical Journal*, *475*(2), pp.441-454.